

Atherton, Dorothy

From: ethos@bl.uk
Sent: 17 June 2011 13:43
To: LIB Digitisation
Subject: British Library EThOS Thesis Request THESIS00349687

Categories: Orange Category

The following thesis has been requested by a user of the EThOS system:

Order number: THESIS00349687
Title: Computational investigation of flow regimes and performance characteristics of a pump operating as a turbine Author Given Name: Arnaldo.
Author Family Name: Rodrigues
Institution: Nottingham Trent University Issue date: 2006-01-01 Ethos persistent id: uk.bl.ethos.442089

Please forward this thesis by first class post to the address below as soon as possible as requested in the Memorandum of Understanding signed between your Institution and The British Library.

PLEASE SEND A COPY OF THIS EMAIL WITH THE THESIS.

If this thesis is at The British Library as part of the UK Thesis Digitisation Project, please forward this email to uktheses-work@bl.uk with a brief covering note.

EThOS Admin
The British Library
Bldg 6A, Ground Floor
Boston Spa, Wetherby
West Yorkshire
LS23 7BQ
Tel: 01937 546189
Email: UKTheses-work@bl.uk

ProQuest Number: 10290218

All rights reserved

INFORMATION TO ALL USERS

The quality of this reproduction is dependent upon the quality of the copy submitted.

In the unlikely event that the author did not send a complete manuscript and there are missing pages, these will be noted. Also, if material had to be removed, a note will indicate the deletion.



ProQuest 10290218

Published by ProQuest LLC (2017). Copyright of the Dissertation is held by the Author.

All rights reserved.

This work is protected against unauthorized copying under Title 17, United States Code
Microform Edition © ProQuest LLC.

ProQuest LLC.
789 East Eisenhower Parkway
P.O. Box 1346
Ann Arbor, MI 48106 – 1346

BL ✓

Digitised

21/7

41 0675834 5



Computational Investigation of Flow Regimes and Performance Characteristics of a Pump Operating as a Turbine

ARNALDO RODRIGUES

A thesis submitted in partial fulfilment of the requirements of
The Nottingham Trent University for the degree of
Doctor of Philosophy

September 2006

432720

NOTTINGHAM TRENT
UNIVERSITY LIBRARY

NOTTINGHAM TRENT UNIVERSITY LIBRARY	

TABLE OF CONTENTS

List of Figures	vi
List of Tables	viii
Acknowledgements	x
Abstract	xi
List of Publications	xii
Symbols	xiii
1 Introduction	1
1.1 Developments in the area of Pumps as Turbines.....	1
1.1.1 Historical Context.....	1
1.1.2 Research Activities	2
1.1.3 Benefits of using Pumps as Turbines.....	4
1.1.4 Challenges with PAT Technology	4
1.1.5 Unattended Areas of PAT Technology.....	4
1.1.5.1 Problem 1: Complexity of PAT Computational Model.....	4
1.1.5.2 Problem 2: Improvement of Internal Hydraulics of a PAT	5
1.2 Outline of the Research Project	6
1.2.1 Research Objectives.....	6
1.2.2 Research Base Outline	6
1.2.2.1 Problem 1: Complexity of a PAT Computational Model.....	6
1.2.2.2 Problem 2: Improvement of the Internal Hydraulics of a PAT ...	7
1.2.3 Appropriate Technology aspects of the Research Project.....	10
1.2.3.1 Unattended Areas	10
1.2.3.2 Contribution to Knowledge	11
1.3 Collaborating Institute	12
2 Computational Fluid Dynamics	13
2.1 CFD - A General Background	13
2.1.1 Governing equations.....	14
2.1.2 Turbulence modelling.....	16
2.1.3 Frame of references.....	17
2.1.3.1 Sliding Mesh	17
2.1.3.2 Mixing Plane	18
2.1.3.3 Frozen rotor	18
2.1.4 Near wall treatment.....	19
2.1.4.1 Y-Plus	19
2.1.4.2 Rough Walls.....	20

2.2	PAT context in CFD Research.....	21
3	Computational Modelling & Discretization	23
3.1	Geometry Description.....	23
3.2	Mesh Generation and Discretization.....	24
3.2.1	Mesh topology.....	24
3.2.2	Mesh Quality.....	26
3.2.2.1	Determinant.....	27
3.2.2.2	Orthogonality.....	27
3.2.2.3	Degeneracy.....	27
3.2.2.4	Aspect Ratio.....	27
3.3	Boundary conditions.....	28
3.3.1.1	Inlet Boundary Condition.....	28
3.3.1.2	Outlet Boundary Condition.....	30
3.3.1.3	Wall Boundary Condition.....	31
3.3.1.4	Periodic Boundary Condition.....	32
3.3.2	Solver Parameters.....	32
3.3.2.1	Advection Scheme.....	32
3.3.2.2	Timestep selection.....	33
3.3.2.3	Grid Convergence (Verification).....	34
3.3.2.4	Error Estimation.....	37
3.3.2.5	Turbulence Modelling.....	39
4	Theory & Methodology	43
4.1	Hydraulic Parameters.....	43
4.2	Hydraulic Loss Methodology - Flow Zones.....	45
4.2.1	Flow Zone- <i>i</i>	47
4.2.1.1	Flow Description.....	47
4.2.1.2	Hydraulic Losses in Flow Zone- <i>i</i>	48
4.2.2	Flow zone- <i>ii</i>	49
4.2.2.1	Flow description.....	49
4.2.2.2	Hydraulic Losses – Flow zone- <i>ii</i>	51
4.2.3	Zones- <i>iii, iv, v</i>	51
4.2.3.1	Flow description & Energy Transfer in Zones- <i>iii, iv, v</i>	52
4.2.3.2	Hydraulic Losses – Flow Zones- <i>iii, iv, v</i>	55
4.2.4	Zones- <i>vi, vii</i>	55
4.2.4.1	Flow description.....	55
4.2.4.2	Hydraulic Losses – Zone- <i>vi, vii</i>	58
4.3	Modelling Methodology.....	59
4.3.1	Geometrical Association – Interface Modelling.....	59

4.3.2	Optimisation of PAT Geometry	61
4.3.2.1	Modification-i - Suction eye enlargement.....	61
4.3.2.2	Modification-ii – Rounding of impeller inlet edges.....	62
4.3.2.3	Modification-iii – Casing ring inserts	62
4.3.2.4	Modification-iv – Sharpening of outer front-shroud and back-shroud edges at inlet	63
4.4	Correlation Between CFD and Experimental.....	64
4.4.1	General Experimental Parameters	64
4.4.2	CFD parameters	65
4.4.2.1	Torque	65
4.4.2.2	Total pressure	67
4.4.3	Flow Zone Combined Hydraulic Losses influence on Variables	67
4.4.4	CFD-Experimental Correlation	69
5	Results.....	70
5.1	Interpretation of Results.....	70
5.1.1	Flow Description	70
5.1.2	Evaluation of Geometry Changes	71
5.2	Comparison of CFD and Experimental Parameters	71
5.2.1	Torque	72
5.2.2	Exit pressure.....	73
5.2.3	Hydraulic Parameters	74
5.2.4	Zonal Losses (Hydraulic Loss Method).....	75
5.3	Discrepancies and Uncertainty in CFD modelling	77
5.3.1	Simulation without draft-tube.....	78
5.3.1.1	No-Draft.i - Single impeller passage modelled.....	79
5.3.1.2	No-Draft.ii - All impeller passages modelled	80
5.3.2	Representation of Leakage	82
5.3.3	General overview of uncertainty with CFD	84
5.4	Interface Modelling - Representing churning.....	85
5.4.1	Comparison between interface- <i>i</i> and interface- <i>ii</i>	86
5.4.2	Comparison between interface- <i>i</i> and interface- <i>iii</i>	89
5.4.3	Interface- <i>i</i> and interface- <i>iv</i>	91
5.4.4	Hydraulic Losses	94
5.4.4.1	Flow Zone-i	94
5.4.4.2	Flow zone-ii.....	95
5.4.4.3	Flow Zone-iii.iv.v	96
5.4.4.4	Flow zone-vi.....	97
5.4.4.5	Flow zone-vii	98

5.4.4.6	Combined Flow Zone losses	99
5.4.5	General overview of interface study	100
5.5	Optimization of Internal Hydraulics Using CFD	101
5.5.1	Modification- <i>i</i> - Impeller eye enlargement.....	101
5.5.2	Modification- <i>ii</i> - Modified-Eye with Inlet Rounding	103
5.5.3	Modification- <i>iii</i> - Modified-Eye with Front-shroud/Shroud outside sharpening	106
5.5.4	Hydraulic Losses	109
5.5.4.1	Flow zone-i.....	109
5.5.4.2	Flow zone-ii.....	109
5.5.4.3	Flow zone-iii.iv.v.....	110
5.5.4.4	Flow zone-vi.....	111
5.5.4.5	Flow zone-vii	112
5.5.4.6	Combined Flow Zone losses	113
5.5.5	Summary of Modification Study	114
6	Discussion.....	115
6.1	Uncertainties Associated with CFD.....	115
6.1.1	Uncertainty in CFD	117
6.1.1.1	Residual Errors	117
6.1.1.2	Draft-tube & Tailrace Conditions	117
6.1.1.3	Modelling of Gravity	119
6.1.1.4	Leakage	119
6.1.2	Uncertainty Analysis for Experimental-CFD correlation.....	120
6.2	Interface Modelling – Zone ii.....	120
6.2.1	Interface- <i>i</i>	121
6.2.2	Interface- <i>ii</i>	121
6.2.3	Interface- <i>iii</i>	122
6.2.4	Interface- <i>iv</i>	122
6.2.4.1	Interface Study.....	123
6.3	Geometrical Optimization.....	123
6.3.1	Modification- <i>i</i>	124
6.3.2	Modification- <i>ii</i>	124
6.3.3	Modification- <i>iii</i>	125
6.3.4	Optimisation study	126
6.4	General Overview.....	126
6.4.1	CFD as a PAT Performance Prediction Tool.....	126
6.4.2	CFD as a Design Tool.....	128
6.4.2.1	Optimisation Study	128

6.4.2.2	Identification of Good Pump Design for PAT Application	128
7	Conclusion and Recommendations	130
7.1	Conclusions	130
7.1.1	Review	130
7.1.2	Modelling and Discretization	131
7.1.3	Comparison of CFD and Experimental Data	132
7.1.4	Interface Study	132
7.1.5	Modification Study	133
7.1.6	CFD for performance prediction	133
7.2	Further work and Recommendations	134
	References	137
	Appendix A Flow Behaviour in a PAT	138
	Appendix B Calculation of Leakage	149
	Appendix C Geometry Verification using CFD	150
	Appendix D Test Specimen	155
	Appendix E Performance Prediction Methods	161
	Appendix F Computational Tool	163
	Appendix G Experimental Work at IWK	164
	Appendix H Experimental Uncertainty	169
	Appendix I Published Papers	176

List of Figures

Figure 1.1 - Hydraulic Regions of a PAT	8
Figure 1.2 – Pump Volute	9
Figure 1.3 - Impeller cross-section	10
Figure 3.1 Hydraulic region of volute, impeller, and inlet of draft-tube	23
Figure 3.2 Mesh in the static components (a) Volute (b) Draft tube	25

Figure 3.3 Mesh of the blade passages.....	26
Figure 3.4 Normalised velocity component along the leading edge span (a) Tangential component (b) Meridional component.....	39
Figure 3.5 Velocity components (a) Q=22l/s (b) Q=26l/s	42
Figure 4.1 Flow zone (a) Volute cross-section (b) Draft tube.....	47
Figure 4.2 Flow zone- <i>ii</i> and sub-zones.....	49
Figure 4.3 Velocity diagram for flow zone- <i>ii_a</i>	50
Figure 4.4 Turbine mode inlet velocity diagram with and without slip (infinite and finite number of blades Chors (1997))	53
Figure 4.5 Pump mode inlet velocity diagram with and without slip	54
Figure 4.6 Theoretical swirl component at the draft-tube, at (a) part-load (b) BEP (c) Overload.....	56
Figure 4.7 Draft-tube head recovery.....	57
Figure 4.8 zone- <i>ii</i> different possible geometrical representation (a) interface- <i>i</i> , (b) interface- <i>ii</i> , (c) interface- <i>iii</i> , (d) interface- <i>iv</i>	60
Figure 4.9 - Modification- <i>i</i>	62
Figure 4.10 Modification- <i>ii</i>	62
Figure 4.11 - Modification- <i>iii</i>	63
Figure 4.12 - Modification- <i>iv</i>	64
Figure 5.1 - Torque comparison from CFD Force Integration and Hydraulic Loss methods.....	72
Figure 5.2 - Comparison of Exit static pressure for non-modified PAT	73
Figure 5.3 - CFD and Experimental hydraulic characteristics for non-modified PAT.....	74
Figure 5.4 - Zone loss distribution for non-modified PAT.....	76
Figure 5.5 - Hydraulic Characteristics for PAT without draft-tube and with periodic boundary.....	79
Figure 5.6 - Zone loss distribution for PAT with periodic boundary and no draft- tube.....	80
Figure 5.7 - Hydraulic Characteristics of PAT modelling all passages but without draft-tube	81
Figure 5.8 - Zone loss for PAT with all blade passages and without draft-tube..	82
Figure 5.9 - Hydraulic characteristics without leakage and with leakage	83
Figure 5.10 - Comparison of Hydraulic Losses for PAT with and without Leakage	84
Figure 5.11 - Dimensionless characteristics comparing interface- <i>i</i> and experimental efficiency and change in (a) Head number (b) Power Number	86

Figure 5.12 - Dimensionless characteristics comparing Efficiency and change in (a) Head number (b) Power Number	87
Figure 5.13 - Percent change	88
Figure 5.14 - Dimensionless characteristics comparing Efficiency and change in (a) Head number (b) Power Number	90
Figure 5.15 - Percentage change	91
Figure 5.16 - Dimensionless characteristics comparing Efficiency and change in (a) Head number (b) Power Number	92
Figure 5.17 - Percent change	93
Figure 5.18 - Losses in Zone- <i>i</i> – Interface Study	95
Figure 5.19 - Losses in zone- <i>ii</i> – Interface Study	96
Figure 5.20 - Losses in zone- <i>iii.iv.v</i> – Interface Study	97
Figure 5.21 - Losses in zone- <i>vi</i> – Interface Study	98
Figure 5.22 - Losses in zone- <i>vii</i> – Interface Study	99
Figure 5.23 - Combined zone losses – Interface Study	100
Figure 5.24 - Dimensionless characteristics comparing Efficiency and change in (a) Head number (b) Power Number	102
Figure 5.25 - Percentage contributions of power and head to change in efficiency	103
Figure 5.26 - Dimensionless characteristics comparing Efficiency and change in (a) Head number (b) Power Number	104
Figure 5.27 - Percent change	105
Figure 5.28 - Dimensionless characteristics comparing Efficiency and change in (a) Head number (b) Power Number	107
Figure 5.29 - Percent change	108
Figure 5.30 - Losses in zone- <i>i</i> – Modification Study	109
Figure 5.31 - Losses in zone- <i>ii</i> – Modification Study	110
Figure 5.32 - losses in zone- <i>iii.iv.v</i> – Modification Study	111
Figure 5.33 - Losses in zone- <i>vi</i> – Modification Study	112
Figure 5.34 - Losses in zone- <i>vii</i> – Modification Study	113
Figure 5.35 - Combined zone losses – Modification Study	114
Figure 6.1 - CFD Torque loading on each blade for a full impeller model	116

List of Tables

Table 3.1 Effect of grid size on head rise	37
Table 3.2 Grid check	37

Table 4.1 – Summary of Interface Models.....	61
Table 4.2 Correlation Table Correlation for power p , CFD and Experimental	69
Table 4.3 Dimensionless groups correlation for CFD-Experiment	69
Table 5.1 - Distribution of zone losses as a percentage of total hydraulic loss for non-modified PAT	76
Table 5.2 - Percent change	88
Table 5.3 – Percentage change	91
Table 5.4 - Summary of dimensionless characteristics.....	93
Table 5.5 - Summary of relative study at each operating region.....	103
Table 5.6 - Percent change.....	106
Table 5.7 - Percent change.....	108

Acknowledgements

I would like to begin by expressing my profound gratitude to my Director of Studies Dr. Eugene Lai for giving me the opportunity to embark on this research project and for all of his constructive criticism and encouragement throughout the entire project.

My sincere thanks to my second supervisor Dr. Arthur Williams for whom without his efforts this project would have not existed. His support and knowledge has been outstanding throughout.

I would also like to acknowledge the collaborative PAT research programme with the Institute of Water Resources Management (IWK) of the University of Karlsruhe, Germany. Through this collaboration I met Dr. Punit Singh a great individual with such competent knowledge and charisma for his work. He provided the experimental data which gave a starting step for this project.

This research would not have been possible without the financial support given by ESPRC and the Nottingham Trent University. A special thanks also to the academic and support staff. A particular thanks to Mr. Gary Griffiths, Mr. Jez Keeling, and also Mrs. Doreen Corlett.

I would also like to thank my colleagues Dr. Drona Uphadyay, Dr. Justyna Mordaka, and also Research Assistant Dr. Robert Simpson for all their support and creating a family-like environment. Thanks also go to all the research students in our memorable FRI for their motivation.

My thanks are also due to my mentor at work Mr. Graham Bradbury for all the support and for allowing me time off work to concentrate on the thesis.

Lastly, I would like to give my heartfelt thanks to the most precious people in my life, my lovely parents and brothers, for all the support, love, and great companionship.

Abstract

This project deals with the investigation of the physical significance of the internal hydraulics of a pump operating as a turbine through the means of computational fluid dynamics. The pump as turbine is a new application area for CFD with very limited studies published. A commercial code is used to enable the modelling of the pump as turbine and thorough discretization is carried out to understand the most suitable solution parameters for the modelling.

The 'Hydraulic Loss' methodology is developed to analyse seven individual zones within the geometry of the pump as turbine with the aim of understanding two major unattended problems. The first concerns methods for translating actual geometry into a mesh which is solvable yet still accurate. Four interface models between the volute and impeller are investigated and compared against already available experimental data. The most accurate interface is the geometrical model that closely represents the actual geometry, whilst the least accurate is the less complex geometrical interface model. CFD has shown that accurate PAT geometry representation is necessary to accurately predict the performance characteristics.

The second is with respect to the improvement of the performance characteristics of the pump as turbine through geometry modification. Four geometrical modification stages are investigated and three are compared to the available experimental data. CFD has shown good agreement with the experimental performance characteristics and has been able to detect the effects on losses and performance due to the different modifications. The modifications have shown that impeller rounding, back-shroud sharpening, and casing rings have improved the performance of the pumps as turbine whilst the impeller eye enlargement has improvement in performance in the part load region only.

The computational method has allowed for practical guidelines on the selection of pumps for turbine operation. Recommendations are made for further work in the area of PATs

List of Publications

Proceedings of the IMechE. Advances of CFD in Fluid Machinery Design, 18 November 2003. One Birdcage Walk, London

- Rodrigues, A., Singh, P., Williams., A., Nestmann, F., Lai., E (2003). Hydraulic analysis of a pump as a turbine with CFD and experimental data. Advances of CFD in Fluid Machinery Design, Proceedings of the IMechE. pp 118 - 131

Symbols

Upper case Roman alphabet

A	Cross-sectional area
B	Casing width
D	Reference impeller diameter
gH	Head,
H	Head
L	Length
N	Rotational speed
P	Power output
Q	Discharge
T	Torque
X	Clearance

Lower case Roman alphabet

e	Exit reference plane
g	Acceleration due to gravity
p	Pressure
p	Power number
r	Radius
t	thickness
u	Peripheral velocity
v	Velocity
z	Vertical elevation

Greek Symbols

α	Absolute flow angle
β	Blade angle
δ	Radial flow angle,
δ	Clearance diameter between casing and impeller
Δ	
Φ	Discharge number
η	Efficiency
λ	Friction coefficient
μ	Dynamic viscosity
ρ	Mass density of water
ψ	Head number

ψ	Work done
ω	Angular speed
ζ	Swirl loss coefficient
ξ	Dynamic coefficient

Subscripts

1	Impeller inlet
2	Impeller outlet
c	casing
a	Atmospheric conditions
A	Axial clearance
e	exit reference plane
Eu	Euler
Exp.	Experimental
Hyd	Hydraulic
i	inlet reference plane
L	Hydraulic loss
Le	Leakage
m	Meridional velocity component
m	modified geometry
mech.	Mechanical
n	non-modified geometry
r	relative velocity component
R	Radial clearance
s	specific
t	throat
u	Peripheral component

Other Abbreviations

FS	Front Shroud
BS	Back Shroud

1 Introduction

This chapter is comprised of two main sections. The opening section gives a general insight into the historical background of hydroelectric energy and 'pumps as turbines' and its current unattended problems. The second section describes the base outline of the project and sets the scene for the research investigation, which has been carried out according to the derived aims and objectives in section 1.2.1.

1.1 Developments in the area of Pumps as Turbines

1.1.1 Historical Context

For many centuries alternative energy has been a subject of research interest and curiosity for mankind. Various forms of natural energy resources have been documented and investigated throughout the centuries leading to the sustained development of diverse technologies, and vitally, playing a role in the well being of society in general.

Hydroelectric energy has been one form of alternative energy that has been around for a long time. The original concept of extracting energy from water to a rotating shaft probably can be traced to waterwheels. Quoting from Nechleba (1957), *"according to rather unreliable sources, the first blade fitted waterwheel was invented by Ctesibios as early as 135 BC"*. In fact the history on waterwheel seems to go even further back to 250 BC (Wolfel, 1987) when the Egyptians used the energy in river currents to turn wheels. It is therefore difficult, or perhaps impossible, to attribute merits to its original inventor(s). Nevertheless its primary concept is what gave way to the development of hydroelectric energy.

The progress of hydroelectric technology has been constant throughout the years owing to the increased demands of expanding societies and industrialisation. This requirement has led to large effort being put into the research of large hydroelectric power schemes. However these schemes are designed to target large populations. It is not economically viable to supply electrical power from a central grid to smaller communities in remote areas due to various technical challenges. In third world countries, the impact resulting from this challenge becomes more apparent. Recently awareness has grown towards this problem, however the current technological advancement of the smaller hydroelectric

systems are lagging behind their larger counterparts and therefore a new effort is being put into microhydro technology research.

A number of developments have already come out as a result of this relatively new area. But most of these turbines are purpose built to suit the particular site conditions. One approach has been to install pumps operating in turbine mode. It is on this technology that this research is based.

1.1.2 Research Activities

The first reported pump operating as turbine was made by Thoma (1931) in the early 1930's who accidentally discovered this while studying the characteristics of sudden power supply failure in pump operation. He realised that a pump could generate energy and operate as a turbine when the direction of flow was reversed. Spetzler (1934) soon after described the installation of a reversible pump-turbine. Towards the 1950s most pump storage schemes were still built with separate pump and turbine units. The state of reversible pump technology hadn't advanced enough to justify its implementation, especially because it was slow to change from pump operation to turbine operation (Strub, 1959). Interest for this technology however grew within this period, as manufacturers and researchers realised the potential benefits from operating pumps in both modes. During this period considerable research and experimental testing of pumps in turbine mode took place as manufacturers wanted to provide information on both modes of operation. However, cost on experimental testing was high, consequently much of the research into the application of pumps-as-turbines was aimed at developing methods to predict the turbine-mode best efficiency point (BEP) from manufacturers pump geometrical and performance data. Kittredge et al (1931), Engles (1957), Stepanoff (1957), and de Kovats (1958) were amongst the first group of individuals to propose various prediction methods. In more recent work a number of prediction methods have been developed however they still lack generality for pumps of different designs as there are many uncertainties to these empirical models. For instance, Ventrone et al (2000) proposed a means for correlating the ideal pump and turbine head-flow parameters in the region of optimum performance in both modes of operation using a runner momentum coefficient obtained experimentally and geometrical information from the runner. However the performance in turbine mode also depends on the strong interaction of the impeller with other components and this is not taken into account. Amelio et al (2004) proposed a one-dimensional numerical code for deriving the turbine efficiency of centrifugal pumps. The code computes the losses through each

component thus determining the PAT performance. The process however is limited as it only takes into account average data and disregards three-dimensional effects.

The concept of using a pump as turbine (PAT) for non power recovery schemes appears to only have come out following the Oil Crisis in the 1970's. The US Department of Energy led investigations through Acres American (1980) and Cooper et al (1981) into low-cost renewable energy supplies of grid connected schemes within the 100-500kW range. They realised that instead of dissipating the energy in a valve a PAT could be installed to recover some energy for use in other parts of the plant. Taylor (1983), however, noted some limitations in this type of application, which are due to the fixed geometry of the pump and the fact that, at low flow rates, a reverse running pump will actually absorb mechanical power. McKinney et al (1983) and Marquis (1983) looked at the application of various types of turbine, including reverse-running of pumps, and found that reverse-running of pumps was cost-effective in the 5-100kW. Practical information was later gathered from various types of installation by Chappell (1982), this brought out some useful information for PAT selection. Other engineers, including Laux (1983), McClaskey et al (1976) and Apfelbacher (1988), realized the application of PATs to industrial processes and in water supply systems.

These research activities brought valuable and practical information associated to the categorisation and application ranges of PATs. This information has aided in the commissioning of PAT technology but has not made progress in the understanding of internal hydraulics of the machine and each individual component. Development and availability of new and advanced research tools has permitted for the revival in interest on the research of PATs. Recently Tamm (2000) carried out an analysis of a reverse operating pump using computational data with intent of understanding the internal hydraulics, but had no experimental data to verify his results. Singh (2003) carried out experimental work and was able to compare his results to computational data but the discrepancies were significant due to lack of knowledge on how to set up the computational model.

1.1.3 Benefits of using Pumps as Turbines

When pumps are operated efficiently in turbine mode they can be more cost-effective than specifically designed turbines, especially for micro-hydropower. These are often decentralized energy systems of capacities below 100kW (and above 20kW). Pumps are generally easy to obtain off the shelf and at lower costs since they are mass-produced and come in a large range of heads and flows. They also involve low-cost maintenance, as parts are generally standard and therefore easier to obtain.

1.1.4 Challenges with PAT Technology

The main disadvantage of a pump operating as a turbine is that it is of fixed geometry, which only allows it to operate efficiently at one set of steady-state conditions, whereas equivalent turbines allow for flows to be regulated by some mechanisms (such as variable guide vanes), allowing the turbine to run efficiently at a range of flow rates. This unconventional hydraulics may lead to less efficient operation if the turbine performance is not identified prior to installation. Very few manufacturers have readily available data on the turbine-mode performance of their pumps, and other manufacturers will supply a pump for operation as a turbine only after carrying out a full performance test, for which the customer would have to pay a significant amount above the usual pump price.

1.1.5 Unattended Areas of PAT Technology

1.1.5.1 Problem 1: Complexity of PAT Computational Model

The use of computational tools is a relatively new methodology for the internal investigation of flow behaviour in a PAT. CFD itself is still in an evolutionary process. One of the main unattended areas of PAT research is with respect to the understanding of effects of geometrical complexity on the behaviour of flow. For significant evaluation of a PAT computational model to be made it is also necessary to understand the associated uncertainties with computational parameters. This also allows for a good level of confidence in the interpretation of the computationally predicted variables.

With experimental data made available computational models of different levels of geometrical complexity can be compared to determine their level of accuracy.

Moreover the critical regions of a PAT which can have a significant impact on the internal flow regimes can be identified. Adequate guidelines for PAT computational modelling can be established.

1.1.5.2 Problem 2: Improvement of Internal Hydraulics of a PAT

Another challenging area in the research of PAT is with respect to the improvement of turbine mode performance characteristics through definite modification of the pump design. Experimental work by Lueneburg (1992), Williams (1992), Cohrs (1997), and field testing described by Mikus (1983) have shown that simple modifications to geometry can bring about efficiency improvements, but their results are not always consistent and they could not explain the reasons behind these inconsistencies. Recently Singh (2004) carried out experimental studies on PATs of different designs. He investigated the effects of minor geometrical modifications and reported significant improvements in the performance characteristics with some modifications. The experimental methodology did not allow his judgement on the hydraulic behaviour of the region of modification. His observations were based on the trend from a number of tested pumps.

Experimental methods are not sufficiently robust to allow for a better understanding of the internal hydraulics of a PAT and therefore when minor changes are made to the geometry very few significant observations can be made. Measuring internal flow parameters is extremely difficult in the experimental procedure and this is a major drawback in the understanding of the influence of geometrical changes. Moreover, the experimental approach has high economical impact on the research due to the resources required.

There is still lack of detailed understating of the hydraulic energy transfer mechanisms resulting from geometrical changes in a PAT, which makes it difficult to make any conclusive judgements of the influence of geometrical optimisation procedure. With the combination of established hydraulic fundamentals, and elaborate computational investigations and with comparison to experimentally obtained data the internal hydraulics of a PAT can be better understood and the benefits of optimisation methods can be better explained. A computational investigation can provide more insight into the flow regimes and phenomena within a PAT and with correlation of experimental data the energy transfer mechanisms can be better understood.

1.2 Outline of the Research Project

1.2.1 Research Objectives

The aim of this project is to employ computational fluid dynamics as an analytical tool to study the flow regimes and performance characteristics, and to carry out design assessments of a pump operating as a turbine. The objectives of this research are:

- i. To correlate the CFD code for 'pump as turbine' (PAT) application to enable confident interpretation and judgement of the computational results against experimental data.
- ii. To identify CFD parameters that are best suited for PAT simulations, namely, the boundary conditions, interface modelling, turbulence model selection
- iii. To investigate methods for analysing the flow within the PAT
- iv. To allow the understanding of the hydraulic loss mechanisms within each component of the machine, and energy transfer mechanisms.
- v. To evaluate geometrical modification procedures for PAT optimisation
- vi. To evaluate the influence of geometrical complexity and identify critical regions that can affect the internal flow prediction of flow regimes of a PAT.
- vii. To evaluate CFD as a performance prediction tool for PAT applications
- viii. To bring out basic pump selection guidelines for PAT applications by understanding geometrical characteristics of pumps that make a 'good' PAT based on numerical assumptions.

1.2.2 Research Base Outline

The research base of this project involves the investigation of computational model geometrical complexity and optimisation of the internal hydraulics of a PAT using computational tools as a mean of investigation.

1.2.2.1 Problem1: Complexity of a PAT Computational Model

In a computational simulation the internal flow regimes of a PAT model can be directly affected by the level of geometrical complexity that it incorporates. For models with low level of geometrical complexity the advantage can be reduced set up time and effortless grid generation, which overall can produce faster set up and computing cycle times. In computational modelling the generated geometry is an approximation of the real physical model. Certain geometrical

assumptions are inevitable due to the limitation of the computational tool(s), such as their lack in the capability of reproducing an exact replica of a physical model. In other cases deliberate assumptions are made which often consist on removal of geometrical features that are considered to not be influential in the overall behaviour of the hydraulics.

1.2.2.2 Problem 2: Improvement of the Internal Hydraulics of a PAT

Various aspects have to be considered to understand what can be classified as optimisation of operating a pump in turbine mode. Although much of the research has focused solely on peak efficiency, other aspects have to be considered when installing a PAT scheme. Due to its fixed operating nature and a single peak efficiency point, the PAT system can only operate at a limited range of flow rates and heads. Often though, the PAT is not an exact match, or, the duty requirements vary seasonally at the installation site, so the PAT does not always run at peak efficiency. (Therefore, when considering optimisation not only the best efficiency point is of interest but the whole performance characteristics of the PAT). Optimisation should therefore satisfy the following criteria:

- Improvement of the overall performance characteristics, including the part-load efficiency. Reduction of losses in the different regions.
- Maintain the best efficiency value over a wider operating range of flows. The observed efficiency curve should display a flatter characteristics rather than a single peak efficiency.
- Through minor geometrical modification, shift the peak efficiency from its current operating flow to the required or new operating flow .

The PAT control volume consists of the hydraulic volume and surfaces of the pump. There are various regions in a pump that can be considered for possible geometrical modification with the aim of improving the hydraulic characteristics for optimum turbine operation. This research investigates the effects of small modifications on the characteristics of the PAT. Geometrical alterations which would require major change in the main design characteristics of the pump, such as alteration of the blade profile, are not considered as these redesign modifications make the idea of operating a pump in turbine mode uneconomical and difficult to implement in practice.

This section highlights regions within the hydraulic control volume of the pump that can be easily modified. The main components or fluid domains of a pump operating as a turbine include the volute, impeller, and draft-tube as shown in [Figure 1.1](#) below.

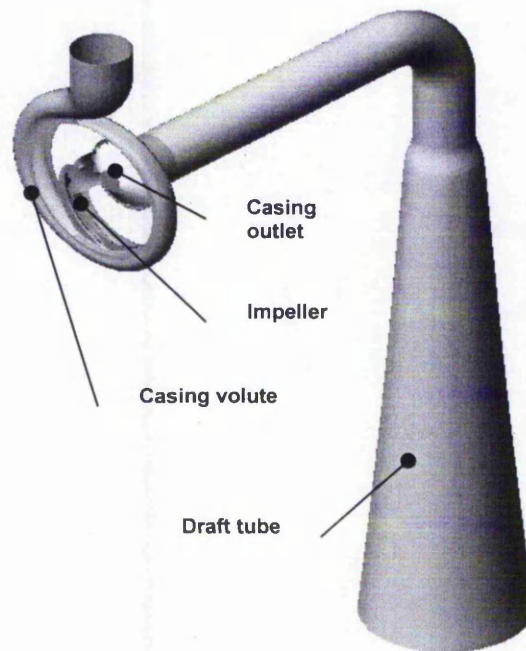


[Figure 1.1](#) - Hydraulic Regions of a PAT

Volute: The volute is the most upstream component of a PAT arrangement and in turbine operation it guides the flow into the impeller. As shown in [Figure 1.2](#) it consists of a pipe region and a semi-enclosed region. In turbine mode of operation the flow enters at the inlet area $A_{c,1}$ and exits through $B_{c,1}$. Usually the volute is also referred to as casing which covers the hydraulic volume around the impeller eye. Generally pump volutes are equally as efficient in both pump and turbine operating modes. The hydraulic characteristics of a volute is affected by a number of geometrical features, namely the volute section areas from the inlet measuring plane to the tongue, volute angle α_v , volute mouth width $B_{c,1}$, and volute base circle (or cutwater) D_B .

Another region which has an influence on the flow behaviour consists of the radial $X_{R,1}$ and axial $X_{A,1}$ clearances between the volute and impeller. In the same region the churning between rotating impeller and stationary volute plays a vital role in the flow characteristics prior to entry into the impeller.

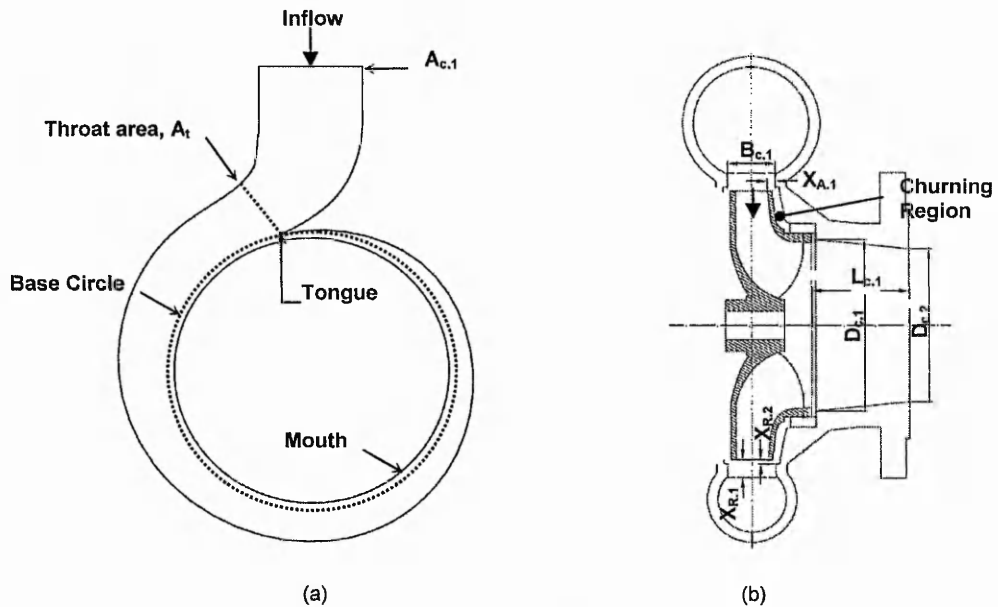


Figure 1.2 – Pump Volute

Impeller: The second component that the flow will encounter will be the impeller. As shown in [Figure 1.3](#) the main parts of the impeller consists of the Front-shroud (FS), Back-shroud (BS) and blades. For each passage, in turbine mode of operation the flow inlet is at leading edge width B_1 and exit is through trailing edge width B_2 , where the flow of all passages join and leave through the impeller-eye D_{2f} . The impeller is responsible for the energy conversion from the incoming flow to the rotating shaft. It consists of a number of blades and it may also be profiled depending on the type of pump and its particular design purpose. The inlet of the impeller, main body or passages and also the outlet are of particular interest as these can play a role on the optimum energy conversion. However modification of the blade profile is out of the scope of minor modifications. Other regions of interest of the impeller include the front-shroud and back-shroud modelling. [Figure 1.3](#) shows the cross-section of a standard pump impeller.

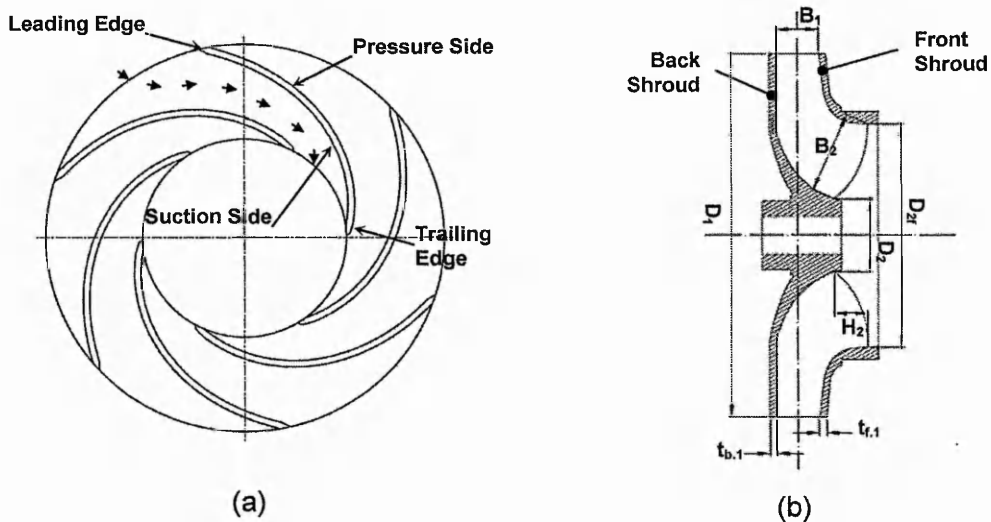


Figure 1.3 - Impeller cross-section

Draft-tube: The last component downstream is the draft-tube and it consists of a long pipe usually with a conical shape at the discharge region as shown previously in Figure 1.1. The draft-tube is responsible for head recovery and also can be used to avoid other problems such as cavitation. The draft-tube inlet diameter is usually the same diameter as the impeller eye diameter D_2 , and is designed to optimise the flow characteristics where both components interface. A pump will not usually come with a draft-tube therefore its overall design always has to be considered for optimum head recovery.

1.2.3 Appropriate Technology aspects of the Research Project

1.2.3.1 Unattended Areas

A lot of effort in pump as turbine research has been focused towards the development of theoretical prediction methods essentially because experimental work is not a cost-effective option. Unfortunately this has made PAT research very contained and focused into isolated areas. The current research considers a new area of investigation for PATs. The use of CFD has certain advantages, for instance some decisions that would be costly to make with a physical model are easily replicated with CFD. A simple yet good example is the ease of removal and addition of material such as increase and decrease of impeller diameter as and when required. In an experimental model this change is often definite.

There is still lack of technical data and information related to the performance of different type of turbines for small applications (specifications for installations and setups are often crucial to obtain maximum power outcomes of the particular scheme). The complex nature of flow within hydraulic machinery has been motive for investigation for several many years. Various techniques and methodologies have originated from the analysis of hydraulic machinery. The use of computational methods on the investigation of 'pump as turbine' is still at a developing stage with very limited literature available.

PATs are increasingly being used for decentralised electricity generation however with lack of suitable information the appropriate selection of a PAT is difficult. The current research provides insight into the operation of PATs and covers the problem areas categorised in section 1.2.2.

1.2.3.2 Contribution to Knowledge

The CFD model of a standard PAT needs to be validated against the experimental data. The computational modelling and discretization for a PAT model needs to be evaluated. A methodology to facilitate the analysis of flow and losses at the various regions of a PAT needs to be developed. The geometrical regions of a PAT which are critical for accurate performance prediction at all operating regions have to be identified. The problems are briefly outlined in the following sections.

This research investigates computational modelling techniques that are suitable for PAT application through the interpretation of the energy transfer mechanisms within a PAT. Further the research also investigates methods for translating actual geometry into a mesh which is solvable yet still accurate. Recommendations are made on best geometrical modelling practices depending on the given application. The computational investigation of simple geometrical modifications which could be made to a standard PAT in order to improve performance are investigated. Geometrical characteristics that make a pump suitable for PAT operation have also been investigated to bring selection guide lines on how to identify pumps suitable for PAT application. This research investigates several innovative areas and the expected outcome is to provide a basis for future PAT work. Most importantly, this research contains practical information that can be of immediate implementation and make a positive contribution to the lives of the end users.

1.3 Collaborating Institute

In the current research, experimental data was made available through the collaboration with the Institute of Water Resources Management (IWK) at the University of Karlsruhe (Germany). The experimental data was used to provide boundary condition input for the current computational model. The experimental data consist only of global hydraulic parameters and therefore local pressures within the PAT domain are not known.

In Karlsruhe an open loop test-rig was commissioned to carry out the experimental research of pumps running in turbine mode only. The test-rig was equipped with measurement instrumentation to capture the global hydraulic parameters, which include pressure head at inlet and outlet (H), discharge (Q), torque (T), and rotational speed (N). Further information about the test rig and accuracy of the instrumentation can be found in Appendix G. More in depth information can be found in the work by Singh (2004).

2 Computational Fluid Dynamics

This chapter is divided into two sections. In the first section the fundamentals of computational fluid dynamic (CFD) are briefly introduced. The second section makes a review on the computational work on PATs and machinery of geometrical similarity.

2.1 CFD - A General Background

Computational Fluid Dynamics (CFD) has rapidly gained an important role in various engineering applications due to its ability of analysing complex problems. The demand for better-designed and more efficient products has led to an increase in interest and investment from various sectors of the engineering field. Research and application of CFD codes started to take larger steps towards the beginning of the last decade, and this is greatly attributable to the ascending power of computer capabilities and their relatively inexpensive costs. Anderson (1995) suggests that CFD has come out as a third approach, following theoretical and experimental fluid dynamic approaches, which quantitatively analyses fluid flow. It does not substitute the other already well-established methods but due to its potential has become a complementary tool to theoretical and experimental methods for simulating, designing and analysing the complex three dimensional flows in turbomachinery (Raw et al, 1989). CFD is now playing an important role in the design of fluid machinery where the design can be analysed, refined, and optimized.

A significant part of the development of CFD codes has been driven by the turbomachinery industry and the need to model areas such as rotor-stator passages, known for the inherent unsteady flow fields, the swirl flow in draft-tubes, and other complex flow regions. This has led to a number of research publications that sought to evaluate and validate the accuracy of CFD codes. For instance, Song et al (1991) developed a Navier-Stokes (N-S) code and carried out numerical simulations on turbine runners and draft-tubes and were able to predict with good accuracy. Other researchers (e.g. Drtina et al, 1999) have used and validated commercial N-S codes such as TASCflow on Francis turbines, and also used an Euler code to predict the performance in Kaplan turbines. With a number of improvements done on numerical codes, CFD is widely applied to design and optimisation. The application of CFD in certain studies (Qian, 1997)

has led to a better understanding of complex flow phenomena. Sick et al (1996) for instance demonstrated the high level of accuracy that can already be achieved with simulations of the draft tube vortex, but at the same time he provides cautious words with regards to the accuracy and limitations of the numerical methods if appropriate care is not taken. De Henau (1997) discussed accurate methods of modelling and demonstrated the importance of component interaction using viscous flow simulations with a suitable level of accuracy for engineering applications. This brought out information on efficiency, power output, cavitation, and other inherent characteristics of a complete system. The reason for component interaction or complete turbine numerical simulation approach is to avoid assumptions at internal boundary conditions (Sabourin, 1997) and further errors on numerical simulations. Keck (1994) has gone further to refer to CFD as a tool which has aided in making turbomachinery components safer and also easier in layout.

It was found that very little numerical work has been carried out on pumps operating in turbine mode as will be later reviewed in [section 2.2](#). Much of the current turbomachinery research is carried out with in-house CFD codes instead of commercial codes. A plausible reason could be that commercial codes are generally used within industry sectors and often research within competing sectors are kept with a certain level of commercial confidentiality. The second aspect is that most of the research in turbomachinery has been carried out on large scale machines such as Francis turbines which are similar in operating principles, but the characteristics are not necessarily scalable.

2.1.1 Governing equations

The first major breakthrough in CFD for water turbine design came with the introduction of the Euler equations, which combined with theoretical design rules allowed for a significant reduction in model testing to achieve satisfactory designs (Keck et al, 1990). The Euler method has the capability of predicting useful characteristics of flow, including inlet and outlet condition of impeller/runners such as swirl, cavitation, incidence levels, and other. However, the Euler terms neglect viscous effects and therefore it has the lack of ability in predicting losses as Drtina et al (1999) showed through numerical modelling. This makes it difficult to predict the performance of the turbine. 3D Euler codes are still used in CFD design analysis as the codes describe the flow field in turbomachines with all typical vorticity effects, including inviscid reverse flows, are modelled by solving

the continuity together with the inviscid momentum equation. Only viscous losses cannot be estimated therefore skin friction is neglected. Reymond (1996) has shown that Euler codes have been used and there is evidence that with the numerical method, the flow through a runner blade can be predicted correctly. This is because the viscous effects are small and confined to thin boundary layers.

Current codes are based on the Navier-Stokes equations. These are based on the equations governing the dynamics of fluid flow problems – continuity, momentum, and energy equations. Numerous studies (Drtina et al, 1999; Lakshminarayana, 1991; Suzuki et al, 1996) have shown that the N-S codes are appropriate in applications where losses and performances have to be included in the prediction for various or individual components.

For the present study the energy equation is not considered, as thermal energy transfer is assumed negligible (Anderson, 1995) and would add to the computing effort. The momentum equations are known as the Navier-Stokes equations, however, it is common in CFD literature to see stated both the momentum and continuity equations as the Navier-Stokes equations. The following is the general continuity equation for compressible-viscous fluid. For incompressible-viscous fluid the density is assumed constant, therefore only the terms within the parenthesis remain.

$$\frac{\partial \rho}{\partial t} + \left(\frac{\partial u}{\partial x} + \frac{\partial v}{\partial y} + \frac{\partial w}{\partial z} \right) \rho = 0 \quad (2.1)$$

The momentum equations expressed in the conventional form for x-, y- and z-directions are:

$$\begin{aligned} \frac{\partial(\rho u)}{\partial t} + \nabla(\rho u V) &= -\frac{\partial p}{\partial x} + \frac{\partial \tau_{xx}}{\partial x} + \frac{\partial \tau_{yx}}{\partial y} + \frac{\partial \tau_{zx}}{\partial z} + \rho f_x \\ \frac{\partial(\rho v)}{\partial t} + \nabla(\rho v V) &= -\frac{\partial p}{\partial y} + \frac{\partial \tau_{xy}}{\partial x} + \frac{\partial \tau_{yy}}{\partial y} + \frac{\partial \tau_{zy}}{\partial z} + \rho f_y \end{aligned} \quad (2.2)$$

$$\frac{\partial(\rho w)}{\partial t} + \nabla(\rho w V) = -\frac{\partial p}{\partial z} + \frac{\partial \tau_{xz}}{\partial x} + \frac{\partial \tau_{yz}}{\partial y} + \frac{\partial \tau_{zz}}{\partial z} + \rho f_z$$

where,

τ_{ij} = Stress in the j direction exerted on a plane perpendicular to the i -axis

f_i = i -component of the body force per unit mass

u, v, w are respectively $x, y,$ and z components of velocity vector V

t = time

$\nabla() = i \frac{\partial()}{\partial x} + j \frac{\partial()}{\partial y} + k \frac{\partial()}{\partial z}$ = vector differential operator

i, j, k = unit vectors along the $x, y,$ and z axes, respectively

2.1.2 Turbulence modelling

Numerical simulation of inviscid or laminar flows does not present great difficulties. Turbulent flow simulations on the other hand demand greater effort and understanding. Direct simulation of fully turbulent flow by the time-dependent Navier-Stokes equations, termed DNS (Direct Numerical Simulation), requires extraordinary computing effort and is as yet only possible for some simple flow cases at low Reynolds numbers (Blazek, 2001). Despite this, it is possible to account for turbulence in an approximate manner by the time-averaged process. The time-averaged method deals with the effect of turbulence on the mean flow and therefore considerably reduces computing requirements. The Navier-Stokes equations consist of four equations each with four unknowns. This is known as the turbulence closure problem as there are more unknowns than there are equations. The equations are solved by the introduction of averaged and fluctuating quantities to produce the Reynolds Averaged Navier-Stokes (RANS) equations (Ansys CFX Solver Theory, 2003) these quantities are known as the turbulence models. The most common ones are listed below:

- Zero equation models (Mixing length model)
- Two equation models (k - ϵ , k - ω)
- Reynolds Stress Models (RSM)
- Algebraic Stress Models

There is no single turbulence model which is capable of predicting all kinds of turbulent flows (Blazek, 2001). The zero equation models do not solve additional transport equations and are completely incapable of predicting any turbulence. It computes a global value for the mean velocity and geometric length scale using

an empirical formula. It is a characteristic of turbomachinery to have separation and recirculation especially at off-design conditions, therefore turbulence models that can incorporate these are of fundamental importance. The two equation models, namely the $k-\epsilon$ and $k-\omega$ are less time consuming when compared to more advanced models such as the RSM. The $k-\epsilon$ model has been successfully applied to a wide variety of fluid machinery applications and has shown less demand in computer capabilities. It is well established in turbomachinery applications and also the most widely validated (Versteeg et al, 1995). The $k-\omega$ model is not as widely validated but has shown certain advantages. Its application is particularly well suited to the sub-layer of a boundary layer. Unlike the previous models, the Reynolds Stress Model is not as widely validated reflecting mainly the relatively large computing costs required for a simulation. It is very accurate in the calculation of mean flow properties (Versteeg et al, 1995), but its advantages are not sufficient to outweigh the use of the two equation models.

2.1.3 Frame of references

Turbomachinery have stationary and moving frames of reference, e.g. the volute and impeller domains respectively. In the numerical approach each domain contains an independent mesh (or cell zone), which can be assembled to form a multiple frame of reference simulation. Currently three approaches are available to treat interface problems between the assembled cell zones i.e. moving and non-moving parts; these are:

- Sliding mesh model
- Mixing plane model (Stage interface)
- Frozen rotor interface model

2.1.3.1 Sliding Mesh

The interaction between rotating and stationary components in a turbine is an unsteady periodic process. This information could be obtained by time-averaging the results of an unsteady calculation. The sliding mesh model assumes that the flow field is unsteady. At the zone interface the moving cell 'slides' against the neighbouring cell. Due to the modelling of unsteady effects and the change in pitch this model is the most accurate but on the other hand it is computationally more demanding (Giles, 1988). In rotor-stator calculation this cost is further increased as the unsteady phenomenon have to be captured in

small timesteps. In the commercial field unsteady three-dimensional calculation is still expensive to make it suitable.

2.1.3.2 *Mixing Plane*

The stage interface approach calculates a steady-state solution of the fluid flow for each fluid zone independent of the solution of the neighbouring frame (Denton, 1992 and Dawes, 1992). At the interface, flow field variables are exchanged and the data averaged circumferentially. The averaged data is then passed to the next zone; because the data is averaged the unsteady effects are not considered.

The stage averaging interface is not appropriate in cases where the circumferential variation of the flow is significant relevant to the component pitch (Ansys CFX Tutorial Manual, 2003), this has been found to be the case for this particular PAT application. Numerical simulations with the stage interface showed that the momentum and mass residuals at the volute/impeller interface were quite high, which did not allow for the solution to converge, particularly at off-design conditions. This is due to the high variation in the flow field in the volute and at the volute/impeller interface.

2.1.3.3 *Frozen rotor*

With the frozen rotor model the rotor is fixed at one position and a steady-state solution is calculated (variation in flow characteristics due to pitch rotation of the impeller is not captured). The absolute velocity is maintained between cell zones, in other words the velocities are just switched from the relative to the absolute frame (Galpin, 1995). The solution is therefore dependent on the position of the blade relative to the spiral volute. All unsteady effects and flow variations at different pitch of the rotor are neglected. This is a potential weakness, particularly at off-design conditions. This weakness can be overcome by pitch rotation and averaging the values of interest (Galpin, 1995). However, if too many pitch rotations are required this process becomes extremely time consuming and therefore a better alternative would be to model using a transient interface with larger time-steps as the global parameters are automatically averaged by the code. The frozen-rotor technique model was adopted throughout to model the interfaces between domains in this research.

2.1.4 Near wall treatment

2.1.4.1 Y-Plus

The wall surface can be described as smooth or rough in simulations using turbulence models. Near the wall boundary region the viscous forces are much larger than the inertia forces. The standard turbulence models are not able to predict the flow accurately due to the extremely low Reynolds numbers (Versteeg et al, 1995)

In the wall-function approach, the viscosity affected sublayer region is bridged by employing empirical formulas to provide near-wall boundary conditions for the mean flow and turbulence transport equations. These formulas connect the wall conditions (e.g. the wall-shear-stress) to the dependent variables at the near-wall mesh node which is presumed to lie in the fully-turbulent region of the boundary layer.

The logarithmic relation for the near wall velocity is given by (Launder and Spalding, 1974):

$$u^+ = \frac{1}{k} \ln y^+ + C \quad (2.3)$$

where,

$$y^+ = \frac{\rho \Delta y u_\tau}{\mu} \quad (2.4)$$

and,

$$u_\tau = \left(\frac{\tau_w}{\rho} \right)^{1/2} \quad (2.5)$$

u^+ is the near wall velocity, u_τ is the friction velocity, U_t is the known velocity tangent to the wall at a distance Δy from the wall, y^+ is the dimensionless distance from the wall, τ_w is the wall shear stress k is the von Karman constant and C is a log-layer constant depending on wall roughness.

While in the wall-function formulation, the first point is treated as being outside the edge of the viscous sublayer, the location of the first mesh point is now

virtually moved down through the viscous sublayer as the mesh is refined in the low-Reynolds (*low-Re*) mode. It is to be emphasised, that the physical location of the first mesh point is always at the wall ($y = 0$).

The recommended maximum y^+ value for a typical small scale pump is around 300 although a lot of debate still remains about this issue. All the domains for the current PAT model were under this limit.

2.1.4.2 Rough Walls

In a rough wall simulation the specified roughness height is the equivalent sand grain roughness, but this is not exactly equal to the real roughness height of the surface under consideration. The equivalent sand-grain roughness depends on numerous factors such as the shape, distribution, and other parameters. Schlichting (1968) and White (2005) provide guidance in the selection of the equivalent sand-grain roughness for each particular problem. The wall functions are appropriate for hydraulically smooth surfaces. For rough walls the logarithmic profile still exists but moves closer to the wall, and therefore the equation becomes a modified log-law equation in the wall function equation.

The wall function equations introduced in [section 2.1.4.1](#) are appropriate when the walls can be considered as hydraulically smooth. Roughness effects are accounted for by modifying the expression for u^+ as follows (White, 1979):

$$u^+ = \frac{1}{k} \ln \left(\frac{y^*}{1 + 0.3k^+} \right) + C \quad (2.6)$$

and,

$$k^+ = y_R \frac{\rho}{\mu} u^* \quad (2.7)$$

y_R is the equivalent sand grain roughness, y^* is the scalable wall function and u^* is the velocity scale in the logarithmic region, and the remaining are as defined for Y-Plus equations.

The first element off the wall should not be much thinner than the equivalent sand grain roughness. If this element becomes too thin, then negative values of

u^* can be calculated, this will result in a solver failure. A comparison is made in Appendix C of smooth and rough wall simulation but the results are not conclusive.

2.2 PAT context in CFD Research

The use of CFD in the analysis of pumps operating in turbine mode is a relatively new field of numerical application owing to the fact that this type of machine operation is not commonly employed and this is therefore reflected through the lack of research and published material in this area. An appraisal of the current status of CFD analysis on machine with similar geometries and operation principles of a PAT has been therefore carried out to establish some basis for this research. In this sense the literature was reviewed with the intent of capturing a spectrum of numerical modelling techniques that could be explored within the current problem. The geometries with some similarities include Francis turbines, turbine-pump, centrifugal pumps, pump-turbines, and centrifugal pumps operating as turbines.

It was found that a lot of research has been carried out on Francis turbines with a variety of modelling approaches. Nichtawitz (2005), reviewed the computational approach for pump-turbine modelling and the limitations and advised further investigation of component interaction. Qian (1997) also noted the limitations in the field of numerical techniques and turbulent models. Other interesting research has been in the area of draft-tube and stator-rotor interaction. Sick et al (1996) model a complete Francis turbine using different interface models and identify the advantages and limitations. Some numerical research has also been carried on turbine-pump systems. The use of a turbine as a pump is a more challenging task than the reverse as the defusing flow of a pump may stall and separate more readily. Baines (1998) used the standard Baldwin-Lomax turbulence model, and demonstrated the effectiveness of CFD as a design tool for successfully predicting the performance characteristics of a cryogenic power recovery turbine, operating in both turbine and pump mode. Within the pump numerical research area Blanco (2000) provides information on volute/impeller interface and boundary conditions in a centrifugal pump. Cao (1998), Michaelidis (2001) and Muggli (1997) have also modelled flow within the diffuser region of a pump and recommend boundary settings. The pump model set up can be

compared to PAT modelling because of the geometry similarity and similar component interaction.

Pump-turbines are designed to operate in both pump and turbine modes. Pump as turbine (PAT) are machines that can incorporate definite changes to the geometry so that they can optimally operate as a turbine. Pumps are also used for power recovery at shut-off period and partial flow condition. A number of research has been found on pump-turbine systems. Guedes (2002) assessed interface models on a pump-turbine rotor-stator model operating in pumping mode using commercial CFD codes. These included the frozen-rotor, stage averaging, and sliding mesh models mentioned previously in [section 2.1.3](#). Included in their analysis was also the use of the periodic method for rotor-stator passages later discussed in [section 3.3.1.4](#). Skotak (2003) carried out a runner design analysis for a pump-turbine using CFD. The pump-turbine was analysed in both modes of operation with a single channel passage at the inlet and outlet stators for which he reported success as a design method.

As for numerical research on pumps operating as turbines only a few research material was found. Kirloskar Brothers Limited (2003) compare experimental and CFD data, but mention discrepancies in the results, and that CFD over-predicted the hydraulic losses through individual passages. A single blade passage model with periodicity was used in this case. Tamm (2000) carried out an analysis of a reverse operating pump using CFD tools, but had no experimental data to verify his results. In the setup he included the whole impeller to enable the study of circumferential variation of the flow caused by the spiral casing. His research compared experimental and CFD data in pump mode, however there were some discrepancies in the CFD performance characteristic predictions. Recently White (2005) carried out CFD analysis on a high specific axial-flow pump operating in turbine mode, but he did not have turbine experimental data to compare his results. However he made a comparison with pump CFD and experimental data and also reported some discrepancies in the results.

3 Computational Modelling & Discretization

This chapter describes the modelling and discretization of the 24.5 rpm PAT computational model. It makes an assessment of the various variables and parameters that are better suited to compute a pump as turbine problem to allow confidence in the judgement of internal hydraulics.

3.1 Geometry Description

The actual model is a Kirloskar NW8 24.5 rpm PAT. The test-specimen data is given in [Appendix D](#). The computational geometry consists of three main domains, namely the casing (or volute), the impeller and the draft-tube. The computational geometry representation consists of the hydraulic-volume (or control volume) of the real machine. Shaded area in [Figure 3.1](#).

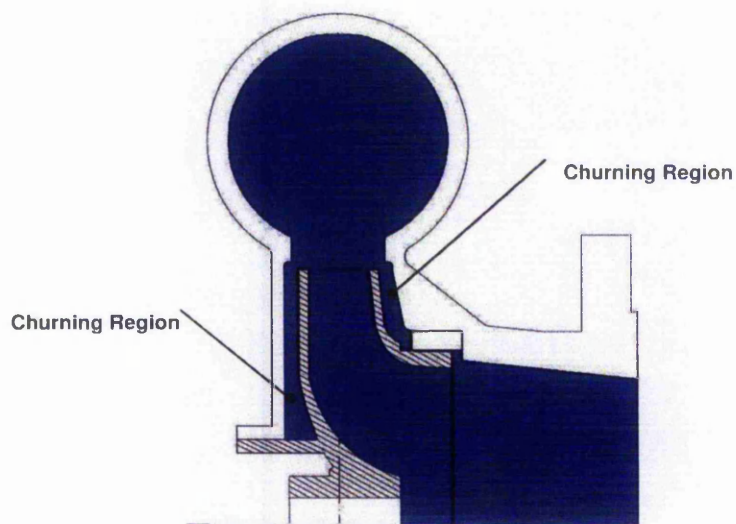


[Figure 3.1](#) Hydraulic region of volute, impeller, and inlet of draft-tube

All the geometries apart from the impeller were created using Pro/E (a generic CAD package) and later exported to a Meshing software. The impeller was developed using BladeGen which is a specific tool for the creation of bladed geometry for turbomachinery.

BladeGen includes specific terminology and tools for the modelling of various types of turbomachinery blades and for defining the framework of grid

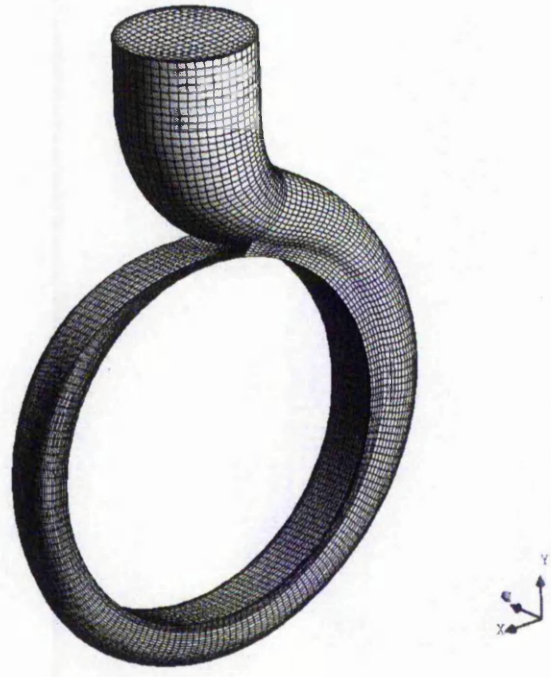
generation. A single blade can be created by defining the profile at different sections between the front-shroud and the back-shroud. The user determines the number of sections required, this normally depends on the complexity of the blade being designed. Each section is independent of the other and allows for alteration of features like the camber, blade angles, thickness and other geometrical details including leading edge and trailing edge rounding. The blade can be repeated in CFX-Build to form the complete impeller.

3.2 Mesh Generation and Discretization

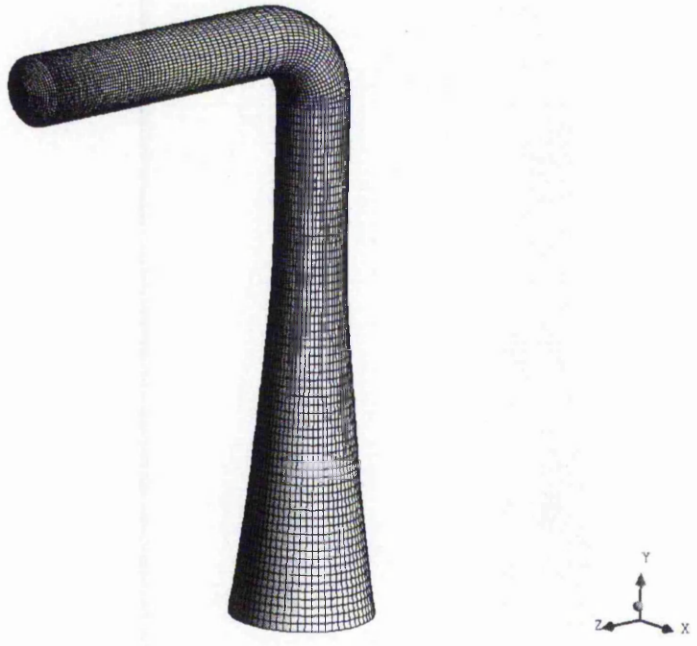
The grid nodes are distributed within the computational domain in terms of x, y, and z coordinates forming a complete three-dimensional matrix of nodes. Each node in the domain is referred to by the index (i, j, k). This node layout is often referred to as structured (or Cartesian) grid. For unstructured grid the nodes are placed in the flow field in an irregular fashion. In any case at each node of the domain, the solver determines the values of all dependent variables.

3.2.1 Mesh topology

The mesh for the stationary domains namely the volute, draft-tube, and churning region were generated using ICEM CFD, whilst the mesh for the Impeller (single-passage) was generated using CFX-TurboGrid. As most grid creation tools ICEM CFD contains an in-built grid generation tool that uses the Finite Volume Method for spatial discretization of the domain to produce the grid. Parameters can be manipulated to produce grids of different types, namely structured and unstructured grid. The grid used by CFX-5 is boundary-fitted. Hexahedral elements have been the choice for the mesh in all of the domains.



(a)



(b)

Figure 3.2 Mesh in the static components (a) Volute (b) Draft tube

TurboGrid is a software designed to create computational meshes for periodic bladed geometry. Blade sections, front-shroud, and back-shroud data, can be

imported and predefined grid topology templates around the blade can be selected to minimize grid set-up time and optimise the mesh for a given application. The Generic Multi-Block Grid template was selected for the 24.5 rpm PAT. This is a template using an O-grid around the blade and an H-grid in the blade passage which is particularly suited for axial and radial blades. Moreover, TurboGrid includes the capability of grid region definition which is useful for boundary condition attachment and solution visualisation in pre- and post-processing stages respectively.

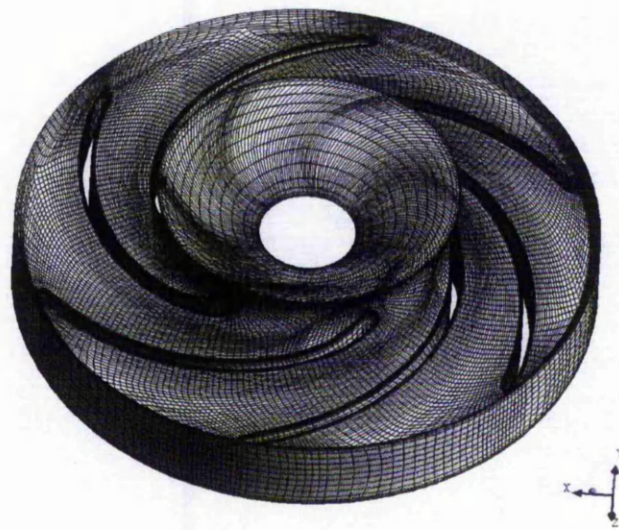


Figure 3.3 Mesh of the blade passages

3.2.2 Mesh Quality

Most grid generation software have an inbuilt tool which allows the user to check or judge the quality of the created grid, this is often termed as a Quality Metrics tool. There are several ways on how to compute the quality of individual elements and how to quantify the overall quality of a mesh. This section only deals with the Quality Metrics employed to analyse the quality of the mesh for this problem, and the terminology associated with the particular packages which were used i.e. ICEM CFD and TurboGrid. The checks performed included those for Determinant, Orthogonality (skew angle), Degeneracy, and Aspect Ratio all of which are explained below.

3.2.2.1 Determinant

The determinant is a parameter that allows checking the deformation of each element in a mesh by computing the Jacobian of each hexahedron. The quality indication may vary in different programs but usually 1 is a perfectly regular mesh element, 0 is a degenerate element in one or more edges, and negative values indicate inverted elements. The value of 0.25 is the minimum recommendation (Ansys ICEM Manual, 2003) and this was achieved in all the domains. Warpage is also similar to Determinant however it measures the computed distortion of a plane, based upon the nodes that compose the surface. A warpage of 0 is flat (preferred) while 90 is degenerate.

3.2.2.2 Orthogonality

Generally the minimum skew angle recommended is 20 degree, however, most solvers cope with even smaller skew angles and recommend a minimum of 15 degree skew angle (Ansys ICEM Manual, 2003). On the volute and draft tube domains all the skew angles were over the 20 degree mark, whilst in the impeller domain 4% of the entire mesh were below the 20 but all elements were over the 15 degree minimum requirement.

3.2.2.3 Degeneracy

An element is said to be degenerate when one edge collapses into a point in a 2D face and when a face collapses into an edge in a 3D element. Some solvers do not accept degenerate elements and it is generally not recommended to have degenerate elements in the domain. Degenerate checks the minimum internal angle for each element - with 0 as degenerate and 90 as perfect. No degenerate elements were present in the current problem.

3.2.2.4 Aspect Ratio

The aspect ratio is the ratio based on the largest and shortest lengths of the elements. Most solvers handle well a maximum aspect ratio of 100:1 and perhaps larger, however this is not recommended as round-off errors can grow when the element aspect ratios exceed this value, and this will also slow convergence. Grid elements with large aspect ratios can lead to numerical diffusion and dispersion problems with the use of single and second order advection schemes. This can be visually identified by the misaligned flow across the grid. In the current model all of the elements were below the maximum limit of 100:1. The largest aspect ratio found was 60:1 and consisted only around 0.25%

of the total mesh. Grid alignment to the flow was also implemented as a precautionary step to avoid numerical problems.

The Quality Metrics explained above are only an indication to assure that the mesh will work in the solver. However, other steps were carried out to assure further quality of the mesh such as refinement of the grid resolution in areas where flow is expected to be more complex and in boundary condition areas, and also attention was paid to the alignment of the grid with regards to the flow direction. The effect of grid alignment and flow direction are discussed further in section 3.3.2.1.

3.3 Boundary conditions

A number of boundary condition options can be specified at any face or surface of the computational domain. Those specified for the current problem are explained below. (It is worth to remember that the upstream region for the pump operating as turbine is the volute and the downstream component is the draft-tube).

3.3.1.1 Inlet Boundary Condition

Two boundary condition combinations at the inlet and outlet were assessed in terms of robustness and correlation with experimental data. The boundary condition combinations included inlet mass-flow and outlet static pressure and inlet total-pressure and outlet mass-flow. The differences of both results were marginal however the overall picture provided by the mass-flow inlet and total-pressure exit agreed better with experimental data and therefore this option was carried throughout. For unsteady simulation these boundary conditions may not be as accurate due to pressure and velocity fluctuations at the boundary. A boundary condition option that might allow for simultaneous unsteady pressure and velocity fluctuations could be total pressure inlet and static pressure outlet, however this combination was not attempted due to the limited computer resources for unsteady type simulation.

For inlet mass-flow specified boundary condition the flow direction was set normal to the inlet face and a constant flow magnitude was assumed along the entire inlet boundary face i.e. a constant value of velocity is set by the code at each nodal location along the boundary face. In reality the inlet velocity value is

not constant along the boundary face due to wall friction and perhaps turbulence in the region, however this is a reasonable approach in the absence of experimental flow profile. Another option is to increase the inlet section to allow for the flow to develop until it reaches this inlet region, but this was not required as the velocity vector visualisation from preliminary simulations indicated that the flow develops quickly within the volute entry portion. Therefore constant velocity at inlet can be used as a reasonable approximation.

CFX allows two ways for specifying the turbulence quantities at the inlet boundary. One way is to specify the turbulence quantities of k and ε , and the second method is to specify the turbulence intensity and length scale from which the k and ε are computed. In the absence of experimental values for the turbulence quantities, the recommendation is to use a value of 0.037 for the turbulence intensity which is sufficient for nominal turbulence through a circular inlet (Ansys CFX Theory Manual, 2003). For cases where there is uncertainty of the turbulence quantities in the inlet region a 5% turbulence intensity is recommended (Ansys CFX Theory Manual, 2003) which corresponds to a viscosity ratio of 10. i.e. ratio of viscosity in a solution to the viscosity of the suspending medium.

In the current research experimental values of k and ε were not available, so these had to be estimated through use of empirical relationships. The turbulence intensity, I at the inlet pipe portion can be estimated by (Lauder et al, 1974):

$$I = 0.16(Re)^{-1/8}$$

Where Re is the Reynolds number. For the current case the Reynolds number was calculated to be around $3,3 \times 10^5$ corresponding to a turbulence intensity of around 3.3% (0.0326). The turbulence length scale, ℓ , is a physical quantity related to the size of the inlet diameter (D) and is given by:

$$\ell = 0.07D$$

The factor of 0.07 is based on the maximum value of the mixing length in fully-developed turbulent pipe flow Naot et al (1993). For the current inlet the length scale for the 100mm diameter is therefore 0.007. The relationship between the turbulent kinetic energy, k , and turbulence intensity, I , is:

$$k = \frac{3}{2} l^2 U^2$$

Where, U is the mean velocity of flow at the inlet. The turbulent kinetic energy for the flow rate of 3.33m/s (26l/s) was calculated to be 0.0176. Finally, with the turbulence length scale known from the above equation, the turbulent dissipation rate, ε can be calculated from (Lauder et al, 1974):

$$\varepsilon = C_{\mu}^{3/4} \frac{k^{3/2}}{\ell}$$

Where C_{μ} is an empirical constant specified in the turbulence model, approximately 0.09 (Lauder et al, 1972). For the current model the turbulent dissipation rate is therefore estimated to be 0.055. A brief sensitivity analysis was also carried out to verify the influence of higher and lower values of turbulence intensity and corresponding k and ε values on flow at the inlet.

For turbulence intensity values higher than 6% (corresponding to $k=0.059$ and $\varepsilon=0.344$), the fully turbulent flow starts early from the inlet plane with increasing magnitude towards the downstream components. This in turn has caused convergence due to high residuals between strong interacting components such as the volute/impeller combination. For turbulence intensity values lower than 1% (corresponding to $k=0.00166$ and $\varepsilon=0.00159$) the onset of turbulent flow occurs further downstream. Lower values of k and ε have not caused convergence problems but have shown that the fully developed flow only takes place further downstream. The turbulence quantities between 3% and 5% generally worked well for the current problem. Lower values were used for low flow rate (lower Reynolds number) whilst higher values for high flow rates (higher Reynolds number).

3.3.1.2 Outlet Boundary Condition

At the outlet boundary face two boundary condition options can be specified namely, an outlet boundary condition and an opening boundary condition. The outlet option can be specified when flow is directed out of the domain, if flow attempts to return into the domain the code places virtual walls to block this condition. The opening option allows free flow traffic both out and into the domain without imposing any constraints on the flow, making it the most robust option out of the two.

For certain operating regions (with the outlet boundary condition specified) it was noticed that the placement of virtual walls was only a temporary situation until the flow was fully developed. In other cases though, the placement of walls persisted, therefore the real geometry was not being modelled. Alternatively the outlet domain can be extended to accommodate the recirculation in the outlet area however, recirculation size and location varies depending on operating conditions and therefore this was not a logical option. For the opening option the turbulence quantities can also be set as there is flow into the domain, and the same guidelines for the inlet boundary condition as explained in [section 2.1.2.1](#), for turbulence quantities is taken.

The placement of virtual walls was noticed at the inlet region with the inlet Total Pressure specified boundary condition and also at the outlet mass-flow specified boundary condition with the outlet option. As a result most of the modelling was carried out with the opening boundary condition option at the outlet and using the inlet mass-flow and outlet static-pressure combination.

It is important to note, that the specified mass-flow, total-pressure, and rotational speed are tied to the experimental data, whilst the remaining parameters are computed.

3.3.1.3 Wall Boundary Condition

A no-slip or a free slip condition can be specified at the wall boundary. For the no-slip wall condition the velocity of the fluid at the wall is set to zero in the mass conservation equation and set equal to the wall velocity for the momentum conservation equations. For the free-slip condition the velocity normal to the wall and the wall shear stress are both set to zero therefore the velocity component parallel and near to the wall is not retarded due to friction effects of the wall and therefore has a finite value. The no-slip boundary conditions were imposed over the volute casing, draft-tube, and impeller blades and walls. The effects of roughness were investigated and are given in [Appendix C](#). Smooth wall was used with the no-slip setting unless if specified otherwise.

In a multiple frame of reference problem the domains can be either stationary, rotating, or in a translation motion. In this context the walls of the casing volute and the draft-tube are in the stationary frame of reference whilst the impeller walls including front-shroud, back-shroud, and blade walls are in the rotating

frame of reference. For the stationary domains all the walls are stationary in the absolute frame of reference, whilst for the rotating domains all the walls are stationary in the relative frame of reference.

3.3.1.4 Periodic Boundary Condition

A periodic boundary condition can be used to model an entire impeller by using only a single blade passage under the assumption that the flow field repeats itself in all blade passages – *rotational periodicity*. This method significantly reduces the mesh by excluding the remaining blade passages, thus saving on computer resources. Numerical simulations of a single-blade passage were compared against those of a complete impeller for the PAT model. The results showed that the flow representation within each blade passage is not axi-symmetric, due to the unequal pressure and velocity distribution at the volute/impeller interface.

Although convergence is easily achieved for a single-blade passage it was noticed that the flow representation within the volute is not realistic, as it is forced to accommodate the periodicity within the blade passages. It was found however, that at near BEP the performance characteristic curves were similar to that of an entire impeller simulation. At BEP there is good matching between volute and impeller flow angles, and therefore more even pressure distribution at the volute/impeller interface. Further discussion on single-blade simulation is given in [section 6.1.1.1](#).

3.3.2 Solver Parameters

3.3.2.1 Advection Scheme

Various options are available in CFX-5 for the setting of advection scheme. These include the Upwind Differencing Scheme (UDS) whereby the advection terms are first order accurate, the High Resolution (HR) with second order accurate advection terms, and Specified Blend of the advection scheme where a numerical value can be given by the user. For complex flow the UDS is a weak choice as diffusion problems may arise depending on the type, arrangement, and quality of the grid.

UDS is the most robust setting but it suffers from Numerical Diffusion and therefore is not suitable for final results. In a structured grid it is usually effective when the flow direction is normal to the faces of each element but in the case

where flow is not normal to the faces of the elements, such as in re-circulating regions, the flow will move from one element to adjacent elements downstream and will create a smeared out pattern of flow. The effect varies according to the alignment of the mesh with the flow direction. It is relatively straightforward to achieve highly accurate solutions to simple flow problems. However, for situations in which the flow is predominantly not aligned with the mesh, numerical diffusion effects limit the accuracy of the solution. In the current problem the UDS setting was used in cases where convergence was difficult to obtain at initial stages of the solving process, and then later switched to a specified blend and second order differentiation scheme.

HR was used throughout for final results as the flow in the turbine was three-dimensional. Visual comparison of the draft-tube swirl was made for both HR and UDS and it was noticed that with the UDS setting the swirl is not carried out through to the outlet of the draft-tube. With the HR setting the swirl was realistic as carried out throughout the domain. In summary, the UDS can be used for initial running of the problem but for fully developed flow and to capture three-dimensional characteristics accurately the HR setting should be used.

3.3.2.2 Timestep selection

The selected timestep is largely dependent on the length scale of the problem. It is generally recommended (CFX Theory Manual, 2003) to use the time step as a fraction of the representative time scale of the problem, which is defined as the velocity scale divided by the length scale of the problem. The velocity scale itself is defined as the root mean square (RMS) of the velocity at each node defined by the initial guess. The length scale is defined as the cube root of the volume open to fluid flow. However the length scale of the problem varies depending on the domain volume and operation nature of the particular component, and therefore this recommendation is not applied throughout an assembly but rather to individual domains. It was found that by using this recommendation and using one timestep value for the whole assembly that convergence was quite rapid at the volute and impeller domains. However, the residuals in the draft-tube took longer to converge. The convergence was achieved at around 200 iterations for the volute and impeller domains, and around 1000 iteration or more were necessary for the draft-tube domain. This means that the suggested timestep values were appropriate for the volute and impeller domains, but too small for the draft-tube domain.

Different timesteps were therefore used within each domain. The volute timestep was based on the length scale and dynamics of each domain. The impeller timestep for instance was based on its rotation cycle.

3.3.2.3 Grid Convergence (Verification)

In order for CFD results to have credibility grid convergence analysis is necessary, in this way the acceptable levels of errors associated with the CFD simulations can be estimated. This is particularly relevant to the current work since the computer resources are limited and hence the grid size is a limiting factor. Generally the errors in CFD consist of modelling errors, computer round-off errors, iterative errors, and Discretization errors.

Modelling errors are those due to uncertainty or deliberate simplifications in the creation of the model. The uncertainty is associated with lack of knowledge in the physical representation of the problem, for instance boundary conditions, surface roughness, and other, whilst deliberate simplifications will consist on geometry alteration such as removal of a specific geometrical feature of the model which is deemed to not have much effect on the overall flow behaviour. Modelling errors are usually difficult to estimate but are on the other hand small. Computer round-off errors arise from the representation of floating point numbers and the accuracy at which they are stored. These however are not considered significant when compared with other errors. Iterative errors are based on the behaviour of the residuals as the solution progresses and a problem is said to be converging as these residuals decrease.

Discretization errors are introduced when the approximated algebraic expressions of the governing flow equations are represented across the boundaries of each control volume of the discrete spatial domain (grid). It is the difference between the exact analytical solution of the partial differential equations and the exact (round-off-free) solution of the corresponding difference equation (Anderson, 1995). As the grid points spacing tend to zero the numerical method will approach the continuum representation of the equations, as a consequence so will the solution, making the solution independent of the number of grid points i.e. *grid independent solution*. However with limited resources achieving a grid independent solution may be difficult due to the extremely fine grid requirements. An alternative is to use a coarser grid and to estimate the discretization errors involved.

Methods for quantifying discretization errors are still a matter of discussion as CFD is yet an emerging tool therefore the existing methods such as the Richardson's Extrapolation and GGI (Roache, 1994) methods were used as a guide rather than a standard. Generally the most commonly used method for judging the spatial and temporal convergence in CFD is that by Roache (1994) using the Grid Convergence Index (GCI). It is based on the use of Richardson's extrapolation. These methods are based on the principle that a solution yields some solution functionals such as pressure recovery or lift which converge after a number of iterations.

Richardson's Extrapolation applies the concept of continuum value which is achieved at zero grid spacing (i.e. high-order discretization) from a series of lower order discrete values (coarser grid sizes). A simulation will yield a solution (f) expressed by a series:

$$f = f_{h=0} + \sum_{i=1}^p g_i h^{i-1} \quad (3.1)$$

where p is the order of discretization. If the solution f is computed on two grids with spacing h_1 and h_2 , then equation 3.1 can be written in the following form:

$$f_{h=0} \cong f_1 + \frac{f_1 - f_2}{r^p - 1} \quad (3.2)$$

Where r is the grid refinement ratio h_1/h_2 , and p is the order of discretization

The actual fractional error A_1 is given as:

$$A_1 = \frac{f_1 - f_{h=0}}{f_{h=0}} \quad (3.3)$$

The estimated fractional error E_1 for f_1 is defined as

$$E_1 = \frac{\varepsilon}{r^p - 1} \quad (3.4)$$

Where ε_{ab} is the relative error defined as:

$$\varepsilon_{ab} = \frac{f_a - f_b}{f_b} \quad (3.5)$$

ε is not used as an error estimator as it does not take into account the grid refinement ratio r or the order of discretization p .

Grid Convergence Index (GCI) was suggested by Roache (1994) to provide uniform reporting of the discretization errors arising from different grid refinement. This provides an error band to establish how far the computed value is away from the value of the asymptotic numerical value. GCI for the fine grid is given as:

$$GCI_1 = \frac{F_s |\varepsilon|}{(r^p - 1)} \quad (3.6)$$

and for the coarse grid it is given as:

$$GCI_2 = \frac{F_s |\varepsilon| r^p}{(r^p - 1)} \quad (3.7)$$

Where F_s is the factor of safety.

For comparisons of two grids the factor of safety $F_s=3$ is recommended. This value is generally recommended for reporting purposes and is quite conservative of the actual errors Roache (1994). Moreover, a higher factor of safety is necessary because the number of grid compared is less. A less conservative, lower limit of the factor of safety is suggested for comparisons of three grids with value of $F_s=1.25$.

The process is only valid if each of the grid levels is within the asymptotic range of convergence. This is checked from two GCI values computed over three grids by using the following expression:

$$GCI_{23} = r^p GCI_{12} \quad (3.8)$$

where r , the grid refinement ratio is given by:

$$r_{ab} = \sqrt[3]{\frac{N_a}{N_b}} \quad (3.9)$$

3.3.2.4 Error Estimation

The errors have been estimated using the Richardson's extrapolation only. [Table 3.1](#) summarises the three different grid sizes and the corresponding head rise used to estimate the errors. The actual setup involved the simulation of all six blade passages.

	Number of Nodes (1 Passage)	Head Rise (m)
1	907392 (150000)	14.619
2	602910 (100000)	14.604
3	300456 (50000)	14.528

[Table 3.1](#) Effect of grid size on head rise

Calculating the GCI, using a safety factor of 3 gives for the fine grid:

$$GCI_{fine} = \frac{F_s |\varepsilon|}{(r^p - 1)} = 0.015691$$

and for the coarse grid the value obtained is:

$$GCI_{coarse} = \frac{F_s |\varepsilon| r^p}{(r^p - 1)} = 0.035792$$

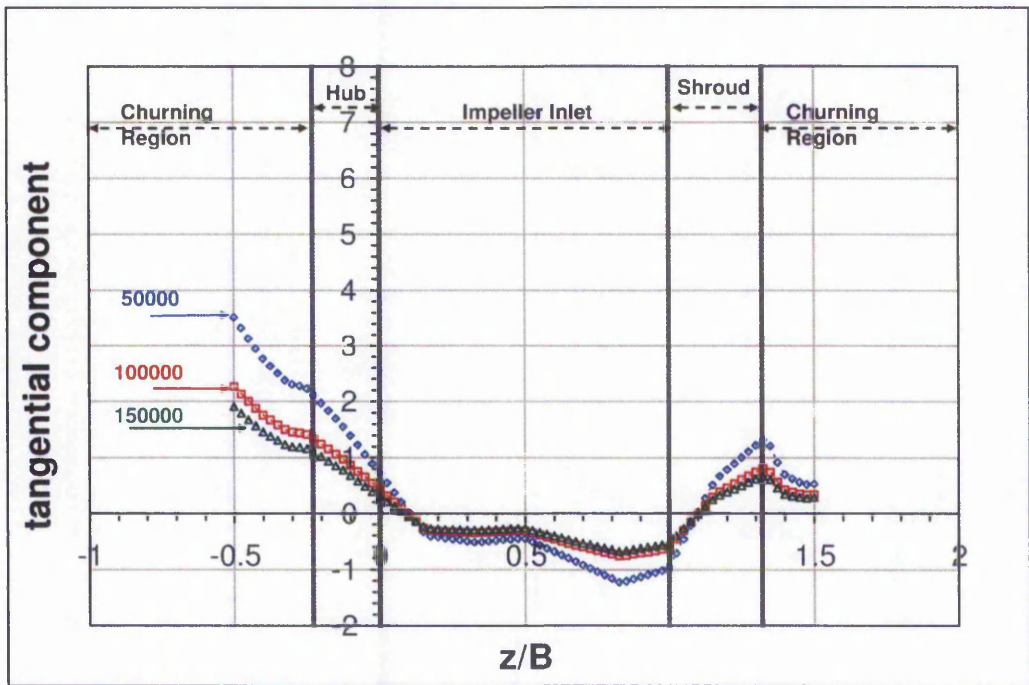
[Table 3.2](#) summarises the GCI for the intermediate grid checks. The GCI results show that the grids are within acceptable limits. The GCI values are quite conservative as seen from the large margins obtained.

Subscript	r	ε	GCI
12	1.146	0.00103	0.009825
13	1.446	0.00622	0.017118
23	1.261	0.00523	0.026456

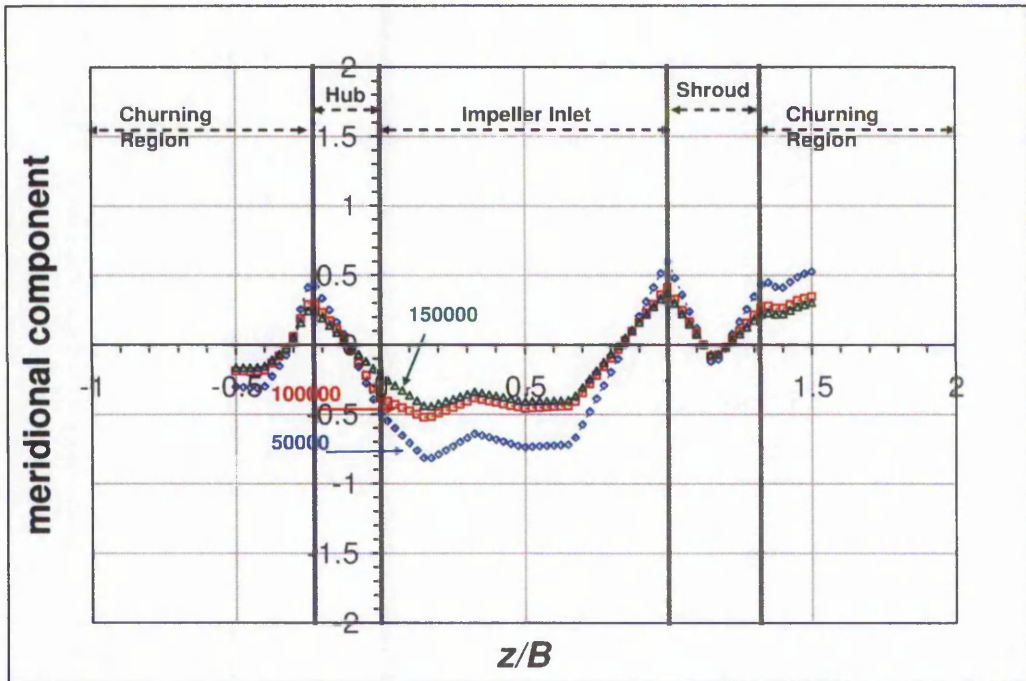
[Table 3.2](#) Grid check

The fine grid represented a high computational effort for the current resources and therefore the medium option was used. A $\pm 2\%$ maximum change on the Net Head parameter between the fine (independent) grid and the medium grid was deemed acceptable for the current application. The medium grid produced less than $\pm 1\%$ change on the net head parameter which is well within the defined limit.

Figure 3.4 show the normalised tangential and meridional components of velocity at the leading edge of the impeller inlet. The velocities are plotted in the spanwise direction from front-shroud to back-shroud. It is clear from the graphs that the coarser grid (50000 nodes) has a substantial discrepancy when compared to the medium and fine grids. The discrepancy between the medium and fine grids is only marginal and mostly noticeable near the wall surfaces. Further refinement of the grid would not produce significant differences between the predicted values.



(a)



(b)

Figure 3.4 Normalised velocity component along the leading edge span (a) Tangential component (b) Meridional component

3.3.2.5 Turbulence Modelling

A brief assessment between the $k-\epsilon$ and $k-\omega$ was carried out to enable the selection of the turbulence model for the current modelling. These models are already well established for turbomachinery problems. Other turbulence models such as the Reynold-stress models were not considered due to the high computer resources required.

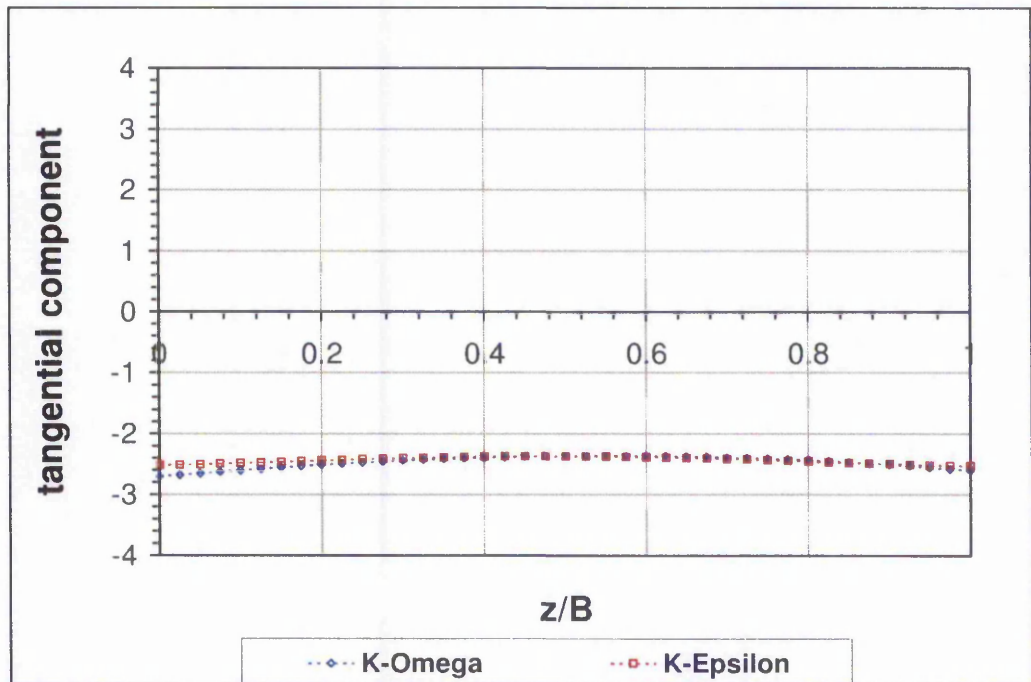
There are limitations to both the $k-\epsilon$ and $k-\omega$ turbulence models. The standard turbulence models based on the ϵ -equation predict the onset of separation too late and under predict the amount of separation later on and have poor performance in a variety of important cases such as some unconfined flows, flows with large extra strains such as curved boundary layers, swirling flows, rotating flows and fully developed flows in non-circular ducts (Versteeg et al, 1995)

The $k-\omega$ turbulence model allows for a more accurate prediction of flow separation from a smooth surface (Menter,1994). Some advantages included near wall treatment for the low Reynolds number computations. The equations

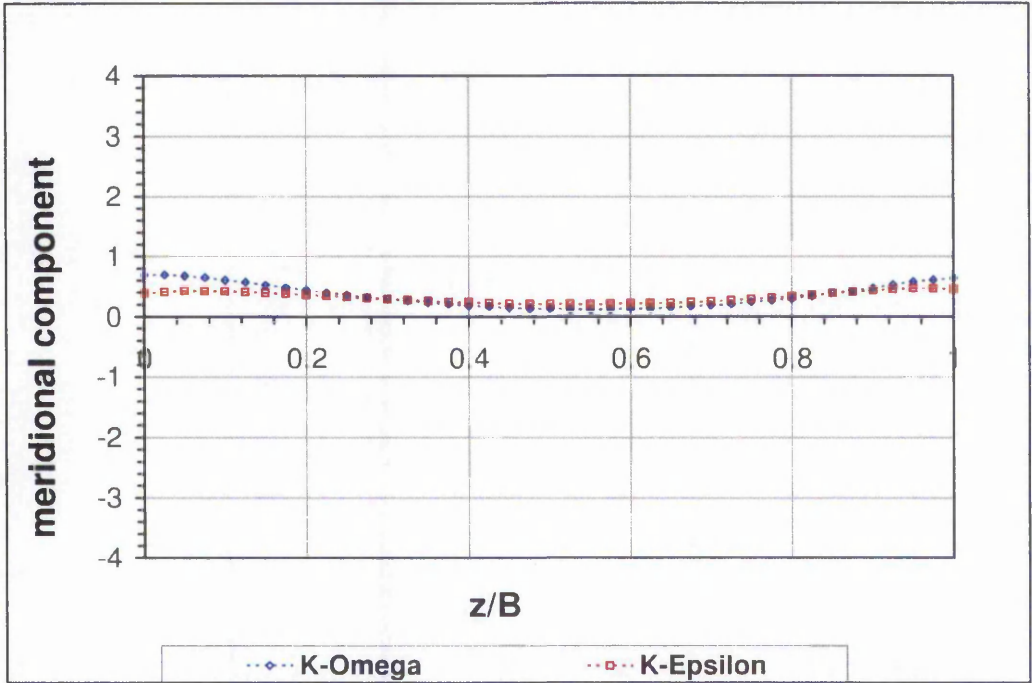
do not involve complex non-linear damping functions required for the $k-\epsilon$ model and therefore is more accurate.

Figure 3.5 compares the normalised tangential and meridional components of velocity at the leading edge of the impeller in a PAT at a normalised spanwise direction from front-shroud to back-shroud and shows the differences between both models. The set of data shows that the velocity components throughout the span of the blade agree for both turbulence models.

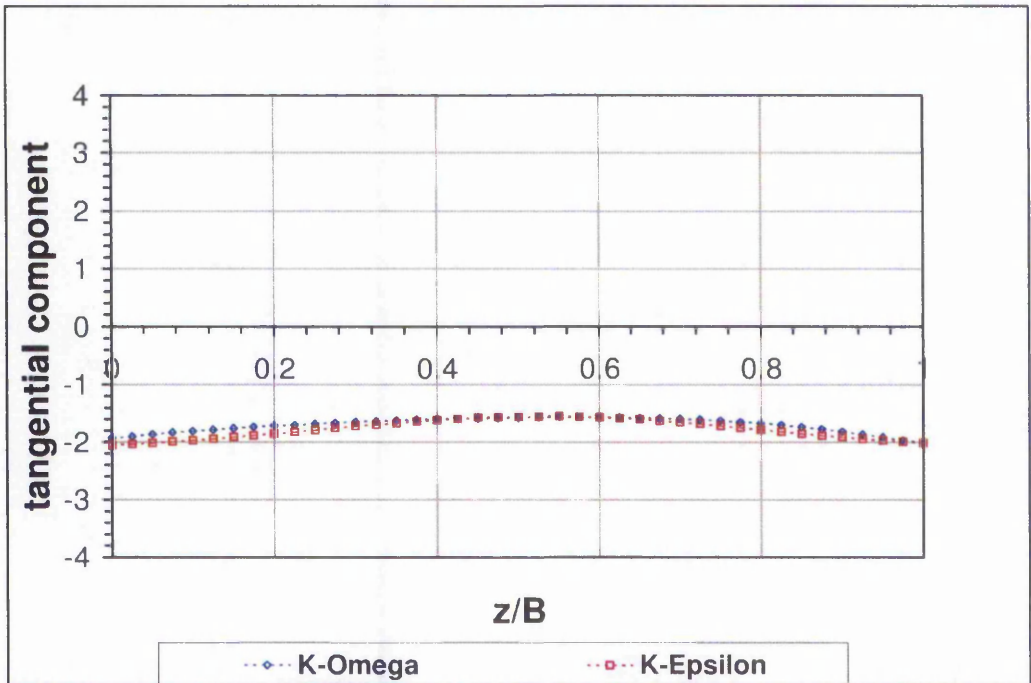
However, the $k-\epsilon$ model over-predicts and under-predicts the axial velocity components near the outlet and inlet boundaries respectively. The $k-\omega$ model however imposes limitation on the size of grid that can be used at the wall boundary condition. This is a limitation since the current geometry model is quite complex. For flexibility the $k-\epsilon$ model has been used throughout. The relative merits of each turbulence model cannot be attributed as experimental data was not available. But the observations agree with the literature.



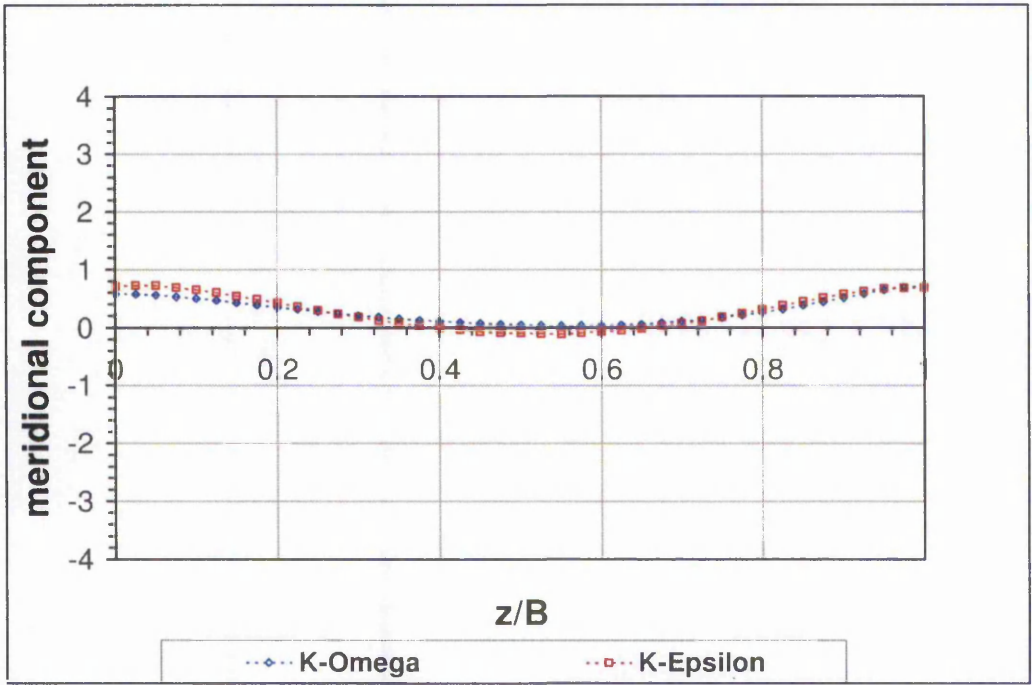
(a_i)



(a_{ii})



(b)



(b_{ii})

Figure 3.5 Velocity components (a) $Q=22l/s$ (b) $Q=26l/s$

4 Theory & Methodology

This chapter describes the method of investigation employed in the current research. It builds on the aims and objectives and research base set out in chapter 1 (section 1.2.1). It starts by defining the Hydraulic Loss (HL) method which describes six flow zones within the entire computational domain that are of interest. The second section deals with different methods of computational representation of the volute/impeller geometrical region. The third section deals with the geometrical modification techniques for optimisation of PAT internal hydraulics. The final section describes the key correlation parameters for CFD and experiment. Throughout this chapter the theoretical basis to support the analysis of the flow in each hydraulic flow zone is given along with the flow description.

4.1 Hydraulic Parameters

In experimental practice or model testing useful information can be obtained which characterises a hydraulic machine. For a turbine (or in this case a PAT) the input variables include the total head (H) across the PAT and the discharge (Q). The output variable comprises the shaft rotation (N) and output torque (T) or the resulting power (P). The torque and power are a function related to each other and can therefore be considered associatively. In a computational setting the input variables are the discharge and impeller rotation (N). The total head across the turbine and torque are a result of the computed solution based on the given input. The discharge and rotational speed are usually termed control variables since they can be manipulated by the user in both Experimental and CFD cases. The definitions for the individual parameters are given briefly below:

- 1) Total head (gH) is defined by the Bernoulli energy components which include static pressures, mean velocity head and the vertical elevations between the respective measurement planes. This parameter is evaluated between the inlet measurement plane and the exit measurement plane.
- 2) Discharge (Q) is the volumetric mass flow through the control volume of the turbine and is also composed of some leakage through clearances.
- 3) Power (P) is calculated from the hydraulic torque which is computed from the energy transferred from the fluid to the impeller blades. There are

differences in experimental torque and CFD torque. Experimental power on the other hand is measured directly measured from the shaft and is associated to power losses mechanisms.

- 4) Rotational speed (ω), this is the rotational speed of the impeller at which energy transfer takes place.

Buckingham π theorem (Buckingham, 1914) suggests five dimensionless groups for turbines which comprise the head number, discharge number, power number, and a fourth and fifth term which is a form of the Reynolds number representing the relative influence of viscous effects, and the relative roughness of the pump/turbine respectively. The last two parameters can be ignored since the flow in a turbine involves high Reynolds number and the irregular shape of the pump volute is usually the predominant factor. Thus the four significant input and output parameters, namely Total head, Discharge, Power, and Efficiency can be interpreted using the following relationships.

$$\text{Head number, } \psi = \frac{gH}{\omega^2 D^2} \quad (4.1)$$

$$\text{Discharge number, } \phi = \frac{Q}{\omega D^3} \quad (4.2)$$

$$\text{Power number, } P = \frac{P}{\rho \omega^3 D^5} \quad (4.3)$$

$$\text{Hydraulic efficiency, } \eta = \frac{\rho g Q H}{P} \quad (4.4)$$

where D , is the impeller diameter and ρ , the fluid density.

The geometry of a pump runner or turbine impeller can be identified from its specific speed ω_s , which allows for its preliminary matching to a fluid system. For preliminary design and pump or turbine selection, it can be used as a performance indicator. The specific speed of a pump is derived from the dimensionless groups where for a pump it is a combination of flow coefficient and the head coefficient in the following manner.

$$[\omega_s]_{\text{pump}} = \frac{(\text{flow coefficient})^2}{(\text{head coefficient})^3} = \frac{\left(\frac{Q}{\omega D^3}\right)^2}{\left(\frac{gH}{\omega^2 D^2}\right)^3} \quad (4.5)$$

$$[\omega_s]_{\text{pump}} = \omega \frac{\sqrt{Q}}{(gH)^{3/4}} \quad (4.6)$$

For a turbine, the duty is usually expressed in terms of power generation at a given speed when operating under a given head. Combining the power coefficient and the head coefficient gives,

$$[\omega_s]_{\text{pump}} = \frac{(\text{Power coefficient})^2}{(\text{head coefficient})^5} = \frac{\left(\frac{P}{\rho\omega^3 D^5}\right)^2}{\left(\frac{gH}{\omega^2 D^2}\right)^5} \quad (4.7)$$

$$[\omega_s]_{\text{turbine}} = \omega \frac{\sqrt{Q/\rho}}{(gH)^{5/4}} \quad (4.8)$$

which, since $\rho = \eta \ell g H Q$ gives alternatively

$$[\omega_s]_{\text{turbine}} = \omega \frac{\sqrt{\eta g H Q}}{(gH)^{5/4}} = \omega \frac{\sqrt{\eta Q}}{(gH)^{5/4}} \quad (4.9)$$

It can be seen that in both cases that the specific speed is dependent on the total head (gH)

4.2 Hydraulic Loss Methodology - Flow Zones

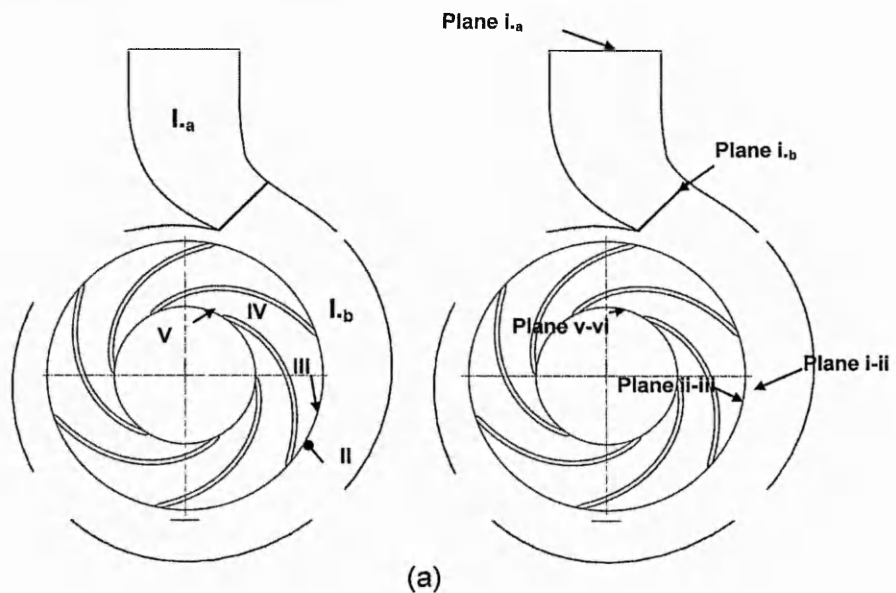
The methodology is developed to study the physical significance of the internal geometrical modification and geometrical complexity of the model with respect to hydraulic loss distribution in various regions of the PAT control volume. The methodology can also help in the following topics:

- reduce modelling uncertainties
- demonstrate the incompatibilities with methods of modelling , and
- identify features in a pump geometry that make it a good PAT.

The different regions (of the hydraulic volume) of a PAT can be divided into different zones as demonstrated in [Figure 4.1](#). Nestmann (2003) first introduced this concept on an experimental application and demonstrated the “flow zone” approach in the optimisation study of medium and low specific speed pumps as turbines. A similar zonal approach concept but in a different application was also

introduced by Fleberger (1994) whereby the flow field of a turbulent plane cascade flow is divided into regions. The application of the flow zone approach in experimental analysis has inherent limitations since it is difficult to obtain measurements of internal parameters. In a computational set up however the potential of this concept can be further explored, as calculated pressure, velocity, and other parameters can be obtained easily and at any region or location within the entire computational domain. This concept is extended by integrating a loss analyses approach termed the "Hydraulic Loss Method" (HL method) which is particularly useful in the computational analysis of PATs. The methodology may be extended to other similar turbomachinery applications. The HL method consists on predicting the losses in each subdivided zone. The division in number of zones is dependent on the study in question and the regions of the hydraulic domain that are of particular interest.

In the current analysis the flow of a PAT is divided into six major zones, as shown in [Figure 4.1](#). This may also include other sub-zones such as the churning region, and the outside front-shroud and back-shroud walls. The modelling of churning will also be described later in [section 4.3.1](#).



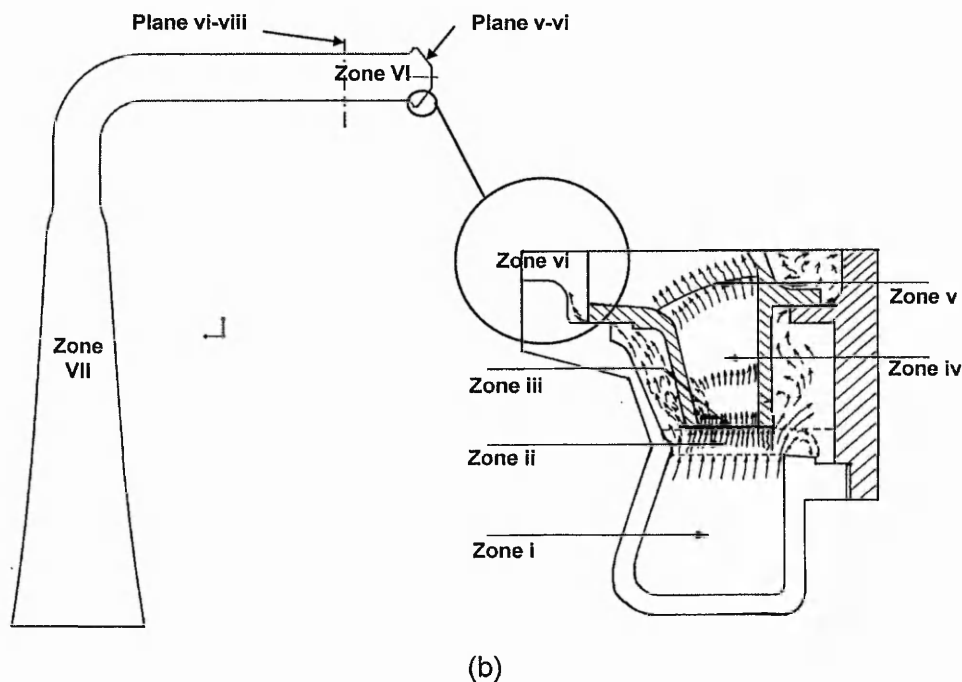


Figure 4.1 Flow zone (a) Volute cross-section (b) Draft tube

4.2.1 Flow Zone-*i*

Flow zone-*i* refers to the whole volute, beginning from the inlet-measuring plane and extending to the volute base circle circumferential plane depending on the particular design of the pump volute. However instead of placement at the cut-water the circumferential plane can be placed at any user location, preferably where there is some geometrical influence on the flow behaviour such as sudden change in section. (Sudden changes in geometry can influence the loss behaviour within a region and therefore it may be advantageous to isolate this feature into the next zone downstream). The design features within this region can vary from pump to pump but in most cases this circumferential plane can be made to coincide with the tongue edge of the volute. Essentially zone-*i* consists of the portion from the inlet-measuring plane to the throat (or tongue) plane plus the entirety of the spiral control volume.

4.2.1.1 Flow Description

Zone-*i*_a, consist of the pipe section of the volute, from the inlet measuring plane up to the throat cross-sectional area. In turbine mode of operation the normal velocity component, v_{ib} of flow leaving the throat section area A_t (A_{ib} for convention) at a given discharge, Q has the following relationship:

$$v_{ib} = \frac{Q}{A_{ib}} \quad (4.10)$$

Zone- i_b , comprises of the semi-enclosed region of the volute. The flow becomes more complex and of a forced vortex nature beyond the throat section. The flow traverses in the radial direction due to the radial opening and gets a meridional velocity component (v_m) and the spiral path creates a tangential (v_u) velocity component. The tangential component is higher in magnitude than the meridional component throughout the spiral section because of the gradual decrease in cross-sectional area. At the throat section the mean tangential component can be assumed to be equal to the throat velocity component (i.e. $v_t = v_u$). Thus, the meridional component of velocity can be estimated as follows.

$$v_m = v_{ib} \tan \alpha_v \quad (4.11)$$

The angle α_v is a property of the volute design. The velocity distribution in the volute throat (c_t) is given by making it proportional to $1/r$ and the resulting shape of the volute is a logarithmic spiral with this constant angle.

4.2.1.2 Hydraulic Losses in Flow Zone- i

Zone- i comprises of two sub regions, therefore the sum of losses is given as follows:

$$H_{L,i} = H_{L,i,a} + H_{L,i,b} \quad (4.12)$$

where $H_{L,i,a}$ is the losses within zone- i_a and $H_{L,i,b}$ is the losses within zone- i_b .

The flow in zone- i_a can be considered similar to that of a pipe, with similar boundary layer formation and energy loss mechanisms. In zone- i_b the flow becomes more complex in nature because of the semi-open section. The friction loss h_f and dynamic loss h_d in flow zone- i can be given as follows (Idel'cick, 1986):

$$h_f = \lambda \frac{v^2}{2g} \left(\frac{1}{D_h} \right) \quad (4.13)$$

and,

$$h_d = \xi \frac{v^2}{2g} \quad (4.14)$$

Where, λ and ξ are the friction and dynamic coefficients. Where D_h is the hydraulic diameter and v is the fluid velocity.

4.2.2 Flow zone-ii

Flow zone-ii starts at the base circle plane and extends to the impeller inlet plane (in turbine mode). It also consists of sub-zones (zone-ii_b and zone-ii_c) which model the churning region. The standard approach in CFD modelling does not model these sub-zones.

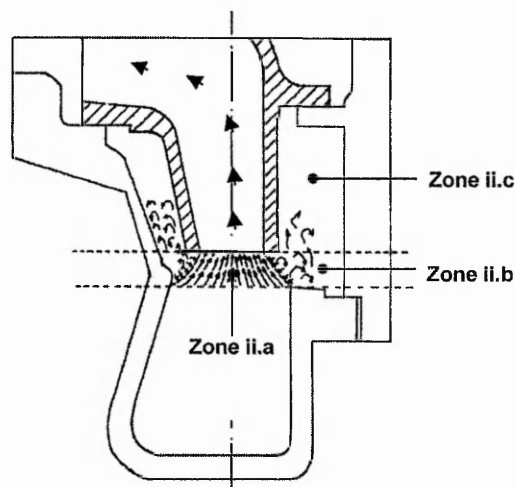


Figure 4.2 Flow zone-ii and sub-zones

4.2.2.1 Flow description

Flow zone-ii is the region in the volute geometry enclosed by the virtual radial plane at the cut-water and impeller inlet plane, i.e. the radial clearance region between impeller and volute, and also the churning region. It is divided into three sub-zones as shown in Figure 4.3. The flow in this zone is highly complex because of the fluid contact with the stationary and rotating walls and also because of the radial and axial clearances between the components

Zone-ii_a: - This region concerns the readjustment of flow prior to leaving the stationary volute domain and entering the impeller rotating domain. It also deals

with the changes in width area from the volute mouth to the impeller inlet. The same mass-flow has to enter a smaller area. The flow in this zone is crucial for the optimum operation of the impeller and is affected by all the surrounding zones. Due to the semi-open section the meridional component v_m increases. When the flow leaves the volute it is exposed to two openings namely, the impeller inlet section and the clearance openings. With losses in this region the total energy of the fluid decreases. Therefore the energy term becomes $(V_{u,ii}^2 / g)_{ii} < (V_{u,i}^2 / g)_i$ and causes the reduction of tangential velocity. The flow components arising in this zone prior to entering zone-*iii*, are shown in Figure 4.3.

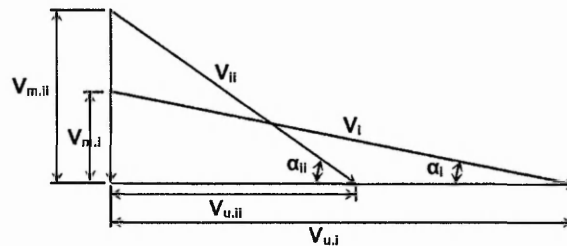


Figure 4.3 Velocity diagram for flow zone-*ii_a*

Zone-*ii_b*: - A pump is not designed to operate as a turbine and some of the geometrical features that distinguish a pump from a turbine include the distinctive differences between widths of the volute mouth and impeller inlet and also the sizeable radial and axial clearances. The width difference permits the front-shroud and back-shroud thicknesses to be in the flow pathway and thus influencing the flow into the impeller.

Zone-*ii_c*: - The rotation of the impeller causes a churning motion of the fluid (eddy formation) in this region as the fluid is essentially trapped by the seals. Only a minute amount of the fluid is lost due to leakage, through the clearance between wear rings and impeller eye.

The sub zones-*ii_b* and zone-*ii_c* are of particular interest in CFD modelling and are dealt with in greater details in section 4.3.1. Generally the front-shroud and back-shroud thicknesses and the churning regions are not fully or accurately modelled in a computational set up as these make the geometrical model and mesh creation more complex.

4.2.2.2 Hydraulic Losses – Flow zone-ii

The total loss in zone-ii is given by:

$$HL_{ii} = H_{Li.a} + (H_{Li.b} + H_{Li.c}) \quad (4.15)$$

The loss mechanisms in zone-ii can include shock losses, possibly at the front-shroud and back-shroud thicknesses, separation, surface friction and other secondary flow effects.

4.2.3 Zones-iii.iv.v

Zones-iii.iv.v refer to the whole hydraulic volume of the impeller. Zone-iii refers to the impeller inlet (in turbine mode) and zone-v refers to the exit plane. Zone-iv consists of blade passage hydraulic volume.

Zone-iii is at the interface of the impeller inlet. This zone refers essentially to the circumferential plane at the tip or leading edge of the blade and can be slightly extended either into zone-ii or into the impeller zone-iv. This will depend on what features are of particular interest. Usually extension into zone-iv will be related to geometrical modification that are carried out at the flow entry region of the impeller and can allow for some simple geometrical alterations to be studied. Zone-iii can be entirely in the rotating frame or part in the rotating frame and part in the stationary frame of reference.

Zone-iv refers to the hydraulic region of the impeller passages. This zone-is entirely in the rotating frame of reference. The energy transferred to the blades takes place within zone-iv. Isolating this region is useful to understand the effectiveness of the impeller design in maximising the flow. Moreover, studying the blade profile also allows an understanding of what features make a good impeller for PAT applications.

Zone-v is at the interface of the impeller exit with the draft-tube. This zone refers to the exit plane of the impeller, and in a computational set up it can be considered as a plane or volume with one grid spacing. Isolation of this zone can allow for a better understanding of the features at the impeller exit that can affect the behaviour of the flow within the draft-tube.

4.2.3.1 Flow description & Energy Transfer in Zones-iii.iv.v

The efficient operation of a turbine is dependent on the optimum transfer of energy from the total head of the fluid to the rotating impeller, and is explained by the Euler head, which is commonly referred to as the net rotational momentum of the impeller. The Euler head gH_{Eu} is described for an infinite blade arrangement however in reality for a finite number of blades the value is a function of the slip $gH_{Eu.slip}$. This value is smaller than the Euler Head gH_{Eu} . The net rotational momentum across the impeller is given by:

$$gH_{Eu} = U_{iii} V_{u,iii} - U_v V_{u,v} \quad (4.16)$$

The energy per unit mass added to the flow by the impeller $U_{iii}V_{u,iii}$ slightly exceeds the energy gH delivered at the diffuser branch (zone-ii.a) owing to irreversibilities in the volute represented by an efficiency η_{ip} (Ventrone, 2000).

$$\eta_{ip} = \frac{gH_E}{U_{iii} V_{u,iii}} \quad (4.17)$$

The efficiency power is also a function of the Euler head gH_{Eu} as given below:

$$\eta_{hyd} = \frac{P_{hyd.shaft}}{\rho Q(gH_E)} \quad (4.18)$$

where, ρ is the fluid density, Q the mass flow.

From the equations above it can be seen that both the total head and output power respectively are affected by the change of the net rotational momentum ($gH_{Eu.slip}$). Relatively if the net rotational momentum increases or decreases then the total head and output power will also increase or decrease accordingly. The power however is only sensitive to the losses within the impeller hydraulic volume and will not be affected by the losses in the other zones. A decrease in the hydraulic losses in zone-iii-iv-v results in a rise in the output power.

The parameter gH_{Eu} is affected by any change in losses occurring in any zone of the PAT domain. Two important observations can be drawn with respect to the losses of the stationary zones and rotating zones.

- 1) As previously mentioned a change in power means that there has been a change in the losses within the rotating hydraulic volume only (i.e. impeller and corresponding hydraulic volume/surfaces).
- 2) Secondly, unchanged power and change in total head means that there is a change in the losses within one or all of the stationary hydraulic zones.

The impeller converts the energy from the available head into mechanical power through the shaft. A good impeller and blade design of a machine is essential in order to make optimum use of this energy, although it also largely depends on the good design of the interfacing components. The Euler's (Head) equation was originally used to analyse the performance of turbine impellers. However it only represents the ideal theoretical situation. In reality the actual head through a pump impeller (H_p) is lower than the Euler head (gH_{Eu}) and for a turbine the Euler head (H_E) is lower than the actual turbine head (H_t). This discrepancy was explained in part by 'head slip' which was evaluated by Busemann (1928). It takes into account the recirculation effects mentioned above. Anderson (1980) later demonstrated that the performance of a centrifugal pump is determined by the interaction of the impeller and the volute. However slip has generally been allowed for only at the outlet of pump impellers. Rholik (1975) and Whitfield et al (1990) demonstrated the role that entrance slip velocity plays on the performance of a turbine rotor. Pfleiderer (1991) also evolved a derivation of slip factor in pumps. He also presented an equation for slip factor in Francis turbines, which was later used by Cohrs (1997) in the application of a PAT system. [Figure 4.4](#) and [Figure 4.5](#) highlight the turbine and pump mode velocity angles and show the ideal and slip-adjusted velocity diagrams for flow entering the tips of the centrifugal impeller.

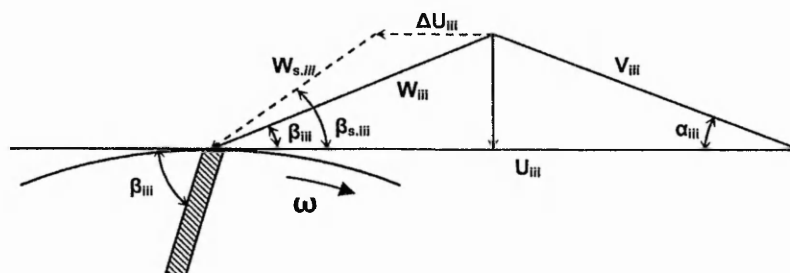


[Figure 4.4](#) Turbine mode inlet velocity diagram with and without slip (infinite and finite number of blades Chors (1997))

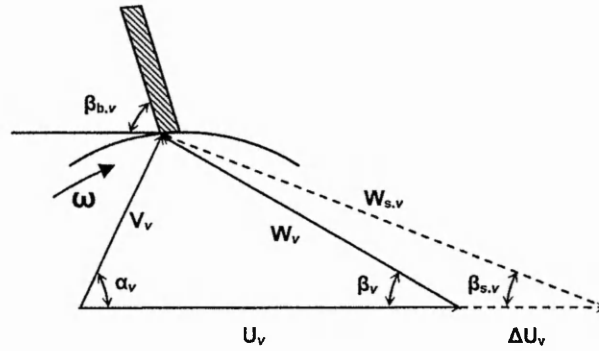


Figure 4.5 Pump mode inlet velocity diagram with and without slip

The counter rotating vortex generated by the spinning motion of the impeller displaces the flow by a quantity ΔU , positive at the impeller inner radius and negative at the outer radius.

The flow approaches a turbine runner with the swirl component.

$$V_{u,iii} = V_{m,iii} \cot \alpha_{iii} \quad (4.19)$$

While in front of a pump runner the swirl is:

$$V_{u,v} = V_{m,v} \cot \alpha_v \quad (4.20)$$

(The suffixes denote the flow zone that is being investigated. In this case suffix *iii* denotes flow zone-*iii*):

For optimum incidence in turbine mode $V_{u,ii} = V_{u,iii}$, while in pump mode $V_{u,v} = V_{u,vi} = 0$. The ideal work ψ done by a pump impeller, in non-dimensional form, with zero pre-rotation, $V_{u,vi}=0$, is,

$$\psi = \frac{V_{u,v}}{U_v} \quad (4.21)$$

While the ideal work done by a turbine runner is:

$$\psi = \frac{gH_E}{U_{iii}^2} \quad (4.22)$$

4.2.3.2 Hydraulic Losses – Flow Zones-iii.iv.v

Zone-iii: - there are a number of elements that can affect the flow prior to its entry into the impeller. At zone-iii itself there are two significant elements that affect the flow. The first include geometrical features, which include the front-shroud and back-shroud edge, and the blade leading edge sharpness. These features create flow discontinuity and may introduce flow separation and disturbance Mikus (1983). The second most predominant effect includes the alignment of the relative flow angle α_1 with the blade inlet angle β_1 . The miss-match of the angles results in “shock” losses. (The terminology shock losses are an effect that occurs in incompressible flows). The flow velocity component will vary in magnitude and assume different directions for each loading condition. Losses occur due to separation, which is due to mismatch of inlet velocity angle and/or sharp edges at the impeller inlet.

Zone-iv: - the blade geometry and profile are difficult to alter. Any modification within this region would therefore make the PAT concept costly. Some associated losses to the blade passages include recirculation losses which occur within blade passages. Profile drag losses arise from the contact of the fluid with the surface, generally with the Impeller blades and other interior surfaces (Ardizzon et al, 1999).

Zone-v: - Ideally at the ‘design point’ the velocity of the fluid leaving the impeller will have no whirl component. In practice this is never achieved due to the complex nature of three-dimensional flow. In the presence of slip, exit shock losses may also arise at changing load condition. Other losses in this region can be due to sudden expansion (Amelio, 2004). The combined losses for all three zones is,

$$HL_{iii-iv-v} = H_{Liii} + H_{LIV} + H_{LV} \quad (4.23)$$

4.2.4 Zones-vi.vii

Zone-vi.vii encompasses the eye region of the impeller/casing interface and extend to the draft tube passage up to the exit-measuring plane.

4.2.4.1 Flow description

The flow characteristics in the draft-tube vary depending on the operating stage

namely the part-load, best efficiency, and over-load operating conditions. Figure 4.6 shows how in theory the velocity components change for each of the operating conditions. In reality the degree by which each of the velocity components changes varies according to each particular machine and individual design and associated losses.

Note: BEP for a PAT is a compromise between optimum flow conditions at impeller inlet, and minimum kinetic energy loss in the draft tube. In practice, these never occur for the same flow rate, because it is designed as a pump and not as a turbine.

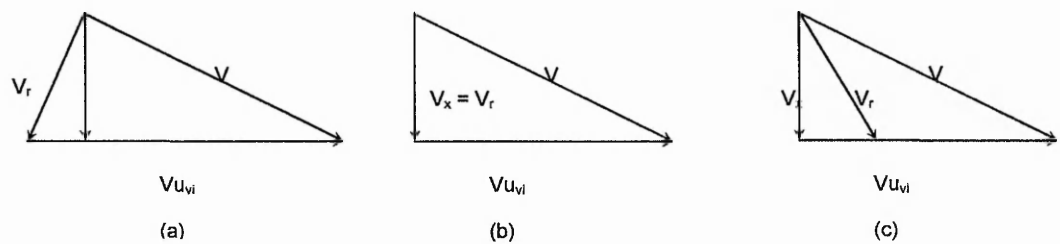


Figure 4.6 Theoretical swirl component at the draft-tube, at (a) part-load (b) BEP (c) Overload

In both part-load and over-load operating stages the absolute component of velocity (v) is at an angle to the axial velocity component (v_x), but ideally in the case of best efficiency the absolute velocity component is coincident with the axial component of velocity. In the over-load operating stage both the absolute and relative components of velocity (v_r) are in the same direction, whilst in the part-load the absolute and relative component of velocity are in opposite directions.

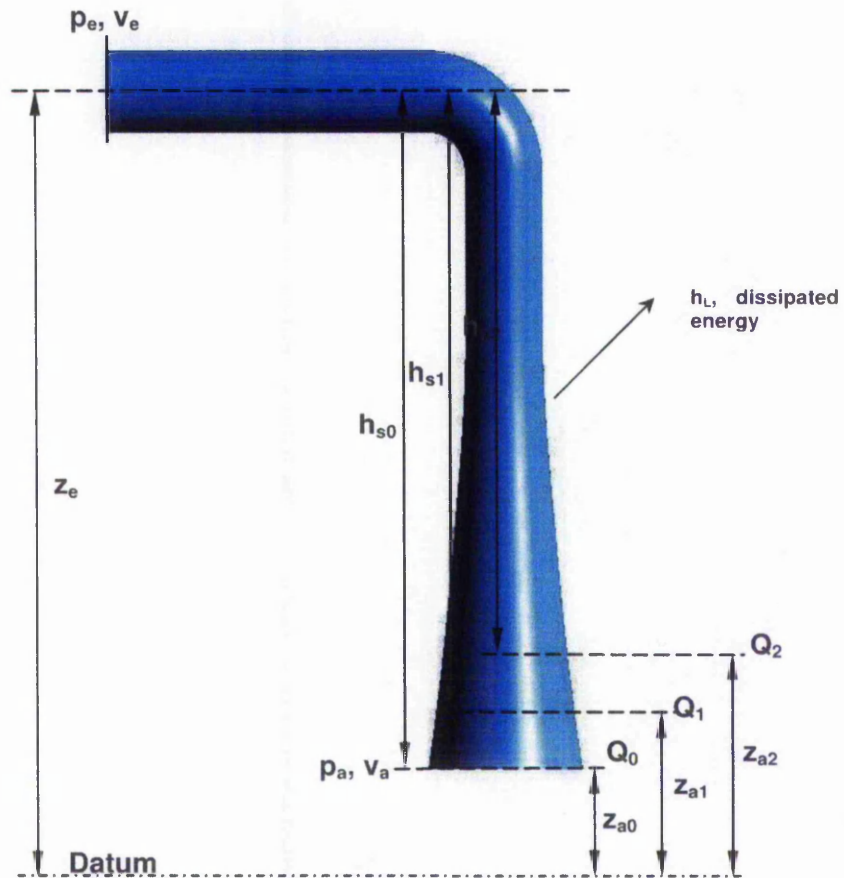


Figure 4.7 Draft-tube head recovery

Applying the conservation of energy principle the conditions at the inlet (subscript a) and outlet (subscript b) of the draft-tube in question has the following relationship.

$$\frac{p_e}{\rho g} + \frac{v_e^2}{2g} + z_e = \frac{p_a}{\rho g} + \frac{v_a^2}{2g} + z_a \quad (4.24)$$

Where subscript e , denotes the inlet of the draft-tube and a , denotes the outlet. Both velocity components are axial at the inlet and at the exit of the draft tube. Suffix a refers to the outlet plane of the draft-tube exposed to the atmosphere and e denotes exit plane which is the interface between flow zone- vi and zone- vii .

The left hand side portion of the equation is the total head at the inlet and the right hand side portion is the total head at the outlet. The performance of a draft-tube can be judged by the energy it can recover from the dynamic head (kinetic

energy) and the static head (potential energy). The respective terms in equation 4.24 can be grouped individually in the following form, where:

$$\text{Dynamic Head} = \frac{v_a^2 - v_e^2}{2g} \quad (4.25)$$

and,

$$\text{Static Head} = z_a - z_e \quad (4.26)$$

The sum of both heads determines the Total Head (H_T) recoverable across the draft-tube and is expressed in the following manner:

$$H_T = \left(\frac{v_a^2 - v_e^2}{2g} \right) + (z_a - z_e) \quad (4.27)$$

Figure 4.7 shows how the loss h_L behaves with effects of submergence at the tailrace of the draft-tube. With increasing tailrace height z_a the static height h_s decreases. The following relationship is derived again from equation 4.24.

$$p_e = -\frac{v_e'^2}{2g} - h_s + h_L \quad 4.28$$

where,

$$h_s = z_a - z_e \text{ and } \frac{v_e'^2}{2g} = \frac{v_a^2}{2g} - \frac{v_e^2}{2g} \quad 4.29$$

The static head h_s decreases with increasing flow rate, Q whilst the dynamic head increases. Therefore the dissipated energy in the draft-tube is affected as follows:

- a) $h_L > \frac{v_e'^2}{2g} + h_s$ then p_e is positive, and if
- b) $h_L < \frac{v_e'^2}{2g} + h_s$ then p_e is negative

4.2.4.2 Hydraulic Losses – Zone-vi.vii

Equation 4.27 is the theoretical total head recovery, in reality there are other

losses within the draft-tube that have to be accounted for, thus the actual Total Head (H_A) recovery is given by:

$$H_A = H_T + \sum h_L \quad (4.30)$$

where, $\sum h_L$ is the sum of the draft-tube losses.

There are various losses in the draft-tube, some of which include those attributable to pipe friction and pipe bends (as in the current case). The frictional losses arising through whirl are the most significant and represent a greater challenge in terms of the impeller exit design as the flow characteristics leaving the impeller are carried through to the draft-tube, thus subsequently influencing the energy recovery process (Amelio, 2004). The losses at the PAT outlet are composed of frictional losses due to the vortex, which is the energy associated to the peripheral velocity, and partially ($\frac{1}{4}$) lost, relative to the energy of the axial velocity (Amelio, 2004).

4.3 Modelling Methodology

To enable direct comparison between CFD and experimental work the geometry of the computational model and the parameters evaluated have to be brought to a common ground. Different possible geometrical models to represent the critical zone-ii/zone-iii interface are considered.

4.3.1 Geometrical Association – Interface Modelling

It is common practice in CFD modelling to remove certain geometrical features that are thought not to influence the machine characteristics by a great amount in order to simplify the mesh creation and reduce modelling time. However, each machine has its own flow characteristic, and simulating the pump in turbine mode should be looked at with a different perspective to modelling the same pump in normal pump operating mode. The flow direction is reversed and the flow path will encounter different 'obstacles' as it travels through the machine, thus the geometry features that can be removed in one direction would need reconsideration when modelling the flow in the opposite direction.

For a pump operating in turbine mode the most critical regions are the interfaces between zone-ii and zone-iii, and also zone-iv and zone-v. In zone-ii of a PAT model the FS and BS thicknesses are in the flow path and therefore can affect

flow behaviour. The axial and radial clearances between volute and impeller, and the churning volume can also affect the flow behaviour within the PAT since there are losses associated to these regions. For the current PAT model preliminary computational results showed that any variations in geometry within flow zone-*ii* could alter the characteristics of a pump when operated in turbine mode but had no influence in pump mode operation. Therefore other geometry configurations were attempted in this region to evaluate the amount of simplification that can be contemplated.

The large clearances and complex geometry in this zone can be modelled in many ways but it is fundamental that the modelled interfaces do not compromise the accuracy of the predicted flow to the extent of altering the operating characteristics of the machine. On the other hand, geometry simplification is also desirable because accurate geometry representation can be time consuming in both set-up and computational time. The acceptable modelling boundaries therefore have to be explored. There are numerous possibilities in the geometrical modelling of the casing-impeller interface. [Figure 4.8](#) illustrates four possible models that have been investigated. The bold lines represent interface planes between component domains.

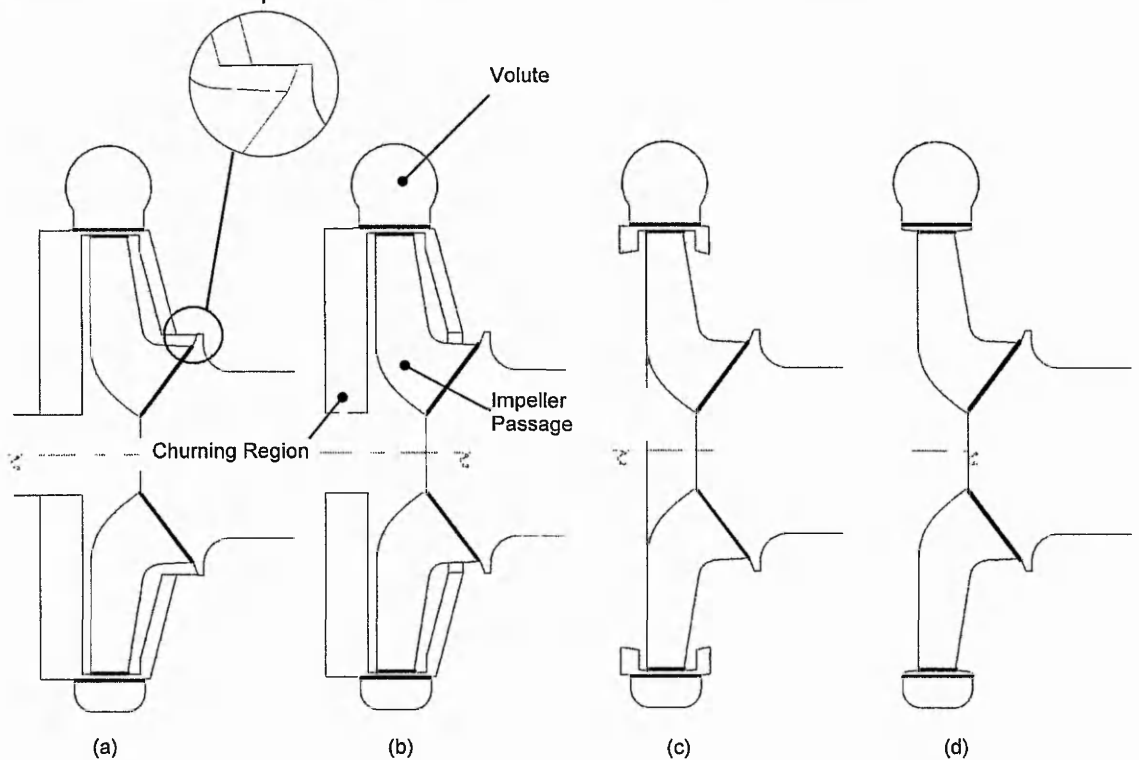


Figure 4.8 zone-*ii* different possible geometrical representation (a) interface-*i*, (b) interface-*ii*, (c) interface-*iii*, (d) interface-*iv*

Interface-i: - This is the most complete model as the geometry representation is the closest to the real geometry. The computational geometry includes the front-shroud and back-shroud complete definition, the churning region, and casing leakage into the draft-tube.

Interface-ii: - A variation of interface-*i*. Includes the whole churning geometry but does not model the leakage into the draft-tube.

Interface-iii: - A variation of interface-*i*, but it does model the churning. It only models the effects of front and back-shroud edges and the axial and radial clearances.

Interface-iv: - Certain features of the impeller including front-shroud and back-shroud thicknesses and churning regions are not modelled. This is a common technique for modelling, which does not include the churning region. This method is normally adopted in pump operating mode as the geometrical features in this region do not influence the flow and machine characteristics.

	Interface- <i>i</i>	Interface- <i>ii</i>	Interface- <i>iii</i>	Interface- <i>iv</i>
Discharge (Q)	$Q_{A,i}=Q+Q_{CFD,Le}$	Q_A	Q_A	Q_A
Churning Volume (V_c)	$V_{C,i}$	$V_{C,ii}<V_{C,i}$	$V_{C,iii}<V_{C,ii}$	$V_{C,iv}=0$
Shroud Thickness t_s	t_s	t_s	t_s	N/A

Table 4.1 – Summary of Interface Models

4.3.2 Optimisation of PAT Geometry

4.3.2.1 Modification-*i* - Suction eye enlargement

Modification-*i* involves the enlargement of the casing eye and impeller eye areas as shown in Figure 4.9. Part of the material is removed to allow a larger volume of flow out of the impeller eye. Preliminary experimental work with the modified eye on the NW8 Kirloskar (24.5rpm) PAT at the operating speed of 800rpm showed a marginal decrease in efficiency of 0.3% (Singh et al, 2002).

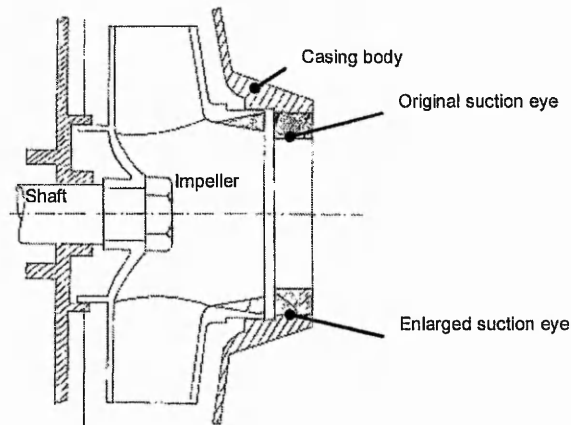


Figure 4.9 - Modification-i

4.3.2.2 Modification-ii – Rounding of impeller inlet edges

Another modification technique for possible optimisation is to round off the inlet edges of the impeller as in [Figure 4.10a](#). If the geometry allows, the front-shroud and shroud edges can also be rounded as shown in [Figure 4.10b](#). Experimental work has shown inconsistent results with this technique. Williams (1992) did not report any improvement in efficiency whilst Singh (2003) reported a 1-2% improvement.

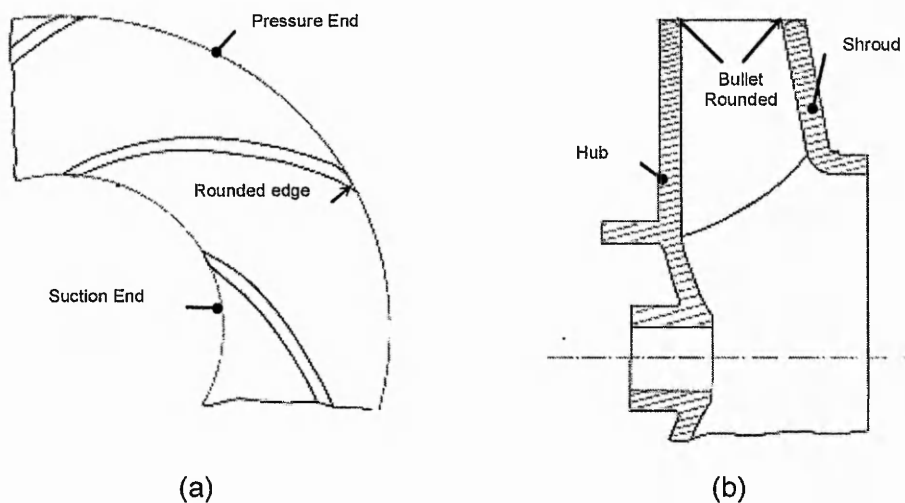
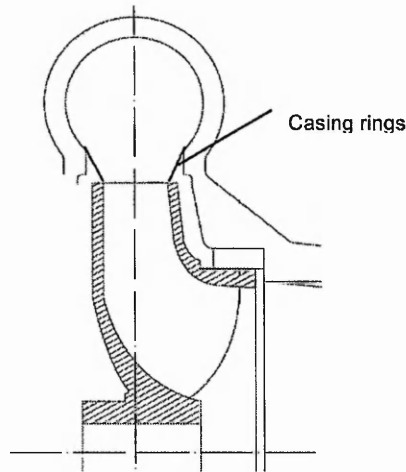


Figure 4.10 Modification-ii

4.3.2.3 Modification-iii – Casing ring inserts

This modification procedure may be new in experimental work but it is often employed in CFD modelling as the churning region is usually not modelled. As

shown in [Figure 4.11](#) rings are attached at the outlet region of the casing and taper down to the inlet of the impeller in the radial direction. The aim is to direct the flow into the impeller and to reduce secondary flows occurring.



[Figure 4.11](#) - Modification-iii

4.3.2.4 Modification-iv – Sharpening of outer front-shroud and back-shroud edges at inlet

This modification procedure consists of sharpening the outer edge of the front-shroud and back-shroud at the inlet region of the impeller as shown in [Figure 4.12](#). The aim with this procedure is to allow less throttling within the inlet region of the impeller by means of increasing the axial clearances between the casing-volute and front-shroud and back-shroud outside walls. The assumption in this case is that with the tapering of the front-shroud and back-shroud outside edges the flow will no longer experience separation and associated losses that may arise due to the sudden change in flow area resulting from the large ratio between the casing outlet and the impeller inlet section widths. Moreover, throttling of the flow can result in less efficient impeller operation.

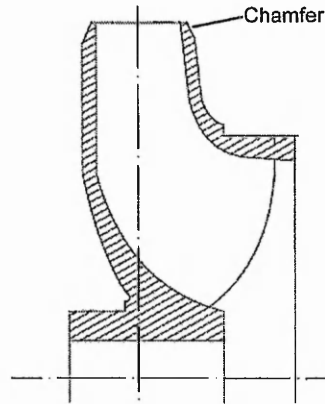


Figure 4.12 - Modification-iv

4.4 Correlation Between CFD and Experimental

4.4.1 General Experimental Parameters

Experimental work normally measures the inlet and exit heads from which the total head across the PAT, H_{total} is obtained. The other parameters to be measured are the discharge, Q , the speed, N , and the shaft torque, T_{shaft} . The shaft torque accounts for the losses from the mechanical system of bearings/seals and the leakage flow, and is different from the hydraulic torque, which is determined by CFD. Therefore, corrections have to be made to the measured quantities, so that experimentally determined hydraulic parameters can be compared with predictions.

The overall experimental efficiency, $\eta_{overall}$ is,

$$\eta_{overall} = \eta_{hyd} \times (\eta_{mech} \times \eta_{leakage}) \quad (4.31)$$

The experimental hydraulic head is defined as,

$$H_{hyd} = \eta_{hyd} \times H_{total} \quad (4.32)$$

From (4.31),

$$H_{hyd} = \left(\frac{\eta_{overall}}{\eta_{mech} \times \eta_{leakage}} \right) \times H_{total} \quad (4.33)$$

The experimental hydraulic losses can be determined as,

$$H_{\text{loss}} = H_{\text{total}} - H_{\text{hyd}} \quad (4.34)$$

and, the experimental hydraulic torque is,

$$T_{\text{hyd}} = \frac{T_{\text{shaft}}}{\eta_{\text{mech}} \times \eta_{\text{leakage}}} \quad (4.35)$$

The factor $\eta_{\text{mech}} \times \eta_{\text{leakage}}$ is difficult to ascertain analytically. Based on Karassik (1986) this factor is approximated to 0.96 for the NW8 Pump as Turbine.

4.4.2 CFD parameters

The CFD model calculates the total head, H_{total} , across the PAT at identical locations of the inlet and exit as in the experimental set up. It also determines the hydraulic losses within the individual zones and the sum of all of these losses is defined as H_{loss} .

The experimental data made available consists of a number of parameters including data measured at the outlet and inlet boundary such as mass flow and pressure, and output data measured at the shaft such as torque, from which performance parameters including efficiency and losses can be calculated.

The computational setup requires the inlet and outlet boundaries and the speed of the impeller for initialisation. The mass flow rate can be varied according to the available experimental data to obtain the complete operating range characteristics.

Several solution parameters can be obtained from the post-processing tools. Some of the parameters of interest include, power output and torque, head rise in each of the identified zones (and respective components), the total head rise, and velocity components in the Cartesian and cylindrical coordinates.

4.4.2.1 Torque

There are two ways of estimating the torque in CFD, one being the force integration method and the other being the hydraulic loss method explained whereby the losses in each domain are added up to calculate the hydraulic

torque.

For the force integration method the torque is calculated from the solution-derived pressures and wall shear values that act upon the blade surfaces, and is given in the following form:

$$T_p = \sum (\rho \cdot A_y \cdot d_x - \rho \cdot A_x \cdot d_y) \quad (4.36)$$

Where Force normal to the surface,

$$F = \rho \cdot A \quad (4.37)$$

$A_{x,y}$ = x,y component of the area of the element on the blade surface
 d_x, d_y = perpendicular distances with respect to the x and y axes coordinate location relative to the coordinate system origin

Similarly the contribution due to shear stress is given as:

$$T_\tau = \sum (\tau \cdot A_x \cdot d_y - \tau \cdot A_y \cdot d_x) \quad (4.38)$$

Where Force due to shear,

$$F = \tau \cdot A \quad (4.39)$$

The total torque is a result of the addition of both the torque due to pressure and due to shear stress:

$$T_{\text{total}} = T_p + T_\tau \quad (4.40)$$

For the Hydraulic Loss approach the hydraulic head across the machine is taken into account the combined losses of every zone. The CFD hydraulic torque is then defined as a function of discharge (Q), hydraulic head (H_{hyd}) and angular speed (ω).

$$T_{\text{hyd}} = \frac{Q \times g \times H_{\text{hyd}} \times \rho}{\omega} \quad (4.41)$$

The Hydraulic Loss calculation is based on the volumetric discretization of the

mesh, whilst the Force Integration calculation is based on the node spacing on the blade surfaces. In both cases the grid spacing will affect the accuracy of the procedure and therefore some discrepancies between the torque values determined from the two methods of calculation is inevitable. However as the grid spacing tends to zero the torque values will be expected to converge.

4.4.2.2 Total pressure

For an experimental setup the total pressure is the sum of the dynamic head, static head, and elevation head (gravitational term). However in CFX-5 acceleration due to gravity is not included in the code therefore the elevation head across any two sections is not calculated. Therefore the calculated total pressure becomes:

$$p_{\text{total}} = p + \frac{\rho v^2}{2} \quad (4.42)$$

where,

p = static pressure

ρ = density of fluid

v = velocity

The assumption in equation 4.42 is suitable for cases where the gravity term is small compared to the other two terms. To enable a direct comparison between experimental and CFD results the elevation terms can also be added to the final predicted total pressure value. Upadhyay (2003) carried out a study with the inclusion of the gravity term and concluded that this had no significant effect in the flow behaviour but caused problems in solution convergence.

4.4.3 Flow Zone Combined Hydraulic Losses influence on Variables

The combined losses of the individual zones contribute to the overall. Substituting the flow zone losses into equation 4.16 gives,

$$gH = gH_{\text{Eu.slip}} + g(H_{\text{L.i}} + H_{\text{L.ii}} + H_{\text{L.iii}} + H_{\text{L.iv}} + H_{\text{L.v}} + H_{\text{L.vi}} + H_{\text{L.vii}}) \quad (4.43)$$

where, the physical significance:

gH = Net rotational momentum + Hydraulic losses in the PAT control

similarly, substituting the combined flow zone losses into equation 4.18 gives,

$$P_{\text{hyd.CFD}} = T_{\text{hyd.CFD}} \cdot \omega = \rho Q \cdot (gH_{\text{Eu.slip}} - gH_{\text{L.iii}} - gH_{\text{L.iv}} - gH_{\text{L.v}}) \quad (4.44)$$

where, the physical significance is,

$P_{\text{hyd.CFD}}$ = Net rotational momentum – Hydraulic losses in the impeller control volume

The hydraulic efficiency η_{hyd} is then defined from equation 4.18 as,

$$\eta_{\text{hyd}} = \frac{(gH_{\text{Eu.slip}} - gH_{\text{L.iii}} - gH_{\text{L.iv}} - gH_{\text{L.v}})}{gH_{\text{Eu.slip}} + g(H_{\text{L.i}} + H_{\text{L.ii}} + H_{\text{L.iii}} + H_{\text{L.iv}} + H_{\text{L.v}} + H_{\text{L.vi}} + H_{\text{L.vii}})} \quad (4.45)$$

and physical significance is,

$$\eta_{\text{hyd}} = \frac{\text{Net rotational momentum} - \text{Hydraulic losses in the impeller control volume}}{\text{Net rotational momentum} + \text{Hydraulic losses in the PAT control volume}} \quad (4.46)$$

From the equations above a number of conditions of interest can arise which relate the power and head. These are of relevance in the interpretation of characteristics of any turbine or pump, these refer to two conditions:

1) Known conditions:

- The increase in power but unchanged total head – efficiency rise
- The decrease in power but unchanged total head – efficiency drop
- The increase in power and increase in total head – efficiency rise
- Unchanged power and increase in total head – efficiency drop
- Unchanged power and decrease in total head – efficiency rise

In known conditions one variable maintains unchanged and the change in the other variable will determine whether any change has occurred in the overall performance.

2) Unknown Conditions:

- The decrease in power and increase in total head – unknown depending on the extent of change in power and total head (i.e. can result in efficiency rise or efficiency drop)

- The increase in power and drop in total head – as above
- The decrease in power and drop in total head – as above

In this occasion both variables change in opposite magnitudes, the extent to which these change will determine whether there was an improvement or drop in efficiency. This method of analysis gives way to a better understanding of the hydraulics that can arise as a result of the study of geometrical modifications and also from the study of geometry modelling of PATs using CFD.

4.4.4 CFD-Experimental Correlation

Table 4.2 and Table 4.3 highlight the differences between CFD and experimental parameters. The main difference to highlight is the different mass flow through the impeller and the calculated torque (and consequently power).

Measured Variables	CFD	Experiment	Correction
Net Discharge, Q	The net discharge (Q) is assumed to flow through the impeller passages	The actual discharge (Q_A) through the impeller is less than the net discharge (Q)	$Q = Q_A + Q_L$ $Q_{\text{exp}} = Q_A = \eta_L \cdot Q$
Output power, P	The CFD evaluates only hydraulic power	The experiment measures the mechanical shaft power, which includes other losses. Therefore output measured power (P) needs to be corrected to the hydraulic power	$P_{\text{exp t.Hyd}} = \frac{P}{\eta_{\text{mech}}}$

Table 4.2 Correlation Table Correlation for power p, CFD and Experimental

Therefore from Table 4.2 the dimensionless number for correlation become as given in Table 4.3 below.

Number	Experiment	CFD
Discharge Number	$\frac{Q_A}{ND^3}$	$\frac{Q}{ND^3}$
Head Number	$\frac{gH_{\text{exp}}}{N^2 D^2}$	$\frac{gH_{\text{CFD}}}{N^2 D^2}$
Power Number	$\frac{P_{\text{exp.hyd}}}{\rho N^3 D^5}$	$\frac{P_{\text{CFD.hyd}}}{\rho N^3 D^5}$
Efficiency	$\frac{P_{\text{exp.hyd}}}{\rho g Q_A H_{\text{exp}}}$	$\frac{P_{\text{CFD}}}{\rho g Q H_{\text{exp}}}$

Table 4.3 Dimensionless groups correlation for CFD-Experiment

5 Results

In this chapter the results are presented in three separate sections. In the first section a comparison between the CFD results and experimental parameters is carried out for the non-modified PAT, to demonstrate any discrepancies between both sets of data. The second section describes the results obtained from different interface configurations in zone-*ii*, explained in chapter 4, [section 4.3.1](#), which model the churning region of the PAT. In the final section the CFD results for the different geometrical modifications introduced in chapter 4, [section 4.3.2](#) presented.

5.1 Interpretation of Results

5.1.1 Flow Description

The results are explained for three distinct regions of operation of a PAT, which are of interest in turbomachinery applications, these are:

No-load to Part-load which consists of the operating region at which insufficient energy is being provided to the impeller for optimum operation. In a turbine this normally refers to the region before reaching best efficiency as the mass-flow rate increases.

Best-efficiency region or point comprises the peak efficiency of the machine itself. However when considering a complete system installation the term region is preferred as usually the system best efficiency does not coincide with the machine best efficiency point due to the further losses that take place in the penstock and other components in the system assembly.

Overload operating region consists of the operating stage where the energy being provided to the impeller is more than what it can cope with for optimum operation. This normally refers to the region after the best-efficiency when the mass-flow is increased.

The post-processing tool in CFX-5 (CFX-post) has a number of flow visualisation techniques which include plotting of streamline, vectors, pressure, and other relevant parameters. The visualisation of internal flow properties is made in Appendix A.

5.1.2 Evaluation of Geometry Changes

In order to interpret any significance between a modified (m) and non-modified (nm) geometry, Singh (2004) suggested the following percentage analysis.

i) Power change between the modified and non-modified PATs is given by the following relationship:

$$\text{Power change} = \frac{P_m - P_{nm}}{P_{nm}} \quad (5.1)$$

The equation above would result in a positive numeric value for an improvement in power and a negative value for a decrease in power.

ii) Head change between the modified and non-modified PAT is given as:

$$\text{Head change} = \frac{H_{nm} - H_m}{H_{nm}} \quad (5.2)$$

From the above equation a negative value would represent a reduction in loss whilst a positive value will represent head rise.

iii) Efficiency change between the non-modified and modified geometry is:

$$\text{Efficiency change} = \eta_m - \eta_{nm} \quad (5.3)$$

A negative value of efficiency signifies that the non-modified geometry had better efficiency, and a positive value will mean that the modified geometry actually gave rise to efficiency. A fuller and better interpretation of efficiency can be made by using equation 4.18 and 4.45 as they relate the efficiency to the power and head.

5.2 Comparison of CFD and Experimental Parameters

Several solutions were carried out to understand the software and its capability of predicting the flow in the current PAT model. Solutions for the non-modified PAT were obtained at various operating points and compared against experimental results.

The solver solution automatically generates the pressure and Cartesian velocity

components. The power output and torque, velocity components in cylindrical coordinates, and pressure terms can be derived by the inbuilt post-processing calculator.

5.2.1 Torque

The predicted Force-integrated (FI) and Hydraulic-Loss (HL) torques (as described in [chapter 4, section 4.4.2.1](#)) have been plotted along with the experimental torque on [Figure 5.1](#). The good agreement between the FI and HL Torques suggests that the chosen CFD model can yield consistent results. The small discrepancies are mainly due to the rounding of errors and the small differential interface pressure readings for neighbouring interface planes. As the HL approach gives a better insight of the internal flow situation in a PAT, it has been used in all subsequent flow analysis and comparisons with experimental results. The HL approach consistently shows a marginally higher torque throughout the entire operating range. In the no-load and part-load region both torques are almost identical. Further it can be seen that the discrepancy between the CFD and experimental torque is large (at least 10% difference). The lower experimental torque may be attributable to various factors in the experimental procedure such as mechanical losses, disc friction losses, and other. On the other hand the higher CFD torque can be attributed to the higher predicted total head which is reported in the subsequent sections.

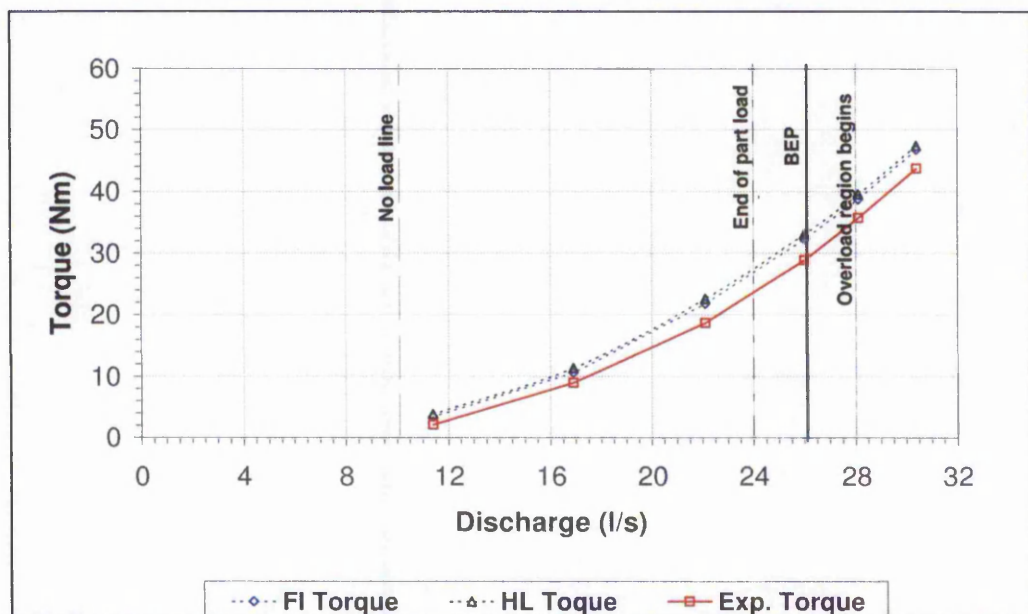
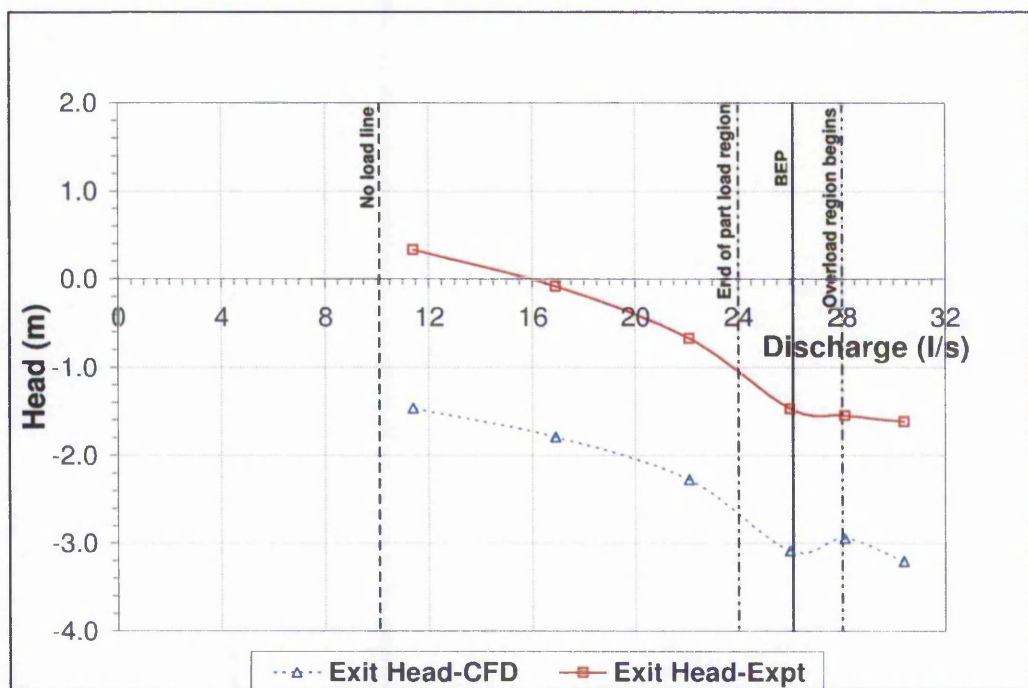


Figure 5.1 - Torque comparison from CFD Force Integration and Hydraulic Loss methods

5.2.2 Exit pressure

The CFD model calculates the relative pressures through the pump, but the absolute values are based on an arbitrary datum. Applying a fixed correction to the computed values to make the inlet pressures equal, allows a direct comparison to be made with the experimental data for exit pressures.

In [Figure 5.2](#), the total exit pressures obtained from CFD and the experiment are compared. The predicted total exit pressure curve follows a similar trend to that of the experiment but have consistently lower values. It can be seen that the difference throughout the whole operating range is significant, at around 1.7m.



[Figure 5.2](#) - Comparison of Exit static pressure for non-modified PAT

The lower values of the predicted exit pressure may be attributed to the flow conditions within the upstream and downstream domains. An inspection of the residuals in each domain indicated that these were higher within the draft-tube. This scenario is aggravated by the use of coarser grids in particular, and in such cases the residuals were either taking longer to drop below the target convergence level or in occasions did not drop below this level. Further investigation with medium grid did not reduce the difference between predicted and experimental exit pressure. Fine grid sizes were also experimented at the exit region and within the entire draft-tube, unfortunately the use of denser grid

led to solver failure due to lack of memory allocation. This aspect therefore remains an unknown as it was difficult to ascertain the computed head recovery and losses within the draft-tube. Another limiting factor was that only steady-state simulations were carried out. The averaging techniques employed at the rotating and stationary component interface caused convergence problems due to the high residuals.

Further studies were carried out without the draft tube in order to understand how the exclusion of any downstream geometry influences the predicted exit head. These results are presented in chapter [section 5.3.1](#).

5.2.3 Hydraulic Parameters

[Figure 5.3](#) compares the computed and experimental values of the total head, hydraulic loss, hydraulic head, and hydraulic efficiency. As in [section 5.2.2](#) the discrepancy between CFD and experimental data is significant for the hydraulic head and hydraulic losses. However, the computed curve profiles are remarkably similar to those obtained experimentally which can also be an indication of machine geometry similarity.

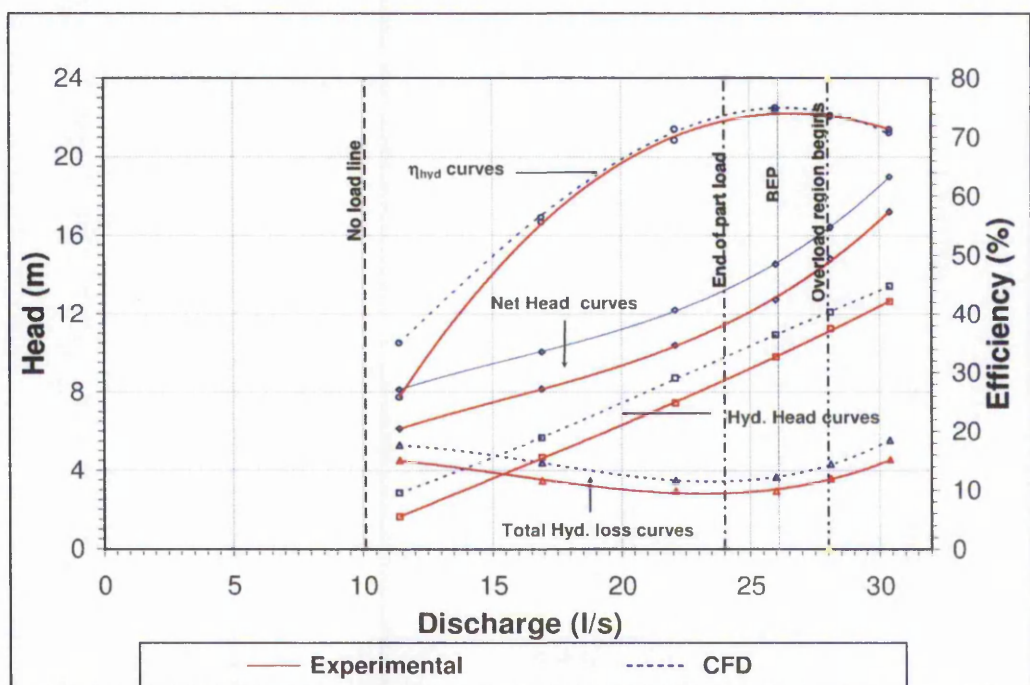


[Figure 5.3](#) - CFD and Experimental hydraulic characteristics for non-modified PAT.

The maximum hydraulic head discrepancy between the sets of data is around 1.7m and occurs at the flow rate of 22.1l/s whilst the lowest of 0.76m occurs at a flow rate of 30.4l/s. Two trends are observed for the CFD hydraulic efficiency. In the part-load and BEP region the CFD efficiency is higher than the experimental data. Towards the best-efficiency and over-load regions the CFD hydraulic efficiency drops marginally below the experimental efficiency curve.

The BEP occur at the same discharge of 26 l/s for both experiment and CFD, achieving 76.9% experimental best efficiency and 75.1% CFD best efficiency. The minimum hydraulic loss occurs at an identical discharge of 22.1 l/s for both experimental and CFD data. The two sets of loss curves follow a similar trend, with the CFD predicting higher losses throughout. The highest difference is around 0.98m and the lowest around 0.56m occurring at the flow rate of 30.4l/s and 22.1l/s respectively.

5.2.4 Zonal Losses (Hydraulic Loss Method)

The hydraulic losses within each flow zone are illustrated in [Figure 5.4](#). The losses in the radial clearance (zone-*ii*) are the lowest in the whole domain. With increase in discharge, the losses initially decrease from the no-load point reaching a minimum towards the part-load region, somewhere between 17.2 l/s and 19.9 l/s. Thereafter the losses increase steadily towards the BEP and over-load regions.

The losses in the impeller (zone-*iii.iv.v*) behave in a similar manner to those of zone-*ii*, however with a more pronounced increase throughout the whole operating range and with increasing discharge. In the BEP and overload region the losses within this zone form a major proportion of the overall losses.

The losses in zone-*vi*, which are mainly associated with the swirl flow within a contracted flow area (casing eye) and the draft tube, show an interesting behaviour. They form a major proportion of the overall losses when the PAT is operating in the part-load region, but the losses reduce rapidly towards the best efficiency reaching a minimum at 28.1 l/s and then it starts to increase again towards the over-load region. This is probably due to the unusual design of the NW8 pump in that the casing on the suction side has a smaller diameter than the impeller eye.

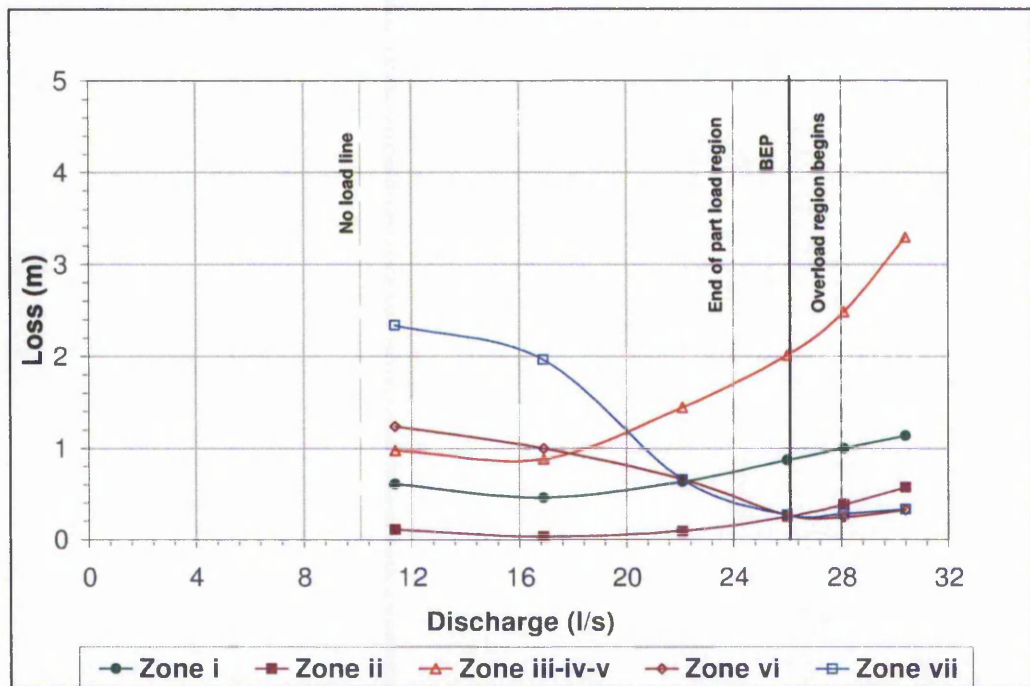


Figure 5.4 - Zone loss distribution for non-modified PAT

The flow-zone and hydraulic-loss approach above has shown to be useful and can form the basis for design optimisation for individual PAT components. In the present study, five major loss components have been identified and analysed separately, these are listed in Table 5.1. The table summarises the percentage losses relative to each zone at a given operating flow.

Load Point	Discharge	Zone-i	Zone-ii	Zone-iii.iv.v	Zone-vi	Zone-vii
Overload	0.132	20.9	10.5	60.5	5.9	6.1
Overload	0.122	18.4	7.0	45.6	4.6	5.2
BEP	0.113	16.0	4.6	36.9	4.9	5.0
Part-load	0.096	11.6	1.7	26.6	12.1	12.1
Part-load	0.074	8.4	0.6	16.2	18.3	36.1
Part-load	0.050	11.1	2.0	17.9	22.8	42.9

Table 5.1 - Distribution of zone losses as a percentage of total hydraulic loss for non-modified PAT

The first component is the volute casing (zone-i) where the losses account for 8% to 21% of the total hydraulic loss. The losses in this region increase with discharge, very similar to frictional losses in pipes. However, optimisation of the main volute casing area is very difficult.

The second component is in the radial clearance (zone-*ii*) and it represents 5% and 11% of the total losses in the BEP and overload regions respectively. There are two possible explanations for the relatively high losses: the rapid acceleration of the flow with a discontinuity of the flow direction near the impeller; and the influence of secondary flows due to large axial clearances. Therefore optimization in this region can be contemplated.

The third component is in the impeller area (zone-*iii.iv.v*), where the loss has shown a minimum value in the early stage of the part-load region. This minimum loss point refers to the shock free conditions at impeller inlet. However, it should be noted that for a given pump, the discharge at minimum impeller loss when it is operating in pump mode is not the same as the corresponding discharge when the same pump is operating as a turbine. Since the pump impeller is not designed for turbine applications, the recorded 37% to 61% of the total hydraulic loss at the BEP and over-load points compares favourably with conventional turbines (Hutton, 1954). However, it may be possible to improve the impeller inlet zone for PAT operation.

The fourth component is the impeller eye and draft tube area (zone-*vi* and zone-*vii*). The losses in this area can be very high in the part-load region accounting for as much as 23% of the total hydraulic loss in zone-*vi* and 43% in zone-*vii*. The contraction in the casing immediately after the impeller eye increases the flow velocity and hence losses. It follows that a reduction of the losses can be achieved by minimising the amount of swirl and the operating flow velocities at the PAT exit. It may be difficult to alter the design of the exit blade profiles, but it is possible to modify the eye region.

5.3 Discrepancies and Uncertainty in CFD modelling

The set up and geometry of a computational model consist of an approximation of an experimental model and therefore modelling discrepancies cannot be entirely avoided. Often the level of complexity of the computational model is reduced by making certain assumptions which may or may not affect the accurate prediction of the hydraulic characteristics of the machine. This section picks up on current modelling trends particular those relevant to PAT modelling and demonstrates that certain assumptions are not suitable for prediction of its

internal flow regimes. These assumptions are generally a consequence of the requirement for reduction in model set up time and complexity.

The following sections are dedicated solely to the assumptions with regards to the modelling of the impeller and leakage in a PAT. Interface modelling in [section 4.3](#) also partially deals with the theme of discrepancies and uncertainty in CFD modelling but has been isolated due to the involved analysis.

5.3.1 Simulation without draft-tube

In [section 5.2.2](#) and [section 5.2.3](#) the computational exit pressures and hydraulic head curves showed a large difference when compared to the experimental data. Both sets of curves however are similar in profile, suggesting that head recovery is not being modelled by the computational model. This may be due to the physical discrepancies between the computational and experimental approach. With the computational model the draft-tube portion at the outlet is not submerged and therefore head recovery may not be 'accurately' represented as in the experimental procedure. This will therefore affect the accurate prediction of the net head across the entire turbine reflecting in the observed head increase. (Head recovery in a draft-tube is briefly described within chapter 4, [section 4.2.4](#)).

To understand this predicament the PAT was modelled without the draft-tube. This allows for the results to be compared with those obtained from a PAT modelled with draft-tube (in [section 5.2](#)). The significance of this study is that if a considerable difference arises between the sets of results, or if an increase in head is witnessed for the case scenario without draft-tube, then it means that the computational approach is modelling head recovery and/or capturing the effects of different geometry setup at the downstream components. If on the other hand the results do not alter comparably then this means that with or without draft-tube the computational model is not capable of modelling head recovery.

Two cases are represented in this section for this study, in which in the first case, [section 5.3.1.1](#), the PAT is modelled without a draft-tube and only uses a single blade passage with periodic boundary conditions. In the second case, [section 5.3.1.2](#), the PAT is modelled without a draft-tube but includes all impeller passages and interface-iv. The first case is labelled No-Draft i, and second case is labelled No-Draft ii as given in the following sections.

5.3.1.1 No-Draft.i - Single impeller passage modelled

The graph below plots the hydraulic characteristics of the turbine for No-Draft.i. The net head curve data for both CFD and experimental show small deviations in the main operating region, however it is difficult to establish whether the cause for this significant reduction is due to draft tube removal or single blade passage modelling.

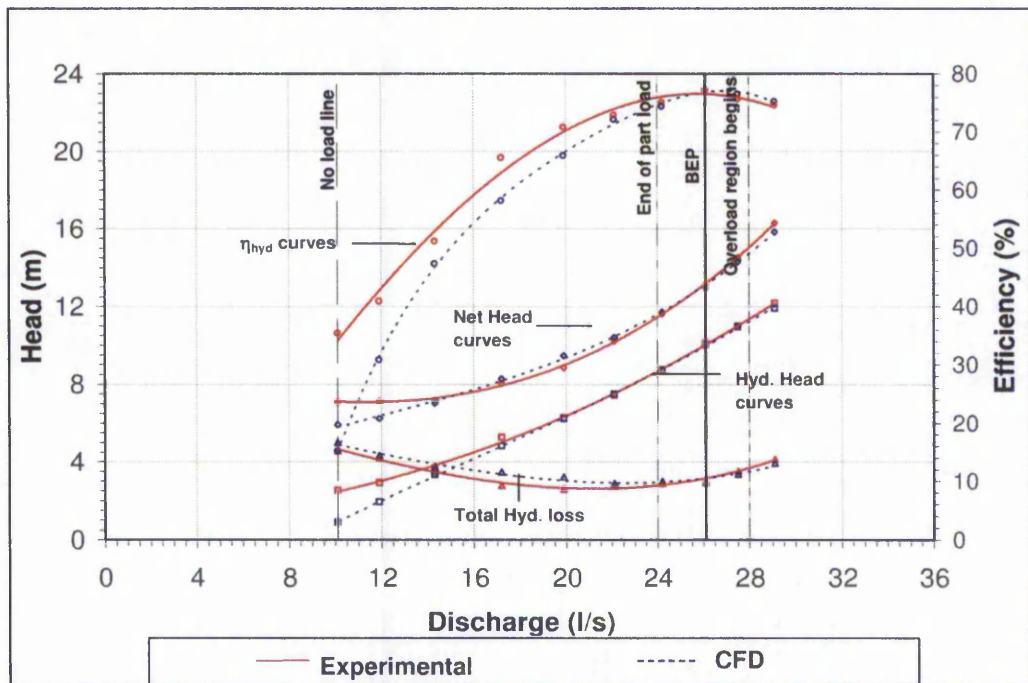


Figure 5.5 - Hydraulic Characteristics for PAT without draft-tube and with periodic boundary

Good agreement is achieved in the determination of the hydraulic head essentially in the main operating region. In the no-load and part-load regions the discrepancies are higher for all the hydraulic parameters. Towards the BEP the computed hydraulic head slowly merges with the experimental data, leading to a gradual convergence of the efficiency curves.

The best efficiency point for experiment (η_{bep} -78.1%) and for CFD (η_{bep} -78.2%) occurs at an identical discharge of 26.1 l/s. The minimum hydraulic loss also occurs at an identical discharge of 22.1 l/s for both CFD and experimental.

The two sets of loss curves follow a similar trend with the CFD predicting identical losses in the BEP and overload regions, but lower losses in the part-

load region. This in turn has led to a higher CFD efficiency curve throughout the part-load region. With the uncertainty in the experimental determination of turbine efficiency estimated to be around 2 % at BEP and 4 % in the part-load region (Singh, 2004), the overall prediction of the hydraulic losses is considered acceptable.

The hydraulic losses within each zone are shown in [Figure 5.6](#) below. Zone-*i* and zone-*ii* losses are combined losses. Zone-*vi* which refers to the losses at the exit of the impeller eye are high in the no-load region and decrease steadily towards the main operating region. The losses in the impeller zone-*iii.iv.v* is similar in curve profile to those seen in [Figure 5.4](#) in [section 5.2.4](#) for a PAT with draft-tube, however they are much lower in magnitude. This is probably due to the use of periodic boundary conditions.

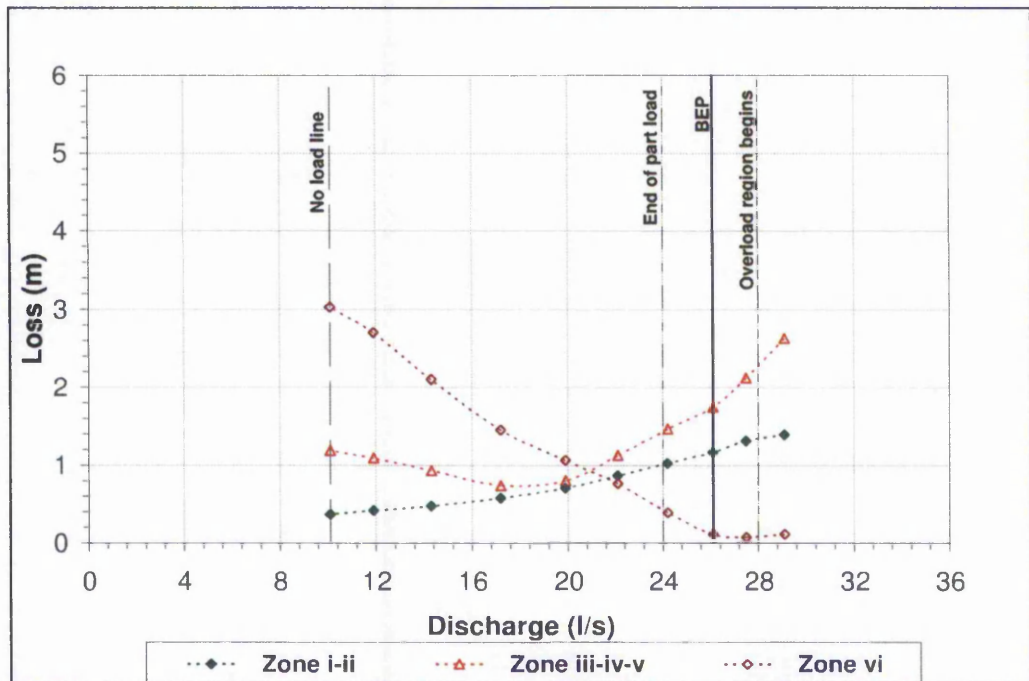


[Figure 5.6](#) - Zone loss distribution for PAT with periodic boundary and no draft-tube

5.3.1.2 No-Draft.ii - All impeller passages modelled

In this set up all the impeller passages are modelled. [Figure 5.7](#) plots the hydraulic characteristics for the PAT without the draft-tube. The performance curves display similar characteristics for both PAT with and without draft-tube. The resemblance in curve profiles indicate geometrical similarity, however since

there has not been any improvement or loss in the hydraulic characteristics this also suggests that with the draft-tube there has not been any head recovery effects.

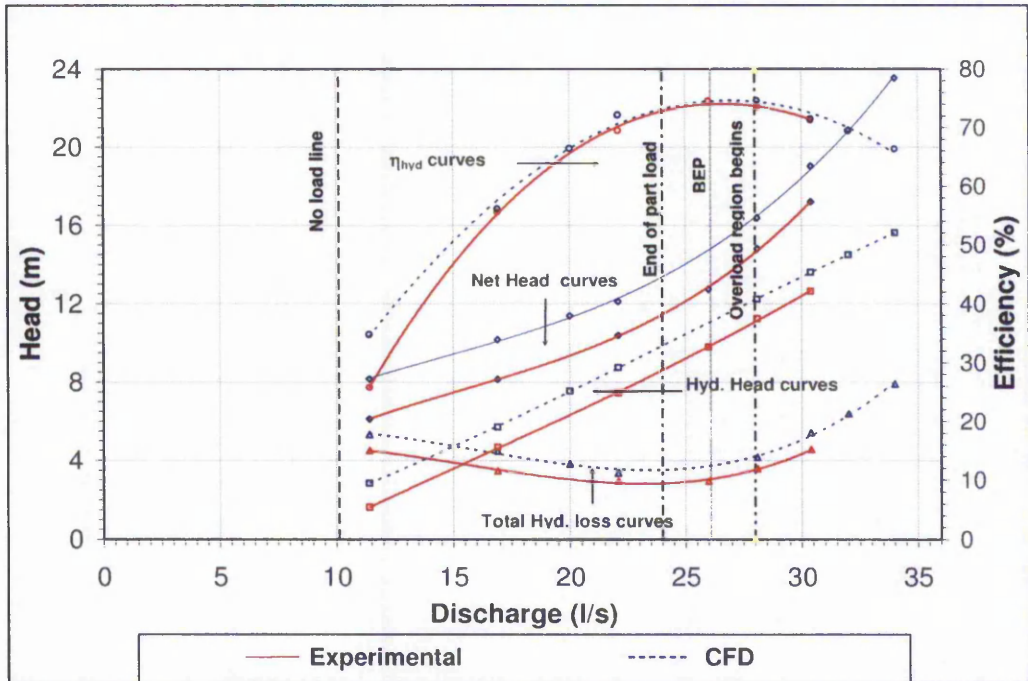


Figure 5.7 - Hydraulic Characteristics of PAT modelling all passages but without draft-tube

The best efficiency point for the experimental setup remains at the discharge of 26l/s for this setup, corresponding to 76.9% efficiency for both experimental and CFD data. The minimum hydraulic loss also occurs at the same discharge of 22.1l/s. Generally the observations for a PAT model without a draft-tube have shown to be very similar to those with a draft-tube (presented in [section 5.2](#))

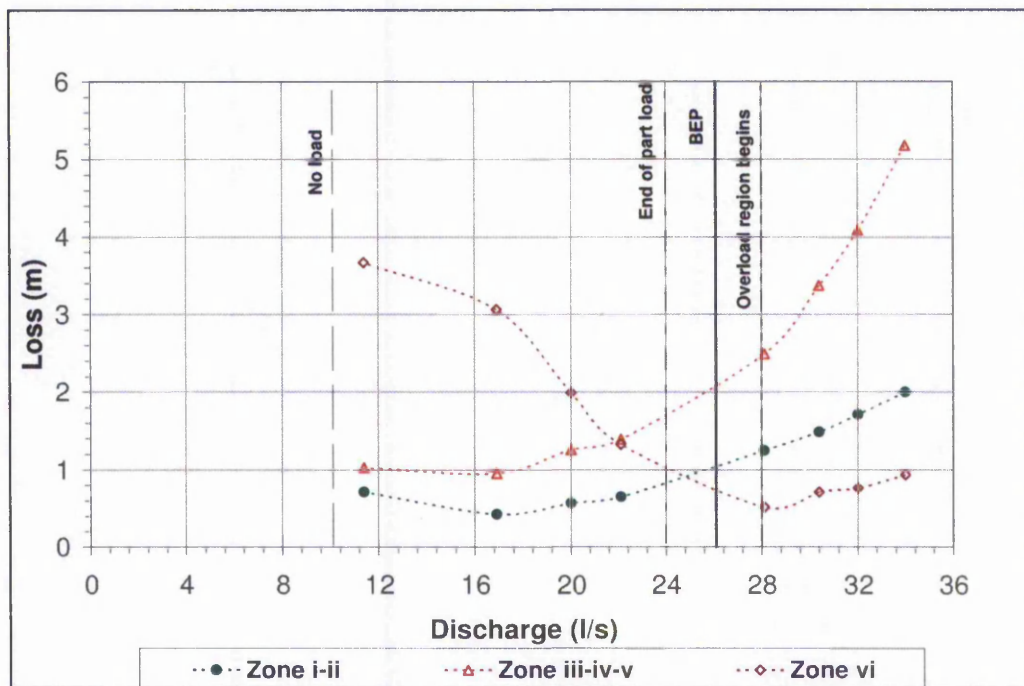


Figure 5.8 - Zone loss for PAT with all blade passages and without draft-tube

The hydraulic losses within each flow zone are illustrated in [Figure 5.8](#). The combined losses in the volute and radial clearance (zone-*i-ii*) are the lowest in the whole domain. With increase in flow they initially decrease reaching a minimum in the part-load region and steadily increase in the BEP and over-load regions. The losses in the impeller (zone-*iii.iv.v*) have a steady trend in the beginning of the part-load region, and rapidly increase thereafter towards the BEP and over-load region. The losses in zone-*vi* maintain the same behaviour as those seen with a PAT with a draft-tube whereby the losses start high in the part-load region and decrease rapidly towards the main operating region.

5.3.2 Representation of Leakage

In the current scenario two approaches were taken to model leakage. In the first case leakage using Thorne's (1982) equation is estimated and incorporated in the overall losses (see Appendix B). In the second case an estimated clearance with controlled flow is modelled computationally which allows flow out of the casing into the draft-tube.

[Figure 5.9](#) shows the hydraulic curves and differences between the PAT without leakage and with leakage. It is interesting to notice a decrease in losses due to

leakage effects at the best efficiency region. The curve profiles remain similar but there is a slight shift of the curves towards the higher operating flows indicating that with leakage the hydraulic curves are closer to an experimental setup. The BEP shifts from 24 l/s to 26.1 l/s.

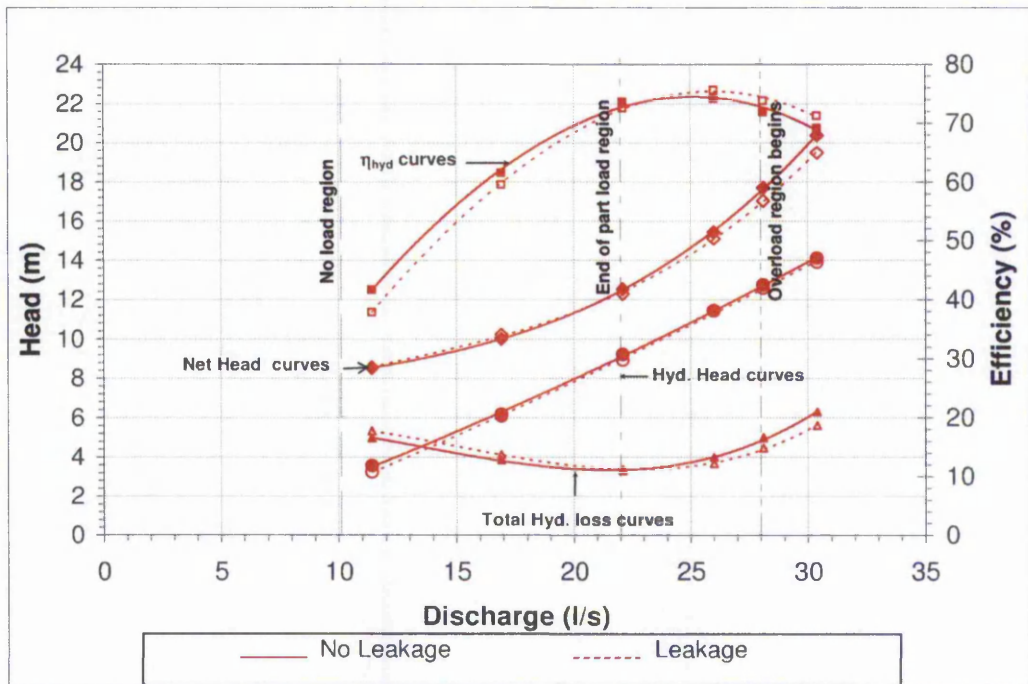


Figure 5.9 - Hydraulic characteristics without leakage and with leakage

In Figure 5.10 the zone losses for both systems without and with leakage are plotted. The dashed line represents the system with leakage and the solid lines represent the same system however without leakage.

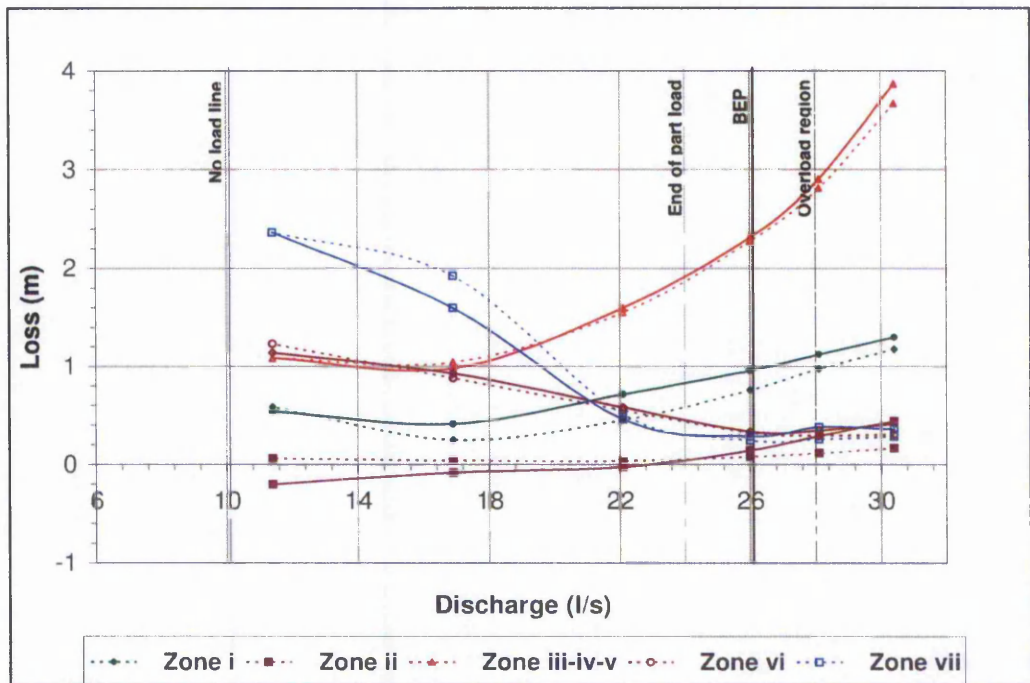


Figure 5.10 - Comparison of Hydraulic Losses for PAT with and without Leakage

The losses within the impeller zone-*iii.iv.v* and within the impeller eye zone-*vi* are very similar for both systems. With increase discharge, for the system with leakage the losses within zone-*i* drop considerably throughout the whole operating region and remain below that of the system with leakage. Losses in zone-*ii* show to increase with leakage within the part-load region but this difference disappears at the end of the part-load region. For higher flow rates beyond the part-load region the losses in zone-*ii* then become lower than those for the system with leakage. Losses within zone-*vii* for the system with leakage are higher within the part-load region. In the BEP region and towards overload region they become lower. Overall the combined loss in the main operating region is better for a system with leakage. Comparison of local pressures for the current model against those of the modified-eye PAT suggest that pressure relief is the cause of improvement in losses within zone-*i* and zone-*vi*. The computational results indicate reduced local pressures for the modified PAT model within these zones after leakage is computed.

5.3.3 General overview of uncertainty with CFD

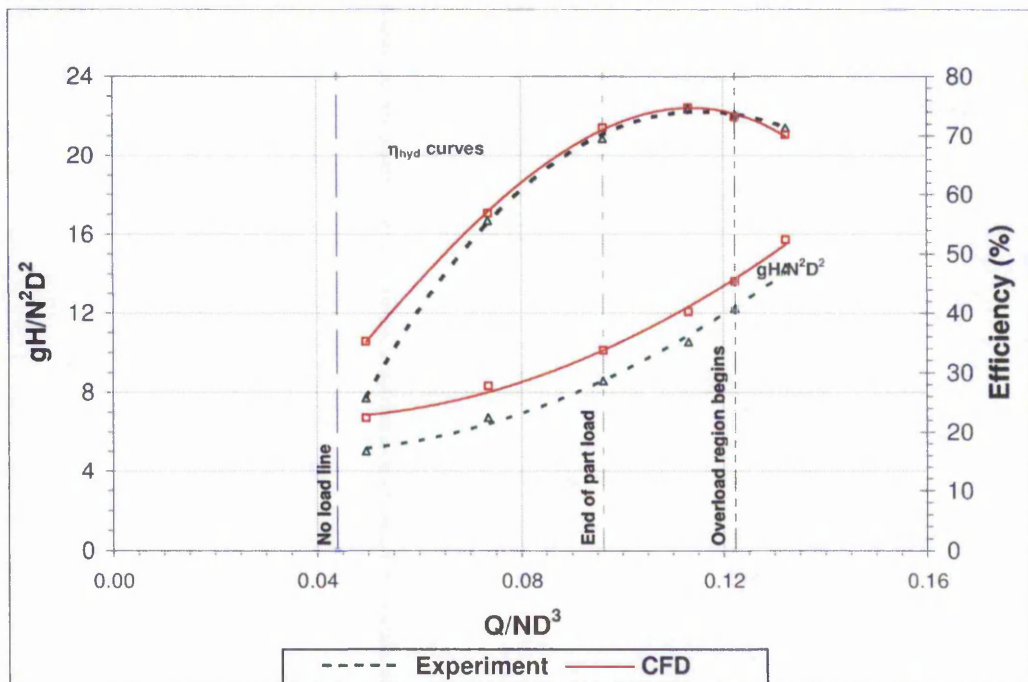
The overall prediction of the hydraulic characteristics for a single-blade PAT model appears accurate as the comparison with experimental data is closely matched however the results are probably incorrect. Generally the loadings

around the impeller for pump operation mode are equal in all blades at BEP (Karasik, 1986), however this is not the case for a PAT as shown in the loadings in chapter 6, [Figure 6.1](#) therefore the predictions for a single blade are probably incorrect. A complete impeller simulation gives a better efficiency match than that for a single blade passage; however the prediction of head and torque is higher. Leakage has shown to have an influence in determination of the BEP of the pump, whereby the efficiency curve undergoes a shift. The main increases in losses for a system with leakage within zone-*ii* occur in zone-*i* and zone-*vii*.

5.4 Interface Modelling - Representing churning

In this section the computed results are compared against each other for the different interface models. The figures in the following sections also include the experimental data for relative visual observation, however the relative comments are made against interface-*i* data.

[Figure 5.11](#) compares the experimental efficiency against the CFD efficiency for the PAT model with interface-*i*. The match of both characteristics is satisfactory in the main operating region which justifies the use of interface-*i* as the basis of comparison for the remaining interfaces. Moreover unlike the other interface models interface-*i* closely resembles that of the real NW8 Kirloskar (24.5 rpm) PAT.



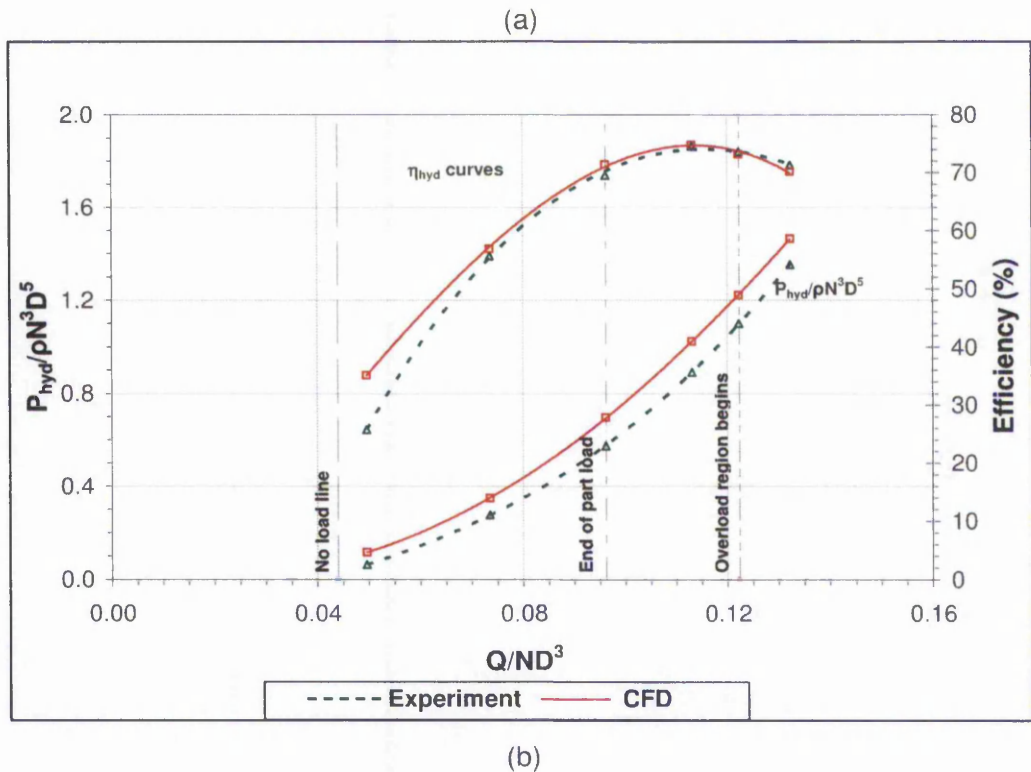
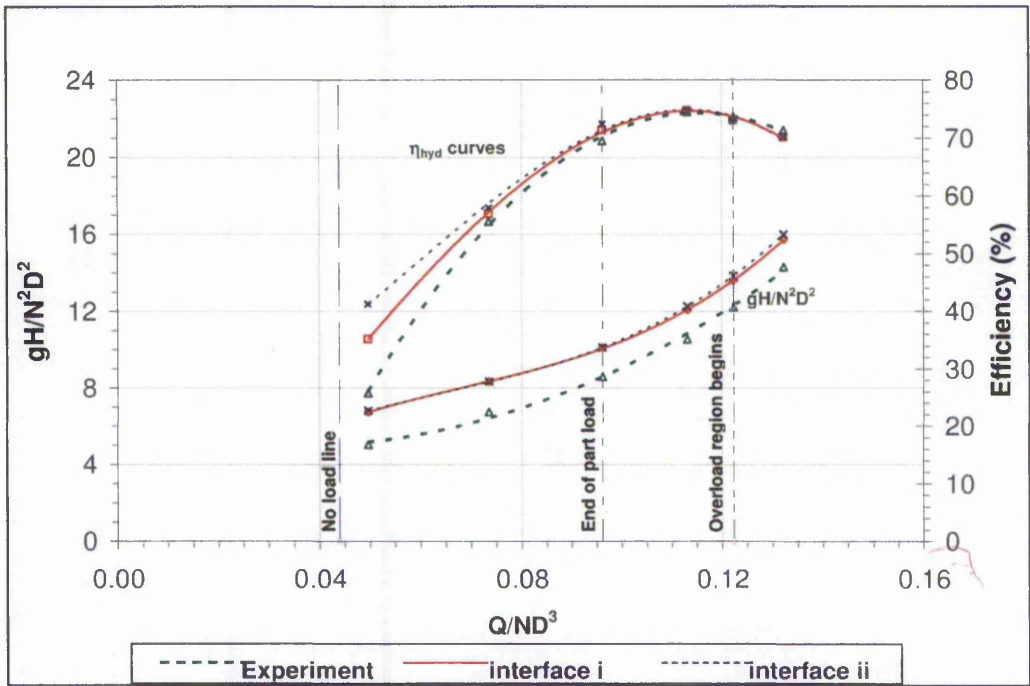


Figure 5.11 - Dimensionless characteristics comparing interface-*i* and experimental efficiency and change in (a) Head number (b) Power Number

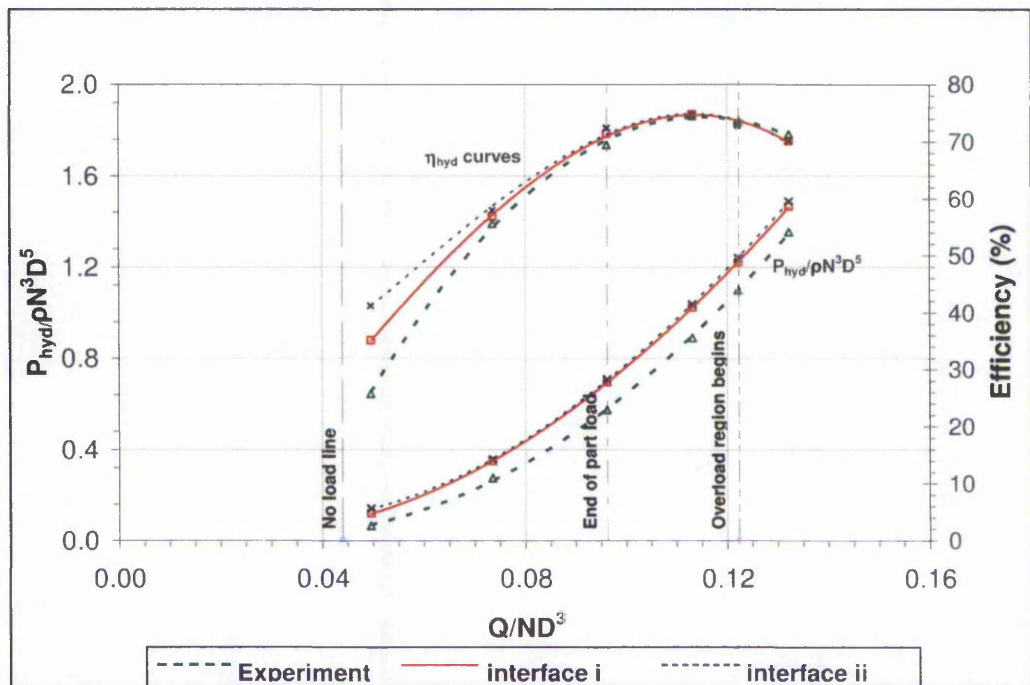
5.4.1 Comparison between interface-*i* and interface-*ii*

Interface-*ii* does not model the clearance into the draft-tube domain. [Figure 5.12](#) compares the head number and power number curves of interface-*i* and interface-*ii*. The head number curve is virtually similar for both interfaces in the part-load region, but interface-*ii* shows an increase in head number at the BEP and overload regions. The power number curve for interface-*ii* is higher throughout the whole operating range.

The unchanged head number and slight increase in power production in the part-load region result in the efficiency rise seen for interface-*ii*. In the main operating region the hydraulic efficiency for interface-*ii* is marginally lower due to the increase in head number.



(a)



(b)

Figure 5.12 - Dimensionless characteristics comparing Efficiency and change in
(a) Head number (b) Power Number

The percentage differences between interface-*i* and interface-*ii* are shown in Figure 5.13 and Table 5.2 whereby positive percentage values denote a positive effect on the observed parameter and a negative percentage value indicates a negative effect on the observed parameter.

The power production undergoes a slight increase for interface-*ii* throughout the entire operating range of the machine, with the highest 18.23% increase being at the discharge number of 0.050 and lowest 1.37% at 0.122. The head number curve shows no improvement with the exception at the discharge number of 0.096 and 0.074.

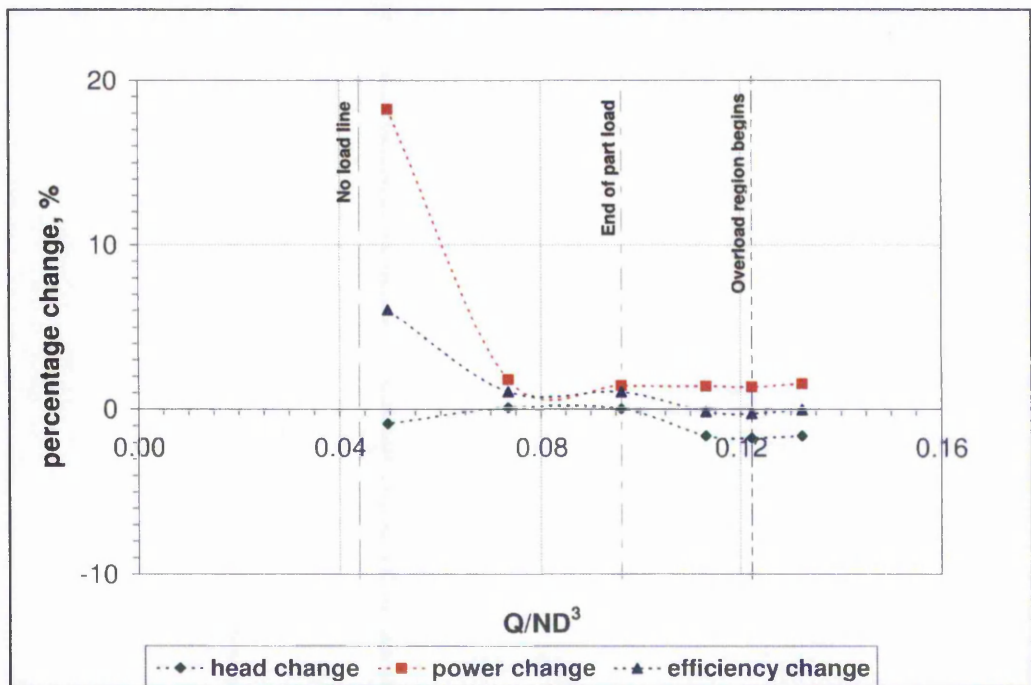


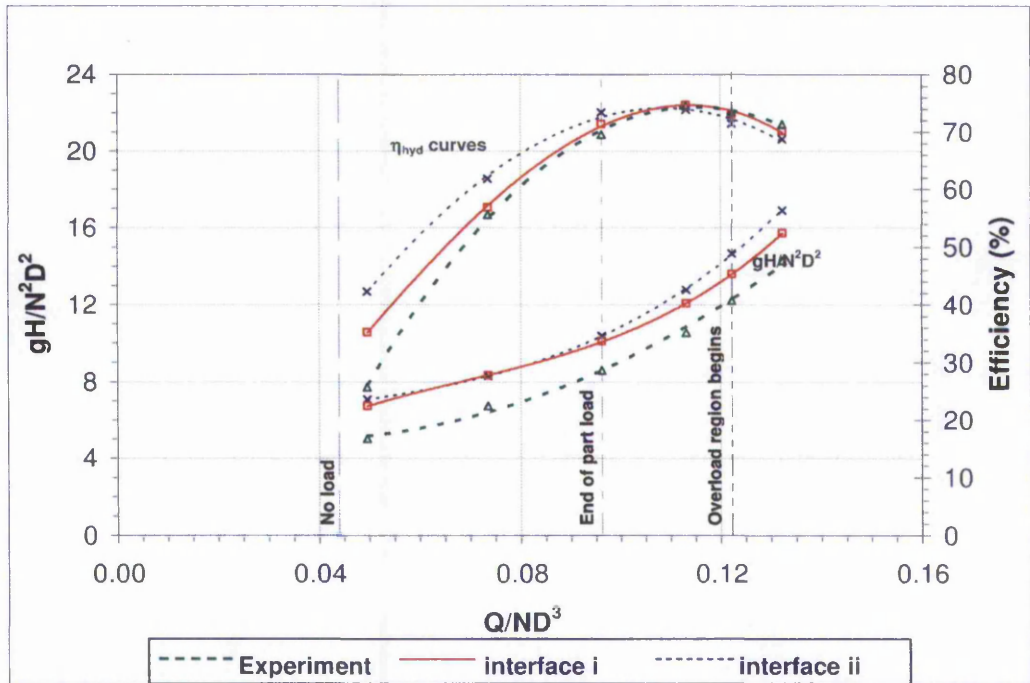
Figure 5.13 - Percent change

Load Point	Q/ND ³	Power Improvement %	Head Reduction %	Actual Efficiency Rise %
Overload	0.132	1.56	-1.59	-0.02
Overload	0.122	1.37	-1.74	-0.26
BEP	0.113	1.40	-1.59	-0.14
Part-load	0.096	1.45	0.02	1.05
Part-load	0.074	1.79	0.08	1.06
Part-load	0.050	18.23	-0.89	6.04

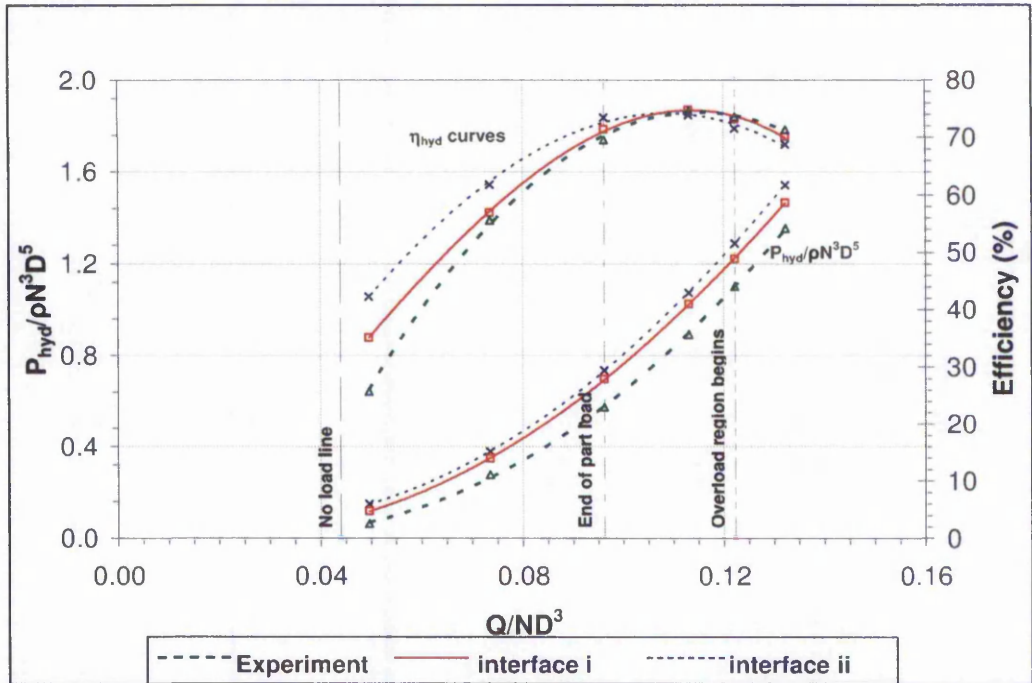
Table 5.2 - Percent change

5.4.2 Comparison between interface-*i* and interface-*iii*

Interface-*iii* only models the front-shroud and back-shroud leading edge thicknesses but does not model the churning region. The dimensionless characteristics for interface-*iii* are plotted against those of interface-*i* in [Figure 5.14](#). There are two trends for the head number, whereby in the part-load region it is almost entirely similar to that for interface-*i*. In the BEP and overload region however there is a significant increase of the head number for interface-*iii*. There is an increase in power production throughout the entire operating range with slightly higher values for the BEP and overload regions. The combined effect of unchanged head and increase in power number in the part-load region results in an efficiency rise. Conversely the substantial increase in head number in the BEP and overload region produces an efficiency drop.



(a)



(b)

Figure 5.14 - Dimensionless characteristics comparing Efficiency and change in
 (a) Head number (b) Power Number

The percentage differences are plotted in [Figure 5.15](#) and summarised in [Table 5.3](#). The head change curve is negative for most of the operating range. The only head number reduction is of 0.32% whilst the highest head number increase is of 7.92%. The power number curve on the other hand is positive throughout the entire operating range. It drops from a maximum power number of 26.23% but maintains an average power gain of around 5% for the remaining operating points.

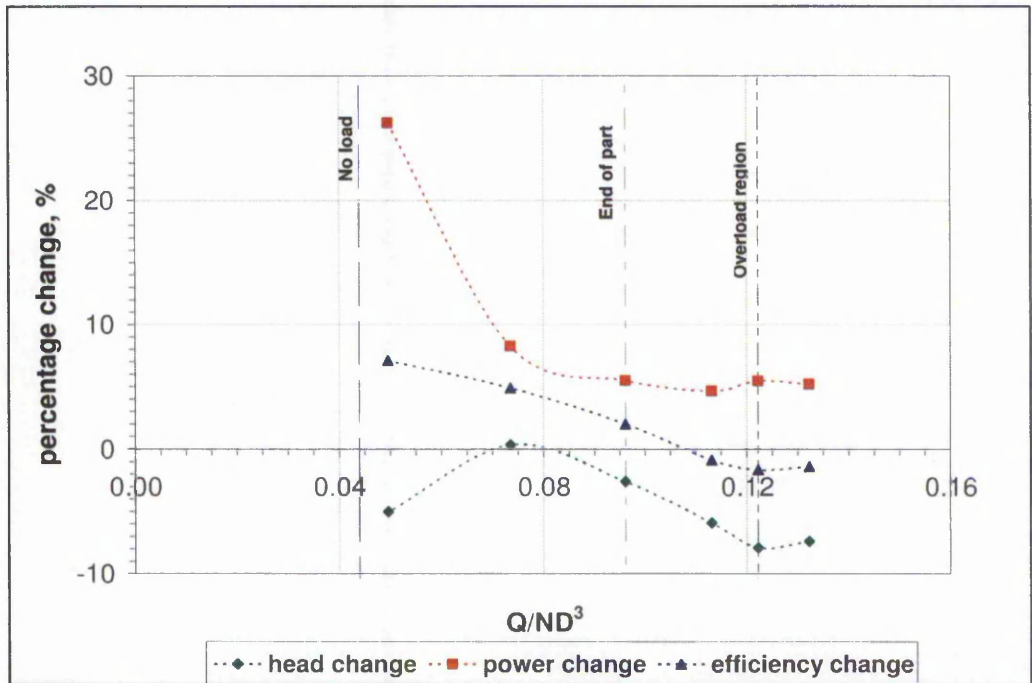


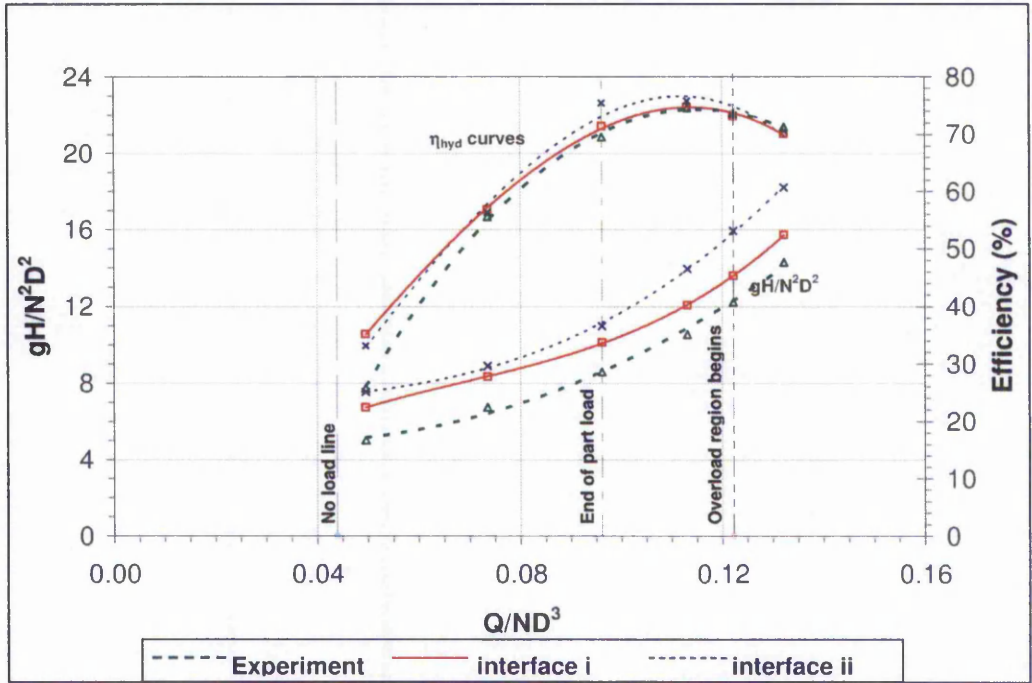
Figure 5.15 - Percentage change

Load Point	Q/ND ³	Power improvement %	Head Reduction %	Actual Efficiency Rise %
Overload	0.132	5.21	-7.39	-1.43
Overload	0.122	5.47	-7.92	-1.67
BEP	0.113	4.68	-5.92	-0.88
Part-load	0.096	5.49	-2.60	2.01
Part-load	0.074	8.26	0.32	4.89
Part-load	0.050	26.23	-5.04	7.10

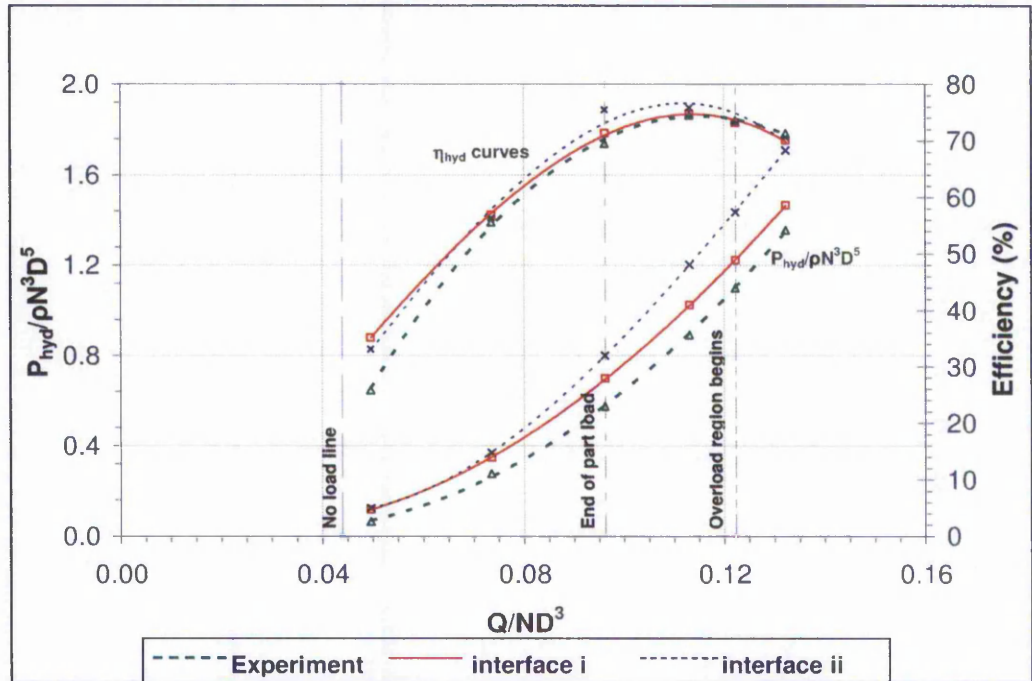
Table 5.3 – Percentage change

5.4.3 Interface-*i* and interface-*iv*

Interface-*iv* is the simplest interface model whereby neither the front-shroud or back-shroud thicknesses nor the churning region is modelled. Figure 5.16 summarises the dimensionless characteristics for interface-*iv* against those of interface-*i*. The head number for interface-*iv* has increased throughout the entire operating range and is more substantial in the main operating region. The power production in the low operating region is similar to that for interface-*i* but increases towards the higher operating flows, being quite significant in the BEP and overload regions. The significant increase in power production compensates for the increase in head number thus resulting in an efficiency rise in the main operating region.



(a)



(b)

Figure 5.16 - Dimensionless characteristics comparing Efficiency and change in
 (a) Head number (b) Power Number

The percentage analysis in [Figure 5.17](#) shows that the head number is negative throughout the operating range for interface-iv. In the part-load region it suffers a maximum increase of 11.98% whilst in the BEP and overload region this becomes even more significant with 15.62% and 17.07% respectively. The power number displays an increase throughout the entire operating range but becomes more significant in the BEP and overload regions where it achieves a maximum improvement of 17.33% and 17.44% respectively. The efficiency rise is only significant for the discharge number of 0.096 at the end of part-load region where it achieves a 4.05%.

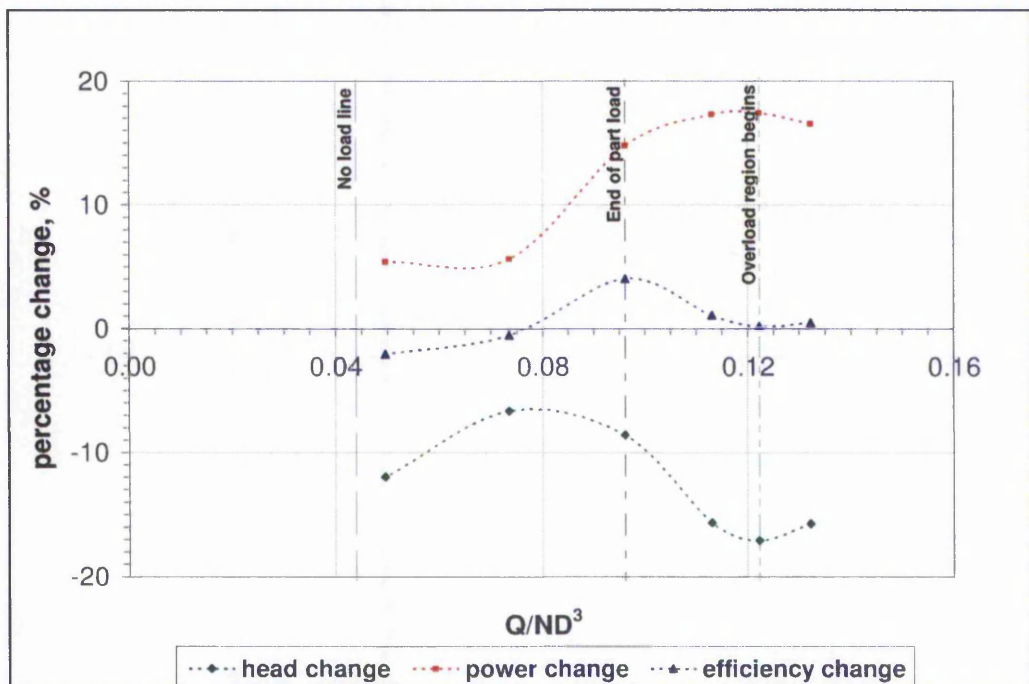


[Figure 5.17](#) - Percent change

Load Point	Q/ND ³	Power Improvement %	Head Reduction %	Efficiency Rise %
Overload	0.132	16.56	-15.72	0.49
Overload	0.122	17.44	-17.07	0.20
BEP	0.113	17.33	-15.62	1.07
Part-load	0.096	14.80	-8.58	4.05
Part-load	0.074	5.64	-6.64	-0.56
Part-load	0.050	5.41	-11.98	-2.08

[Table 5.4](#) - Summary of dimensionless characteristics

5.4.4 Hydraulic Losses

This section describes the behaviour of losses within each flow zone for the different PAT interface models through the use of graphical representation. Supporting and corresponding tables and description can also be found in [Appendix A](#).

For ease of explanation, the losses in each flow zone are generally explained relatively to the losses of the PAT model with interface-*i*, since this geometrical set up, out of the four interface modelled, is the closest representation to the physical model.

5.4.4.1 Flow Zone-*i*

[Figure 5.18](#) shows the hydraulic losses for each of the interfaces in zone-*i*. Between the no-load and mid part-load region the losses for interface-*ii* are lower than those for interface-*i*. Beyond the mid part-load region and up to the end of BEP region the losses for the PAT model with interface-*ii* are similar to the interface-*i* losses. In the overload region the losses of interface-*ii* start to increase above the interface-*i* losses with rising flow rate. A more distinctive increase in loss is noticed with the PAT model with interface-*iii* for the entire operating range, with the exception of a single operating point in the part-load region, where the loss margin with interface-*i* is not significant. The loss for the model with interface-*iv* is the most significant in comparison with the other interface models, particularly in the main operating region. It is only lower than both interface-*i* and interface-*iii* losses near the no-load line and lower than interface-*iii* loss in the overload region. Overall the loss curves maintain a similar trend for all the modelled interfaces with interface-*iv* having the highest losses.

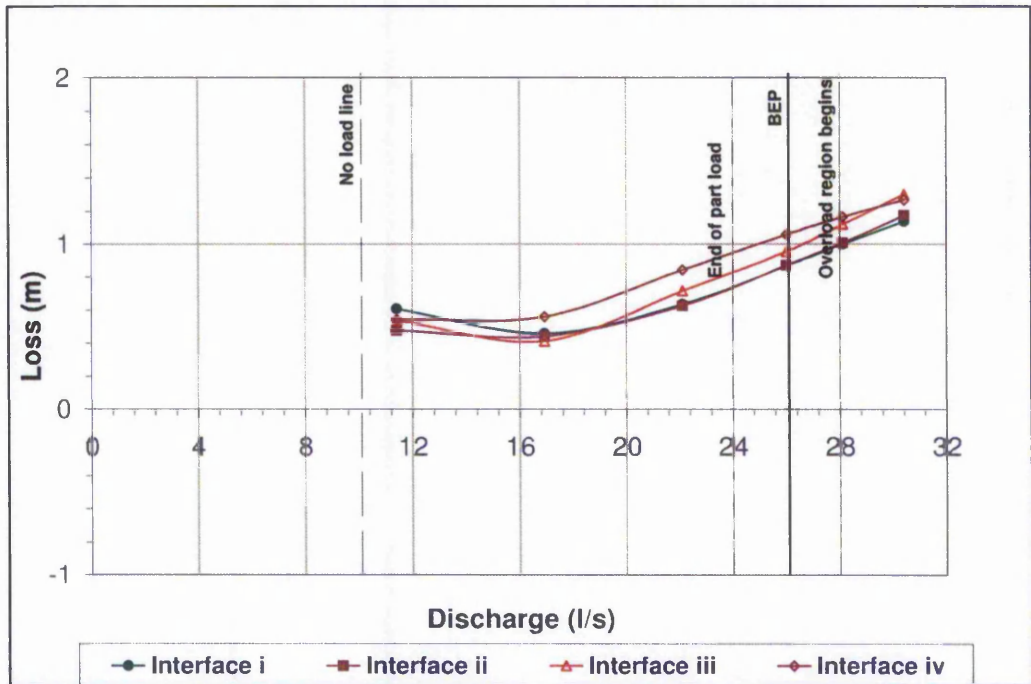


Figure 5.18 - Losses in Zone-*i* – Interface Study

5.4.4.2 Flow zone-*ii*

Various loss trends are observed in zone-*ii* for the different interface PAT models. Throughout the entire operating region both the interface-*ii* and interface-*iii* PAT models display decrease in losses when compared to interface-*i*, with interface-*iii* displaying the lowest losses throughout the entire operating range. Interface-*iv* displays a completely different curve trend to that of the other interface models, whereby the losses are high in the no-load to mid part-load region and progressively decrease towards the overload region becoming the lowest losses compared to the other interface models.

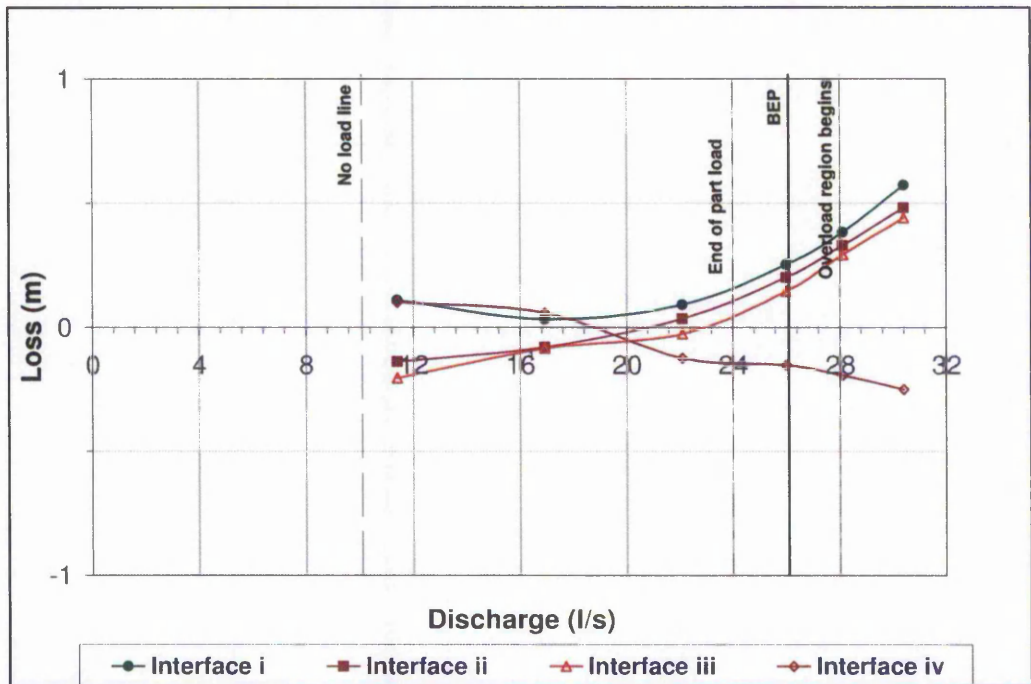


Figure 5.19 - Losses in zone-ii – Interface Study

Zone-ii is the actual region where the geometrical modelling of different interface set up is carried out. Therefore the visible loss variations (and curve dissimilarities) of each interface was expected. On the other hand the curve trends for interface-i, interface-ii, and interface-iii, display quite similar behaviour albeit with large loss discrepancies. The loss trend for interface-iv however is completely distinct in comparison to the loss trends of the other models. This suggests that the flow has been significantly compromised due to the radical simplification of geometry within this region.

The relative contribution of losses in zone-ii to the overall losses is comparatively small to the losses in the other zones. The different loss behaviours for each of the interfaces have clearly demonstrated that accurate geometry modelling within this region is crucial for realistic hydraulic predictions.

5.4.4.3 Flow Zone-iii.iv.v

In zone-iii.iv.v, all interface models have predicted similar loss trends as shown in Figure 5.20. Interface-i and interface-ii display very similar loss values throughout the entire operating region with interface-ii in a few operating points predicting marginally higher losses. The losses for the model with interface-iii are lower in comparison with the losses of interface-iv but at the same time these are

consistently higher than the losses of interface-*i* and interface-*ii*. It can be clearly noticed that the highest losses is displayed by the PAT model with interface-*iv*, particularly in the main operating region.

It is evident that the losses within zone-*iii.iv.v* contribute significantly to the overall losses of the PAT. The interface study has shown that the geometry representation of zone-*ii* in a computational set up is critical to obtain valuable PAT flow predictions.

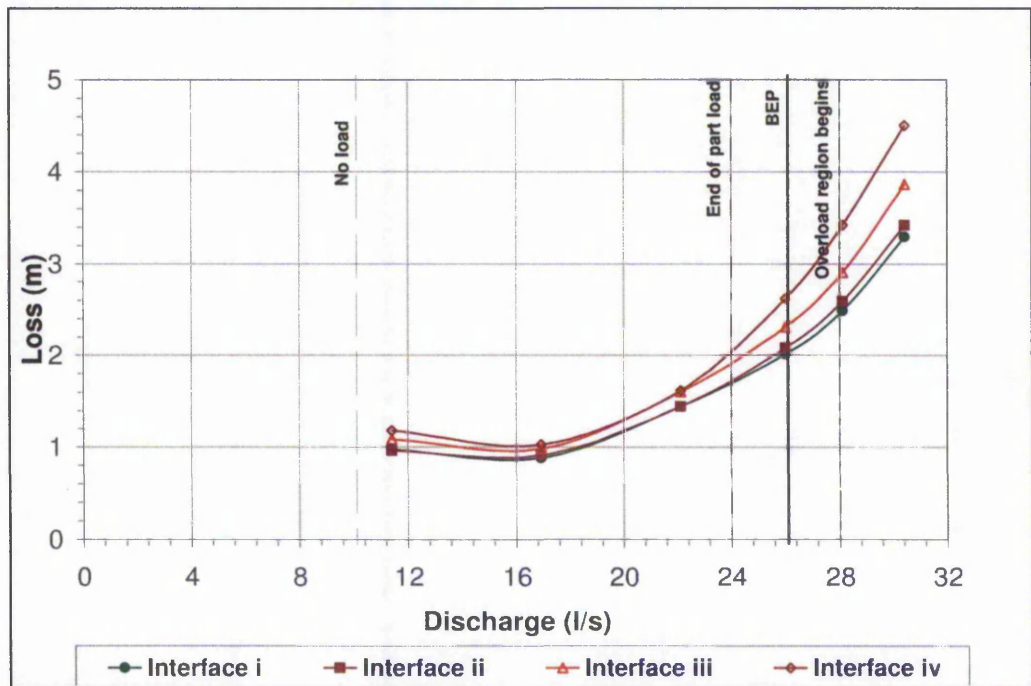


Figure 5.20 - Losses in zone-*iii.iv.v* – Interface Study

5.4.4.4 Flow zone-*vi*

As [Figure 5.21](#) shows, flow zone-*vi* is the only region where interface-*i* and interface-*ii* have displayed a more significant loss discrepancy which occurs in the part-load and up to the BEP. The interface-*ii* losses are lower than those of interface-*i* in the part load region however with increasing flow rate the loss difference reduces, with the difference becoming negligible beyond the BE. The losses in interface-*iii* displays good similarity with the losses of interface-*ii* between the no-load and end of part load region, thereafter it increases. The losses for the PAT model with interface-*iv* are distinct from the losses of the other interfaces. They start off the same as the losses for interface-*i* model up to mid part-load region and steep further to come to a similar loss value of interface-*i* at

BEP. Thereafter the losses increase significantly compared to the other losses.

The losses in zone-*vi* have a smaller contribution to the total losses of the PAT, particularly in the main operating region. Overall the loss behaviour for the PAT model with interface-*iv* has been the most distinct.

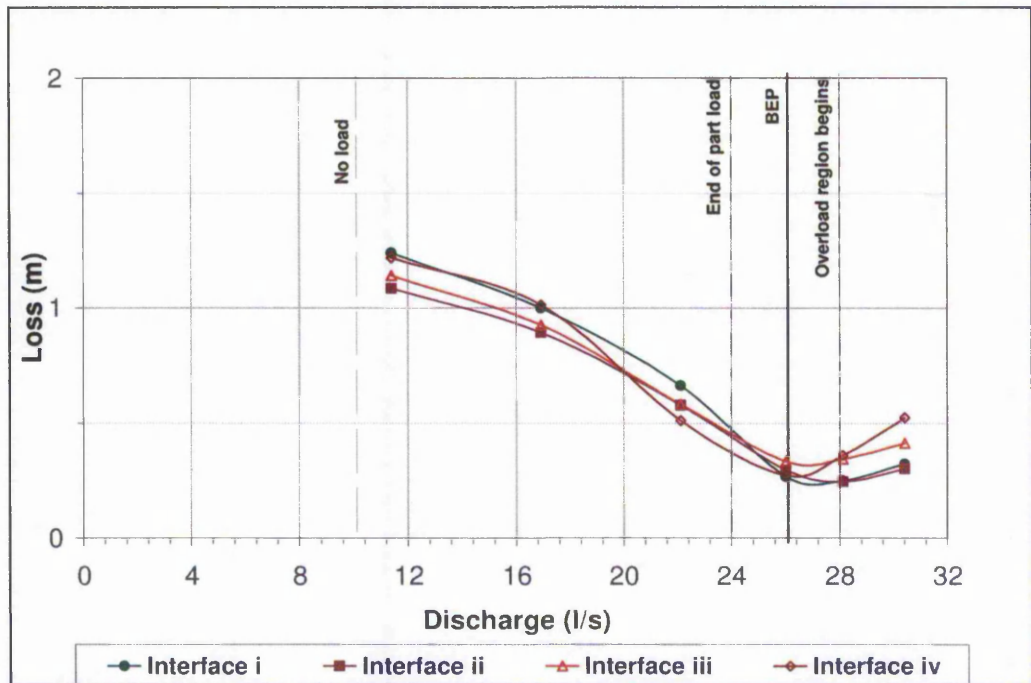


Figure 5.21 - Losses in zone-*vi* – Interface Study

5.4.4.5 Flow zone-*vii*

Observations within flow zone-*vii* show that there are two distinctive behaviours of the hydraulic losses for the studied interfaces, one for interface-*i* and interface-*ii* and another for interfaces *iii* and *iv*. In the part-load region the loss curves for interface-*iii* and *iv* are decreasing almost linearly whereas the curves for interface-*i* and interface-*ii* possess a more prominent bend. All simulated interfaces display similar losses between the BEP and up to the last overload point.

With regards to the loss discrepancies, interface-*i* and interface-*ii* display almost identical losses throughout the entire operating region. The losses for interface-*iii* are lower than those of interface-*i* in the part-load region and increase marginally beyond the BEP. The loss for the PAT with interface-*iv* is higher than those for interface-*i* within the no-load to mid part-load region. Beyond mid part-load point

with increasing flow, these losses become lower than the loss for the interface-*i*. Thereafter the loss difference for interface-*iv* becomes almost negligible.

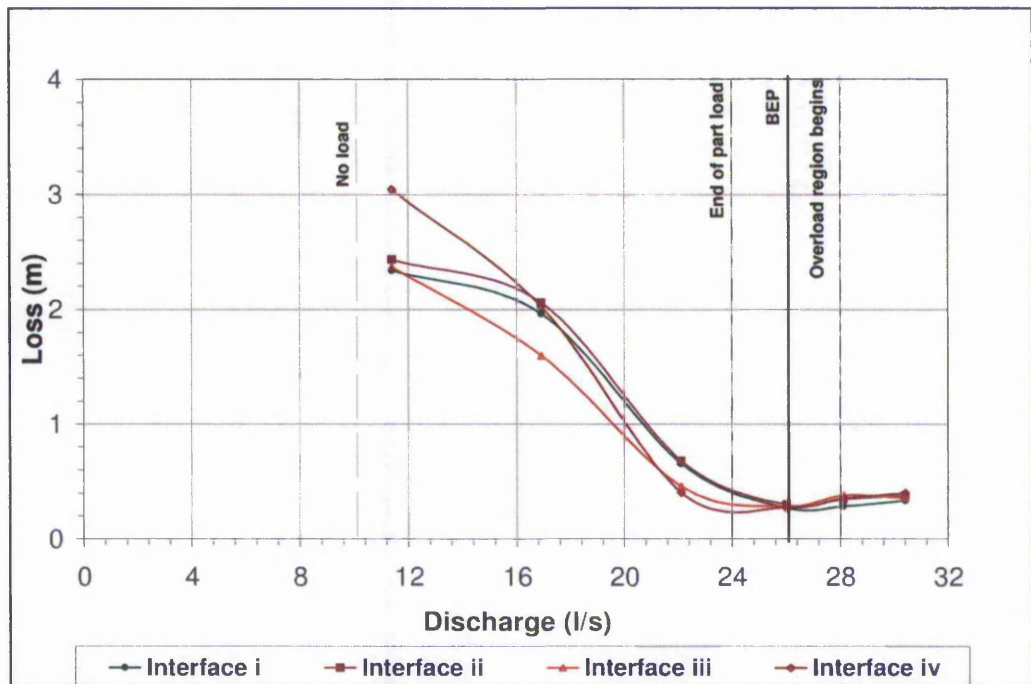


Figure 5.22 - Losses in zone-*vii* – Interface Study

5.4.4.6 Combined Flow Zone losses

An overall comparison of the losses within each zone shows that interface-*i* and interface-*ii* consistently display the most similar loss behaviour throughout the entire operating range, albeit with some marginal discrepancies in the magnitude of losses. Interface-*iii* also displays similar yet 'weaker' curve trends in most zones but also displays a larger loss discrepancy when compared to interface-*i* and interface-*ii*. Finally, the loss curve-trends for the PAT modelled with interface-*iv* are only similar to the other interfaces in zone-*i* and zone-*iii.iv.v*. The behaviour of losses in zone-*ii* and zone-*vi* suggest that hydraulic flow behaviour within the machine has changed compared to the other models.

The combined losses of all zones for all the interfaces are plotted in [Figure 5.23](#). It can be seen that interface-*i* and interface-*ii* display similar overall losses apart from a small operating range between the no-load and mid part-load. The overall losses for these interfaces are the lowest in the main operating region. Interface-*iii* displays the lowest overall losses in the part-load region whilst interface-*iv* shows the highest losses within this same operating range.

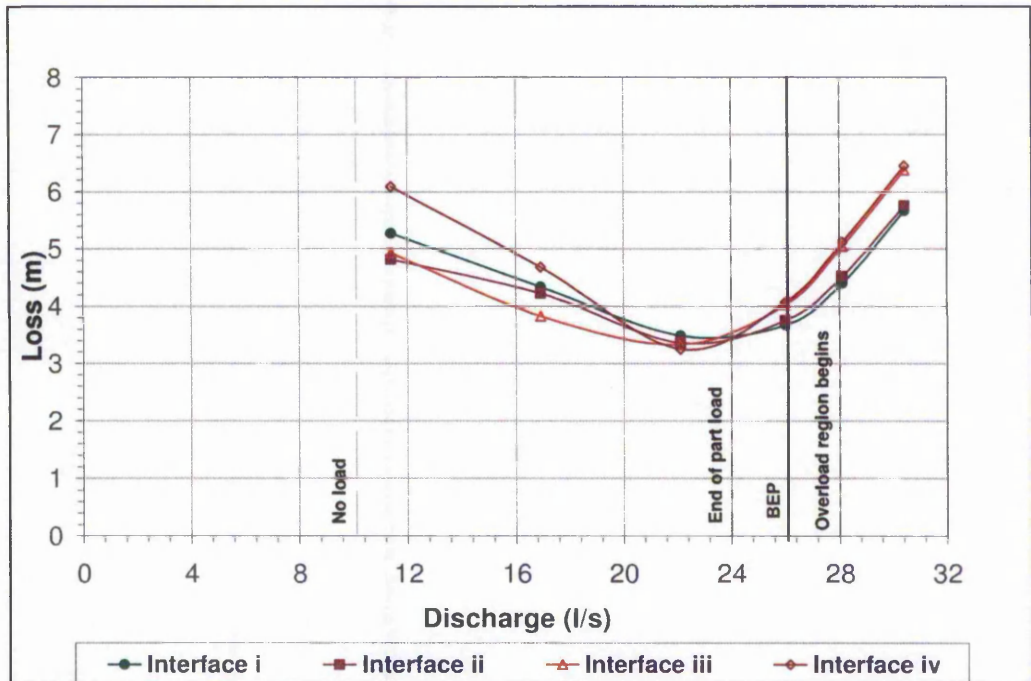


Figure 5.23 - Combined zone losses – Interface Study

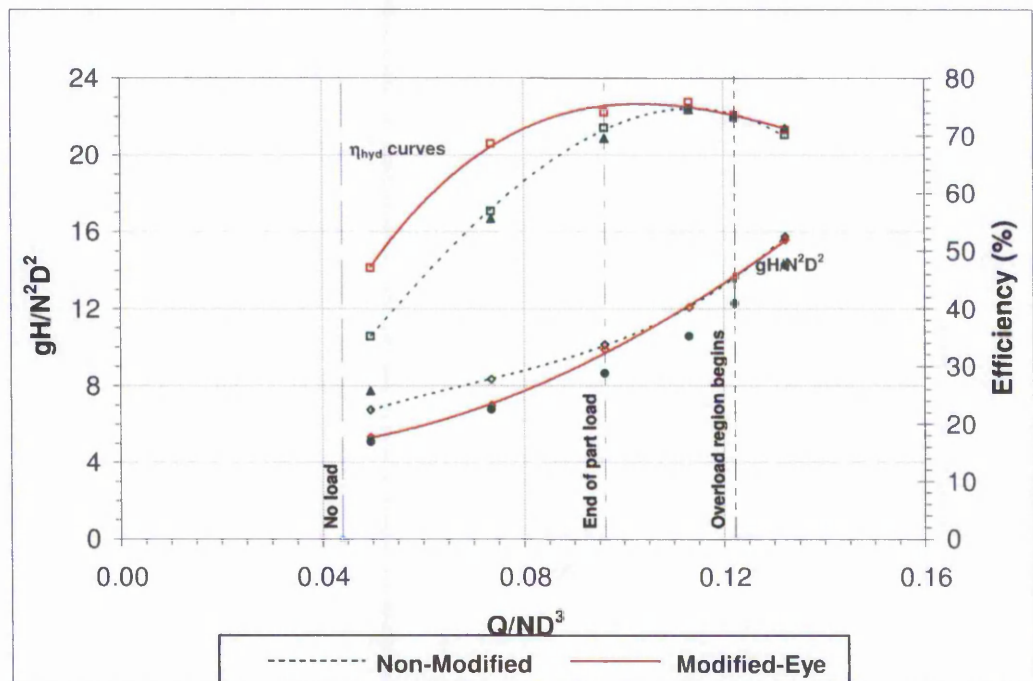
5.4.5 General overview of interface study

The results of the PAT model using interface-*i* has shown that this model favourably compares with the experimental data as shown in [section 5.2](#), with efficiency match from mid part-load region to overload region. The head number and power number curves are higher than experimental but retains similar profiles particularly in the main operating region. The comparison of interface-*ii* against interface-*i* has shown very little difference in terms of head number, power number, and flow zone losses. The comparisons of interface-*iii* against interface-*i* has shown that there is an increase in power number throughout the whole operating region, whilst the head number is similar in the part-load region and higher from BEP and with increasing flow rate. The loss difference for interface-*iii* tends to be higher for certain zones. The comparison of interface-*iv* against interface-*i* has shown that both the head number and power number are higher with both curves possessing different profiles in comparison with the experimental data. Generally the analysis of all parameters shows that interface-*iv* does not retain the characteristic behaviour of head number, power number, and loss in comparison with the other interface models.

5.5 Optimization of Internal Hydraulics Using CFD

5.5.1 Modification-*i* - Impeller eye enlargement

This geometrical modification consists of the enlargement of the impeller eye region and draft-tube inlet diameter. This increase of diameter is maintained constant throughout the length of the draft-tube. The effects of the modified eye region are shown in the dimensionless plots in [Figure 5.24](#). It is found that the head number drops significantly below that of the non-modified. This is mainly evidenced in the whole of the part-load region and only partially in the BEP region where it actually increases slightly over the non-modified head number. At the last operating point ($\Phi = 0.132$) the drop in head number is re-established albeit marginally. However, further operating points in the overload region were not modelled to verify whether this trend would be maintained. The power characteristics for the modified eye only marginally increase above that of the non-modified PAT, this difference is almost unnoticeable particularly in the part-load region, hence resulting in very similar curve profiles without any distinct differences. The resulting efficiency for the modified-eye shows a considerable increase in the part-load region. This increase in efficiency is coming largely from the drop in head number. In the best efficiency and overload region the efficiency curve maintains marginally above, only noticeable by the plot points. After the BEP point the contribution is essentially from the slight power increase, and beyond this point it is due to both head drop and power increase.



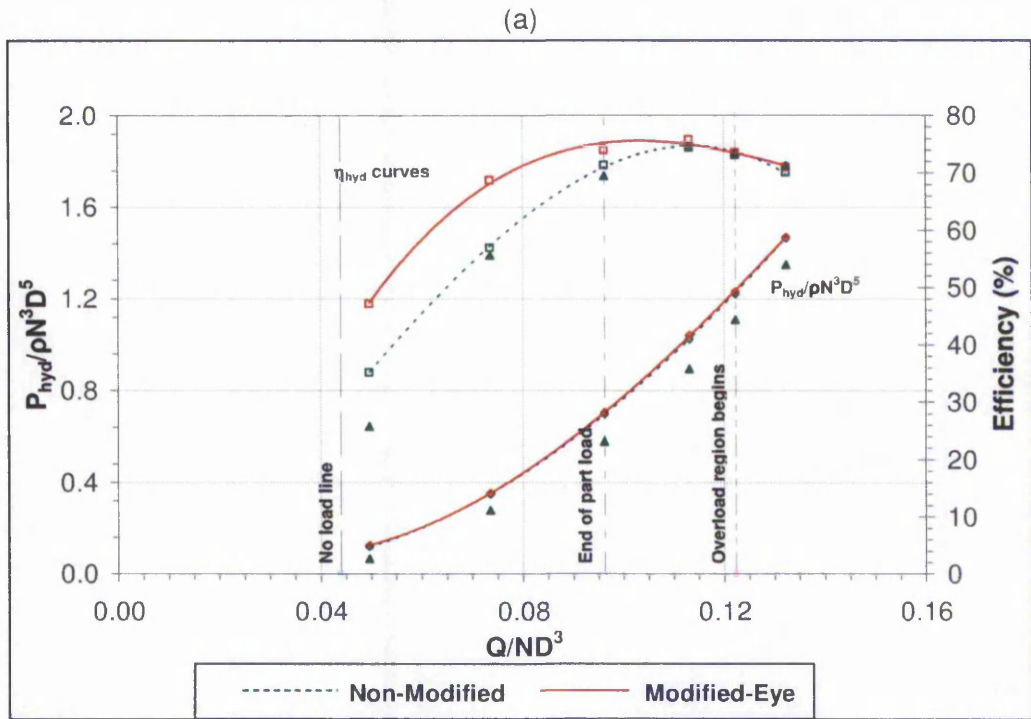


Figure 5.24 - Dimensionless characteristics comparing Efficiency and change in
 (a) Head number (b) Power Number

From the percentage analysis plot in [Figure 5.25](#) a clearer picture can be obtained of the effects of the modification on head number, power number, and efficiency. The relative influences are also summarised in [Table 5.5](#). For most of the part-load region the head number for the modified PAT benefits from a head reduction going from a maximum of 20.95% to a minimum of 2.5%. In the BEP region the head number for the modified PAT increases by 0.30% at the discharge number of 0.122. In the overload region the head reduction is re-established by 0.93%. The power generation is increased marginally from a maximum of 5.84% occurring in the part-load region dropping to a minimum 0.31% improvement in the overload region. The power number maintains positive throughout the computed operating range. The increase in efficiency is significant in the part-load region owing to both the considerable reduction in head and the slight improvement in power. The efficiency change curve shows that there is an efficiency rise throughout the entire operating range for the modified PAT. The minimum efficiency rise of 0.42% occurs at the corresponding flow number of 0.122 whilst the maximum of 11.92% occurs at the discharge number of 0.050.

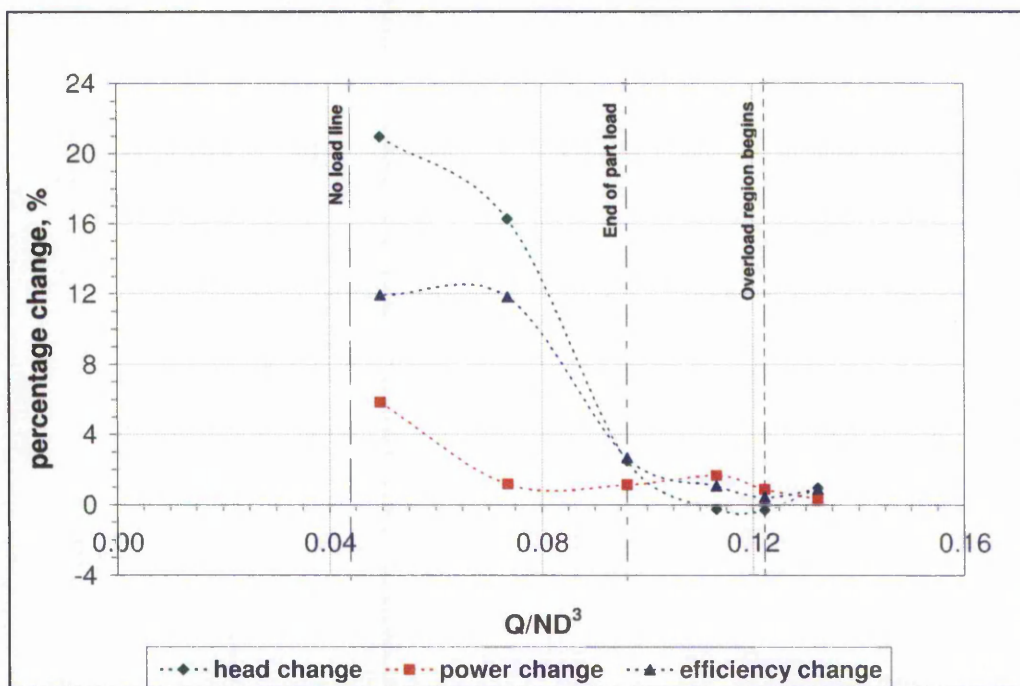


Figure 5.25 - Percentage contributions of power and head to change in efficiency

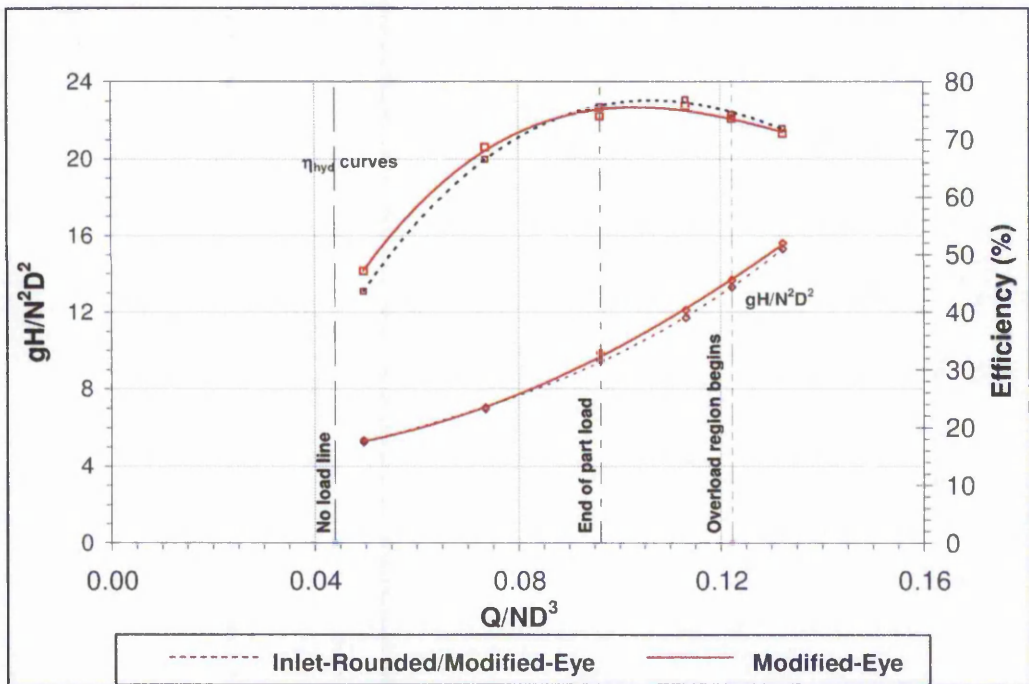
Load Point	Q/ND ³	Power improvement %	Head Reduction %	Efficiency Rise %
Overload	0.132	0.31	0.93	0.88
Overload	0.122	0.88	-0.30	0.42
BEP	0.113	1.66	-0.25	1.05
Part-load	0.096	1.14	2.50	2.67
Part-load	0.074	1.16	16.27	11.83
Part-load	0.050	5.84	20.95	11.92

Table 5.5 - Summary of relative study at each operating region

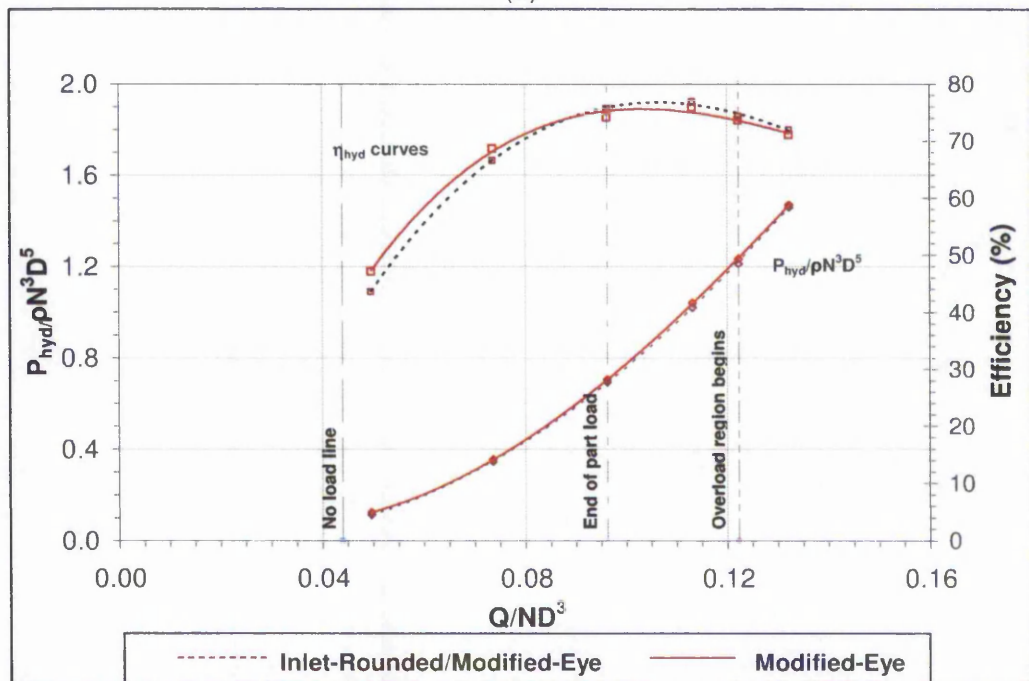
5.5.2 Modification-ii - Modified-Eye with Inlet Rounding

This modification consisted of rounding the blade, front-shroud, and back-shroud edges at the leading edge. The comparison of the characteristics is made in [Figure 5.26](#). Within the part-load region there is practically no head reduction and the two characteristics overlap. However, towards the best efficiency and overload regions there is a considerable drop in the head number for the inlet-rounded PAT. The power number curve for the inlet-rounding displays a marginal decrease in power production throughout the entire operating range. The combined effect of unchanged head number and decrease in power production in the part-load region results in a decrease in efficiency for the inlet-rounded PAT. This scenario is changed towards the main operating region due to the reduction

in head number. This makes the power production the sole contributor for the decrease in efficiency in the part-load region.



(a)



(b)

Figure 5.26 - Dimensionless characteristics comparing Efficiency and change in
(a) Head number (b) Power Number

The effects of the modifications can be better understood by analysing the individual characteristics as shown in [Figure 5.27](#). The percentage head change curve displays a varied trend. In the part load region it can be seen that there is a decrease of 0.74% in head occurring at the discharge number of 0.074. The most significant head reduction occurs within the best efficiency region where a 3.78% head reduction is achieved. The power change curve shows no improvement throughout the entire operating range for the inlet-rounded PAT. The highest power drop of 9.43% occurs in the part load region and the lowest drop of 0.68% in the overload region.

The rise in efficiency is only witnessed in the main operating region. The contribution to efficiency rise is solely coming from the head reduction as there is no power improvement throughout the entire operating range. The relative contributions to head rise from the head and the power are summarised in [Table 5.6](#).

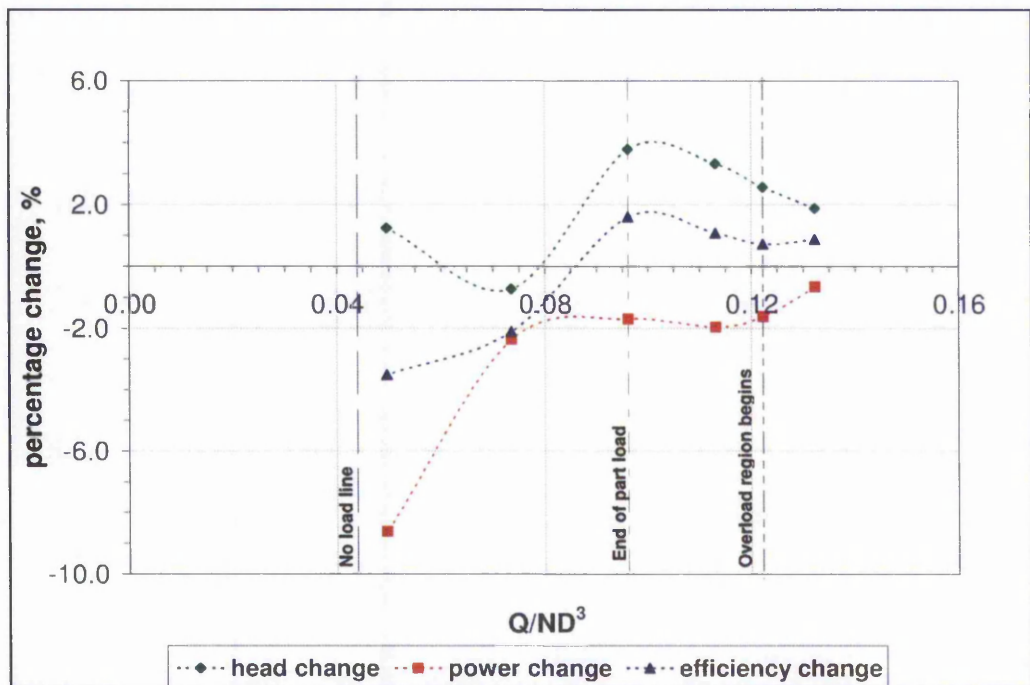


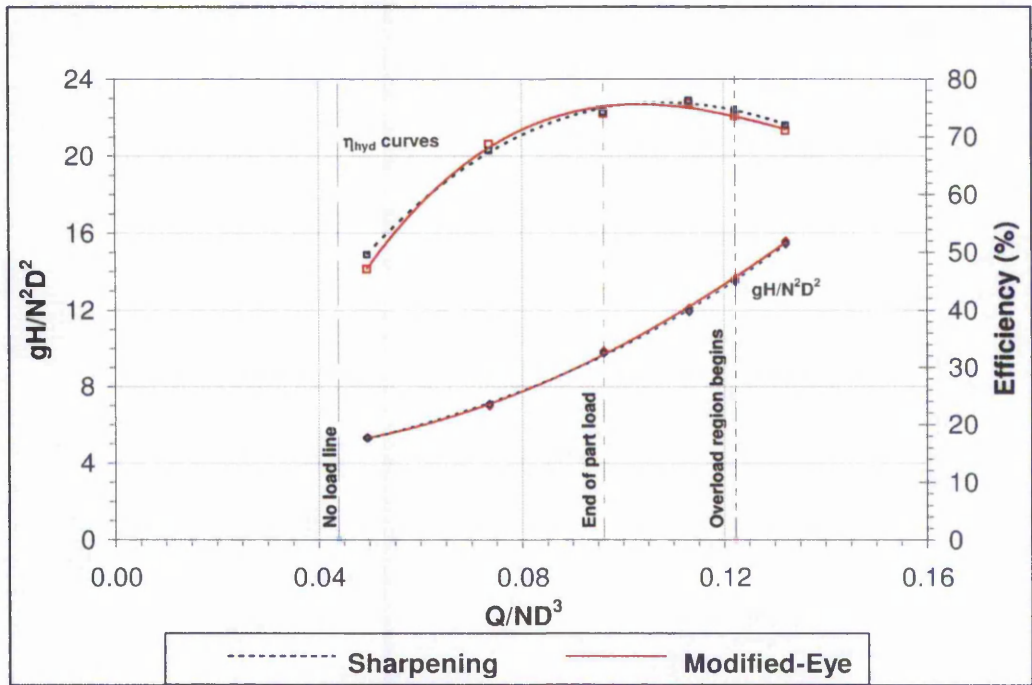
[Figure 5.27](#) - Percent change

Load Point	Q/ND3	Power improvement %	Head Reduction %	Efficiency Rise %
Overload	0.132	-0.68	1.88	0.87
Overload	0.122	-1.65	2.57	0.71
BEP	0.113	-2.00	3.32	1.06
Part-load	0.096	-1.73	3.78	1.60
Part-load	0.074	-2.42	-0.74	-2.11
Part-load	0.050	-9.43	1.24	-3.52

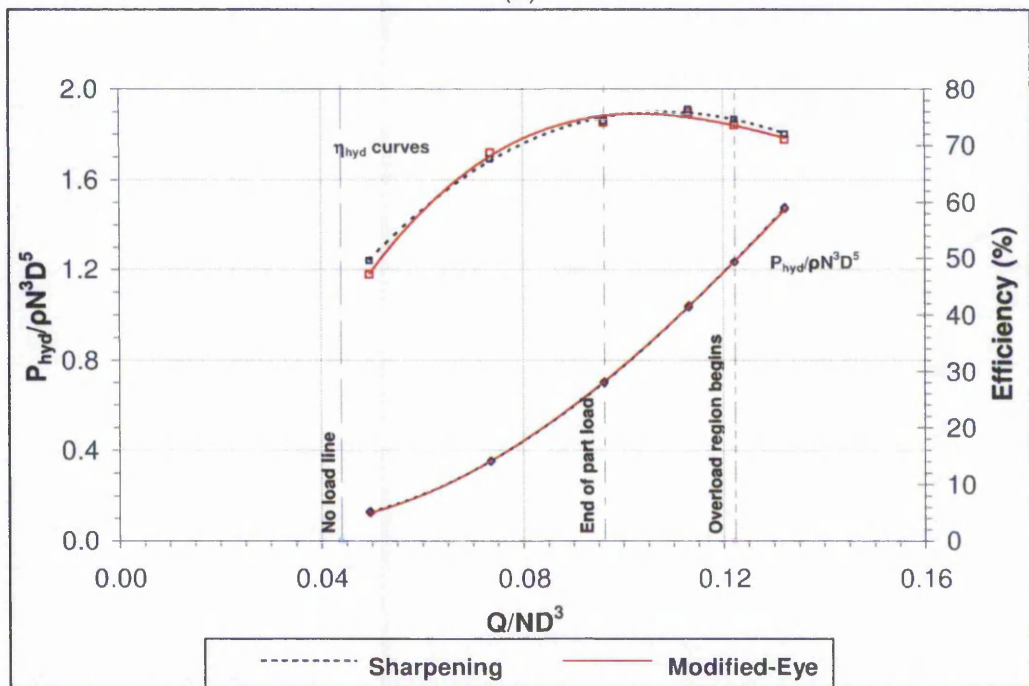
Table 5.6 - Percent change

5.5.3 Modification-III - Modified-Eye with Front-shroud/Shroud outside sharpening

The modification on the PAT comprises of removing material from the outer edges of both front-shroud and back-shroud at the leading edge. This has the effect of increasing the axial clearance between impeller and churning region. Figure 5.28 summarises the dimensionless characteristics for this modification procedure. The head number curves practically show any difference within the entire part-load region. However within the best efficiency and overload condition there is marginal reduction in head for the outside-sharpened PAT. Similarly for the power number it is seen that there is no increase in power production where the two characteristics overlap and maintain the same trend. The joint contribution of power and head to the efficiency changes is difficult to establish within the part-load region, however in the main operating region it is visible that the efficiency rise is due to the reduction in power.



(a)



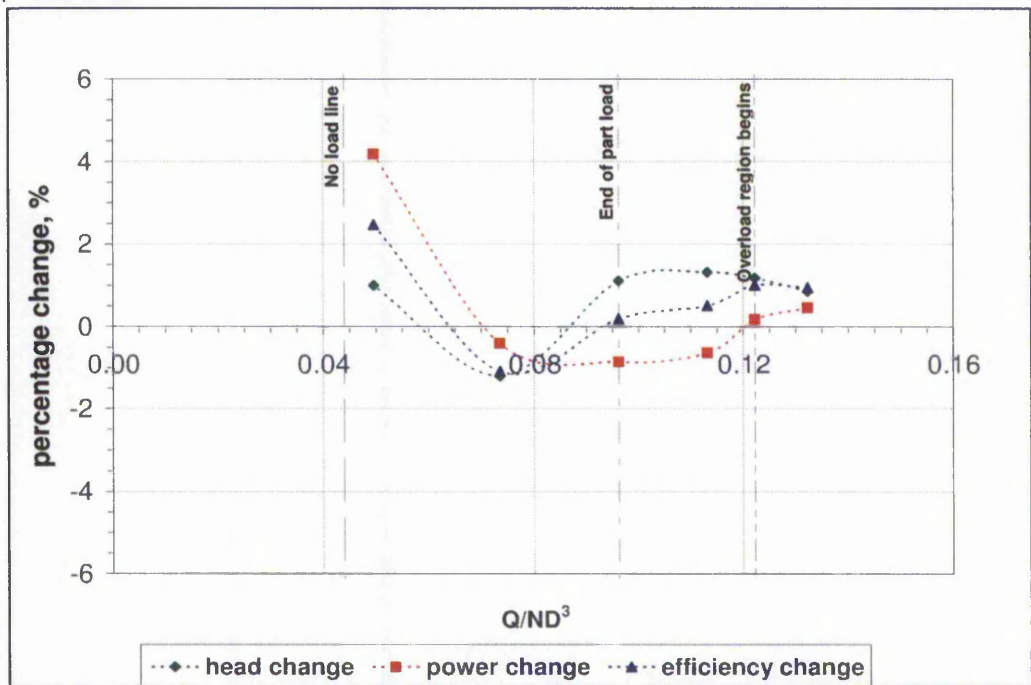
(b)

Figure 5.28 - Dimensionless characteristics comparing Efficiency and change in
(a) Head number (b) Power Number

The percentage analysis plot in Figure 5.29 gives a better indication of the relative contribution of head and power number to the efficiency rise. The head

number curve profile resembles to that seen in [Figure 5.26](#) for the inlet-rounded procedure, with a head rise of 1.21% occurring at the same discharge number of 0.074. Power improvement is only seen near the no-load region and at the start of the overload region. However the efficiency rises for most of the operating points apart from the single discharge number of 0.074.

The observed improvements due to modifications are relatively small and are not necessarily definite as indicated by the results, since there is uncertainty in both CFD and experimental findings. The only distinct and also significant improvement shown has been in the part-load region for the modified-eye procedure.



[Figure 5.29](#) - Percent change

Load Point	Q/ND ³	Power Improvement %	Head Reduction %	Efficiency Rise %
Overload	0.132	0.454	0.855	0.938
Overload	0.122	0.171	1.172	1.001
BEP	0.113	-0.642	1.308	0.512
Part-load	0.096	-0.858	1.106	0.186
Part-load	0.074	-0.403	-1.207	-1.092
Part-load	0.050	4.185	0.994	2.464

[Table 5.7](#) - Percent change

5.5.4 Hydraulic Losses

The effect of the geometrical modifications can be better understood by analysing the individual losses in each flow zone. In the following sections the comparison of the modifications are generally made against the non-modified geometry. Experimental data was not available for this study and therefore a comparative study was not possible.

5.5.4.1 Flow zone-i

The losses within zone-*i* plotted in [Figure 5.30](#) show similar curve trends for all the compared geometries. The only distinct difference is noticed for the non-modified PAT whereby there is a slight difference in the no-load point, mid part-load point, and overload region which suggests that none of the modifications have improved or affected the losses in zone-*i*.

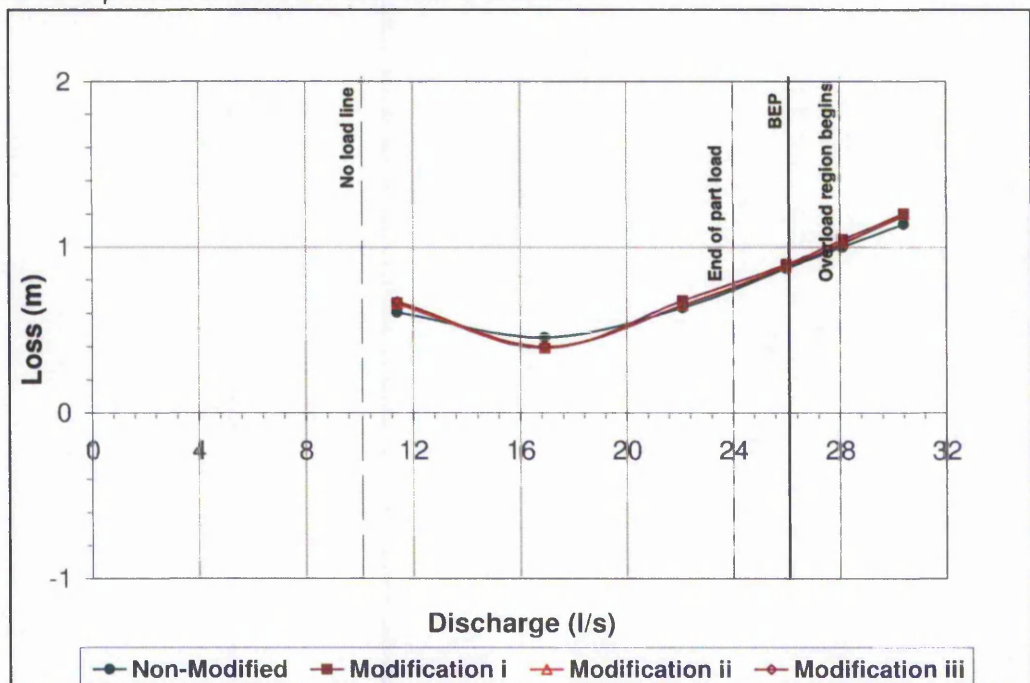


Figure 5.30 - Losses in zone-*i* – Modification Study

5.5.4.2 Flow zone-ii

Again in flow zone-*ii* the curves shown in [Figure 5.31](#), display similar trends but there are distinct differences in the hydraulic losses for each geometry. In the no-load to mid part-load the losses are relatively similar, however beyond this point the losses for modification-*i* and modification-*ii* in flow zone-*ii* actually increase

compared to the losses of the non-modified PAT. Modification-*iii* which consists of the outside chamfer of the front and back-shrouds displays similar losses to that of the non-modified PAT in flow zone-*ii*. Therefore none of the modification procedures have any positive effects on the losses within zone-*ii*.

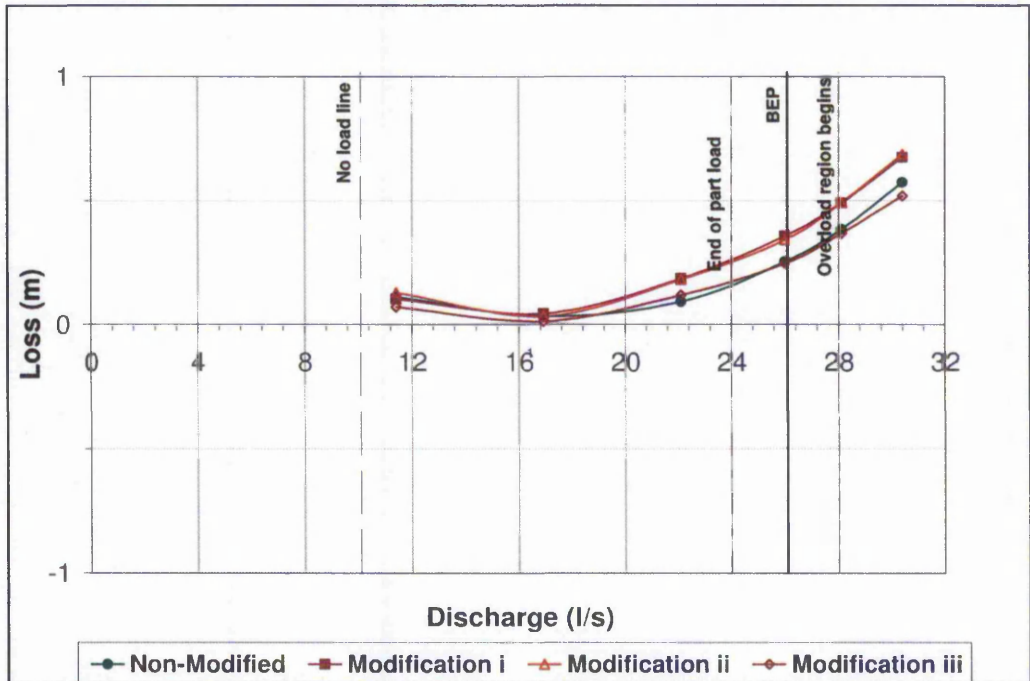


Figure 5.31 - Losses in zone-*ii* – Modification Study

5.5.4.3 Flow zone-*iii.iv.v*

Figure 5.32 shows the losses in flow zone-*iii.iv.v*. It can clearly be seen that modification-*i* is the only modification procedure that is able to improve the losses within zone-*iii.iv.v*. This occurs in the main operating region. Modification-*i* and modification-*ii* procedures do not display an improvement in the losses within this zone. The curve trends are similar throughout the entire operating range and only negligible loss difference is observed.

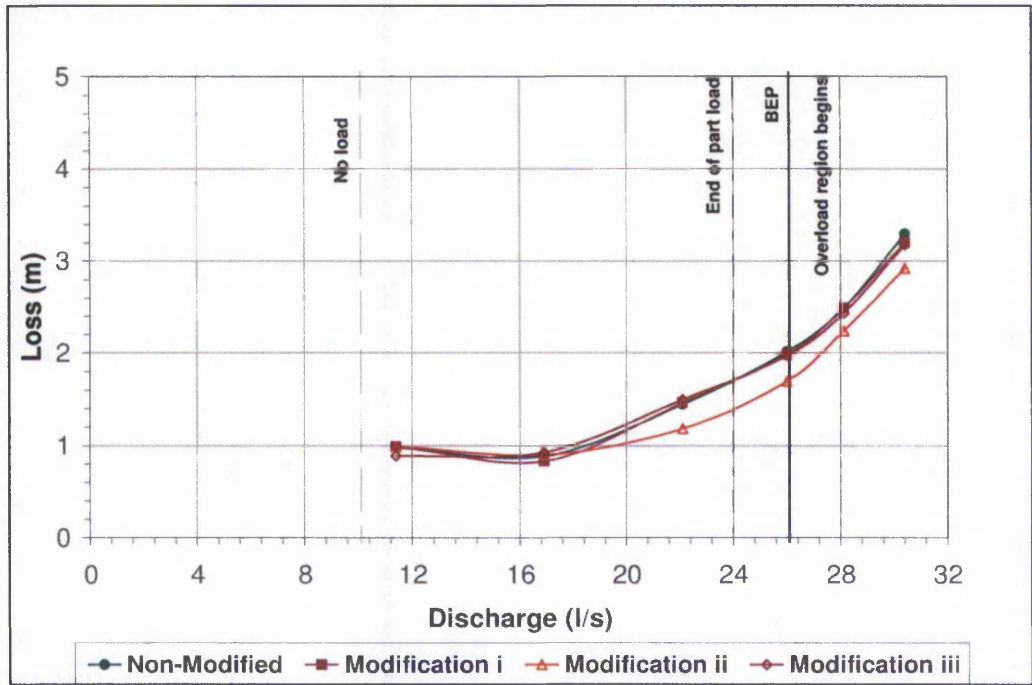


Figure 5.32 - losses in zone-iii.iv.v – Modification Study

5.5.4.4 Flow zone-vi

Figure 5.33 shows the losses in zone-vi. There is a clear improvement of the losses within flow zone-vi as a result of the enlargement of impeller eye and casing eye (modification-i). Both modification-ii and modification-iii also benefit from the same geometrical modification and therefore display similar loss behaviour as modification-i. In the BEP region the losses are slightly higher for the PAT with modification-ii. The overall contribution of the losses within flow zone-vi for the non-modified geometry is high therefore the modifications have shown a good improvement, particularly in the part-load region.

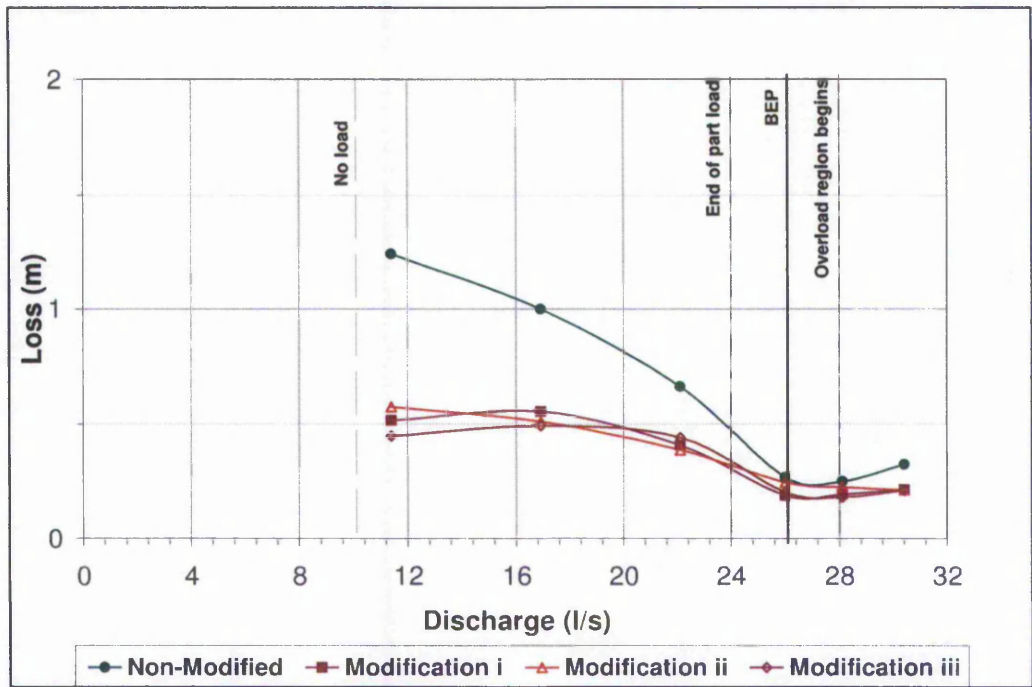


Figure 5.33 - Losses in zone-*vi* – Modification Study

5.5.4.5 Flow zone-*vii*

Within flow zone-*vii* (as shown in [Figure 5.34](#)) the losses improve in a similar manner to the losses observed within flow zone-*vi*. Within the main operating region the losses for all three modifications are similar. In the part-load region however the discrepancies increase slightly. Within this region it can be seen that the losses for modification-*iii* are the lowest. The contribution of losses of flow zone-*vii* to the overall losses is significant and therefore the observed decrease in losses as a result of the modifications is a significant improvement.

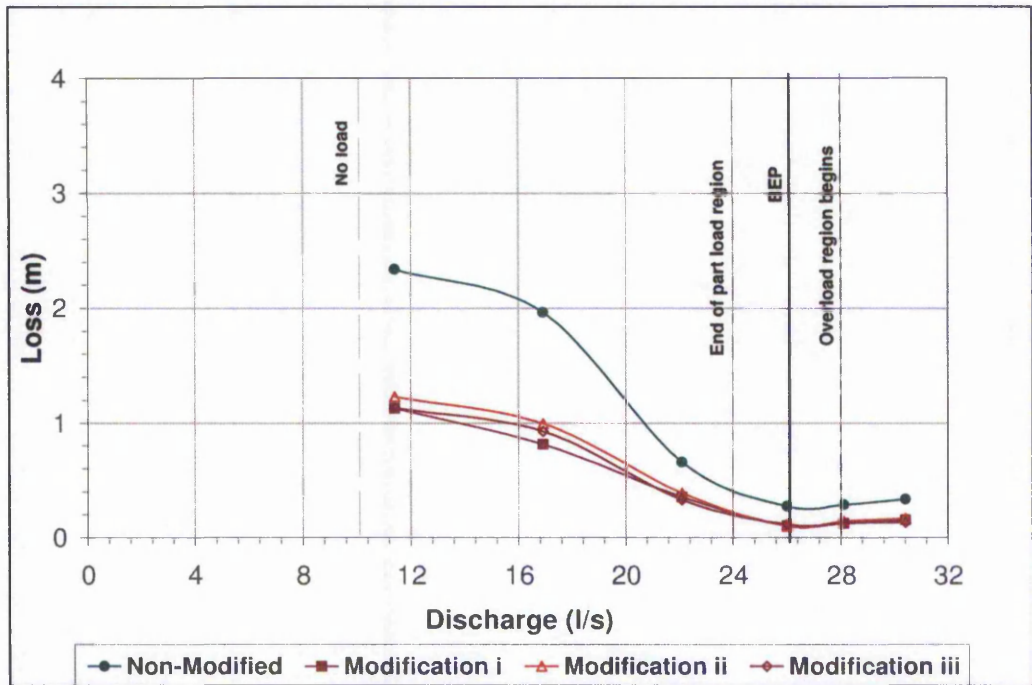


Figure 5.34 - Losses in zone-*vii* – Modification Study

5.5.4.6 Combined Flow Zone losses

The combined losses of flow zone-*vii* for all the modelled geometries are shown in Figure 5.35. It can be seen that the combined effect of eye enlargement and impeller rounding (Modification-*ii*) has the best improvement in the overall losses within the main operating region. The combined effect of outside chamfer and eye enlargement (modification-*iii*) shows partial improvement of losses in the part-load region and BEP region, and a similar improvement to that of modification-*ii* in losses from the beginning of overload region.

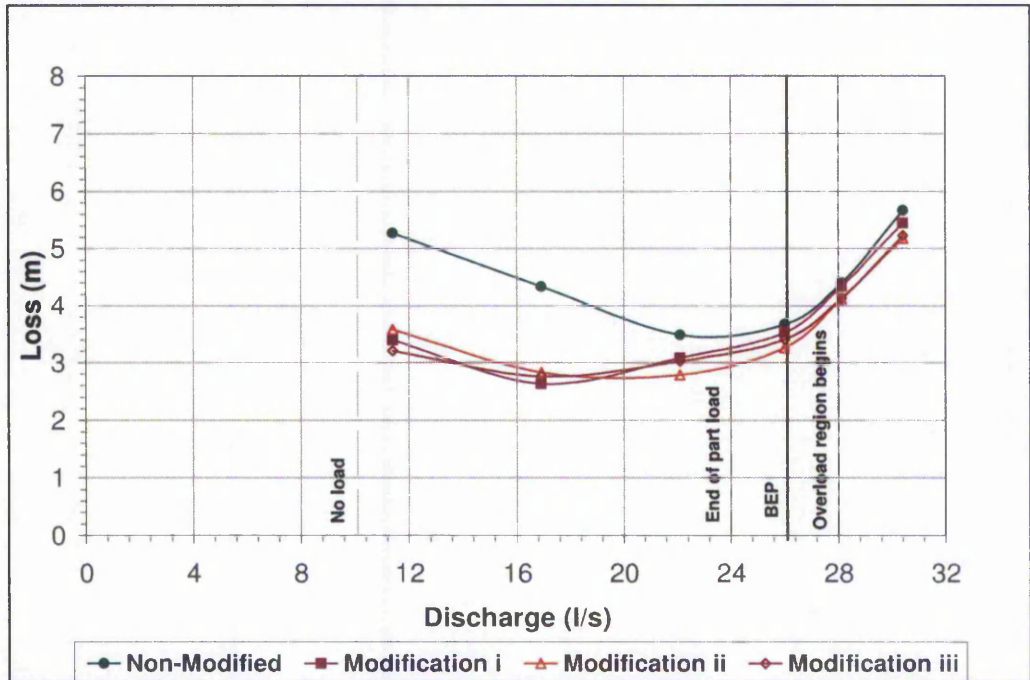


Figure 5.35 - Combined zone losses – Modification Study

5.5.5 Summary of Modification Study

The enlargement of the impeller and casing eye (modification-*i*) has significantly reduced the head number mainly in the part-load region whilst the power number has remained unchanged throughout the entire operating range. The greatest loss reduction occurred in zone-*vi* and zone-*vii*. Modification-*ii* has shown slight decrease in head particularly in the main operating region and only marginal decrease in power number throughout the entire operating range with greatest loss improvement in zone-*iii.iv.v*. Finally modification-*iii* has shown slight improvement of the head number in the main operating region with no change in power number. The best improvement of losses for modification-*iii* occurred within zone-*ii* whilst the losses within the other zones were similar to those of modification-*i*.

For all the modified geometries the losses in zone-*ii* are the lowest and very similar throughout the entire operating range. This could be because zone-*ii* consists of a very small region between the volute and impeller interface.

6 Discussion

Four main issues are discussed pertaining to the results (in chapter 4) and also to the approach and outcomes of this research. The first section discusses the validity of the computational model. The second section discusses the geometrical modification techniques investigated, and the third section discusses the modelling of the interface between volute and impeller. The fourth and final section gives an overview of the general findings.

6.1 Uncertainties Associated with CFD

The match of CFD results with the experimental data has been encouraging, particularly within the main operating range. But CFD tends to be less accurate away from the design conditions. Drtina et al (1999) also predict similar trends at off design conditions and with better performance matching to experimental at main operating region. They suggest that separation zones are one of the causes for this discrepancy. The predicted head has consistently been higher for the PAT modelling all blade passages but similar to experimental data for the PAT modelled with a periodic blade passage. However, the losses within zone-*iii.iv.v*, which refers to the impeller, were much higher for the PAT modelled with all blade passages. This indicates that the losses within each passage can be considerably different due to the unequal mass flow distribution between the different blade passages. Karassik (1986) suggests that at BEP the blade loading (in pump mode) is equal for all blades but this is not the case for the current PAT as evidenced by the different blade loadings observed in Figure 6.1. Consequently, the velocity distribution at the exit of the impeller will also be non-uniform and causes residuals to be high at the interface between impeller and draft-tube.

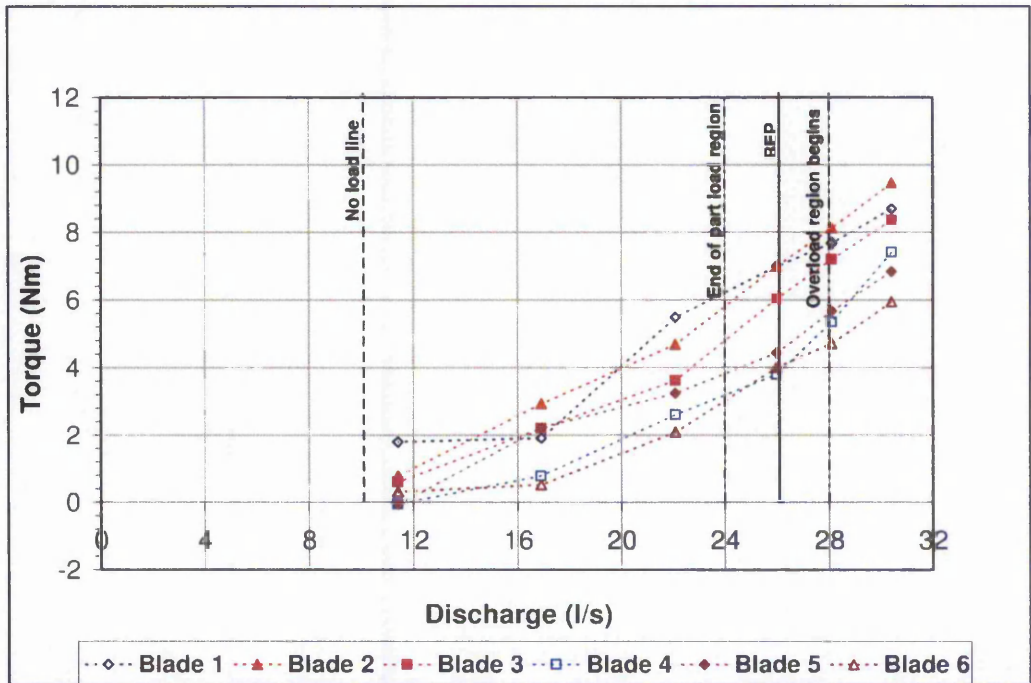


Figure 6.1 - CFD Torque loading on each blade for a full impeller model

Although the results for single blade passage seem correct it is unlikely that this is the case mainly because the hydraulics are different within each passage, particularly at off-design conditions. Although not accurate, at BEP the single blade model can be a reasonable approximation to a full impeller model as the averaged mass flow is close to a full impeller model. The prediction of efficiency at BEP can be an indication of this but it is unlikely that this holds for all PAT designs.

Kirloskar Brothers Limited (2003) used single-blade passage with periodic boundary conditions to model the flow within a PAT but the predicted performance characteristics showed high deviations in comparison with the experimental data. They were not able to make any further conclusions. The hydraulic characteristics curves show different trends which also indicate geometry dissimilarity. The suggestion in this case was that the discrepancy in computational and experimental results could also be due to the computational set up including mesh size. Kirloskar Brothers Limited make the same observation of head behaviour. The smaller discrepancy between CFD and experimental head is likely to be due to the periodic conditions. This creates a symmetrical flow within the draft-tube which reduces the overall flow complexity and calculation effort.

6.1.1 Uncertainty in CFD

6.1.1.1 Residual Errors

The residuals at the impeller exit and draft-tube did not converge to the required level for the PAT model with all impeller passages. This suggested that either the interface treatment between stationary and rotating domain was not suitable or, that recirculation was occurring at the exit of the draft-tube. Generally the latter can be solved through extension of the draft-tube domain (Ansys CFX Manual, 2003) however this proved not to be the case as the residuals did not improve.

Both stage interface and frozen-rotor steady-state treatment between rotating and stationary domains have caused convergence problems. The stage averaging technique caused instability problems and solver failure, particularly at off-design operating flows, perhaps due to the averaging technique. Frozen-rotor was the opted treatment between interfaces but increased residuals in the draft-tube were still observed. The resource limitations did not permit the use of unsteady simulations to allow for comparison.

Most turbomachinery literature employing a steady-state approach show the use of mixing plane (stage interface) boundary condition between stator and rotor components. In these cases however the flow at the interface is assumed to be periodic through all stator and rotor passages. It is a reasonable assumption as the vaned (stator) system creates flow periodicity. Uphadyay (2003) suggests that by increasing the density of grid points immediately after the stage interface allows for much easier convergence, but this is found to not be the case in the current model as convergence is not achieved. Due to the averaging technique of the stage interface it does not reproduce complex flow pattern (Guedes, 2002).

The grid modelling and refinement would also be different for smaller and larger scale models due to their individual flow characteristics. Dixon (1998) and earlier Turton (1995) demonstrated that dynamic similarity between prototype turbines and the models is not maintained due to the change in Reynolds number, which can effectively alter the flow regimes of the machine.

6.1.1.2 Draft-tube & Tailrace Conditions

The higher exit head suggested that the computational model was not capable of predicting the head recovery in the draft-tube. Modelling with and without draft-

tube confirmed that this was in fact the case, since both set ups showed similar exit pressures. Part of the explanation can be due to the turbulence model employed not being capable of modelling large scale eddies (Ansys CFX Manual, 2003).

Perhaps a more considerable cause can be the tailrace conditions of the draft-tube as this was not replicated in the computational model.

It is evident that there can be some influence of submergence on the hydraulic loss and head recovery within the draft-tube. The draft-tube plays a major role in the overall performance of the turbine, but it is always difficult to evaluate its exact performance by analytical or theoretical means as the performance depends on the operating conditions. Hutton (1954) actually states that $1/3^{\text{rd}}$ is the maximum ratio of loss in the draft-tube relative to the impeller losses and Turton (1995) suggests quoting recent IAHR symposia, that the draft-tube losses contribute only 8% of the total losses in the turbine. These values are only recommendations based on rule-of-thumb from practical turbine tests, but this does not mean that they would hold for a PAT. Uphadyay (2003) found that the ratio of draft-tube to impeller losses is more or less $1/4$ and $3/4$ between them when the turbine is operating near the best efficiency condition which agrees with the current model for the non-modified model. Mauri et al (2000) modelled through CFD a standalone draft-tube with an external tank at the draft-tube outlet but the set up did not capture the influence of other components. He reported that in an optimised draft-tube up to 40% of the total energy can be recovered through the transformation of kinetic energy unused by the runner to potential energy. Mauri also reported that the complexity of the flow in the turbine causes instabilities and is usually badly predicted by most of the turbulence models. The flow visualisation within the draft-tube of the current model (in Appendix A) shows recirculation effects at the outlet. There is also separation and recirculation effects at the trailing edge (zone-v) of the suction side of the impeller which adds further to the complexity of the flow calculations at the impeller/draft-tube interface (zone-v/zone-v). Another contributor to the instabilities downstream is the non-uniform mass flow exiting each blade passage.

The residuals in the draft-tube are higher relative to the other regions but this is unlikely due to the chosen variables. Most computational work on draft-tube flows employ similar settings including the standard k- ϵ model with wall function. Shyy, W, and Braaten, M. (1986), Vu and Shyy (1988), Ruprecht, A. (1990), Tanabe, S.

et al (1990), Wu Y.L and Guilbaud M. (1998) and many others. In some of the computational modelling such as Soula V., 1997 uniform boundary conditions have been used at the inlet and therefore swirl was not modelled. In this case a better convergence is expected due to relatively low complexity of flow.

6.1.1.3 Modelling of Gravity

In the current set up the gravity term was not included as the vertical height between inlet and exit planes (elevation term) is added to the CFD result. However the vertical height between the exit measuring plane and outlet plane (at the draft-tube exit) was not included as the head recovery was not established. The accurate correlation of heights between CFD and experimentally obtained data was not conclusive and therefore remains an area for further investigation.

The CFX code does not calculate gravity by default. Uphadyay (2003) found that there was virtually no difference in the calculated power output of the turbine when the gravity term was added to the code. However the head rise predicted with gravity had to be corrected with the vertical height of the domain to obtain the actual head rise. Inclusion of the gravity term caused problems with convergence of the CFD model.

6.1.1.4 Leakage

The PAT modelling leakage shows a shift of the BEP and head curves but generally the curve profiles remain similar in comparison with the PAT without leakage. The best efficiency does not decrease with leakage. The losses have shown an interesting behaviour whereby there is actually a significant improvement in the losses in zone-*i* and zone-*ii*. Including leakage out of the control volume has caused the results to match less well to experiment. Tamm (2001) modelled leakage on a pump through CFD, and found that head and efficiency shift slightly towards lower flow rate values compared to the experimental data. Theory also indicate that if the leakage flows decrease the pump curves shift to higher flow rate and in a turbine to lower flow rate values (Pfleiderer, 1957), which agrees with the current findings. Comparison with Thornes (1982) method (in Appendix B) also shows the same trend however the compared values are different. It is likely that Thornes value over predicts the losses since a first estimate of leakage is required and with a high safety factor. If an experimental set up has leakage out of the control volume (such as through

packing gland) then this can add to further uncertainty in the CFD model.

The geometry of a pump is not optimum for turbine operation as its inherent geometrical features can have a detrimental effect on the flow behaviour and consequently performance characteristics. A good indication is the large difference in widths of casing outlet ($B_{1,c}$) and impeller inlet (B_1) (as shown in [Figure D.1, Appendix D](#)). The flow into the impeller is not ideal due to the sudden change in section areas, with the possibility of the impeller having to take more fluid flow than what it can optimally cope with. This creates a throttling effect of the flow. It appears that leakage deals with the 'excess' fluid and allows for a better flow transition.

6.1.2 Uncertainty Analysis for Experimental-CFD correlation

The computational uncertainty limits are difficult to establish due to the numerous modelling variables involved in a computational simulation. However the Richardsons Extrapolation and GGI (Roache, 1994) methodology employed to achieve grid independence are well accepted methodologies within the computational community and allow for confidence in the accuracy of the obtained data. There are also associated uncertainties with the experimental procedure which in the current case accounts for $\pm 5\%$ at the best efficiency region. The CFD results fall within this range in the main operating range. The correlation of CFD-Experimental uncertainty is given in [Appendix H](#).

6.2 Interface Modelling – Zone ii

The results for the four interfaces modelled have shown that zone-*ii*, which consists of the churning region and interface between volute and impeller, is critical for the accurate prediction of flow regimes within a PAT. However the limited literature available on PATs has shown that the churning region has not previously been modelled. In both of the cases found (Kirloskar Brothers Limited, 2003; Tamm, 2000) only zone-*ii.a* is modelled. In Kirloskar Brothers Limited approach a similar model to interface-*iv* is employed but does not consider its influence on the prediction of flow regimes within the PAT. The CFD results generally show poor matching to the experimental data but this could also be due to the fact that a single-blade passage model as previously discussed. Tamm (2000) models a PAT with all impeller passages and with a similar interface-*iv* but did not have

experimental data available to compare.

The significant discrepancies in losses, head number, and power number that can arise from small geometrical changes has underlined the importance of modelling zone-*ii* as closest as possible to the real geometrical model. These parameters are discussed in more detail in the following sections.

6.2.1 Interface-*i*

The validation of the PAT model has been carried out against the PAT model with interface-*i*. Generally it has been found that the characteristics of the PAT with interface-*i* compare favourably with those of the experimental model. The discrepancies between the compared parameters are thought to be due to the reasoning laid within section 6.1.1.2.

The results suggest that the higher torque and head observed is due to the increase in the exit net rotational momentum from the impeller. This could be from each or a combination of the three factors explained in section 6.1.1 and perhaps the contribution of loss increase within each zone. The performance characteristic curve trends for both the PAT with interface-*i* model and the experimental model are similar, which suggest that the predicted losses are a good description of the hydraulic internals of the real model but probably over predicted in zone-*vi* and zone-*vii*.

6.2.2 Interface-*ii*

A detailed view of the losses suggest that there is a rise of the net rotational momentum as the overall losses do not increase significantly compared to those for interface-*i*. On the other hand there is a decrease in the losses within the no-load to part-load region for zone *iii-iv-v*, suggesting that the power improvement is due to the decrease in the net impeller losses rather than increase of net rotational momentum across the impeller.

A general comparison of interface-*i* and interface-*ii* show that the main differences are the behaviour of losses within zone-*ii* and zone-*vi*. There is evidence of loss reduction in zone-*ii* for the entire operating range when these are compared against zone-*ii* losses of the PAT model with interface-*i*. In zone-*iv*

there is also reduction of losses mainly in the no-load to BEP region. A change of loss behaviour within this region was expected as this interface does not model leakage into the draft-tube domain.

6.2.3 Interface-*iii*

The interface study shows that the discrepancy with experimental data increases further with geometry simplification. Interface-*iii* evidences this as it excludes the whole of the churning region (and only models the front and back-shroud thicknesses).

The head number increases for interface-*iii* particularly in the main operating region and the power number is higher throughout the entire operating range. Examination of the losses shows that there is an increase in the losses in zone-*iii.iv.v* which suggests that the power increase is due to increase in net rotational momentum rather than decrease in losses. Therefore the head number increase is due to both increase in net rotational momentum and increase in overall losses including losses in zone-*iii.iv.v*. A comparison of the losses of the interface-*iii* model with interface-*i* model shows that there is a reduction of losses within zone-*ii* and zone-*vi* whilst the losses. The remaining zones display similar losses.

6.2.4 Interface-*iv*

Interface-*iv* has shown the highest increase in required head patterns relative to the other interface models for the entire operating range. The increased head required is mainly caused by the relative increase in losses within zone-*iii.iv.v*, which are quite significant when compared to the other interface models, and also net increase in rotational momentum. The increased power number is caused by the net increase in rotational momentum alone since the losses also increased within zone-*iii.iv.v*. In comparison with the other interface models, interface-*iv* has shown the highest increase in hydraulic losses within zone-*iii.iv.v* and completely distinct loss behaviour within zone-*ii* and zone-*vi*.

Singh (2005) investigated an experimental set up similar to interface-*iv* on a 79.1rpm PAT model by introducing casing rings in zone-*ii*. A small radial clearance still exists with the physical model and churning is therefore present (unlike the computational model). He also observed similar increase in head

required throughout the entire operating range and also similar power behaviour as the CFD predictions. However, he suggested that the increase in power in the overload region was due to improved hydraulics in the impeller zone, which is not borne out by the CFD flow predictions on the 24.5 rpm PAT. The overall change in head number and power number in the experimental set up was not as significant as that predicted by CFD for the 24.5rpm PAT. Singh (2005) also suggested that the contraction caused excessive losses in zone-*ii*, which was not the case in the CFD model. However, the experimental set up does not measure local pressures and therefore this parameter is difficult to measure within the flow domain. The highest losses in the CFD model were witnessed in zone-*iii.iv.v* instead. It was noticed that the 79.1rpm PAT had almost similar casing outlet and impeller inlet widths which suggests that this could be the primary cause for the different observations in losses. The combined findings from both studies suggest that a large difference in width, such is in the 24.5rpm PAT, causes significant losses in zone-*iii.iv.v*.

6.2.4.1 Interface Study

The observations have shown that there is a relationship between the geometrical complexity of zone-*ii* and the loss behaviour mainly in zone-*iii.iv.v*. This suggests that the velocity components and mass flow at the inlet of the impeller are affected by the change in axial and radial clearances within the churning region.

For PATs with a significant volute to impeller width ratios the losses in zone-*iii.iv.v* will be high due to the throttling effect caused by the smaller width of the impeller (i.e. in this case the impeller is receiving more fluid than it can optimally cope with). A pattern was noticed with the losses in zone-*iii.iv.v* whereby they increased with reducing volume of the churning zones (zone-*ii_b* and zone-*ii_c*).

6.3 Geometrical Optimization

The results for the three levels of modifications have been given in [chapter 5 section 5.5](#). It was found that each modification technique affects the losses in independent zones. The enlargement of impeller eye (modification-*i*) significantly decreases the draft-tube (zone-*vi* and zone-*vii*) losses, whilst inlet-rounding/enlargement of impeller eye (modification-*ii*) technique shows some improvement in the impeller losses, and outside-sharpening (modification-*iii*)

shows a slight reduction in the losses within flow zone-*ii* and also zone-*iii.iv.v*. The evidence from CFD analysis suggests that each geometrical improvement has the effect of reducing the losses in the zones immediately downstream of the modification.

6.3.1 Modification-*i*

The computational results for the modification-*i* PAT model have shown that significant performance improvement can be achieved mainly between the no-load to end of part-load range. The performance behaviour of the predicted results compare favourably to those obtained experimentally in the work carried out by Singh (2005). The performance curves for both CFD and experimental results display remarkably similar trends. Singh (2005) suggested that the suction eye enlargement in zone-*vi* had a great influence on the power number behaviour within the no-load and BEP, indicating that either the hydraulics within impeller zone-*v*, zone-*iv*, and zone-*iii* had improved or there was a decrease of the exit rotational momentum giving a net increase of the rotational momentum across the impeller. Due to the positive and substantial head reductions Singh also suggested that the losses within the impeller dropped tremendously with only a slight decrease of the losses occurring within zone-*vi*. The computational evidence does not support this conclusion. The predicted power number only improves marginally throughout the entire operating region, with almost unchanged losses in zone-*iii.iv.v*. This suggests that the hydraulic effects within the impeller are insignificant when compared to the other regions. The most significant improvements are in the combined losses observed in zone-*vi* and zone-*vii*. This loss improvement is responsible for the significant increase in efficiency in the whole of the no load to end of part load range. The losses in the remaining zones have not altered significantly relatively to the losses of the non-modified PAT. This modification has shown no evidence of changes of the rotational momentum across the impeller.

6.3.2 Modification-*ii*

The PAT model with modification-*ii* has shown significant reduction in head number between the part-load to overload range whilst the power number decreases marginally throughout the entire operating range, resulting in an increase in efficiency. The combined losses of all flow zones are the primary

cause for this head reduction. The decrease in power signifies two possibilities namely, the increase of losses within the impeller control volume or the decrease of the net rotational momentum across the impeller for the modification-*ii* PAT. Since the losses within zone-*iii.iv.v* have improved it means that there is a decrease in the net rotational momentum across the impeller. Therefore the combined behaviour of the power and head number can be the result of the combination of loss mechanisms in the PAT control volume and decrease in net rotational momentum across the impeller.

Singh (2005) also reported consistently greater magnitude in head reduction compared to the power improvement. However, he suggested that their combined behaviour was due only to the loss mechanisms in the PAT control volume. He also suggested that the loss component in zone-*ii* had reduced as a result of the inlet-rounding modification. However, in the computational study the comparisons of losses within zone-*ii* of modification-*ii* against modification-*i* have shown that the inlet rounding modification has not influenced the losses in zone-*ii*.

6.3.3 Modification-*iii*

The performance curves for this modification procedure display similar characteristics of the PAT model with modification-*ii*. The loss mechanisms however are quite different in the different flow zones. The main difference seen for modification-*iii* is the reduction of losses that occur within zone-*ii*. These are associated with the increase in the axial clearance between the back-shroud outside walls and casing inside walls.

The head number shows a decrease for the main operating region whilst the power production decreases marginally in the main operating region and increases in the overload region. The reduction of the head number in the main operating region indicates either a decrease in the losses within the PAT control volume or decrease of the net rotational momentum. The flow zone losses show that the combined losses for modification-*iii* are lower than for modification-*i* in the main operating region therefore the head reduction is mainly because of the loss reduction. The improvement of loss has only occurred in zone-*ii*. The decrease in power number in the main operating region can only suggest either increase in the impeller losses or decrease of the net rotational momentum. Since the losses in zone-*iii.iv.v* have not changed it can be quite confidently said

that the net rotational momentum across the impeller has decreased. This impact can be directed to the decrease of losses more specifically in zone-*ii*. The modelling of this modification procedure was only carried out computationally and therefore experimental basis for comparison is not possible.

6.3.4 Optimisation study

The 24.5 rpm PAT is peculiar in that the area at the impeller eye is restricted. This is not a common characteristic in centrifugal pump designs. Singh (2005) tested the effects of (eye enlargement) modification-*i* on the 24.5 rpm PAT and on a 35.3 rpm PAT. He reported similar behaviour of the performance characteristics on both PATs, with evidences of increase efficiency in the part-load region and marginal decrease in efficiency at the BEP and overload region. However he observed that for the 24.5rpm PAT the losses increased in zone-*iv.v* and reduced in zone-*vi*, whilst the 35.3rpm PAT displayed a contrasting effect with presence of increased rotational momentum in addition to decrease of losses in the zone-*iv.v* and zone-*vi*. The observations he made for the 35.3 rpm agree with the CFD observations for the 24.5 rpm PAT model but the experimental method could not measure the individual zone losses.

Singh (2005) also tested the effects of modification-*ii* on several PAT designs with different specific speeds and showed consistent improvement of the overall performance of all the tested PATs in the BEP and overload region. He suggested that the modification reduced the losses in zone-*ii* and zone-*iii*. The observations in CFD show that only the losses in zone-*iii.iv.v* reduce with insignificant changes on the losses within zone-*ii*.

6.4 General Overview

6.4.1 CFD as a PAT Performance Prediction Tool

The current study has shown that there are a number of parameters that influence the accuracy of the CFD results. The level of geometrical complexity is one of the main parameters and this has been verified through the study of blade passages, leakage, and interfaces. This underlines that three-dimensional flow is critical for accurate predictions. The interface study has shown that variation in geometry complexity in critical areas of the PAT has a high impact on the accuracy of the predicted results. The study of leakage has also shown that the

predicted flow rate for BEP of a PAT can be changed significantly by inclusion of relatively small leakage flows, representative of actual leakage flows that are likely to occur in small PATs.

Previous PAT performance prediction methodologies are not capable of capturing critical geometry features as they are not able of evaluating the geometrical characteristic of an individual machine. Recent prediction models which are based on analysis of basic flow geometry in a PAT are still based on some elements of previous methodologies. For instance, Amelios (2004) method calculates the losses through the PAT to estimate the best performance, whilst Ventrone et al (2000) estimate the peak efficiency of the PAT by establishing two factors, one being the angle of the absolute flow approaching the turbine runner which is derived from the geometry of the runner, and the other a parameter depending on the allowable value of the energy losses which is based on experimental observations. The computational evidence has shown that the hydraulic losses within a PAT are sensitive to small geometrical changes including the effects of radial and axial clearances between impeller and casing spaces.

In the current computational study when the most accurate geometrical models are employed the prediction of BEP occurs at exactly the same flow rate as experiment. At off-design operating regions the performance prediction deteriorates mainly because of increasing complex flow behaviour. According to Bohn, (1998) for flows where there is separation (as in case of off-design conditions, or where the flow is highly curved or rotation, e.g. pumps), the effects of turbulence models can be significant. Goto (1997) investigated the flow fields within a diffuser pump and showed that coarse grids tend to under-predict the losses for a mesh independent solution. In the current case the computed hydraulic losses are over-predicted but this is due to the significantly higher predicted head. De Henau et al (1997) have also shown that grid density and turbulence models can affect the loss prediction.

The current study has shown that the single-blade periodic model predicts the BEP at the same operating flow as experimental, but it is highly inaccurate for off-design conditions. Skoták (2003) also modelled a pump-turbine with only one runner channel and reported the same findings. He suggested that the off design inaccuracies were caused by back flow at the turbine-runner outlet, whereby the back flow is produced by the angular momentum at the turbine runner outlet at

partial load turbine operation. The fluid is then pressed by the angular momentum to the back-shroud walls while the flow near the rotation axis is decelerated and the back flow is appeared as its consequence. Kirloskar Brothers Limited (2003) also evaluated a CFD model of a PAT with single-blade passage and compared with experimental data but the BEP did not match. However they only carried out a preliminary study with suggestions for further scrutiny of the CFD approach, particularly with regards to the meshing. Modelling of the complete impeller has been more accurate in determining the hydraulic characteristics of the PAT and is considered the most accurate approach as it considers the individual mass flow and losses within each individual passage. The high residuals in the draft-tube require further investigation.

6.4.2 CFD as a Design Tool

6.4.2.1 Optimisation Study

The investigation on geometrical modifications has shown that the computational results agree well with the experimental data and therefore can predict well the influence of geometrical changes on the performance characteristics. Denton (1999) is of the view that the N-S solver should be able to predict trends in loss variation with design changes and can point the way to more efficient designs. When CFD is used to investigate the change in performance due to change in design the prediction of incremental design changes can be more accurate than prediction of absolute quantities due to some of the errors cancelling each other Benek (1998). This agrees with results from the current study, which show that the relative changes due to key geometrical improvements match closely with the experimental results, whereas there are still some inaccuracies in the prediction of overall performance.

6.4.2.2 Identification of Good Pump Design for PAT Application

The current research has brought out some useful information on identification of good pump designs for PAT application. The computational observations have shown that zone-ii and zone-v.vi are the two most critical zones that can have a significant impact on the overall losses behaviour of a PAT. Both these zones deal with flow moving from a large area to a contracted area. Some pump selection guidelines are given below based on the above findings:

The width ratio of the volute outlet and impeller inlet should be as close as possible to the value of one, with the volute outlet width being slightly bigger than the impeller inlet width. Another aspect to inspect on the pump is the thickness of the front and back-shroud and how much they protrude into the flow path. Less protrusion into the flow is preferred as separation effects can be avoided. Similar widths will create less obstruction to the flow delivered to the impeller, subsequently optimising the flow behaviour within flow zone-*ii*. Generally, any sudden decrease in flow path area (in the turbine flow direction) should be inspected. Another critical zone is the impeller and casing eye region. The casing eye area should be equal or larger than the impeller eye area, or the geometry of the pump eye should allow enlargement modifications.

Close radial clearance in zone-*ii* between impeller and casing is also preferred, as large clearances will create flow disturbances and secondary flow behaviour. Extremely small clearances do not have any particular advantage and are not critical. Axial clearances between impeller and casing are un-avoidable but generally it was noticed that this does not affect the performance of the PAT as the flow between the casing and impeller is only churning. In this case only the surface roughness of the components will play a role on the efficiency of this region.

A study was carried out to analyse the effects of shortening of blades for which results are given in [Appendix C](#). It was noticed that as the blades are shortened at the impeller eye the efficiency of the PAT decreases. Although simple, this study shows that preference should be given to pumps that have a larger blade span. Blades that extend further into the draft-tube create less separation and recirculation at the exit of the impeller and into the draft-tube.

7 Conclusion and Recommendations

Effort has been made to tie analysis and discussion not only to the results but also to the literature review. The focus of this chapter is to draw conclusions shown by the whole results and project. Essential limitations of the work and recommendations are also included.

7.1 Conclusions

7.1.1 Review

Extensive literature review has shown that a 'pump as turbine' is a technology that can have a positive role in the quality of lives of the people in developing countries for whom electricity is still not easily accessible. It has been found that the PAT technology when operated efficiently it is appropriate for the 20kW to 100kW range where an equivalent turbine would be too expensive to operate. Pumps of the centrifugal type are generally most suitable for these applications (Williams, 1992). These pumps can usually be obtained locally straight from the shelf and can be easily installed. The relative simplicity of the machine allows it to be maintained without expert knowledge as only basic understanding is necessary. The main disadvantage of a pump as turbine is that it is of fixed geometry, which only allows it to operate efficiently over a limited range of steady-state conditions and obtaining experimental data is expensive. For this reason it has been found that several studies attempt to predict best performance characteristics. The empirical methods developed to date lack consistency and can only be used as a first estimate.

One important aspect of previous PAT research has involved the investigation of the influence of small geometrical alterations. These have been shown to bring some improvement in the overall performance of the PAT. It was concluded that a lot of effort has been put through theoretical and experimental methods.

In recent years CFD has emerged as an analysis and design tool and has been used in a variety of applications thereby aiding in the understanding of the internal flow phenomena of machines. Today CFD technology is increasingly being used as a tool to aid research and development of new designs. It has been found that a significant number of studies have been carried out on various types of turbomachinery particularly on large scale turbines, some of which have

a similar operating principle to the PAT. However, there is practically little computational work in the field of pumps operating as turbine, and consequently there is lack of information on how to model and set up a PAT computational simulation appropriately. This gap in PAT research motivated the investigation with aid of CFD to analyse the internal flow regimes and effects of geometrical alterations.

7.1.2 Modelling and Discretization

A preliminary investigation was carried out, first with intent of assessing the CFD parameters that are appropriate for modelling the flow in the 3D generated PAT computational model, and secondly to test the performance capabilities of the workstation. The following conclusions from the examined parameters were drawn.

The suitability of the $k-\epsilon$ and $k-\omega$ turbulence models was evaluated for pump as turbine applications. In literature the $k-\epsilon$ turbulence model is the common option in numerical investigation of turbomachinery flows, however theory suggests that the $k-\omega$ model incorporates the capability of modelling flows near wall more accurately. Compared results showed virtually similar outcomes in the domain but the $k-\omega$ turbulence model was less accurate in predicting axial flow components at the inlet and outlet regions. To understand further the capabilities of the turbulence models a finer grid resolution would be required.

Appropriate boundary condition selection at the inlet and outlet has shown to be important as otherwise can result in the failure of the solver. For PAT application it was found that either inlet mass-flow and outlet total pressure, or, inlet total pressure and outlet mass-flow to be appropriate. The compared results showed only marginal differences. However with outlet mass-flow specified boundary condition the code only allows for an outlet direction of the flow, which during calculation creates virtual walls that stop the flow re-circulation into the domain if there is any, which is not true to the real model. Therefore the recommendation is to obtain the final solution with an "opening" on the outlet face, hence inlet mass-flow and outlet total-pressure.

The steady state frozen-rotor interface has been used between rotating and stationary domain. The steady state stage interface was found to be

inappropriate for the particular model because the different mass-flow distribution within each blade passage created high residuals at the interface between rotating and stationary domains which caused the problem to not converge. Rotating the pitch of the impeller by a certain degree and averaging the data results in little difference relative to a single position simulation. Unsteady transient simulation would require much higher computation resources.

7.1.3 Comparison of CFD and Experimental Data

The CFD results were compared against the experimental data for the non-modified geometry to establish the discrepancy between both sets of data. The following conclusions were drawn:

- i. The CFD predictions of the hydraulic parameters compare reasonably well with experimental results, with deviations of efficiency within 3% in the part-load and overload regions and matching in the BEP. In the no load-region the discrepancy was around 8%. The experimental uncertainty is estimated to be in the region of $\pm 5\%$.
- ii. The chosen CFD model parameters namely, grid size/construction, meshing, turbulence modelling, and wall function have been shown to be appropriate for analysing PAT applications.

A hydraulic loss method was devised to facilitate the analysis and understanding of the individual losses in each domain and the effects of geometrical changes. The concept of dividing the complex flow regime within a PAT into four major flow regions so that each region can be analysed individually by means of CFD has been shown to be very useful and the results are conclusive. However, the research also shows that a sub-zone, the churning regions on either side of the impeller, should also be included. This concept should provide a strong basis for optimising the performance of a PAT.

7.1.4 Interface Study

Interface study has shown that modification zone-ii including the churning region is required to accurately predict performance characteristics of the PAT. All interface models have predicted the BEP at the same flow as experimental data.

However, interface-i has shown the best match with experimental data for the entire operating range. Interface-iv has shown completely distinct loss patterns compared to the other models within zone-i and particularly zone-ii. This has suggested that interface-iv is not suitable for predicting the PAT characteristics and its internal hydraulics.

7.1.5 Modification Study

The enlargement of the pump eye region (modification-i) has shown considerable improvement in the part-load region with only marginal improvement in best efficiency region. The computational results agree well with the experimental data available.

The inlet rounding procedure with modified-eye (modification-ii) has shown improvement in efficiency at the BEP. In the part-load region the efficiency is lower than that for the modification-i. The best improvement in losses occur in zone-iii.iv.v. The overall characteristics agree with experimental data available. Modification-ii has shown the best overall improvement.

Front shroud and back shroud sharpening (modification-iii) has also shown slight improvement in efficiency at BEP and overload region. The best improvement in losses occur in zone-ii.

Casing rings (modification-iv) is a version of interface-iv however as mentioned in [section 7.1.4](#). The loss characteristics became completely distinct. Modification-iv shows increase in efficiency in the main operating region. However, the CFD results do not match the experimental observations from Singh (2005).

7.1.6 CFD for performance prediction

The extensive modelling carried out has shown that the flow within a pump as turbine is highly complex and three dimensional. CFD has predicted the peak efficiency for the 24.5 rpm consistently at the same flow rate as the experimental set up. However at the part load and over load regions there is some over and under prediction respectively, partly because in this case the exact conditions of the tail race were not replicated in the computational set up.

Although CFD results cannot be taken as conclusive, it has shown that even small modifications to the geometry can be accurately predicted. However CFD results have also shown that other parameters can influence the overall efficiency of the PAT. Change in characteristic behaviour has been noticed from the study of leakage. This particular conclusion demonstrates that predicting the efficiency of a PAT through theoretical methods is very difficult as the overall performance has shown to be influenced by various independent factors.

7.2 Further work and Recommendations

In the current research through the interface and modification studies it was verified that simple geometrical or flow manipulation in the vicinity of the volute outlet, impeller inlet, and churning regions can significantly affect the overall performance characteristics of the PAT. A limited number of configurations were attempted leaving still other options unstudied. Of interest would be a parametric study with variation of the volute width whilst maintaining the rest of the geometry unchanged. This will enable the understanding of the influence of the impeller/casing width ratio on the impeller loss behaviour. It is expected that the 'parabolic' characteristic impeller loss curve would flatten, and if such is the case this will confirm that width ratio should be a criteria to select a suitable pump for turbine operation. If the performance of the casing remains unchanged or even if it decreases without surpassing the improvement in efficiency of the impeller this means that the overall performance of the PAT will increase.

Another modification of interest is the combination of modification-ii and modification-iii which should have a combined improvement of losses in zone-iii.iv.v and zone-ii respectively. There is no published work yet on outside sharpening of blades. The objective is to increase the flow entry to the churning region to avoid "throttling" in the impeller mainly for pumps with large volute to impeller width ratio. The recommended research strategy would be firstly through the use of CFD and theoretical analytical methods, at a later stage the results should be confirmed experimentally or through field testing.

Although the CFD procedure has shown to accurately predict the best efficiency point it has not been able to accurately predict the performance of the full range of operating flows. A number of factors owe to this at the computational model. It

is thought that the draft-tube is the major influence on this as the head recovery was not appropriately predicted. It is recommended that the draft-tube is setup to replicate similar tail race conditions of an experimental set up.

Computationally there are many parameters that have not yet been investigated for PATs. It is recommended that further analysis is carried out using unsteady calculation methods. Depending on the computer power it could be beneficial to investigate large eddy simulation (LES) in the draft-tube.

More work can be carried out in the theoretical arena for Performance prediction. The computational results have shown that the 3D aspects have an influence on the accuracy of the performance prediction.

More work can also be carried out in the churning region domain to improve performance of the entire PAT. There is evidence of efficiency improvement in the part-load region with modelling of interface-iii. The influence of churning geometries should be investigated to verify if pumps with different churning volumes or labyrinth geometry within the churning have any effect on overall performance characteristics. This may have significance in a practical setup, perhaps by inserting labyrinth style geometry or valve control measures to control the pressures within zone ii.

A study of effect of impeller diameter reduction using CFD would also be useful, as this is a simple technique for modifying PAT performance in the case that a pump has been installed on site, but does not give the expected output. Williams (1992) tested this on a PAT in case study in Thima in Kenya.

Further computational studies are required on PATs operating in both turbine and pump mode to evaluate the accuracy of assumptions made by current empirical PAT performance prediction models. Local parameters can be compared for both modes of operation to determine if any relationship exists between pump performance and turbine performance.

Solution matching strategy can be used to reduce computing effort and improve solution capability. Large domains such as the draft-tube can be eliminated from the computational assembly and predefined boundary conditions can be used instead. Moreover, definition of boundary conditions at the vicinity of the geometry of interest allows for parametric analysis to be carried out.

Optimising the performance of a PAT through geometrical modifications should be investigated further. For instance in pump applications balance holes are used to relief the axial loading on the impeller and to also deflect flow. This approach can also be attempted on PATs to improve flow uniformity within each blade passage. Flexible baffles installed between volute and impeller can also be investigated with the same purpose of improving flow uniformity between blade passages. CFD also allows for surface roughness to be investigated, therefore it would be of interest to investigate compliant surfaces that are standard in hydraulic applications, such as investigation of roughness equivalent to belzona paint finish.

References

1. Acres American Inc, Small Hydro Plant Development Program U.S. Dept of Energy, Idaho National Engineering Lab., Oct 1980 Report No. DOE/ID01570-T21
2. Amelio, M; Barbarelli, S; (2004). A one-dimensional numerical model for calculating the efficiency of pumps as turbines for implementation in micro-hydro power plants. Proceedings of ESDA04. 7th Biennial Conference of Engineering Systems Design and Analysis. ASME
3. Ansys ICEM CFD (2003) Tutorial Manual
4. Ansys CFX (2003) Tutorial Manual
5. Ansys CFX (2003) Theory Manual - Solver Theory
6. Anderson, H H, (1955). *Modern Developments in the use of large single-entry centrifugal pumps*, Proc. IMechE, Vol. 168, pp743-762.
7. Anderson, H H, (1980) 'Centrifugal Pumps', Trade & Technical Prss, 3rd edition, pp95-96
8. Anderson, J.D. (Jr.) (1995). *Computation Fluid Dynamics: The basics with applications*. McGraw-Hill series in Mechanical Engineering, pp154-155
9. Ardizzon, G., and Pavesi, G., (1999) Funzionamento inverso di una pompa centrifuga: previsione delle prestazioni e confronto con I dati sperimentali 54th ATI Congress, L'Aquila
10. Baines N C, Oliphant K N, Kimmel H E, Habets G, (1998) *CFD analysis and test of a fluid machine operating as a pump and turbine*. IMechE seminar publication 1998-13, pp 71 - 78
11. Blanco E, Fernandez J, Gonzalez Jose, Santolaria C. (2000), *Numerical flow simulation in a centrifugal pump with impeller-volute interaction*. ASME FEDSM200-11297
12. Blazek, P (2001). *Computational Fluid Dynamics: Principles and Applications*. Elsevier, pp 53-55 & 225-255
13. Buckingham, E. (1914) On physically similar systems: Illustrations of the use of dimensional equations. *Physical Review*, IV(4):345-376
14. Busemann, A, (1928) 'The delivery head of radial centrifugal pumps with logarithmic spiral blades', *Z. angew. Math. Mech.* Vol. 8, No. 5, p372.

-
15. Cao, S.L.; Goulas, A.; Yakinthos, K ;Wu, Y.L. ;Tsukamoto, H; Deliporanides., G (1998). *Numerical Simulation of three-dimensional turbulent flow in a centrifugal pump impeller. Third International Conference on Pumps and Fans*, Tsinghua University, Beijing, pp 411-418
 16. Chen, WC et al (1995). *CFD as a turbomachinery design tool: Code Validation*. ASME FED- Vol. 227
 17. Ciocan, G.D. Desvignes, V. Combes, J.F. Parkinson, E. Kueny, J.L. *Experimental and numerical unsteady analysis of rotor-stator interaction in a pump-turbine*. Proceedings of the 19th IAHR Symposium, Singapore, vol. 1. pp. 534-543
 18. Cohrs, D. (1997). *Untersuchungen an einer mehrstufigen rückwärtslaufenden Kreiselpumpe in Turbinenbetrieb*. Verlag und Bildarchiv, W. H. Faragallah.
 19. Cordier, O. (1953), *Aehnlichkeitsbedingungen für Strömungsmaschinen*; BWK (Brennstoff-Wärme-Kraft) Bd. 5, Nr. 10, October, pp 337-340.
 20. Cooper, P & Worthernm, R, Feasibility of using large vertical pumps as turbines for small-scale hydropower, U.S. Dept of Energy, Idaho Nat. Eng. Lab., 1981, Report No DOE/ID?12160-T1
 21. Dawes, W.N. (1992) Towards improved throughflow capability: the use of three dimensional viscous solvers in a multistage environment, Trans. ASME Journal of Turbomachinery, Vol. 114, pp. 8-17
 22. De Henau, Vincent; Michel Sabourin; Yves Labrecque; Benoit Papillon. (1997). *Hydraulic Turbine Design: Will CFD replace model testing?* AEA Technology International Users Conference
 23. Denton, J.D. (1992) The calculation of three-dimensional viscous flow through multistage turbomachines, Trans. ASME Journal of Turbomachinery, Vol. 114, pp. 18-26.
 24. Drtina, P; Sallaberger, M. (1999). *Hydraulic turbines - basic principles and state of the art computational fluid dynamics applications*. Proceedings of the Institution of Mechanical Engineering, Vol 213 Part C.
 25. Dixon, S.L. (1998). *Fluid Mechanics and Thermodynamics of Turbomachinery*. Fourth Edition. Butterworth-Heinemann.
 26. Engel, L. 1957 Die Rucklaufdrehzahlen der kriselpumpen', doctoral dissertation. Tech. Hochschule Braunschweig

-
27. Fleberger, G. Schneider, W. Keck, H. (1994). Zonal computational method for turbulent plane cascade flow. *Acta Mechanica Springer-Verlag Suppl 4*: 233-240
 28. Galpin, P.F., Broberg, R.B., and Hutchinson, B.R. (1995) Three dimensional Navier-Stokes predictions of steady state rotor/stator interaction with pitch change, Third Annual Conference of the CFD Society of Canada, June 25-27, 1995 , Banff, Alberta, Canada.
 29. Giles, M.B. (1998) Calculation of unsteady wake rotor interaction, *AIAA Journal of Propulsion and Power*, Vlo. 4, No. 4, pp. 356-362
 30. Guedes, A., Kueny J. L., Ciocan G. D., Avellan F., (2002) *Unsteady Rotor-Stator analysis of a hydraulic pump-turbine – CFD and Experimental Approach*. Proceedings of the XX1st IAHR Symposium on Hydraulic Machinery and Systems. pp. 767-780
 31. Goto, A. (1995). Numerical and experimental study of 3D flow fields within a diffuser pump stage at off-design condition.
 32. Hutton, S P, (1954). *Component losses in Kaplan turbines and the prediction of efficiency from model tests*. Proc. IMechE, Vol. 163, pp 81-89.
 33. Hwang, R; Jaw, SY (1998). *Second-Order Closure Turbulence Models: Their Achievements and Limitations*. Proceedings of the National Science Council. Vol. 22, No6. pp. 703-722
 34. Idel'cick, E., 1986, "Memento des Pertes de Charge", Eyrolles Edition, Paris, France. (in French)
 35. Iti, H., (1959), Friction factors for turbulent flow in curved pipes, *Journal of Basic Engineering*.
 36. Karassik, Igor J. (1986). *Pump Handbook*, Second Edition. pp 2.22
 37. Kirlosakar Brother Limited (2003), Report on CFD Analysis of NW4+ Pump as Turbine, Corporate Research and Engineering Division, Pune, India
 38. Keck, H., Goede, E. and Pestalozzi, J. *Experience with 3D Euler flow analysis as a practical design tool*. In Proceedings of IAHR Symposium, Belgrade, September 1990.
 39. Keck H. (1994). *Flow calculation and model tests for water turbines tools for potential evaluation and optimisation of modernisation* (In German). Bulletin de L'Association Suisse des Electriciens (Organe Commun de L'Association Suisse des Electriciens (Ase) et de L'Union des Centrales Suisses D'Electricite (Ucs)), vol.85, no.2, pp.17-20.

-
40. Kittredge, C. P. Thoma, D. 1931, *Centrifugal Pumps Operated under Abnormal Conditions; Power*, pp 881-884. (Translated version of: Thoma, D, 1931 'Vorgänge beim Ausfallen des Antriebes von Kreiselpumpen', Hydr. Inst. Tech. Hochschule München, Vol. 4, pp 102 -104)
 41. Kubota, T. Takimoto, S. Aoki, H. (1977). *Development of model turbine by computerised numerical experiments*. Fuji Electric Review, vol. 23, no.2, pp.66-71.
 42. Kuntz, M et al. (2002). *Numerical investigation of turbomachinery performance of a pump-turbine*. Proceedings of the XXI IAHR Symposium on Hydraulic Machinery and Systems, Lausanne
 43. Lakshminarayana, B. (1991). *An Assessment of computational fluid dynamic techniques in the analysis and design of turbomachinery. The 1990 Freeman scholar lecture*. Journal of Fluids Engineering, Transactions of the ASME, v 113, n 3, p 315-352
 44. Launder, B.E. and Spalding, D. B., (1974) The numerical computation of turbulent flows. *Comp Meth Appl Mech Eng*, 3:260-289
 45. Laux, C H, (1976) 'Reversible Multistage Pumps as Energy Recovery Turbines' ASME Conference, paper 76-Pet-65
 46. Lueneburg, R, and Nelson, R M. (1992). *Hydraulic Power Recovery Turbines*. Chapter 14 of *Centrifugal Pumps-Design & Application*. Second Edition by Val S. Lobanoff and Robert R. Ross. Gulf Publishing Company, Houston, Texas.
 47. Mauri, S. Kueny, J.L. Avellan, F. (2000) *Numerical prediction of the flow in a turbine draft tube influence of the boundary conditions*. Proceedings of FEDSM'00. ASME Fluids Engineering Division Summer Meeting, Boston, Massachusetts, USA
 48. Menter, F.R. Two equation eddy-viscosity turbulence models for engineering applications *AIAA-Journal*, 32 (8) 1994
 49. McClaskey, B M, & Lundquist, J A, (1976) Hydraulic Power Recovery Turbines ASME Conference, Paper 76-Pet-65
 50. Michaelides, K; Tournlidakis, A; Elder, R L. (2001). *Use of CFD for the 3-D Hydrodynamic Design of Vertical Diffuser Pumps*. Advances of CFD in Fluid Machinery Design, London, June , IMechE.
 51. Mikus, K, (1983). *Erfahrungen mit Kreiselpumpenanlagen zur Energierückgewinnung aus dem Trinkwassersystem*. Das Gas und Wasserfach, Vol 124, pt. H.4 pp 159-163.

-
52. Muggli, F A; Eisele, K; Casey, M V; Gulich, J; Schachenmann, A. (1997). *Flow analysis in a pump diffuser - Part 2: validation and limitations of CFD for diffuser flows*. Journal of Fluids Engineering, Vol 119 December.
 53. Nestmann, F., Singh, P., Maskey, R. (2003) Optimization Study on Medium and Low Specific Speed Pumps as Turbines; Sechtes Internationales Anwenderforum, Kleinwasserkraftwerke, Passau, pp 74-78
 54. Nechleba, M(1957). *Hydraulic Turbines: Their Design and Equipment*. Artia Press. Prague
 55. Nichtawitz, A., Parkinson, E., sallaberger, M., and Sebestyen (2005) State of the art of the review in pump-turbine hydraulic development. VA TECH HYDRO. IAHR, Beijing Proceedings
 56. Pfeleiderer, C; Petermann, H. 1991, Stromungsmashinen; neubearbeitete 6. Aufl., Springer-Verlag, pp 43-50, 191-203
 57. Roache, P.J. (1994). *Perspective: A Method for Uniform Reporting of Grid Refinement Studies*. Journal of Fluids Engineering Trans ASME Vol. 116, September. pp 405-413
 58. Reymond JD.; Sottas G.; Vilmin S.; Eichenberger M.; Gode E. (1996). *Blade runner hydraulic turbine modelling*. International Water Power & Dam Construction, vol.48, no.2, pp.24-8.
 59. Rodrigues, A. Sing, P. Williams, A. Eugene, L. Nestmann, F. (2003) *Hydraulic analysis of a pump as a turbine with CFD and Experimental data*. IMechE, *Advances of CFD in fluid machinery design*, Proceedings of the Institution of Mechanical Engineering.
 60. Rohlik, H. E. Radial-inflow turbines. NASA SP 290, 1975, pp. 279-306
 61. Ruprecht, A (1990), Numerical analysis of the flow in the elbow draft tube of a Kaplan turbine, Proc IAHR 15th Symposium Belgrade, Vol. 1, G6
 62. Sabourin, M. Labrecque, Y. De Henau, V (1997). *From components to complete turbine numerical simulation*. Gec Alsthom, Tracy, Qc, Canada
 63. Seminar proceedings (2003). *Advances of CFD in Fluid Machinery Design*. IMechE
 64. Shyy, W, and Braaten, M. (1986), Three-dimensional analysis of flow in curved hydraulic turbine draft tube, International Journal for Numerical Methods in Fluids, Vol. 1.6, 861-882

-
65. Sick, M. Drtina, P. Casey, M. V. (1998). *The use of stage capability in CFD for turbomachinery, with application in a Francis turbine*. International Journal of Computer Applications in Technology, Vol. 1, Nos 3/4/5.
66. Singh, P; Nestmann, Franz (2002). *Technical report: NW8 Kirloskar Pump as Turbine*. Institute for Water Resources Management, Hydraulic and Rural Engineering. Univeristy of Karlsruhe, Germany.
67. Singh, P; Khirsagar, JT; Nestmann, Franz (2003). *Experimental and Numerical Studies on a Pump as a Turbine*. The 7th Asian International Conference on Fluid Machinery. Fukuoka, Japan.
68. Singh, P; (2004) Optimization of Internal Hydraulics and of System Design for PUMPS AS TURBINES with Field Implementation and Evaluation. PhD Thesis. Institute fur Wasser und Gewasserentwicklung Unveristat Karlsruhe. Heft 232
69. Schlichting, H. (1968). *Boundary-Layer Theory*. Sixth Edition. McGraw-Hill Book Company
70. Skotak, A., (2003) *The CFD prediction of the dynamic behaviour of a pump-turbine*. CKD Blansko Engineering, a.s. (CBE Blansko) Czech Republic
71. Sick, M., Casey, M. V. (1996) Validation of a stage calculation in a Francis turbine. E. Cabrera et al. (eds.), *Hydraulic Machinery and Cavitation*, Kluwer Academic Publishers 257-266
72. Sick, M., Stein, P., Dorfler, P., Sallaberger, M. *Part load Instabilities in Francis Turbines and Pump Turbines*.
73. Song, C. C. S. He, j. Chen, X Y. (1991). *Calculation of turbulent flow through a Francis turbine runner and an elbow draft tube*. American Society of Mechanical Engineers. pp. 1-6
74. Soula V., (1997), Analyse experimentle et numerique de l'ecoulemet dane unde bache d'alimentation de turbine Francis Diplome d'Etude Approfondies, Université de Poitiers.
75. Spetzler, O 'Die Turbinenpumpe im Stauwerk Baldeney', Zeitschrift Vereines deutsche Ing., Vol 78, No 41, 13 Oct 1934, pp1183-1188
76. Stepanoff A J. (1957). *Centrifugal and axial flow pumps*. John Wiley & Sons, Inc., Chapman and Hall Ltd, New York
77. Strub, R A, 'Investigations and Experiments on Pump-Turbines', Sulzer Tech. Review, 1959, No 2, pp 87-94

-
78. Suzuki, T; Nagafuji, T; Komiya, H; Shimada, T; Kobayashi, T; Taniguchi, N. (1996). *Flow behavior around stayvanes and guidevanes of a Francis turbine*. Journal of Fluids Engineering, Transactions of the ASME, v 118, 1, p 110-115
79. Tamm A, Braten A, Stoffel B, Ludwig G. (2000). *Analysis of a standard pump in reverse operation using CFD*, 20th IAHR-symposium, Charlotte, North Carolina USA
80. Tamm, a. Ludwig, G. Stoffel, Bernd (2001). Numerical, experimental and theoretical analysis of the individual efficiency of a centrifugal pump. Proceedings of ASME FEDSM'01. ASME Fluids Engineering Division Summer Meeting, New Orleans, Louisiana.
81. Tamm, A. Gugau, M. Stoffel, N. (2002). *Experimental and 3-D Numerical Analysis of the Flow Field in Turbomachines Part I*. International Congress on Quality Assessment of Numerical Simulations in Engineering, QUANSE
82. Tanabe, S., Ikegawa, M., Takagi, T. and Sato, J. (1990), Turbulent flow analysis in water turbine draft tube. Proc. IAHR 15th Symposium, Belgrade, Vol. G2
83. Thoma, D, (1931) '*Vorgänge beim Ausfallen des Antriebes von kreiselpumpen*', Hydr. Inst. Tech. Hochschule Munchen,
84. Thorne, E W, Design by the area ratio method, 6th Technical Conference of the BPMA, 1979.
85. Turton, R.K. (1995). *Principles of Turbomachinery*. London: E & F. N Spon.
86. Uphadyay, D (2003), *Low head turbine development using computational fluid dynamics*. PhD thesis, Nottingham trent Univeristy
87. Ventrone, G. Ardizzon, G. Pavesi, G. (2000). *Direct and reverse flow conditions in radial flow hydraulic turbomachines*. IMechE Vol 214 Part A
88. Versteeg, HK; Malalasekara, W (1995). *An introduction to computational fluid dynamics: The finite volume method*. Longman Scientific & Technical.
89. White, D. Holloway, A. G. L., Gerber, A. G. (2005) *Predicting turbine performance of high specific speed pumps using CFD*. Proceedings of FEDSM2005 2005 ASME Fluids Engineering Division Summer Meeting and Exhibition June 19-23, 2005, Houston, FEDSM2005-77460
90. White, F. M (1979) *Viscous Fluid Flow*. McGraw-Hill

-
91. Whitfield, A. and Baines, N. C. Design of radial turbomachines, 1990 (Longman Scientific and Technical Harlow).
 92. Williams, A A. (1992). *Pumps as Turbines used with Induction Generators for stand-alone Micro-hydro Electric Power Plants*, PhD Thesis, Nottingham Trent University.
 93. Williams A A. (1994), *The turbine performance of centrifugal pumps: a comparison of prediction methods*. Proceedings of the IMechE, Part A, vol 208
 94. Worster, R. C., (1957), "The effect of skin friction and roughness on the losses in centrifugal pump volutes", B.H.R.A, Research Report 55&.
 95. Wolfel, Wilhelm, (1987), *Das Wasserrad: Technik und Kulturgeschichte*, Verlag fur Bauswesen, Berlin, p177
 96. Wu, Y.L, and Guilbaud, M. (1996), *Three-dimensional turbulent flow simulation through a hydraulic turbine draft tube*, Proc. of ISFMEFE, Beijing, Sept., 139-149
 97. Yi Qian (1997). *Application of numerical flow analysis technologies to hydraulic turbines and pump-turbines*. Fuji Electric Review, vol. 43, no. 1, pp. 19-22
 98. Yi Qian, Chuichi Arakawa (1998). *The Development of CFD Technology in Hydraulic Machinery*. Third International Conference on Pumps and Fans, Tshingua University, Beijing, pp 79-93
 99. B. E. Launder and D. B. Spalding, (1974) 'The Numerical Computation of Turbulent Flows', *Computer Methods in Applied Mechanics and Engineering*, 3, 269-289 (1974).
 100. B. E. Launder and D. B. Spalding. (1972). *Lectures in Mathematical Models of Turbulence*. Academic Press, London, England
 101. Naot, D., Nezu, I. and Nakagawa, H.(1993) "Hydrodynamic behaviour of compound rectangular open channel", *J. Hydr. Engrg.*, ASCE, 119(3), 390-408.

APPENDIX A	Flow Behaviour in a PAT	146
A.1	Flow zone- <i>iii.iv.v</i>	146
A.2	Flow Description: Zone- <i>vi.vii</i>	149
A.3	Internal Hydraulics - Optimization & Model Complexity	151
A.3.1	Interface Modelling	151
A.3.2	Losses interfaces.....	155
APPENDIX B	Calculation of Leakage loss	157
APPENDIX C	Geometry Verification using CFD	158
C.1.1	Blade Angle	158
C.1.2	Rough Walls	160
APPENDIX D	Test Specimen	163
D.1	Geometry Description	163
D.2	Test Specimen.....	164
D.2.1	Volute, Impeller, and Draft-tube dimensions	164
D.2.2	Impeller Inlet and Outlet flow areas	165
D.2.3	Volute section areas	165
D.2.4	Suction-modified pump.....	168
D.2.5	Inlet rounded pump.....	168
APPENDIX E	Performance Prediction Methods	169
E.1	Theoretical prediction methods	169
E.2	Use of Cordier Diagrams.....	169
E.3	Recent Performance Prediction Methods	170
E.3.1	Amelios methods	170
E.3.2	Ventrone Method	170
E.3.3	Prediction using numerical approaches	170
APPENDIX F	Computational Tool	171
F.1	CFD Code - CFX.....	171
F.1.1	Other salient features in CFX 5.6	171
APPENDIX G	Experimental Work at IWK	172
G.1.1	Test-Rig	172
G.1.2	Experimental Optimisation.....	173
APPENDIX H	Experimental Uncertainty	177
H.1	Uncertainty Analysis for Experimental-CFD correlation	177
APPENDIX I	Published Papers	178

APPENDIX A Flow Behaviour in a PAT

A.1 Flow zone-*iii.iv.v*

Figure A.3, Figure A.2, and Figure A.1 show the velocity vectors within the impeller passages for part-load, BEP, and overload operation respectively. The general trend of the flow at all three operating stages shows that the velocity magnitude is higher at the pressure side of the blade, particularly at the trailing edge region. Generally the flow imparting on the blade at the pressure side is separated at mid-span, with the relative velocity heading in opposite direction towards the leading edge and trailing edge.

At partload Figure A.1 there is no evidence of recirculation at the leading edge. At the trailing edge suction side of the blade there is evidence of flow separation and recirculation effects. The swirl component gains the same direction of the impeller rotation.

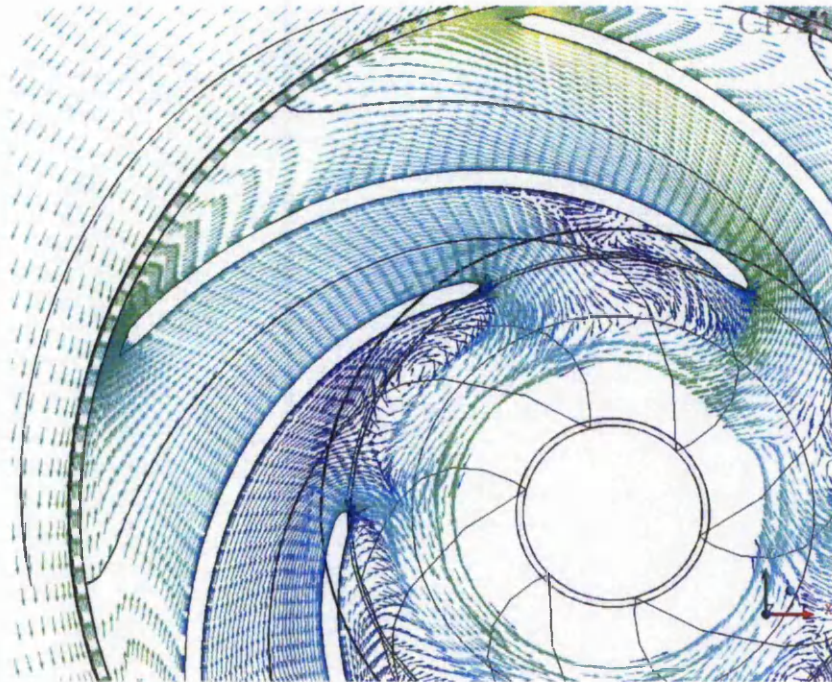


Figure A.1 Velocity vector plot at partload

At BEP, Figure A.2 there is evidence of recirculation at both leading edge and trailing edge suction side of some blades. The flow carries less swirl component at the exit. The swirl component has weak counter-rotating direction relative to the impeller, which would translate to swirl-less flow in the draft-tube (zones-vi.vii)

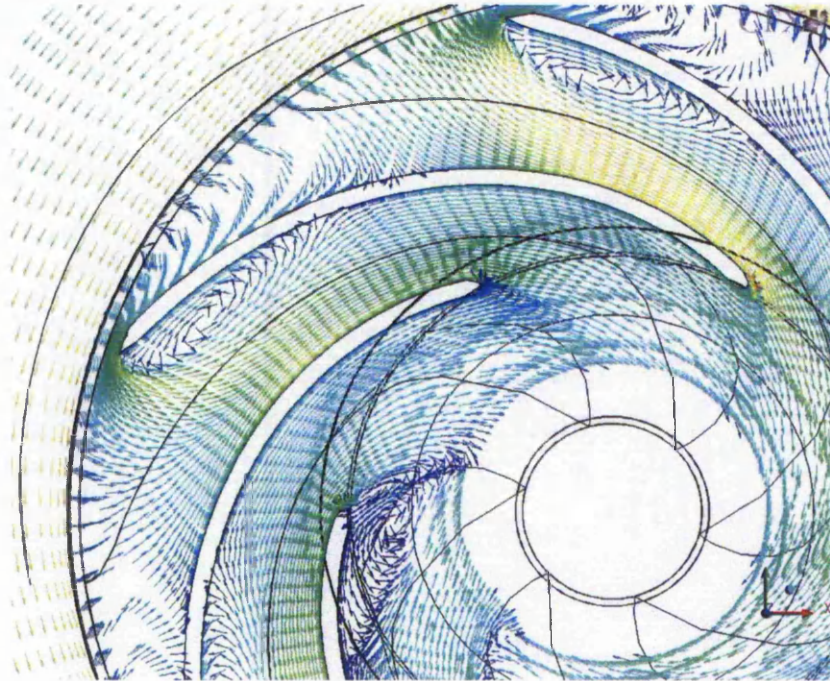


Figure A.2 Velocity vectors at BEP

At overload Figure A.3 operation there is evidence of recirculation at the leading-edge suction side of the blades. At the trailing edge there is sum evidence of flow separation. The swirl velocity component has counter rotating direction relative to the impeller.

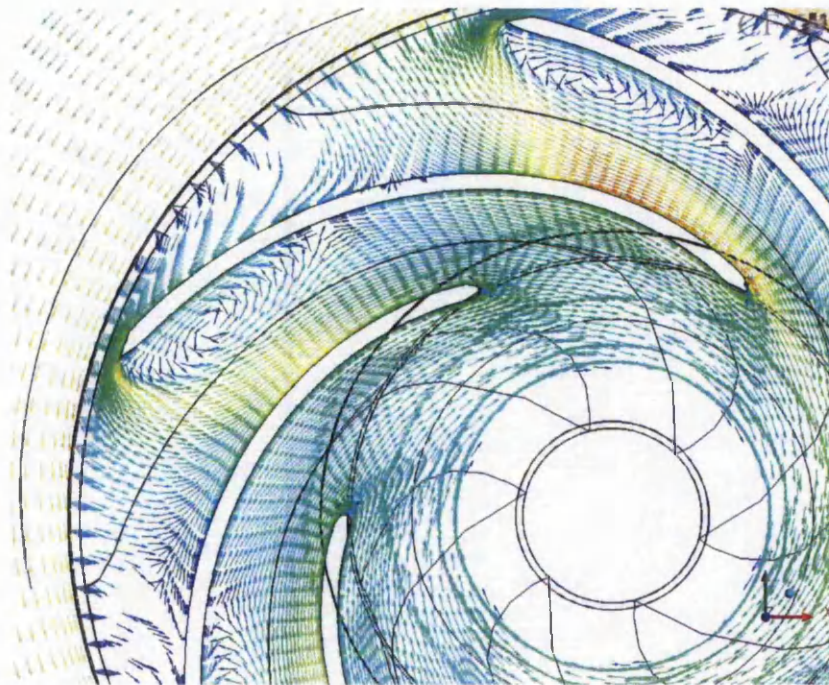


Figure A.3 Velocity vectors at Part-load

Summary

At the suction side around the leading edge region there is evidence of separation and recirculation, the size of which depends on the operating stage of the machine. Generally the velocity magnitude of the flow passing through the first passage (seen just under the volute tongue) is much larger than for the other passages. The velocity decreases for each passage in the counter clock direction. The general description of the flow pattern within all blade passages are relatively similar, however the detailed analysis of the velocity and pressure within each passage is quite distinct for each passage.

Recirculation at the leading edge suction side is present for all the regions of operation, the size of which increases as the flow rate increases i.e. larger recirculation at overload. At the trailing edge suction side there is also recirculation in some of the blade passages at the best efficiency operating point. In the part-load operating stage recirculation is seen at all blade passages, with some blades having counter recirculation motions. At the overload operating condition the recirculation is no longer seen at the trailing edge, with the velocity vectors following the blade profile throughout the passage.

A.2 Flow Description: Zone-vi.vii

Figure A.4 illustrates the computational observations of the flow streamline in the draft-tube at the different operating stages. It can be seen that the flow is quite complex and three-dimensional.

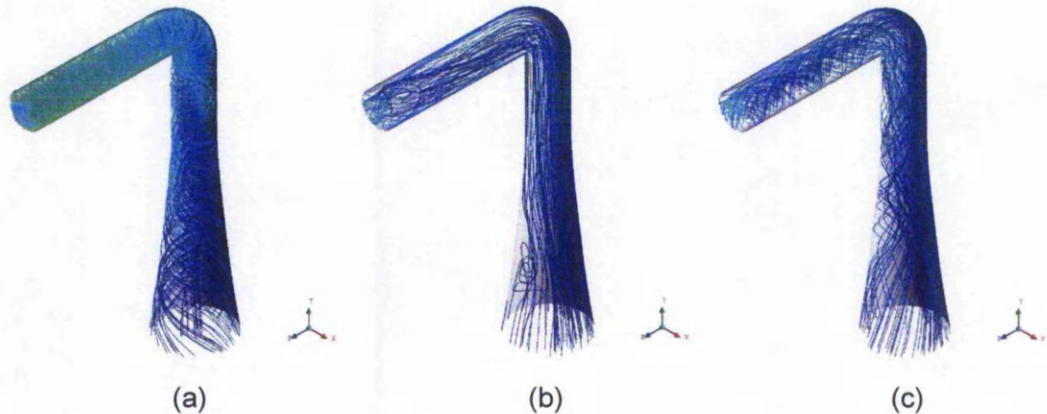


Figure A.4 Flow visualisation in the draft-tube (a) Part-load (b) BEP (c) Overload

At the part-load stage the flow consists of an inner and outer core of flow rotating in opposite directions. The inner core rotates at the opposite direction to that of the impeller, and the outer core flow rotates in the same direction of the impeller.

At the best efficiency region it can be noticed that the flow is predominantly axial. A slight rotation of the flow is visible at the portion before the bend and a more pronounced rotation as the cross-sectional area increases just after the bend. The increase in cross-sectional area allows the tangential components of the flow near the draft-tube wall to become more predominant as the axial components slow down due to the area increase.

In the over-load operating stage the velocity component is tangential throughout the draft-tube carrying the same direction of the impeller rotation.

In the computational setup zone-vi and zone-vii comprise the whole of the draft-tube, from the interface with zone-v to the outlet measuring plane. The draft-tube ensures that the turbine is full of water. In practical applications it can be submerged below the level of water at the tail race in order to regain part of the potential energy. Moreover, the design of a draft-tube allows a gradual reduction in the velocity of the discharged water so that the kinetic energy lost at the outlet

is also minimised. This is achieved through a gradual increase in the cross-section in direction of the flow (i.e. from the inlet to the exit of the draft-tube).

Figure A.5 shows the flow streamline distribution at a meridional plane. It can be seen that at the larger cross-sections in the radial direction that the flow pattern is inward at the centre of the volute section and also at the walls. In the smaller cross-section the same is observed at the centre of the volute section i.e. the flow path is directed directly into the impeller, but the presence of hub and shroud thicknesses creates some flow recirculation effects and disturbances in the flow pattern. The observed flow pattern changes slightly depending on the cross-sectional area and shape variation.

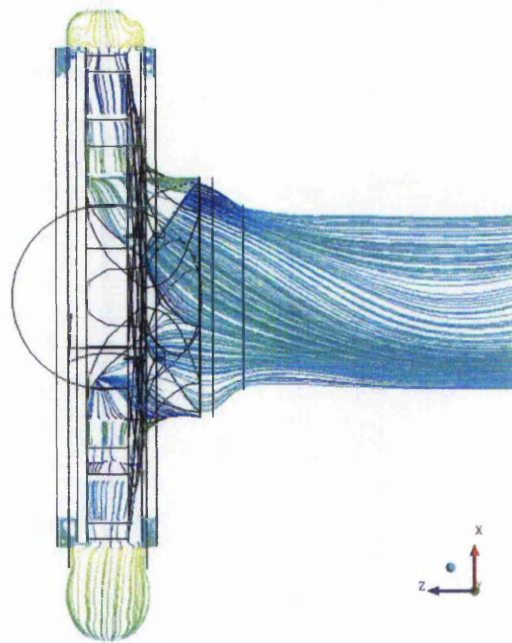


Figure A.5 Velocity vectors at volute cross-sections

In turbines, with similar geometry and operating principle of a PAT, it is usual for the volute mouth, to feed into guide vanes, which have the same width as the impeller inlet and therefore the flow disturbances are minimised in this area. The hub and shroud thicknesses will not be in the flow pathway thus not creating an obstruction. Moreover, the radial clearances in a turbine are usually kept to a minimum in order to reduce further flow disturbances.

An ideal volute/impeller combination will permit a uniform velocity distribution along the interface between both components so that energy is transferred equally to all blades. This can be achieved to a reasonable extent by the use of guide vanes in turbines. However, the current PAT computational model does not include guide vanes.

A.3 Internal Hydraulics - Optimization & Model Complexity

A.3.1 Interface Modelling

Figure A.6 through to Figure A.9 show the total pressure and velocity distribution in stationary frame of reference in the volute and the impeller.

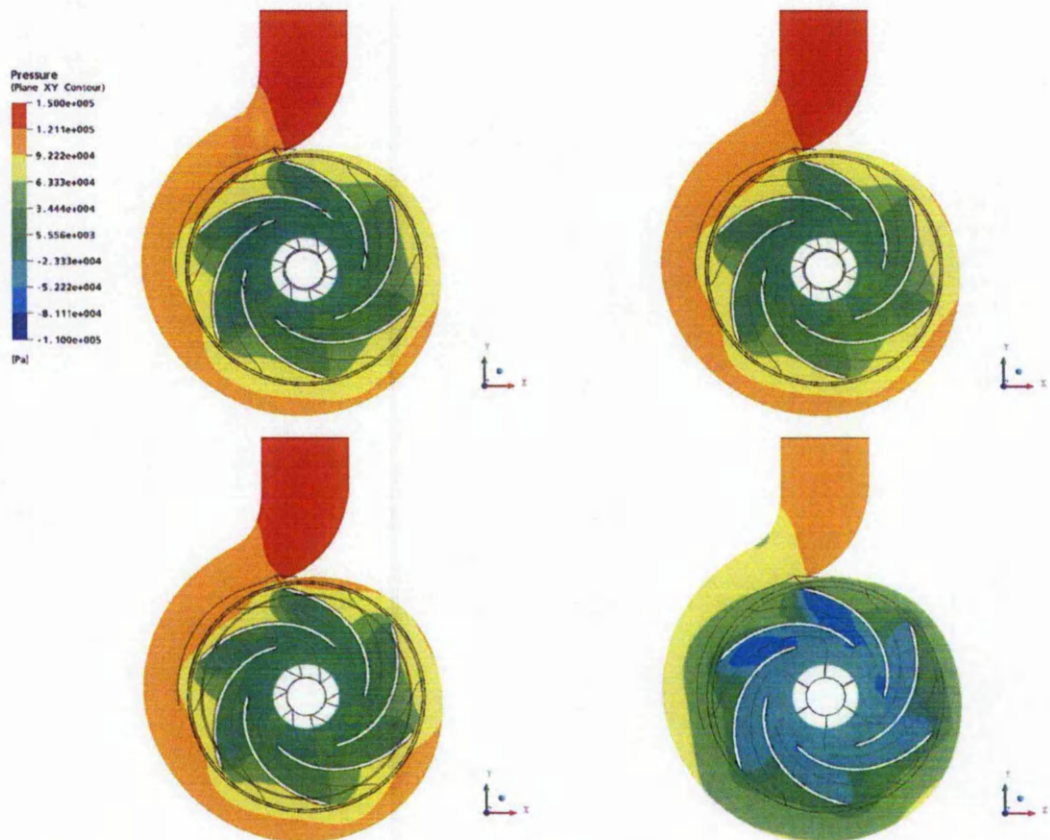


Figure A.6 Pressure distribution – plane XY a) interface i, b) interface ii, c) interface iii, d) interface iv

The trend shows that, as the churning geometry volume is reduced the pressure. For interface-i, interface-ii, and interface-iii, the pressure distribution and gradient along the casing and impeller are quite similar, however for the v-shape interface iv, the pressure.

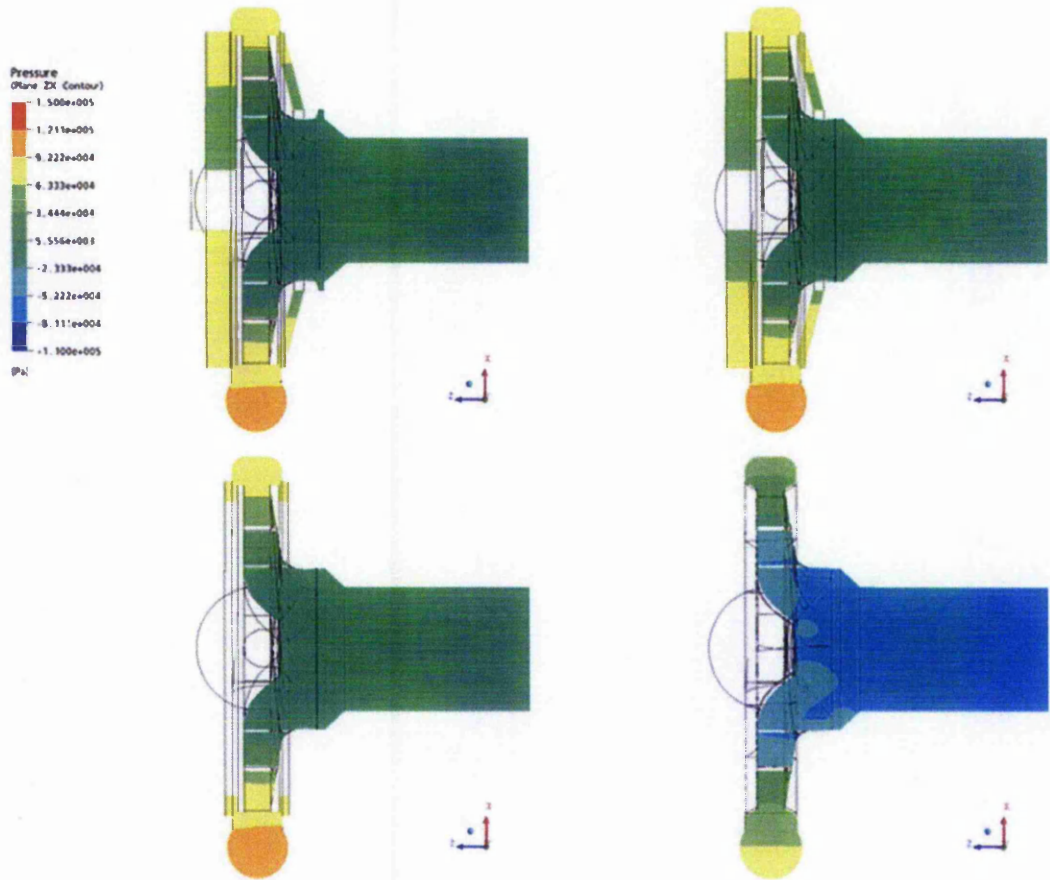


Figure A.7 Pressure distribution - plane XZ a) interface i, b) interface ii, c) interface iii, d) interface iv

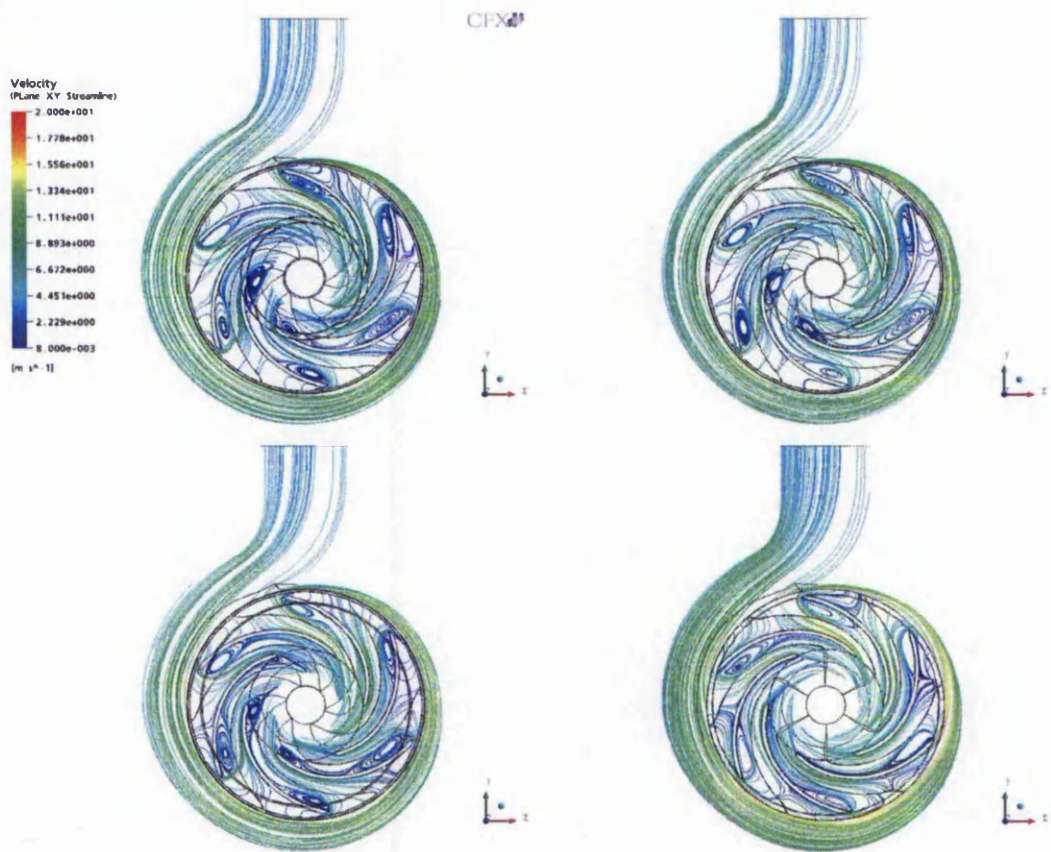


Figure A.8 Velocity Streamline – Plane XY a) interface i, b) interface ii, c) interface iii, d) interface iv

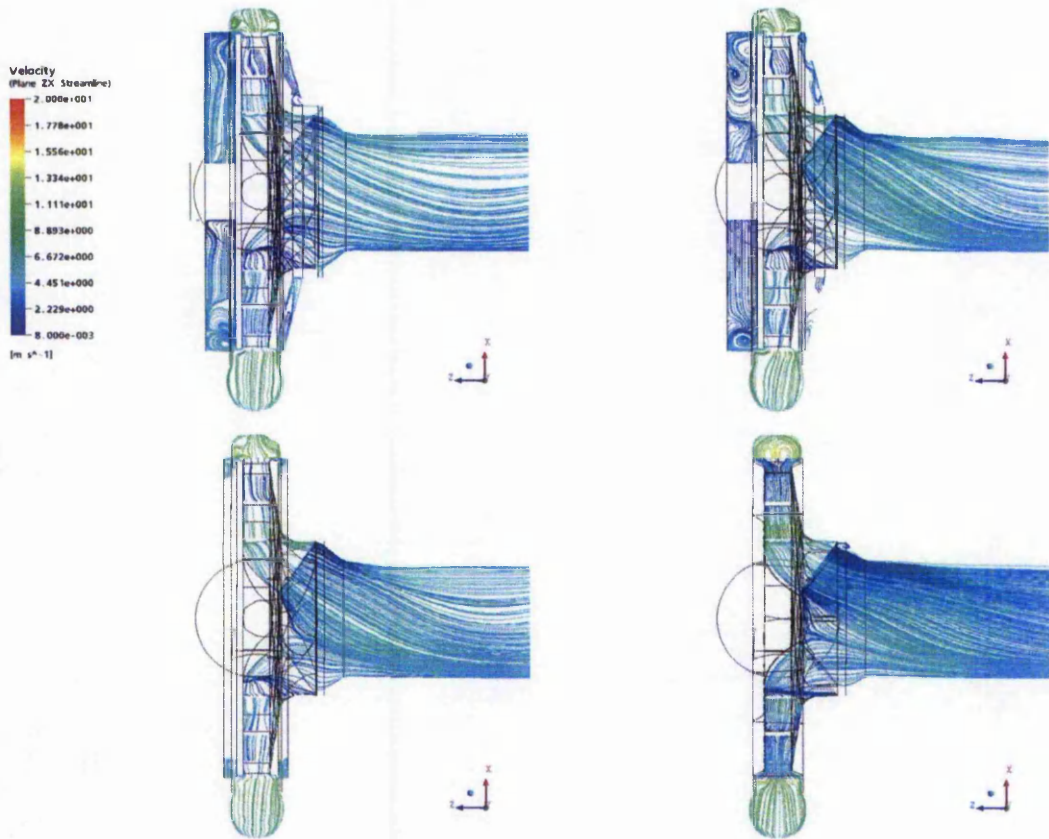


Figure A.9 Velocity Streamline – Plane XZ a) interface i, b) interface ii, c) interface iii, d) interface iv

The interaction of the fluid with the hub and shroud thicknesses in zone ii_c and ii_b respectively show disturbance in the flow and presence of complex turbulent and secondary flow. The flow is compressed locally and also some flow separation is noticed. Because the hub and shroud thicknesses are in the flow path this causes shock losses, and this can be seen by the large decrease of the meridional component of velocity plotted in graph +++. Subsequently the streamline path is somewhat affected which fundamentally contributes to further losses.

A.3.2 Losses interfaces

The tables in the following sections are the percentage losses within each zone for the different interface models. These refer to the results in Chapter 5, section 5.4.

A.3.2.1 Interface i

Load Point	Discharge	Zone i	Zone ii	Zone iii-iv-v	Zone vi	Zone vii
Overload	0.132	20.1	10.1	58.2	5.7	5.9
Overload	0.122	17.7	6.7	43.9	4.4	5.0
BEP	0.113	15.4	4.5	35.5	4.7	4.8
Partload	0.096	11.2	1.6	25.5	11.7	11.6
Partload	0.074	8.1	0.6	15.6	17.6	34.7
Partload	0.050	10.7	1.9	17.2	21.9	41.2

Table A.3.1 Percentage losses in each zone for interface i

A.3.2.2 Interface ii

Load Point	Discharge	Zone i	Zone ii	Zone iii-iv-v	Zone vi	Zone vii
Overload	0.132	20.7	8.5	60.5	5.3	6.6
Overload	0.122	17.8	5.8	45.7	4.3	6.1
BEP	0.113	15.4	3.6	36.8	5.2	5.3
Partload	0.096	11.1	0.6	25.5	10.2	12.0
Partload	0.074	7.7	-1.4	16.1	15.7	36.4
Partload	0.050	8.4	-2.4	17.0	19.2	43.0

Table A.3.2 Percentage losses in each zone for interface ii

A.3.2.3 Interface iii

Load Point	Discharge	Zone i	Zone ii	Zone iii-iv-v	Zone vi	Zone vii
Overload	0.132	22.9	7.8	68.2	7.3	6.3
Overload	0.122	19.8	5.2	51.3	6.1	6.7
BEP	0.113	16.9	2.6	40.8	5.9	5.0
Partload	0.096	12.6	-0.5	28.3	10.3	8.1
Partload	0.074	7.3	-1.5	17.3	16.3	28.2
Partload	0.050	9.5	-3.6	19.2	20.1	41.8

Table A.3.3 Percentage losses in each zone for interface iii

A.3.2.4 Interface iv

Load Point	Discharge	Zone i	Zone ii	Zone iii-iv-v	Zone vi	Zone vii
Overload	0.132	22.4	-4.4	79.6	9.2	7.0
Overload	0.122	20.6	-3.4	60.5	6.4	6.2
BEP	0.113	18.7	-2.7	46.3	4.8	4.8
Partload	0.096	14.9	-2.2	28.6	9.0	7.1
Partload	0.074	9.9	1.0	18.1	17.9	35.8
Partload	0.050	9.6	1.8	20.9	21.5	53.7

Table A.3.4 Percentage losses in each zone for interface iv

APPENDIX B Calculation of Leakage loss

Volute leakage can be calculated using Thornes expression (1979).

$$H_f = 0.74H_p - \frac{U_2^2 - U_r^2}{8g} = \frac{1}{2g} \left(\frac{2q_p}{\pi D_r \delta} \right)^2 \left(\frac{fl}{\delta} + 1.5 \right) \quad (\text{B.1})$$

δ , is the clearance diameter between the impeller and the casing at the impeller eye, l is the length of the clearance, D_r is the external diameter of the impeller eye and f is a dimensionless friction coefficient found from the Moody diagram.

The exact clearance was not known from the experimental set up. But the CFD was modelled with the following characteristics.

$D_r = 130$ mm; $l = 10$ mm; ; $\delta = 0.1$ mm; $Q_p = 26$ l/s; $H_p = 18.15$ m

The calculation is made according to Williams (1992). The leakage passage area is given by:

$$A_L = \frac{\pi D_r \delta}{2} = \frac{\pi \times 130 \times 0.1}{2} = 20.4 \text{ mm}^2 \quad (\text{B.2})$$

The value of Reynolds number is given by:

$$\text{Re} = \frac{V_L \delta \rho}{\mu} = \frac{q_L \delta \rho}{A_L \mu} \quad (\text{B.3})$$

Assuming that the flow is 5% of the total flow, as a first estimate, i.e. $q_L = 26 \times 0.05 = 1.3$ l/s

$\text{Re} = 6372$

$F = 0.044$, which, when substituted into equation () gives:

$q_L = 1.41$ l/s

This value is slightly higher than the original value and is within $\pm 10\%$ of the original value. Comparatively to the CFD flow this is much higher. The CFD leakage flow was $q_l = 1.12$ l/s. Thornes method seems to over predict the losses.

APPENDIX C Geometry Verification using CFD

C.1.1 Blade Angle

The inlet blade angle was measured manually, since this was a critical parameter a study was carried out to verify whether any error in measurement would cause a large discrepancy in the results in the prediction of performance. Figure C.1 shows the actual (measured) inlet blade angle (102 deg) as reference and variation of 4 degrees to either side of reference blade angle.

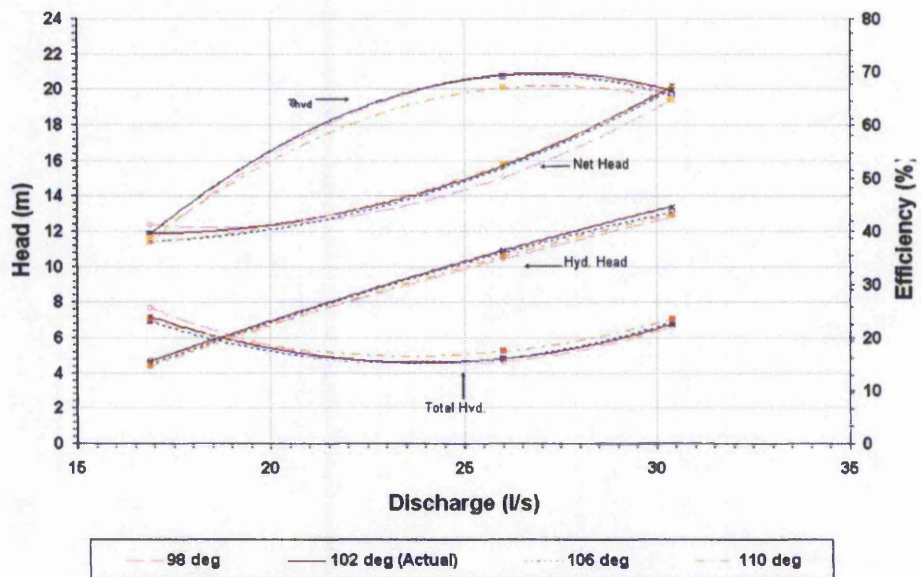


Figure C.1 Effects of blade angle change at the Impeller Leading Edge

It can be seen that there is not much influence for the blade angles with ± 4 degrees, the hydraulic parameters are reasonably well matched. However for the 110 degrees inlet angle the losses increase and with that the overall efficiency. It is safe therefore to say that even if there is slight error on measurement of the actual blade angle the overall performance characteristics will not vary immensely. It is unlikely that an error in measurement of more than 4 degrees is made.

Another observation that can be made from this evaluation is that with the increase in blade angle, the span of the blade increases at the leading edge, and

therefore it can be determined that this has a detrimental effect on the overall performance characteristics of a PAT. Lower angles than 98 degrees were not simulated. This is also a useful exercise to carry out during the design of impellers for PAT applications.

The effect of blade reduction at the leading edge was carried out with the same intent of investigating any errors that might arise due to inaccuracies in measuring the blade length. Incremental reductions of 5mm at a time were carried out. The results in [Figure C.2](#) show that reduction in leading edge blade angle cause the an efficiency decrease. The losses and head rise in the main operating region. The efficiency curve maintains the same profile but shifts to lower operating flows.

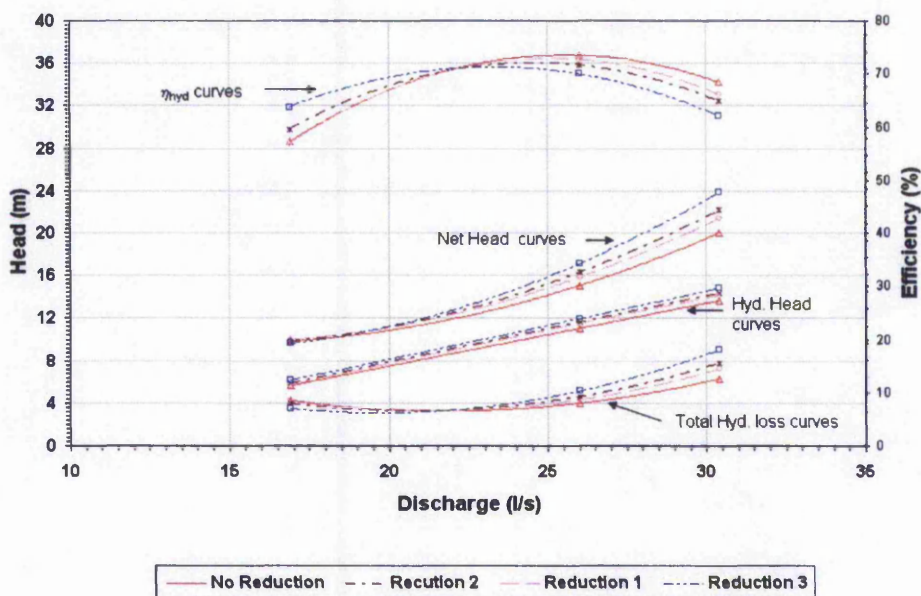


[Figure C.2](#) Effects of blade reduction at the impeller leading edge (turbine)

Similarly reduction of 5mm at the impeller trailing edge was carried out with the same objective. It can be seen that this has the effect of increasing the losses in the part load region which has consequent negative effect on the overall efficiency. The efficiency curves do not shift unlike the leading edge.

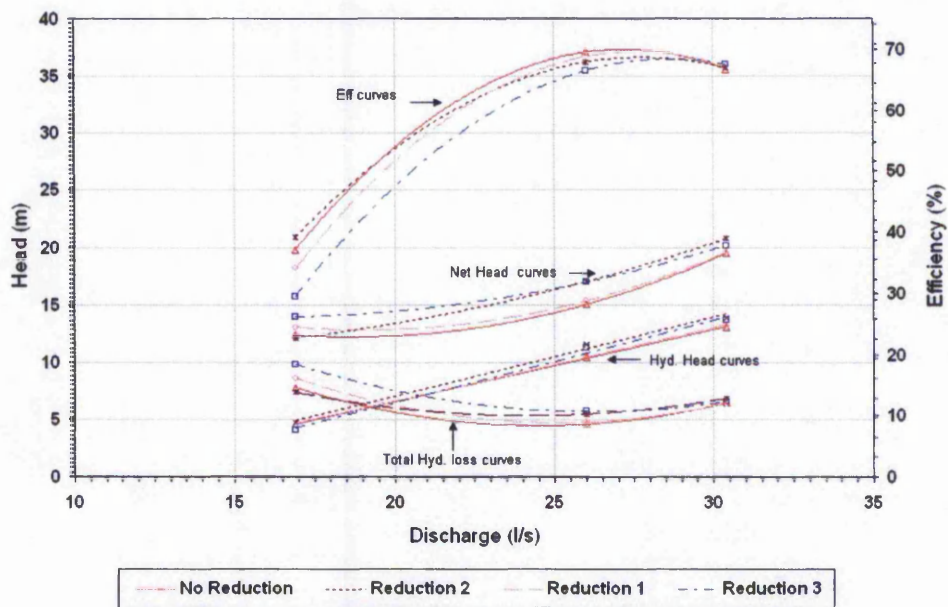


Figure C.3 Effects of blade reduction at the impeller trailing edge (turbine)

This study has shown a useful aspect of CFD, whereby it can be used to design efficient impellers with simple parametric variations. The study suggests that longer impeller spans are more efficient than shorter impeller spans. On the other hand there are many other aspects that influence the overall performance such as the volute/impeller combination.

C.1.2 Rough Walls

An attempt was made to investigate the influence of rough walls on performance characteristics of a PAT. However the real wall sand grain roughness was not known for the 24.5 rpm PAT.

Figure C.4 Shows the performance characteristics for a PAT with rough walls and smooth walls. It can be seen that the PAT model with rough walls is under predicting the losses in the part-load region. Part of the reason is because the calculation was not allowed to converge due to the high number of iterations required. It can be seen however, that in the main operating region the prediction of net head and losses is relatively similar to the smooth wall PAT.

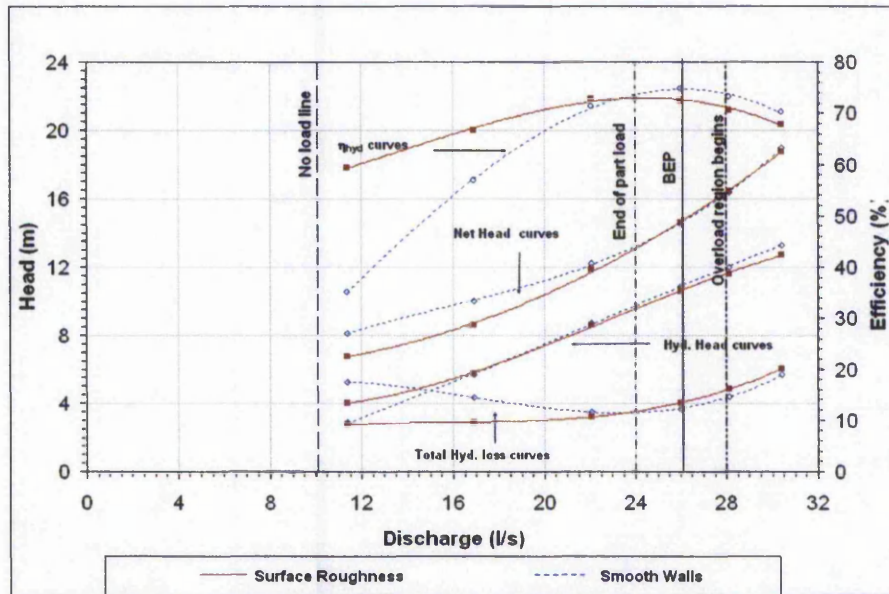


Figure C.4 Performance characteristics for PAT with smooth and rough walls

Figure C.5 shows the torque calculation for both smooth and rough walls. The torques are comparatively similar with only marginal discrepancies in the part load region and overload region.

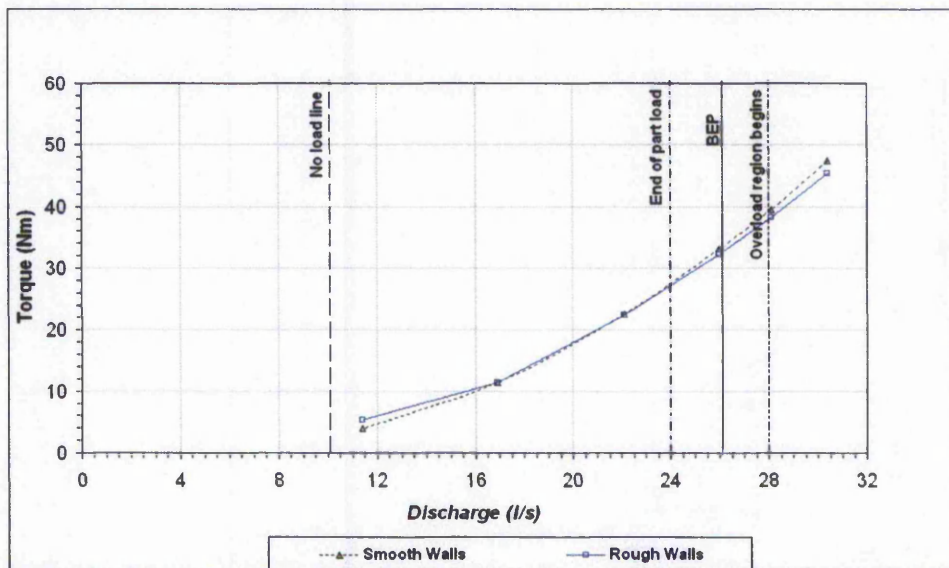


Figure C.5 Torque distribution for PAT with smooth and rough walls

Figure C.6 shows the individual flow zone losses as a result of rough walls. All losses have undergone significant changes. The solutions seem to be quite erratic particularly in the part load region.

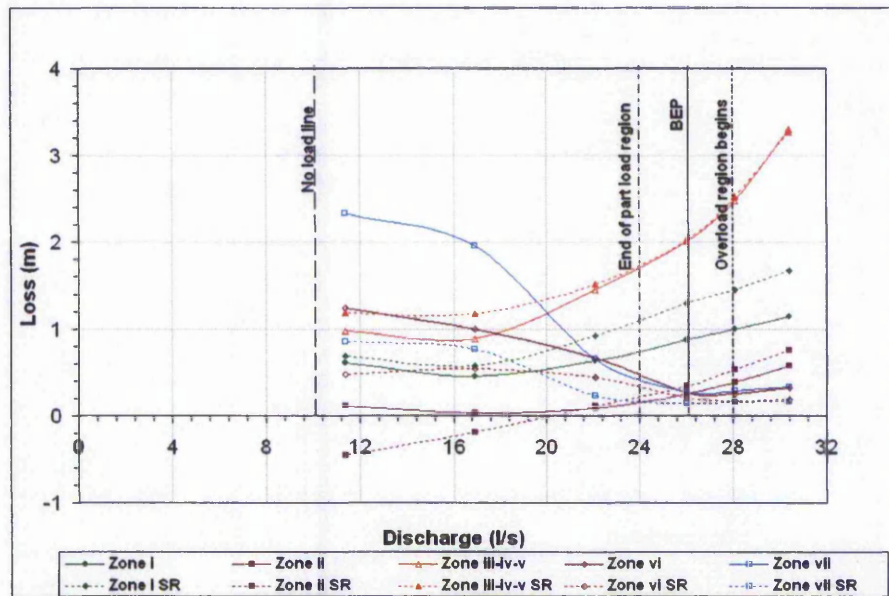


Figure C.6 Zone losses for PAT with rough and smooth walls

Summary

The study of rough walls has been inconclusive. Difficulties were encountered in the set up of rough wall simulation due to the distance limitation of the wall to the first grid node. The roughness modelled is expected to be less than that for the real model. Higher sand grain roughness caused instabilities of the solver and ultimately failure. Therefore, the results obtained are unreliable and significant conclusions can not be made. This is an area that remains to be investigated further.

APPENDIX D Test Specimen

D.1 Geometry Description

Figure D.1a and Figure D.1 show the volute and impeller cross-sections respectively.

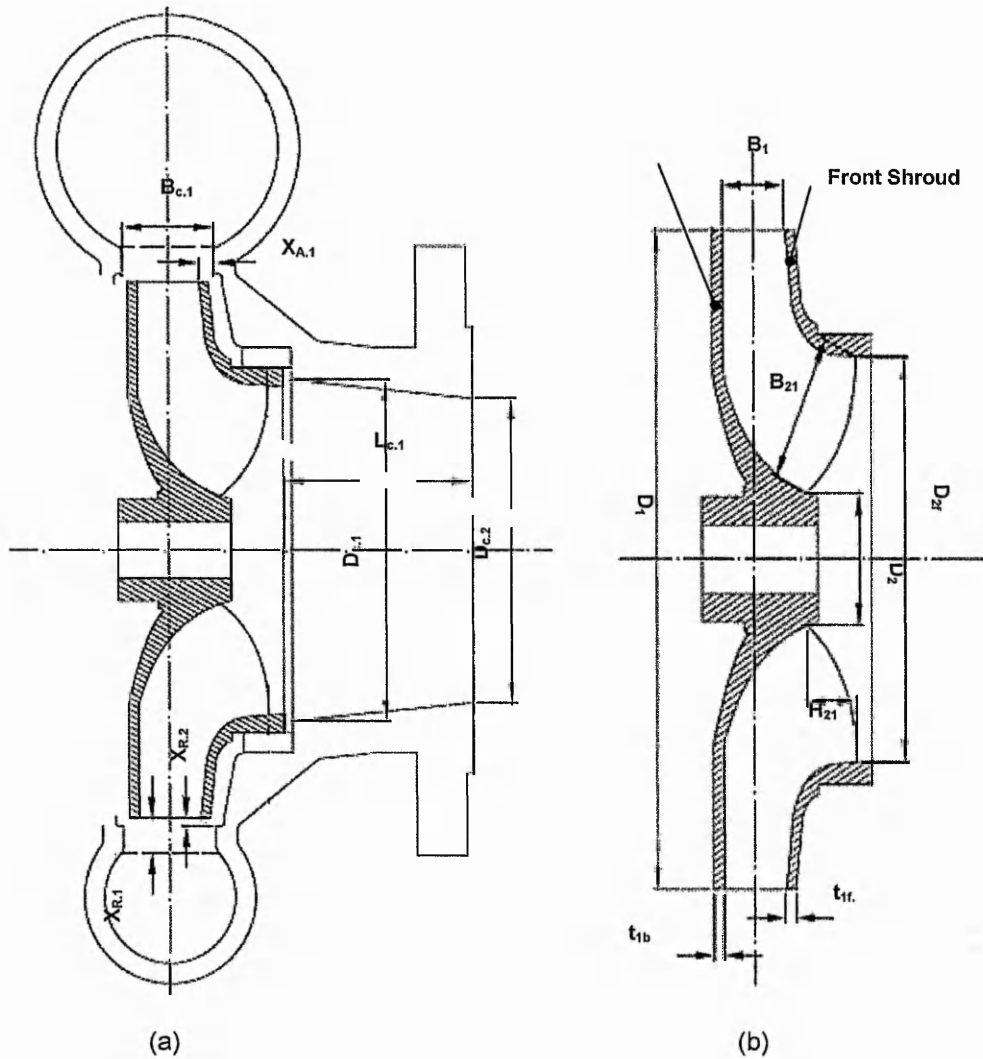


Figure D.1 Volute and Impeller cross section

D.2 Test Specimen

D.2.1 Volute, Impeller, and Draft-tube dimensions

The volute and impeller critical dimensions of the 24.5 rpm NW8 Kirloskar pump are summarised in

Table D.2.1.

Symbol	Description	Dimension
D_1	Impeller inlet diameter (turbine)	$\Phi 258\text{mm}$
D_{2f}	Impeller eye diameter	$\Phi 130\text{mm}$
$D_{2\text{Out}}$	Impeller eye diameter (outer plane)	$\Phi 132\text{mm}$
$D_{2\text{in}}$	Impeller eye diameter (inner plane)	$\Phi 132\text{mm}$
β_{1f}	Inlet blade angle (front shroud)	16.4°
β_{1b}	Inlet blade angle (back shroud)	16.4°
β_{2f}	Exit blade angle (front shroud)	24.3°
β_{2b}	Exit blade angle (back shroud)	24.3°
B_1	Inlet blade width (at leading edge)	21.8mm
B_2	Exit blade width (at trailing edge)	39mm
H_2	Height of the exit blade	39mm
t_1	Inlet blade thickness	4.25mm
t_2	Exit blade thickness	4.25mm
t_{1f}	Front shroud thickness	7.25mm
t_{1b}	Back shroud thickness	5mm
n	Blade number	6

Table D.2.1 Volute and Impeller Dimensions

D.2.2 Impeller Inlet and Outlet flow areas

The important flow areas pertaining to the impeller are, the inlet flow area, the exit flow area (at the end of the blade) and impeller eye area. The different areas for the test specimen are given in the table below:

Description	Calculation	Area
Blade inlet	$(\pi D_1 b_1) - (nt_1 b_1)$	17147 mm ²
Blade Exit	$(\pi D_2 b_2) - (nt_2 b_2)$	14885.9 mm ²
Impeller Eye	$\pi D_e^2/4$	13273.2 mm ²

Table D.2.2 Impeller Inlet and Exit flow areas

D.2.3 Volute section areas

The volute casing of the 24.5 rpm non-modified pump has been described in Figure D.2 Volute section dimensions. It displays the overall layout of the volute with eight radial sections.

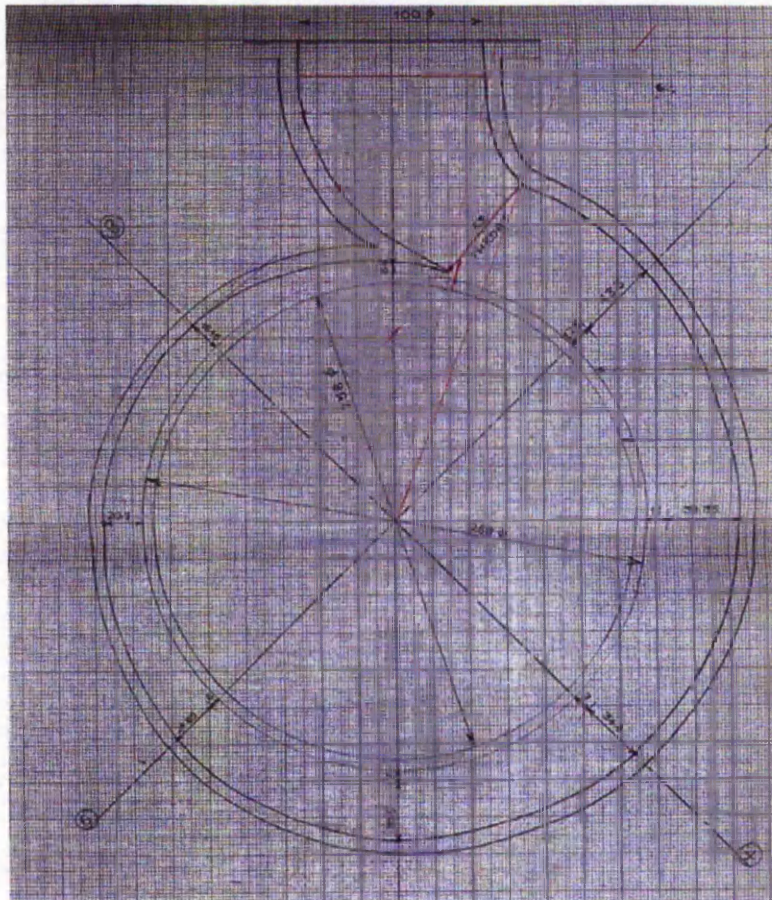
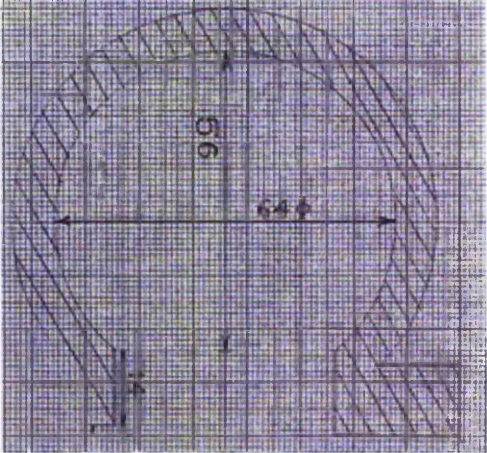
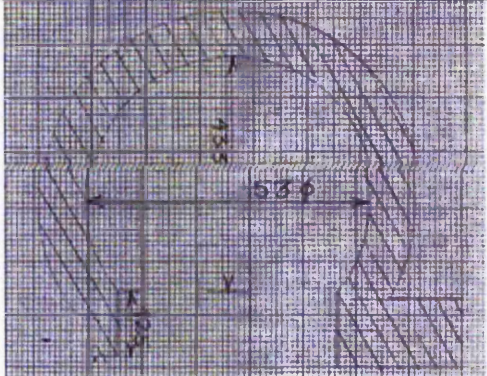
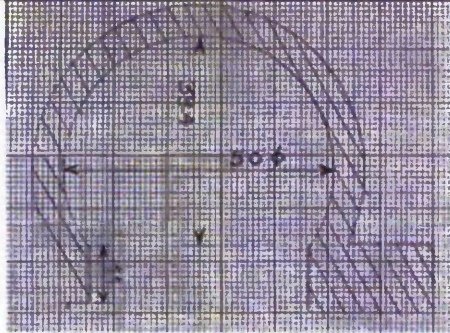
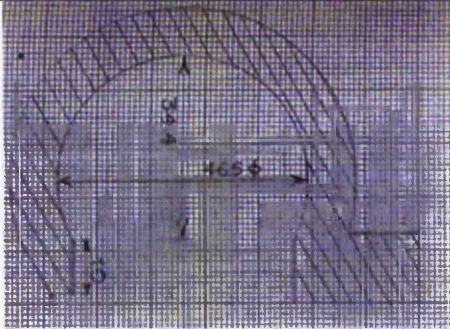
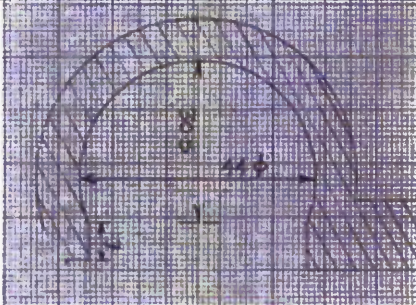
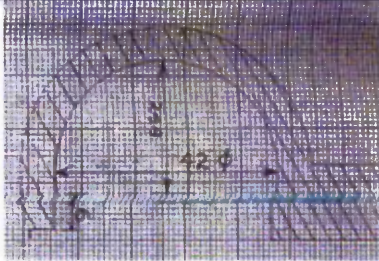
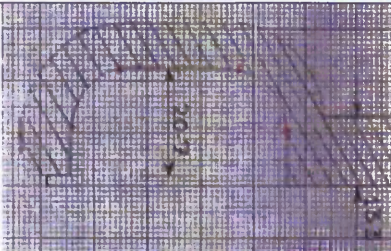


Figure D.2 Volute section dimensions

Each individual section is summarised in Table D.2.3 below

Table D.2.3 Summary of the radial volute profiles

Volute	Drawings	Area
Section 1		235.4 mm ²
Section 2		2164 mm ²
Section 3		1801 mm ²

Section 4		1395.7 mm ²
Section 5		1400 mm ²
Section 6		1102.2 mm ²
Section 7		801.8 mm ²
Section 8		671.1 mm ²
Throat	Circular cross-section	3350.6 mm ²
Inlet	Circular cross-section	7853.9 mm ²
Uniform Clearance Area		226.05 mm ² .

Uniform clearance area - This refers to the uniform area between impeller outlet diameter and reference diameter on the casing.

D.2.4 Suction-modified pump

Suction-modification (modification-i) was carried out on both the impeller and the casing. The eye of the impeller has been increased to 140 mm from 130 mm. A diffuser type enlargement extending 21 mm into the impeller with a diffuser angle of 11° , was given. The casing eye was given a constant enlargement with diameter 140 mm.

D.2.5 Inlet rounded pump

The rounding was carried out on the interior and exterior shrouds. The interior shroud has a round of R 2.0 mm, while the exterior shroud has a round of R 2.25 mm. In the Experimental setup the profiles were rounded off to a constant round of R 2.25 mm.

	Non- Modified		Modified-Eye		Percentage increase, %
	Original diameter, mm	Original Area, mm ²	Enlarged diameter, mm	Enlarged Area, mm ²	
Impeller eye	130 mm	13273.2 mm ²	140 mm	15393.8 mm ²	16 %
Casing eye	100 mm	7854 mm ²	140 mm	15393.8 mm ²	96 %

Table D.2.4 Summary of the suction modification done to impeller eye and casing-eye

APPENDIX E Performance Prediction

Methods

E.1 Theoretical prediction methods

Theoretical performance prediction methods have already been exhaustively covered and evaluated in many other previous research. Some of the contributors include Kittredge (1931) and Stepanoff (1957) amongst many other. Williams (1992) gathered the most common methods and evaluated them individually. He advised that any method can only serve as a first estimate rather than a definite result due to the many uncertainties involved. Williams also developed an area-ratio method, but this gives inaccurate predictions for some pumps.

E.2 Use of Cordier Diagrams

The Cordier diagram was developed by Otto Cordier (1953) which brings various turbo-machines under a common platform and it shows the interdependence between the specific speed number and specific diameter number. Singh (2005) suggested the use of the Cordier diagram as a means to select an appropriate pump to suit given site boundary conditions. It provides a range of impeller reference diameters that could suit different boundary conditions. The diameter is selected via the pump manufacturers catalogue and is expected to fall within this range preferably near to the mean diameter. After the selection Singh suggested a two fold selection which consists on:

1. Finding out if the selected pump would suit the head and discharge conditions.
2. And if the selected pump satisfies the above conditions then the synthesis of the complete characteristics needs to be done followed by a number of procedures.

E.3 Recent Performance Prediction Methods

E.3.1 Amelios methods

Amelio et al (2004) proposed a one-dimensional numerical code for deriving the turbine efficiency of centrifugal pumps. The code estimates the sizing of each component using information such as impeller diameter, specific speed, head, and flow rate at pump BEP, machine overall dimension which are provided in manufacturers catalogues, to deduce geometrical parameters of the machine. It then calculates the losses through each component thus determining the PAT performance. The process however is limited as it only takes into account the average data and disregards the three-dimensional effects. The reported error is around $\pm 10\%$ but it has only been established for the particular case scenario rather than a range of pumps.

E.3.2 Ventrone Method

Ventrone et al (2000) proposed a means for correlating the ideal pump and turbine head-flow parameters in the region of optimum performance in both modes of operation using a runner momentum coefficient obtained experimentally and geometrical information from the runner. The reported error is around $\pm 4\%$ for the case studies given. It should be stated that the study was carried out on vaned diffusers can allow the flow angle to be adjusted prior to entry, making it possible to adjust the turbine to suit best efficiency.

E.3.3 Prediction using numerical approaches

Computational fluid dynamics has emerged as a good tool to investigate the hydraulics of various machines. A lot of this investigation has been successfully carried out and CFD has shown some considerable potential particularly in the research of turbomachinery. CFD is still an evolutionary process and there are many variables yet that need to be understood which may be useful for predicting efficiency in PATs.

APPENDIX F Computational Tool

F.1 CFD Code - CFX

Most general-purpose CFD commercial codes integrate three main stages, namely pre-processor, solver, and post-processor with individual user-friendly interfaces which are for input of problem parameters and examination of results. The pre-processor allows the input of physical elements, fluid properties, boundary and so forth. The solver is designed around numerical algorithms capable of solving complex fluid flow problems. It interacts with the pre-processor by obtaining the input data, solves the problem, and writes an output file. The results can be analysed on the post-processor. Since the geometry and mesh generator is built separately from the pre-processor CFX.5.6 incorporates four interfaces or modules:

- CFX-Build - generic geometry and mesh generator, including automatic mesh generator with capability for unstructured grid
- CFX-Pre - selector of physical elements, fluid properties, and boundary conditions, etc.
- CFX-Solver - the environment where the problem is solved numerically
- CFX-Post - results can be visually and numerically analysed in this module.

F.1.1 Other salient features in CFX 5.6

CFX.5.6 incorporates the most common validated turbulence models, namely the standard $k-\epsilon$, the $k-\omega$ by Menter, and the Reynolds Stress Model (RSM). The available frame change options are frozen-rotor interface, stage interface, and transient interface. The first two options assume that the flow field is steady (Tamm et al, 2002), and the third option allows for unsteady effects to be modelled. A final point to be highlighted is the various boundary conditions options available; these are wall, inlet and outlet, periodic and symmetry, and opening.

APPENDIX G Experimental Work at IWK

A brief description on the experimental set up of the PAT test rig is given in the following sections. The experimental work was carried out by Singh (2004) at IWK in Karlsruhe. His work has contributed immensely to PAT research areas and is thoroughly covered in his thesis. Singh tested the physical test specimen that was investigated in the current research.

G.1.1 Test-Rig

Figure G.1 shows the schematic view of the test facility. The input energy is supplied by four identical pumps connected in parallel. Each pump is capable of delivering 140 l/s of water at a head of 16 m. A transparent acrylic draft tube is fitted at the PAT exit and is submerged in a discharge tank 1.3 m below. The loading device used is a DC generator. The hydraulic circuit for the PAT test-rig is an open loop type and hence study of cavitation is not possible.

The instrumentation used on the test-rig is described in detail in Table F.1.1. The data was processed using the 'Labview' software package from National Instruments and the measurements were made over a time interval of 10 seconds. Transient conditions were not studied.

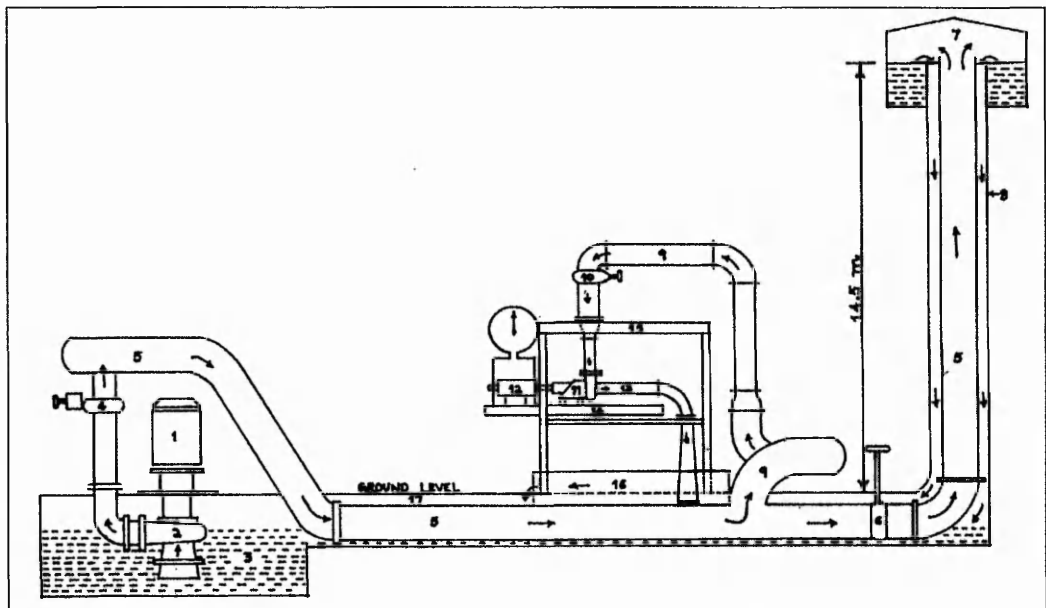


Figure G.1 Schematic Layout of Test Facility

<u>Parameter</u>	<u>Measurement Principle</u>	<u>Make</u>	<u>Range</u>	<u>Accuracy</u>	<u>Output Signal</u>
Discharge	Faradays Magnetic law	Turbo	0-1000 <i>m³/h</i>	±1% of full scale	0-20 <i>mA</i>
Inlet Pressure (Positive)	Wheatstone bridge	Hottinger Baldwin Messtechnik	0-2 <i>bar</i>	±1% of full scale	0-8 <i>mV/V</i>
Exit Pressure (negative)	Wheatstone bridge	Hottinger Baldwin Messtechnik	0-1 <i>bar</i>	±2 % of full scale	0-8 <i>mV/V</i>
Torque	Wheatstone bridge	Hottinger Baldwin Messtechnik	+/-100 <i>Nm</i>	±0.1% of full scale	5-15 <i>kHz</i>
Speed	Optical counts	Self assembled		1 <i>r/min</i>	Pulses

Table G.1.1 Instrument Summary

G.1.2 Experimental Optimisation

The CFD procedure includes the enlargement of impeller eye. The experimental procedure only includes inlet-rounding.

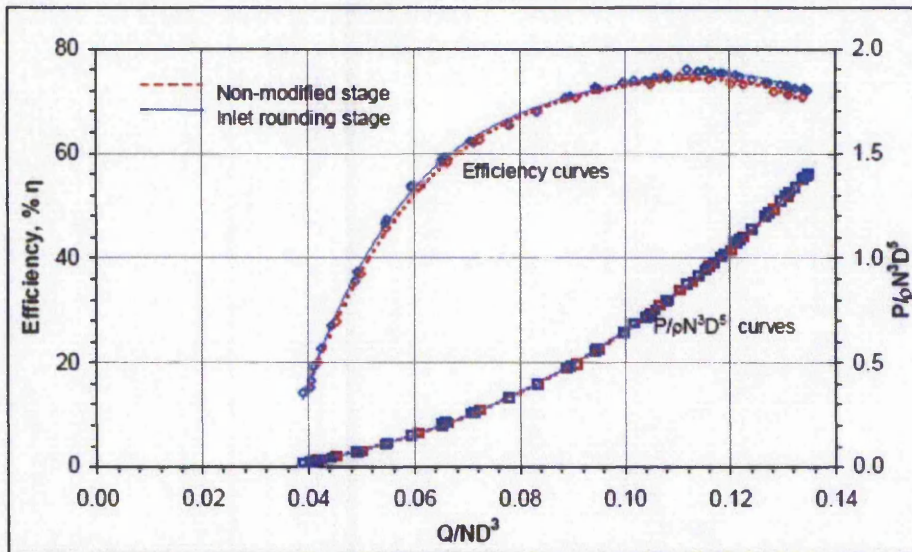
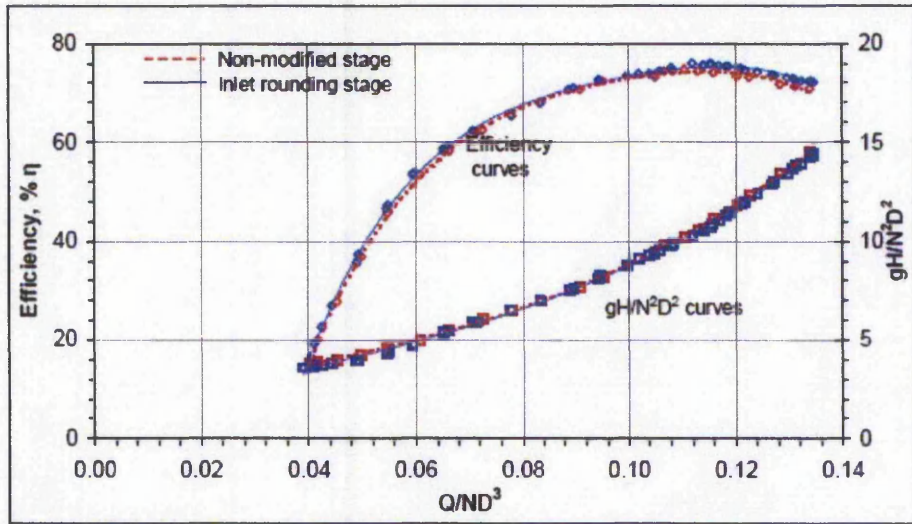


Figure G.2 Inlet rounding procedure on 24.5 rpm PAT – Experimental work from Singh (2004) Setup equivalent to modification-ii CFD

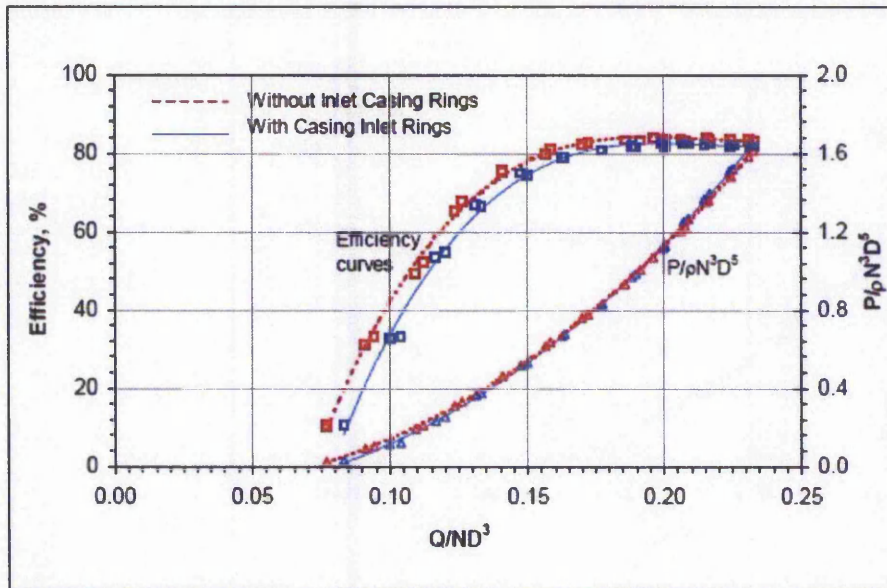
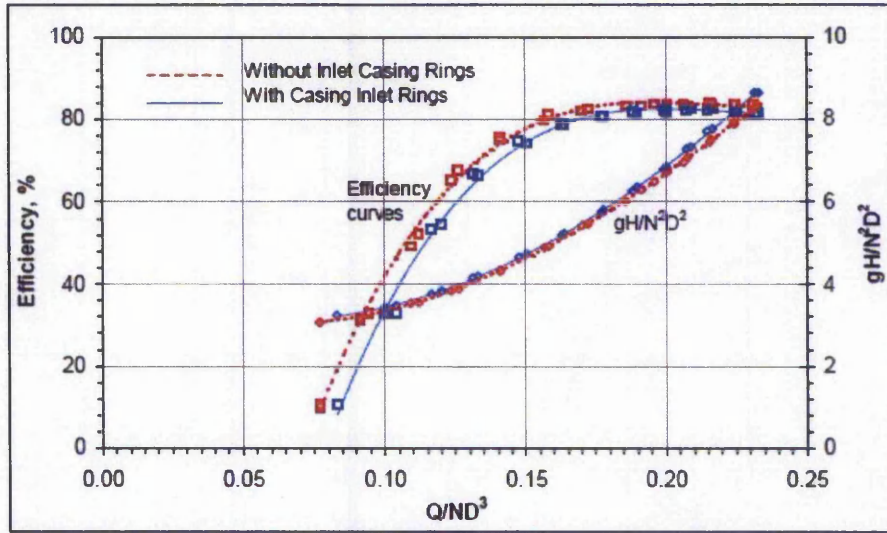


Figure G.3 - Casing Rings Optimisation-ii on 39.7 rpm PAT – Experimental work
Singh (2004) Set up equivalent to interface-iv CFD

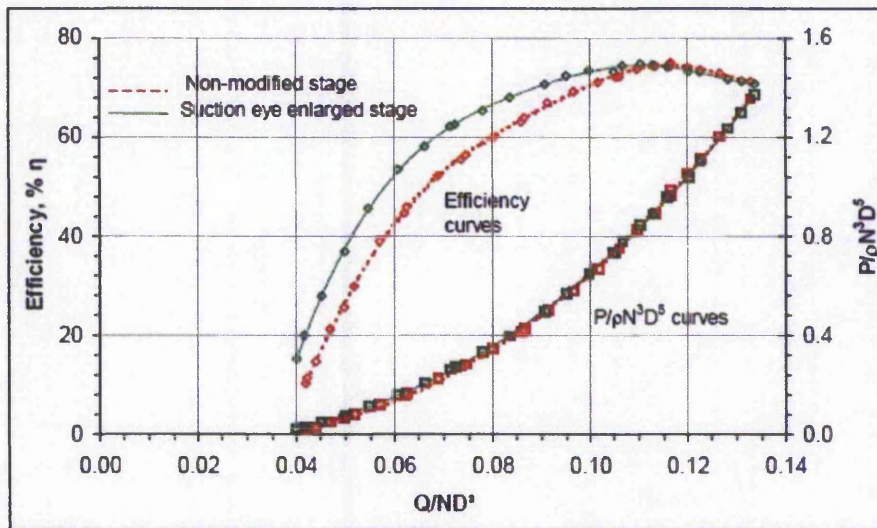
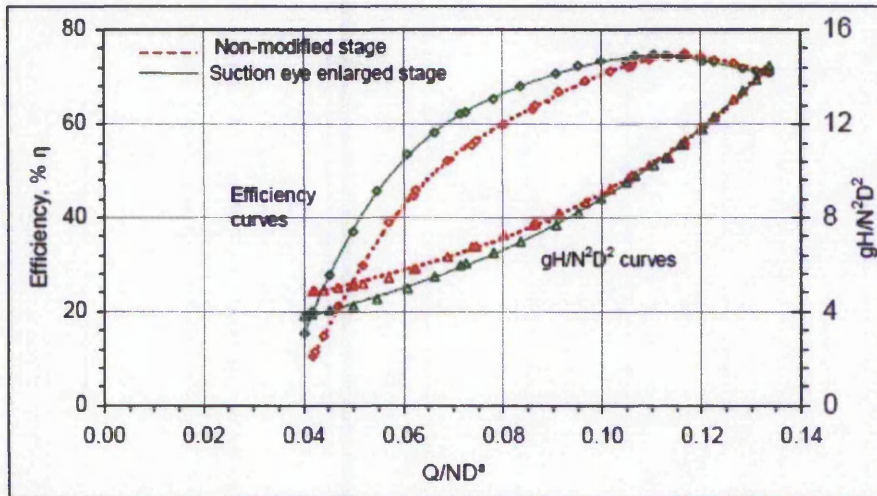


Figure G.4 Enlargement of casing and impeller eye on 24.5 rpm PAT – Experimental work Singh (2004) Equivalent to modification-i CFD

APPENDIX H Experimental Uncertainty

H.1 Uncertainty Analysis for Experimental-CFD correlation

Uncertainty for experimental-CFD correlation of the 24.5 rpm PAT is given in the tables below (Singh, 2004).

Variable	Maximum Uncertainty
$(\Delta\rho_{Le})$	$\delta = \pm 0.168$ or 1648 N/m^2
t_{Le}	$\delta = \pm 0.2 \text{ mm}$

Table H.1.1 Summary of the fundamental uncertainties associated with variables for leakage discharge calculation

PAT	Q	Q_{Le} (l/s)	δQ_{Le} (l/s)	$\delta Q_{Le}/Q$ (l/s)	P_{hyd} (W)	δP_{hyd} (W)	$\delta P_{hyd}/P_{hyd}$ (%)
24.5rpm	24.4	1.66	± 0.83	$\pm 3.4\%$	2527	± 52.1	$\pm 2.1\%$

Table H.1.2 Absolute uncertainty table for the Q_{Le} and P_{hyd} of the tested PAT (experiment-CFD) at respective BEPs

PAT	N (rpm)	Q (l/s)	H (m)	T (Nm)	P_{hyd} (W)	η_{hyd} (%)	$\delta H/H$ (%)	$\delta Q/Q$ (%)	$\delta P_{hyd}/P_{hyd}$ (%)	$\delta \eta_{hyd}/\eta_{hyd}$ (%)
24.5rpm	803	24.4	13.0	29.6	2527	81.3%	$\pm 1.3\%$	$\pm 9.6\%$	$\pm 2.1\%$	$\pm 9.9\%$

Table H.1.3 Relative uncertainty table for the tested PATs (experiment-CFD) at the respective BEP

APPENDIX I Published Papers

Hydraulic Analysis of a Pump as a Turbine with CFD and Experimental Data

Arnaldo Rodrigues¹, Punit Singh², Arthur Williams¹, Franz Nestmann², Eugene Lai¹

1. Nottingham Trent University (NTU), England

2. Institut für Wasserwirtschaft und Kulturtechnik (IWK), University of Karlsruhe, Germany

SYNOPSIS

This paper compares experimental and numerical results of a non-modified centrifugal pump operating as a turbine (PAT). The pump is a Kirloskar India make with specific speed of 24.5 *r/min*. The experimental work at IWK reveals overall performance characteristics of the PAT whilst the numerical study at NTU brings out detailed analysis of the three-dimensional flow behaviour in such a system. The hydraulic flow path within a PAT is divided into six different zones and each zone is independently analyzed. The interpretation is based on parameters namely the total system head, hydraulic losses, and hydraulic efficiency. The comparisons are performed at a speed of 800 *r/min* covering the full range of operating conditions of the machine. A very good match is achieved in the best efficiency region, with best efficiency occurring at the same flow rate of 26.1 *l/s* giving 78.1 % experimental efficiency and 78.2 % numerical efficiency. However, within the part-load region the discrepancy of efficiency values is significant within a range of 5 % to 10 %.

KEYWORDS

Flow zones, optimisation, swirl flow, draft tube, hydraulic losses

ABBREVIATIONS

CFD-Computational Fluid Dynamics

PAT- Pump As Turbine

BEP-Best Efficiency Point

NOMENCLATURE

D	Impeller outer diameter, <i>m</i>
g	Acceleration due to gravity, 9.81 <i>m/s</i> ²
H	Head, <i>m</i>
N	Speed, <i>r/min</i>
Q	Discharge, <i>l/s</i>
P	Shaft power, <i>kW</i>
T	Torque, <i>Nm</i>
η	Efficiency, %
ρ	Mass density, <i>kg/m</i> ³
ω	Angular velocity, <i>rad/s</i>

1. INTRODUCTION

Running pumps in reverse as turbines is a concept that has been around for many years and proven to be cost-effective mainly in micro-hydro applications. This concept was first introduced for power recovery purposes in industry, which gave way to a rich era of research with experimental testing of pumps but operating in turbine mode. Stepanoff's [2] work aided this new concept as it brought out information on pump performance under special operating conditions. However, obtaining empirical data became expensive and the several performance prediction methods that were brought out, based on the pump data at best efficiency, lacked generality for pumps of different designs. Williams [3] studied the prediction methods available and established limits for a first estimate. He also developed a performance prediction method based on the area ratio method by Anderson [1].

With the availability of new (study) approaches such as state of the art computational tools, a greater understanding of the complex flow patterns inside the machine is possible. Baines [4] demonstrated the effectiveness of CFD as a design tool by successfully predicting performance characteristics of a cryogenic power recovery turbine, operating in both turbine and pump mode. Tamm [5] also carried out CFD work on a centrifugal pump but no comparison was made with experimental data. Blanco [6] was able to describe the flow characteristics within a centrifugal pump using numerical studies.

Previous studies have not carried out detailed optimisation of PAT geometry. Experimental work by Lueneburg [7], Williams [8], and Cohrs [9], and field testing described by Mikus [10] have shown that simple modifications to geometry can bring about efficiency improvements, but the results are not consistent.

In this paper a new approach of data interpretation is evolved considering different internal hydraulic zones in a pump as turbine. The power of the CFD software has been exploited to provide information of the flow conditions within these zones. The objective of the present study is to find out which of the zones within a PAT can be modified, and in what manner, in order to optimise its hydraulic performance.

2. THEORY

2.1 Flow Zones in a PAT System

The flow within a PAT can be divided into six major zones as shown in Figure 1 and Figure 2. Zone 1 refers to the whole volute casing beginning from the inlet measuring plane. The zone 2 is the radial clearance between the casing outlet and impeller inlet (in turbine mode). Zone 3 is at the interface of the impeller inlet, zone 4 is within the impeller passage, and zone 5 is at the interface of the impeller exit. Zone 6 encompasses the eye region of the impeller/casing and the draft tube entrance passage until the exit-measuring plane.

However, for the build up of the present hydraulic analysis the flow zones have been broadly regrouped into four major regions which are,

- i. **Zone 1:** the volute casing
- ii. **Zone 2:** the radial clearance zone
- iii. **Zone 3-4-5:** the rotating impeller zone
- iv. **Zone 6:** the eye and draft tube zone

Figure 1, Flow zones –View 1

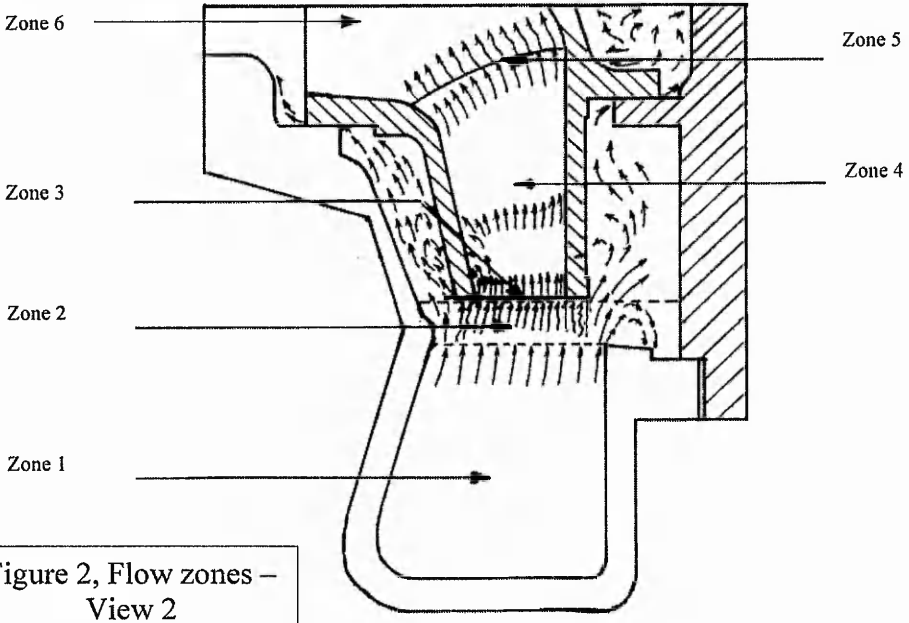
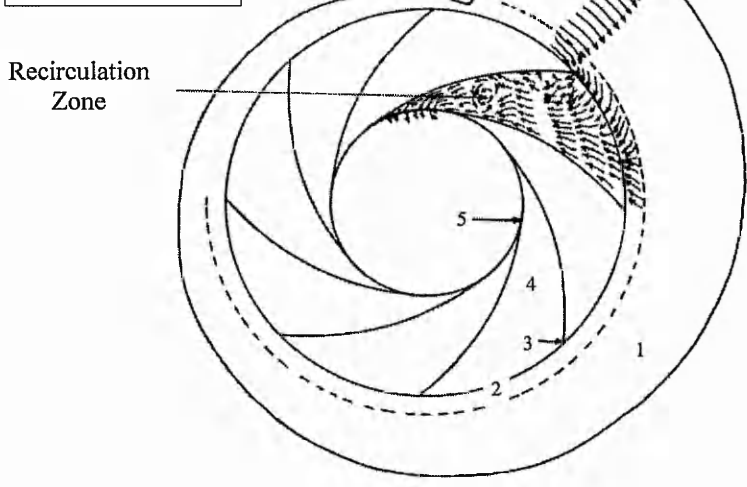


Figure 2, Flow zones –View 2

2.2 Hydraulic Parameters

To compare the experimental results directly with the numerical study, the hydraulic parameters have been evaluated separately. The basis for the calculations is illustrated in the following sections.

2.2.1 Parameters from Experiment

The experimental work measures the inlet and exit heads from which the total head across the PAT, H_{total} is obtained. The other parameters measured are the discharge, Q , the speed, N , and the shaft torque, T_{shaft} . The shaft torque includes the losses from the mechanical system of bearings/seals and the leakage flow, and is different from the hydraulic torque, which is determined by CFD. Therefore,

corrections have to be made to the measured quantities, before experimentally determined hydraulic parameters can be compared with predictions.

The overall experimental efficiency, $\eta_{overall}$ is,

$$\eta_{overall} = \eta_{hyd} \times (\eta_{mech} \times \eta_{leakage}) \quad (1)$$

The overall experimental efficiency, $\eta_{overall}$ is,

$$\eta_{overall} = \eta_{hyd} \times (\eta_{mech} \times \eta_{leakage}) \quad (2)$$

From (1),

$$H_{hyd} = [\eta_{overall} / (\eta_{mech} \times \eta_{leakage})] \times H_{total} \quad (3)$$

The experimental hydraulic losses can thus be determined as,

$$H_{loss} = H_{total} - H_{hyd} \quad (4)$$

Finally, the experimental hydraulic torque is,

$$T_{hyd} = T_{shaft} / (\eta_{mech} \times \eta_{leakage}) \quad (5)$$

The factor $(\eta_{mech} \times \eta_{leakage})$ is difficult to ascertain analytically and based on Karassik [11] this factor is approximated to 0.96 for the NW8 Pump as Turbine.

2.2.2 Parameters from CFD

The CFD model is set to calculate the total head, H_{total} , across the PAT at identical locations of the inlet and exit as the experiment. It also determines the hydraulic losses within each of the previously described zones, and the sum of all of these losses is defined as H_{loss} .

The hydraulic head is then calculated as in (4) and the hydraulic efficiency η_{hyd} is obtained from (2). The CFD hydraulic torque is then defined as a function of discharge (Q), hydraulic head (H_{hyd}) and angular speed (ω).

$$T_{hyd} = (Q/\rho)(gH_{hyd})/\omega \quad (6)$$

This is one of the methods of determining CFD torque and is termed the 'Hydraulic Loss' approach.

3. EXPERIMENTAL STUDY

3.1 Test Setup

Figure 3 shows the schematic view of the test facility. The input energy is supplied by four identical pumps connected in parallel. Each pump is capable of delivering 140 l/s of water at a head of 16 m. A transparent acrylic draft tube is fitted at the PAT exit and is submerged in a discharge tank 1.3 m below. The loading device used is a DC generator. As can be seen from Figure 3, the hydraulic circuit for the PAT test-rig is an open loop type and hence study of cavitation is not possible.

The instrumentation used on the test-rig is described in detail in Table 1. The data was processed using the 'Labview' software package from National Instruments and the measurements were made over a time interval of 10 seconds. Transient conditions were not studied.

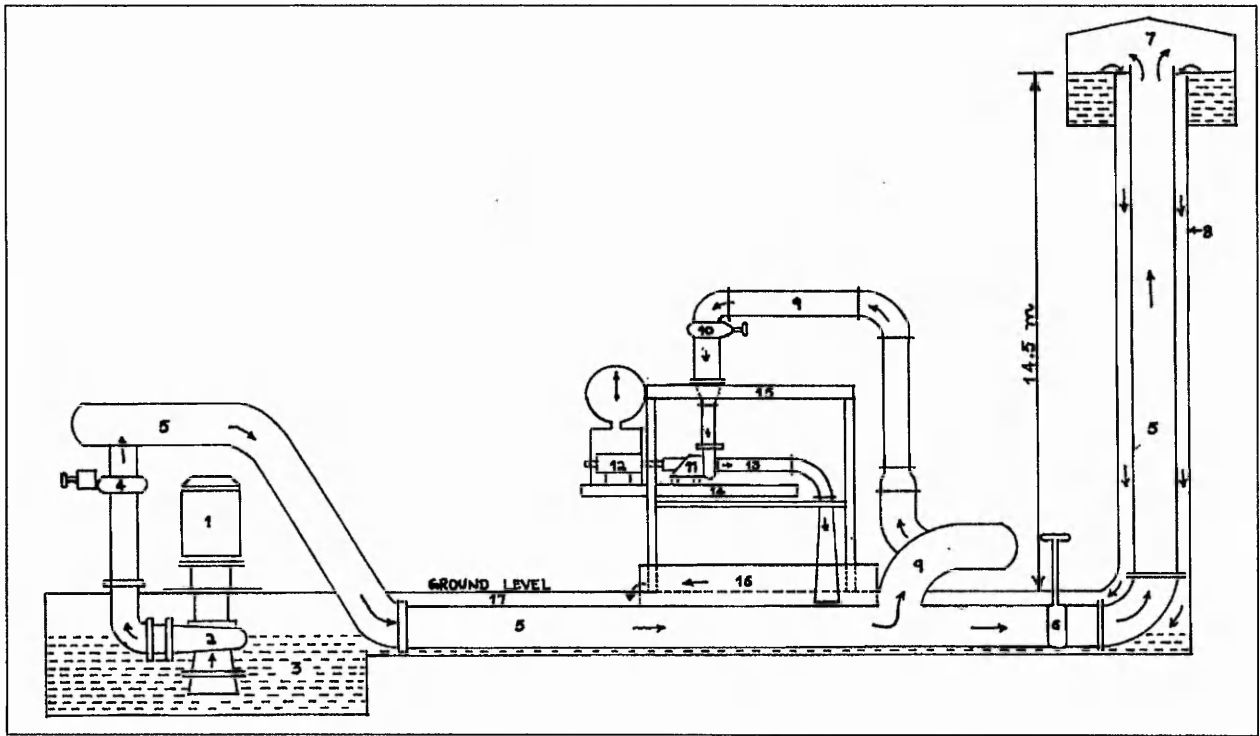


Figure 3. Schematic Layout of Test Facility

Table 1. Instrument Summary

Parameter	Measurement Principle	Make	Range	Accuracy	Output Signal
Discharge	Faradays Magnetic law	Turbo	0-1000 m^3/h	1% of full scale	0-20 mA
Inlet Pressure (Positive)	Wheatstone bridge	Hottinger Baldwin Messtechnik	0-2 bar	0.5 % of full scale	0-8 mV/V
Exit Pressure (negative)	Wheatstone bridge	Hottinger Baldwin Messtechnik	0-1 bar	2 % of full scale	0-8 mV/V
Torque	Wheatstone bridge	Hottinger Baldwin Messtechnik	+/-100 Nm	0.1% of full scale	5-15 kHz
Speed	Optical counts	Self assembled		1 r/min	Pulses

3.2 Procedure

Tests were carried out at different operating speeds. The characteristics have been determined for the whole operating range starting from no-load to maximum load attainable under the prevailing running condition. All the results were analyzed using the following non-dimensional numbers:

$$\begin{aligned} \text{Discharge number} & - Q/ND^3 \\ \text{Head number} & - gH_{total}/N^2D^2 \end{aligned}$$

Power number $- P_{shaft}/(\rho N^3 D^5)$

3.3 Test Specimen

The specimen under investigation is a single stage, end-suction pump. It has a low-medium specific speed of 24.5 *r/min* (pump mode). The chief design parameters are summarized in Table 2.

Table 2, Summary of pump design

Parameter	Dimension
Number of blades	6
PAT inlet impeller diameter D_1 (Outer)	258 mm
PAT inlet blade angle β_1	16.3 ⁰
PAT Inlet impeller width, b_1	21.8 mm
Exit blade diameter D_2	132 mm
Exit blade angle, β_2	24.3 ⁰
Exit blade width, b_2	39 mm
Casing Throat Area	3350.6 mm ²

4. CFD MODELLING

4.1 Modelling

The flow in the PAT is simulated using the CFX.5 commercial code, which incorporates the 3-D incompressible Reynolds-averaged Navier-Stokes equations. A steady state simulation is carried out using the standard *k-ε* turbulence model, with standard log-law for near wall modelling. First order advection scheme is imposed and the computation is considered to be converged when the maximum normalized equation residual is less than 10⁻⁴.

4.2 Geometry and Mesh

A 3-dimensional model based on the geometry data of the hydraulic volume and surfaces of the NW8 Kirloskar pump is generated. The geometry consists of four domains namely the casing volute, impeller, casing outlet, and draft tube as shown in Figure 4. Axial clearances between casing and impeller are not modelled. The total grid size consists roughly of 400 000 nodes. Due to periodic characteristics in the impeller, a single blade passage is modelled and the periodicity is taken into account in the circumferential direction of the impeller. The measuring planes at inlet and outlet are at an identical location to those specified in the experimental procedure.

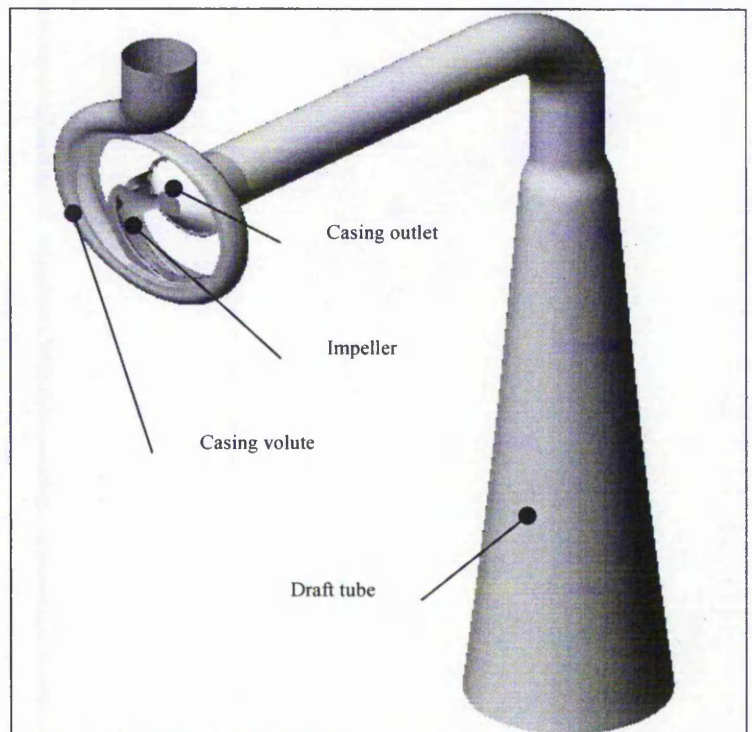


Figure 4. Centrifugal pump domains

4.3 Boundary Conditions

Mass flow is imposed as the inlet boundary condition with the velocity vectors normal to the boundary. At the draft tube outlet, static pressure is given and the boundary set to open conditions to allow possible back flow. Non-slip condition is imposed for all hydraulic surfaces. The casing and draft tube domains are set to stationary in the relative frame of reference, and the impeller set to rotating. Frozen rotor interfaces are used between casing volute and impeller, and between impeller and casing outlet.

4.4 Torque Calculations

Torque is directly calculated from the CFX calculator menu. This is an inbuilt calculation obtained by integrating forces over the impeller radius and is called the 'Force Integration' method. It is an alternative method as compared to the torque calculated from (6). The results from these two methods are to be compared, giving an indication of the reliability of the CFD model.

5. RESULTS

5.1 Experimental Performance Characteristics

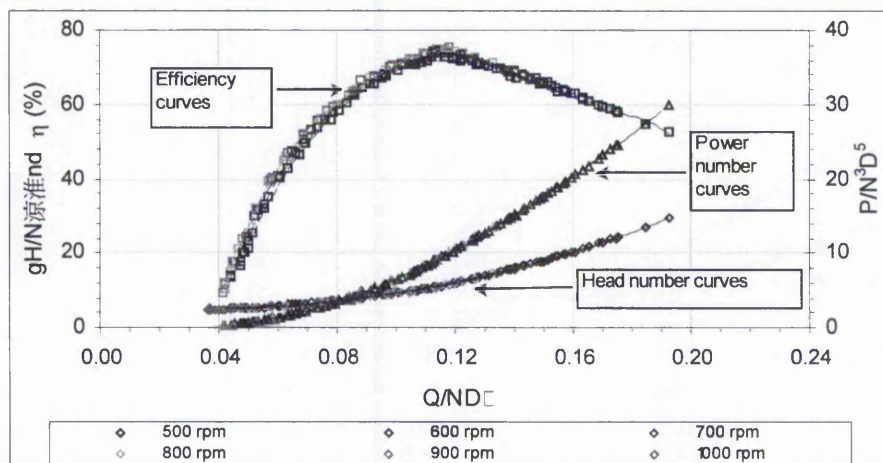


Figure 5. Overall dimensionless characteristics

The performance characteristics are plotted in Figure 5 at speeds of 500, 600, 700, 800, 900 and 1000 *r/min*. When plotted in dimensionless form, the head values and the power values each lie on a single curve, thus confirming the consistency of experimental measurements. The efficiency curves however have small variations mainly due to changes in the ratio of mechanical to hydraulic losses.

5.2 CFD Torque

In Figure 6, the hydraulic torques calculated by the CFD model using the Force-Integration and the Hydraulic-Loss approaches are compared. In the no-load and part-load regions the hydraulic-loss approach shows a higher torque.

The opposite is true in the main operating region (20 – 26 *l/s*) where the force-integration method reports a higher torque. However, the difference between the two torque values over the entire range is marginal.

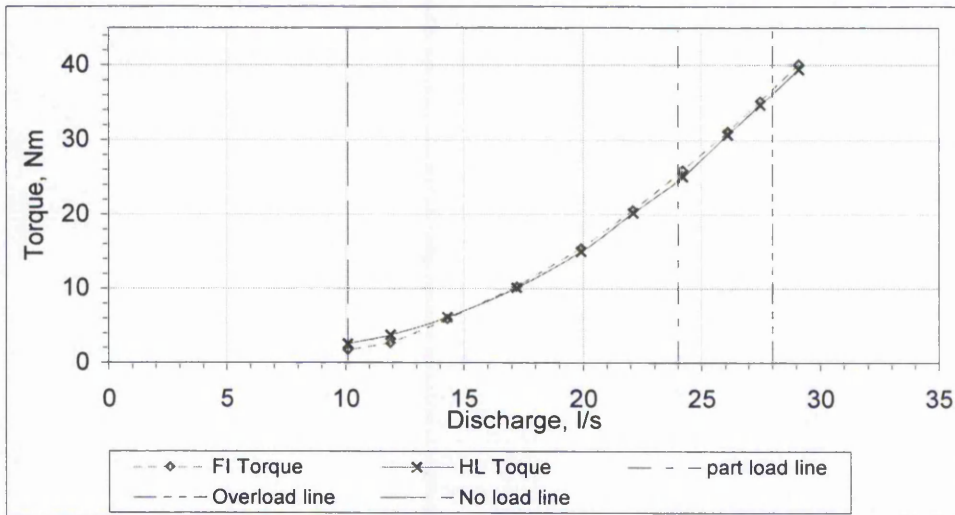


Figure 6. Torque comparison between two methods: force-integration and hydraulic-loss methods

5.3 Comparisons of CFD with Experimental Results at 800 r/min

5.3.1 Total Exit Pressure

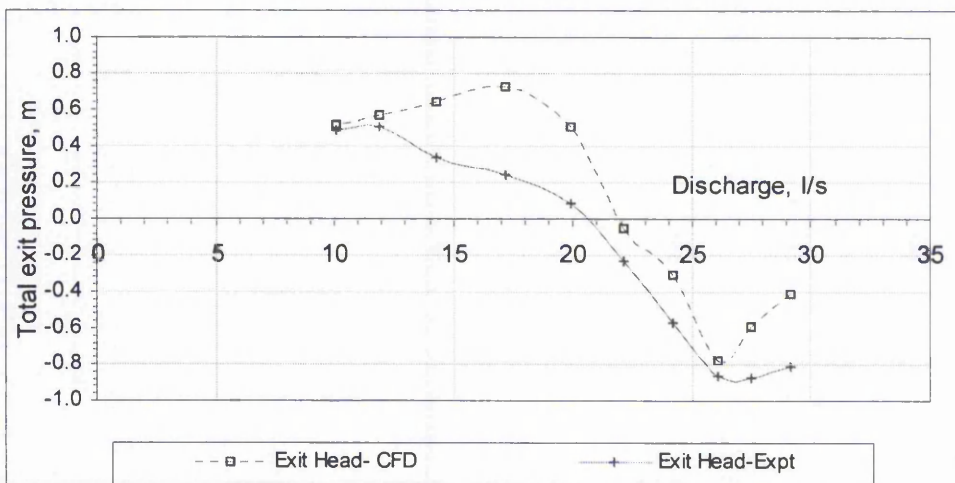


Figure 7. Comparison of total exit pressures

The CFD model calculates the relative pressures through the pump, but the absolute values are based on an arbitrary datum. Applying a fixed correction to the computed values to make the inlet pressures equal, allows a direct comparison to be made with the experimental data for exit pressures.

In Figure 7, the total exit pressures obtained from CFD and the experiment are compared. The CFD curve exhibits similar trend to that of the experimental curve, but predicts slightly higher values. At discharges of 17.2 l/s, 19.9 l/s and 29.1 l/s the difference is more than 0.4 m.

5.3.2 Hydraulic Parameters

Figure 8 compares the total head, hydraulic loss, hydraulic head and hydraulic efficiency curves. The total head curves (in Figure 7) show a reasonable matching, with the computed values consistently

below the experimental values.

The next important parameter to be considered is the total hydraulic loss. The experimental loss curve is higher in the part-load region, but as the BEP region is approached the difference between the two curves vanishes. It can be seen that the minimum hydraulic loss occurs at an identical discharge of 22.1 l/s for both methods.

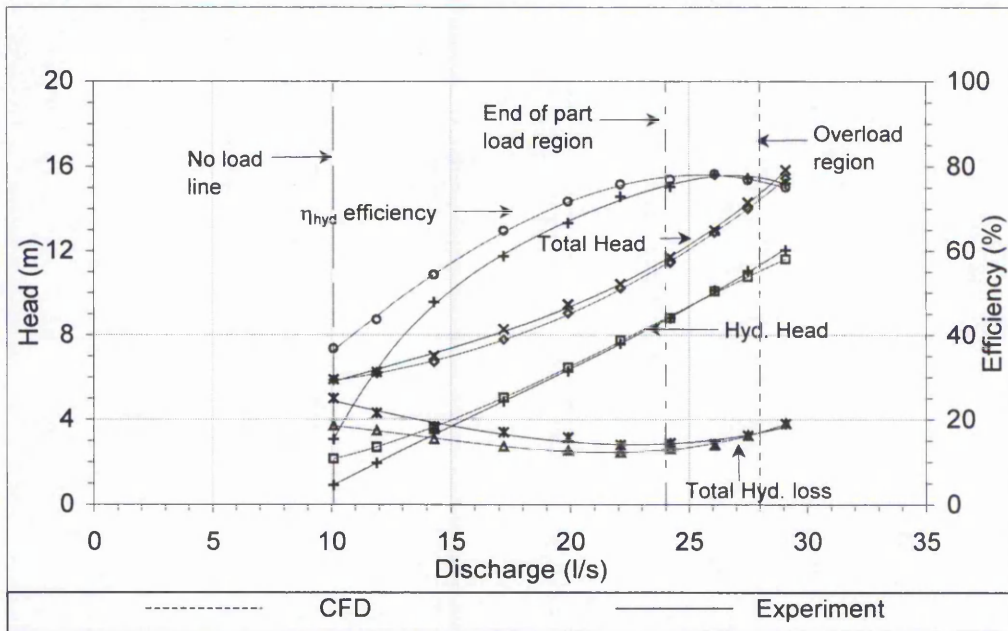


Figure 8. Comparison of Hydraulic Parameters

Good agreement is also achieved in the determination of the hydraulic head. Due to lower losses in the part-load region, the corresponding computed hydraulic head has increased and hence the hydraulic efficiency. However, the computed hydraulic head slowly merges with the experimental data near the BEP, leading to a gradual convergence of the efficiency curves. In the over-load region the experimental efficiency curve is slightly better, as a result of a drop in the computed hydraulic head.

The best efficiency point for experiment (η_{bep} -78.1%) and for CFD (η_{bep} -78.2%) occurs at an identical discharge of 26.1 l/s.

5.4 Zone Loss Distribution

As mentioned in section 2.1, the entire PAT hydraulic system has been divided into four hydraulic zones for ease of analysis. Figure 9 compares the hydraulic losses in the different zones. The losses in zone 1 (casing) show a steady increase with discharge, except for a discontinuity at 26.1 l/s.

The losses in the radial clearance (zone 2) follow a parabolic pattern. These initially decrease from the no-load point, reaching a minimum in the part-load region (between 17.2 l/s and 19.9 l/s) and steadily increase in the BEP and over-load regions.

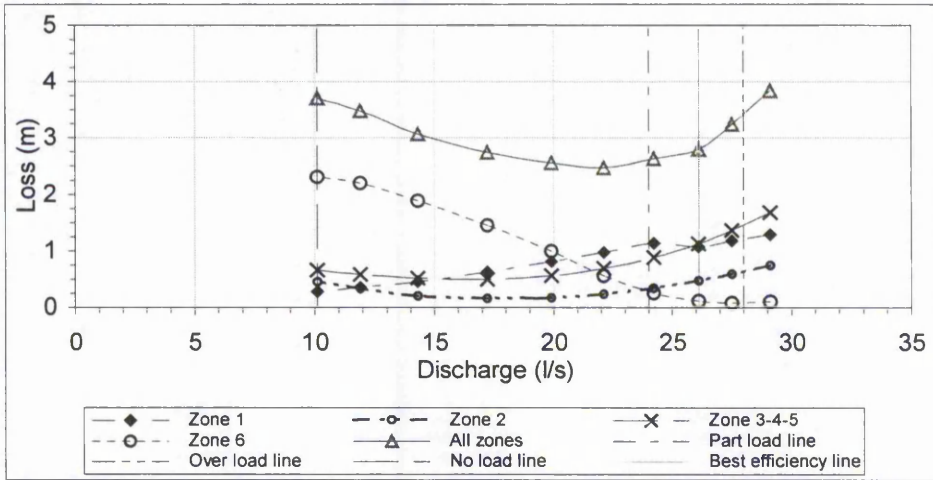


Figure 9. Zone Loss Distribution

Similar to the zone 2, the losses in the impeller (zone 3-4-5) initially decrease, reaching a minimum at 17.2 l/s (part-load region only) and rapidly increase thereafter in the BEP and over-load region.

The losses in zone 6, which are mainly associated with the swirl flow within a contracted flow area (casing eye), show an interesting behaviour. They form a major proportion of the overall losses when the PAT is operating in the part-load region, but the losses reduce rapidly towards the best efficiency and over-load regions. This is probably due to the unusual design of the NW8 pump in that the casing on the suction side has a smaller diameter than the impeller eye.

The swirl angles of the flow at the draft tube wall have been determined experimentally using high speed camera and are shown in Figure 10 along with the losses in zone 6. When the swirl is large (smaller swirl angles), the losses in zone 6 are high. As the swirl diminishes the losses become negligible.

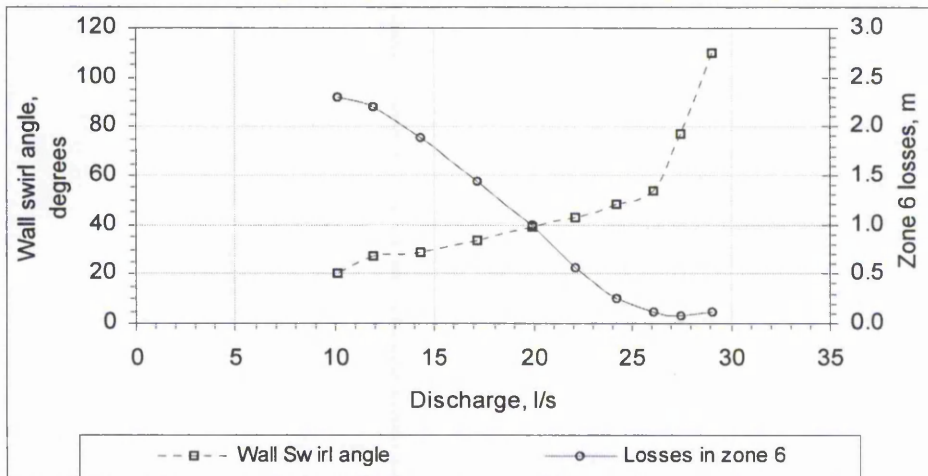


Figure 10. Wall Swirl Angle

Table 3 summarises the percentage distribution of the zone losses with respect to the total hydraulic loss at five specified discharges. It is evident that at the BEP and over-load points the impeller and casing losses assume a greater proportion. In contrast, at part-load, the hydraulic losses occur mainly in zone 6.

Table 3 Distribution of zone losses as a percentage of total hydraulic loss

Serial number	Load point	Discharge (l/s)	Zone 1 (%)	Zone 2 (%)	Zone 3-4-5 (%)	Zone 6 (%)
1	Overload	29.1	34	20	44	3
2	BEP	26.1	38	17	40	4
3	Part load	22.1	39	10	28	23
4	Part load	17.2	23	6	18	53
5	Part load	11.9	10	10	17	63

6. DISCUSSION

Two methods, namely the force-integration method and hydraulic-loss method, have been used initially within the CFD for the determination of the torque. The good agreement between the two sets of results (Figure 6) suggests that the chosen CFD model can yield consistent results. As the hydraulic-loss approach gives a better insight of the internal flow situation in a PAT it has been used in all subsequent analysis and compared with experimental results.

The predicted total exit pressures (Figure 7) follow a similar trend to that of the experiment but have consistently higher values. The higher values of CFD exit pressure may be attributable to the fact that the flow conditions (and hence the measurements) at the exit plane are often affected by both upstream and downstream conditions including the entire draft tube zone. Relatively coarse grids were used to represent the draft tube in the CFD analysis and this may be one reason why the CFD has not been able to predict the flow conditions accurately.

Encouraging results were obtained when comparisons were made between the predicted and experimentally-determined hydraulic losses (Figure 8). The two sets of loss curves follow a similar trend with the CFD predicting identical losses in the BEP and overload regions, but lower losses in the part-load region. This in turn has led to a higher CFD efficiency curve throughout the part-load region, revealing a limitation of the CFD model when the PAT is not operating at the design condition. With the uncertainty in the experimental determination of turbine efficiency estimated to be around 2 % at BEP and 4 % in the part-load region, the overall prediction of the hydraulic losses is considered acceptable.

The concept of 'flow-zone' analysis has been applied to the computational study of PAT performance. This approach has been shown to be useful and can form the basis for design optimisation for individual PAT components. In the present study, four major loss components have been identified and analysed separately. The first component is the volute casing (zone 1) where the losses account for 30% to 40% of the total hydraulic loss (Table 3). The losses in this region increase with discharge, very similar to frictional losses in pipes. However, optimisation of the main volute casing area is very difficult.

The second component is in the radial clearance (zone 2) and it represents 17% and 20% of the total losses in the BEP and overload regions respectively. There are two possible explanations for the relatively high losses: the rapid acceleration of the flow with a discontinuity of the flow direction near the impeller; and the influence of secondary flows due to large axial clearances. Therefore optimization in this region can be contemplated.

The third component is in the impeller area (zone 3-4-5), where the loss has shown a minimum value in the early stage of the part-load region. This minimum loss point refers to the shock free conditions at impeller inlet. However, it should be noted that for a given pump, the discharge at minimum impeller loss when it is operating in pump mode is not the same as the corresponding discharge when the same pump is operating as a turbine. Since the pump impeller is not designed for turbine applications, the recorded 40% to 45% of the total hydraulic loss at the BEP and over-load points compares favourably with conventional turbines [12]. However, it may be possible to improve the impeller inlet zone for PAT operation.

The fourth component is the eye and draft tube area (zone 6). The losses in this area can be very high in the part-load region accounting for as much as 60% of the total hydraulic loss. The relationship between the extent of the losses and the wall swirl angle of the flow at the PAT exit is shown in Figure 10. The wall swirl angle in the no-load region is large, falls rapidly as the discharge increases and becomes very small at the BEP and over-load region. The contraction in the casing immediately after the impeller eye increases the flow velocity and hence losses. It follows that a reduction of the losses can be achieved by minimising the amount of swirl and the operating flow velocities at the PAT exit. It may be difficult to alter the design of the exit blade profiles, but it is possible to modify the eye region.

7. CONCLUSIONS AND RECOMMENDATIONS

1. The CFD predictions of the hydraulic parameters compare reasonably well with experimental results, with deviations within 5% to 10% (excluding the no-load region) for most of the parameters. The experimental uncertainty is estimated to be in the region of 2% - 4%.
2. The chosen CFD model parameters namely, grid size/construction, meshing, turbulence modelling and wall function have been shown to be appropriate for analysing PAT applications.
3. The concept of dividing the complex flow regime within a PAT into four major flow regions so that each region can be analysed individually by means of CFD has been shown to be very useful and the results are conclusive. It should provide a strong basis for optimising the performance of a PAT.
4. The PAT research of this particular pump design (Kirloskar NW8) suggests optimisation may be considered in two areas.
 - i) A relative straightforward design modification could be made to the turbine inlet zone with respect to the radial clearance region and the impeller inlet interface. Additional casing rings could be used to reduce the extent of the radial clearance. This would help to reduce entry losses. The sharp edges of the blades and the shrouds could be rounded to minimise undesired flow turbulence and associated losses.
 - ii) Enlargement of the pump eye region would help to reduce the local flow velocities and hence losses.

8. REFERENCES

- [1] Anderson, H H, 1955. Modern Developments in the use of large single-entry centrifugal pumps, *Proc. IMechE*, Vol. 168, pp743-762.
- [2] Stepanoff A J. 1957. *Centrifugal and axial flow pumps*. John Wiley & Sons, Inc., Chapman and Hall Ltd, New York
- [3] Williams A A. 1994, The turbine performance of centrifugal pumps: a comparison of prediction methods. *Proceedings of the IMechE*, Part A, vol 208

- [4] Baines N C, Oliphant K N, Kimmel H E, Habets G, 1998 CFD analysis and test of a fluid machine operating as a pump and turbine. *IMechE seminar publication 1998-13*, pp 71 - 78
- [5] Tamm A, Braten A, Stoffel B, Ludwig G. 2000. Analysis of a standard pump in reverse operation using CFD, *20th IAHR-symposium*, Charlotte, North Carolina USA
- [6] Blanco E, Fernandez J, Gonzalez Jose, Santolaria C. 2000, *Numerical flow simulation in a centrifugal pump with impeller-volute interaction*. ASME FEDSM200-11297
- [7] Lueneburg, R, and Nelson, R M. 1992. *Hydraulic Power Recovery Turbines*. Chapter 14 of *Centrifugal Pumps-Design & Application*. Second Edition by Val S. Lobanoff and Robert R. Ross. Gulf Publishing Company, Houston, Texas.
- [8] Williams, A A. 1992. *Pumps as Turbines used with Induction Generators for stand-alone Micro-hydro Electric Power Plants*, PhD Thesis, Nottingham Trent University.
- [9] Cohrs, D. 1997. *Untersuchungen an einer mehrstufigen rückwärtslaufenden Kreiselpumpe in Turbinenbetrieb*. Verlag und Bildarchiv, W. H. Faragallah.
- [10] Mikus, K, 1983. Erfahrungen mit Kreiselpumpenanlagen zur Energierückgewinnung aus dem Trinkwassersystem. *Das Gas und Wasserfach*, Vol 124, pt. H.4 pp 159-163.
- [11] Karassik, Igor J. 1986. *Pump Handbook*, Second Edition. pp 2.22-
- [12] Hutton, S P, 1954. Component losses in Kaplan turbines and the prediction of efficiency from model tests. *Proc. IMechE*, Vol. 163, pp 81-89.